THE MECHANICAL PROPERTIES AND FORMABILITY OF DUAL-PHASE STEEL

MOHAMED BASHIRU OLUDARE OKANLAWON SHITTA

A thesis submitted in supplication for the degree of Doctor of Philosophy

Department of Metallurgy and Materials Engineering
University of Aston in Birmingham

July 1981

Summary

The University of Aston in Birmingham.

Title: Mechanical Properties and Formability of Dual Phase Steel.

Author: Mohamed, Bashiru, Oludare, Okanlawon, Shitta.

Degree: PhD, 1981.

In recent years dual phase steels comprising of 5-20% martensite in a ferrite matrix have come into the limelight of high strength cold formable steels because of their potential for vehicle weight saving.

They show the following features: no yield point; relatively low initial flow stress; high initial work-hardening rate; well sustained work hardening.

As a consequence of these characteristics, dual phase steels exhibit a better combination of strength and elongation than other HSLA steels. In this thesis, a broad view of the factors which influence their properties is presented. Mechanical properties and forming ability of a commercially available dual phase steel and an AL-Si killed steel processed to dual phase form are investigated to ascertain the effect of their microstructure on their properties. It is found that the yield phenomena are masked by the transformation induced stresses present during processing and so yield point could be recovered under suitable ageing treatment; that apart from giving the above properties dual phasing gives rise to very low strain-rate sensitivity and a low R value $\sim$ 1; that the mechanical response under rolling conditions is not different from those under tension; that there is a danger of damage to tooling during forming operations of these steels if fracture should precede instability as a result of grain size dependent strength found for these steels. It is also found that very little deformation of the martensite islands took place during deformation except at high strains. The work-hardening and the strength levels can be controlled by either decreasing the grain size or increasing the martensite volume fraction, but it is found that increasing martensite has a detrimental effect on ductility and the ductility and fracture strength can be controlled better by refining the grain size. A remarkable effect found in the dual phase steel tested is that the compressive strength is higher than the tensile strength. The reason for this observation is not yet clear but it is suggested that it might be due to the introduction of emissary type dislocations into the ferrite lattice as a result of twins formed in the martensite during transformation from austenite. The twins are envisaged to be {111} <112> in character.

Key Words: Steel; Dual-Phase; Work-hardening, Formability; (S-D) effect.

CONTENTS

LIST OF TABLES

LIST OF FIGURES

CHAPTER 2 INTRODUCTION

In recent years there has been a worldwide awakening of the need to conserve our energy resources. In particular the United States and Japanese governments have legislated for safety, pollution control and fuel economy. This has presented a challenge to the Automobile industries, where it is envisaged that a major fuel saving could be achieved, to try and reduce the fuel consumption of an average family car.

The attempt to reduce fuel consumption can be approached either by designing more efficient engines, which will require a greater amount of capital out-lay for research and development, or by reducing the vehicle weight. The latter is a more easily tractable approach and can be done in a number of ways.

1. Using lightweight plastic materials and fibre-glass (some car s' bodies are currently made in this way, e.g. Scimitar and Lotus).

2. Using lightweight metals, e.g. Al, Mg, and Be alloys.

3. Reducing the size of the vehicles and its weight by reducing the gauge of metals currently in use during manufacture.

The first of these has been estimated to cost the consumer an additional 50% or so on the amount currently spent on cars apart from the normal inflationary

tendencies of the price of goods. The second route will also increase prices by about another 20-30% because of the higher cost of alloying elements. The last route is a more practical approach but there is a limit to the size reduction of an average family car that consumers can be expected to tolerate hence attention has been focussed on gauge reduction. This moreover requires that the strength of the metal sheet used should be increased to do the same job as the conventional gauges of sheet metals.

The metallurgical variables necessary for increasing the strength of metals and alloys are already well established and these include among other things:

a. Solid solution strengthening
b. Grain refinement
c. Precipitation and dispersion hardening, and
d. Thermomechanical treatment, etc.

Earlier efforts were concentrated on producing high strength low alloyed steel will yield strengths of the order of 80 Ksi (∿550 MPa). The structural properties of these steels have been investigated in detail (2.1). The strength was achieved by a combination of grain refinement, precipitation hardening and solid solution strengthening, which came from the addition of manganese, silicon, titanium, vanadium, niobium and molybdenum to low carbon steel. Since inclusion shape has been shown to affect the response

of metals to deformation and the subsequent failure some Pure-Earth metal additions were also added to control the shape of the inclusions.

An increase in strength causes a reduction in formability compared to mild steel. The increased strength gave rise to loss of ductility and a major redesigning of press-shop components is necessitated to accommodate the thinner gauge and allow greater radii and less severe drawing of pressed parts so that their breaking strains are never reached during forming operations.

This approach means another increase in production costs and time spent in the press-shop as a result of the alloying additions. Therefore it was not altogether acceptable to the automotive industry to utilize completely the weight reduction offered by these HSLA steels; their forming ability must be improved upon and made comparable to, if not better than, that of current plain-carbon steels.

It was in the search for this improvement that by accident the first Dual-Phase steel was produced in the Physics Laboratory of General Motors Corporation in the U.S.A. by Donald J. Bailey in the early seventies while investigating the effect of thermomechanical treatment on the properties of plain carbon steel. His work stems from the earlier work of D.P. Koistinen, also of General Motors, who found that, by rapidly heating a rimmed steel in to the temperature range 400-600^{o}C and rapidly cooling at a rate of the order of 4000^{o}C per

second, he could suppress the yield point and the Luders strain in this steel (2.2) [2,3].

The steel which Bailey (2.4) was investigating at the time, an ageing Nitrogenised Low Carbon Cold Rolled steel, was accidentally heated into the alpha plus gamma region of the Fe-C phase diagram. The resultant product, now referred to as Dual-Phase steel because it contained essentially the two phases Ferrite and Martensite, gave remarkable properties compared to conventional Hot-Rolled steels. The properties observed were:

1. Lower yield strength
2. No sharp yield point
3. No Lüders strain
4. Comparable UTS to conventional HSLA steels
5. Rapid work-hardening at low strain state and high work-hardening coefficient (n) sustained to high strains.
6. Large uniform and total elongation.

A U.S. patent was applied for by Bailey in December 1974 for the product and the related process. The thermo-mechanical processing route that he employed is shown in Figure 2.1a together with the nominal stress/strain curves he obtained at each stage of his treatment shown in Figure 2.1b.

The high rate of work-hardening gives a flow stress which after 2-3% strain is similar to that of a conventional HSLA steel. The improvement in uniform elongation and n value is particularly interesting from the formability point of view as it will allow the material to distribute strain fairly uniformly up to high strain levels during forming operations.

In the tensile test the uniform elongation should be equal to the n value, according to the considered condition, and it is found that in conventional steels e_u is approximately equal to n and that it usually decreases with increase in strength following the Holloman relation $\sigma_y.n$ = constant irrespective of the strengthening mechanism.

The discovery of Dual-Phase steels then provides the first significant departure from this rule.

A method of representing the forming performance of sheet steel by plotting, against each other, the major and minor strain at failure for different strain states has been proposed by S.P. Keeler (2.5), called The Forming Limit Diagram (FLD); shown in Figure 2.2. S.P. Keeler and S.S. Hecker (2.6) have shown that there exists a linear relationship between FLD and n values such that as the n value increases the plane-strain intercept of FL (FLD_o) also increases linearly for a given sheet thickness, Figure 2.3.

The FLD for Dual-Phase steel is shifted upwards in comparison with current HSLA steels and approaches that of mild steel, Fig. 2.2. This upward shift in FLD of Dual-Phase steel means that, because of the improvement in its cold-formability characteristics, existing dies designed for mild steel can be used for this steel.

Much work has been done on the forming and production aspect of this steel notably on a commercial vanadium strengthened type referred to as GM980X by M.S. Rashid (2.7) at General Motors and in Japan. Various automobile parts have been formed out of this steel with considerable success (2.8).

Although much work has been done on the development, production and characterisation of Dual-Phase steels complete elucidation of its outstanding properties have not yet been further advanced. R.G. Davies' work is particularly noteworthy (2.9). His work has led to a definition of properties that a Dual-Phase steel should have. These are:

1. No sharp yield point
2. No yield point elongation
3. A yield strength of 305-385 MPa at 0.2% off set strain
4. A flow strength of 520-550 MPa at 2-4% strain
5. A U.T.S. of 620-655 MPa

6. A total elongation in excess of 27% over a gauge length of 2 inches (50.8 mm)
7. A volume of martensite ranging from 5% to 20%.

There have been three major ideas put forward to explain the properties observed but some doubts still exist as to the true micromechanism governing their behaviour.

The primary aim of this work is to attempt to investigate what governs some of these properties. The disappearance of yield point in Dual-Phase steel cannot just be explained by interstitial solute element removal from the main ferrite matrix alone, but it probably also involves residual stresses due to the martensite formation and perhaps the thermal contraction due to rapid cooling. The enhanced ductility is probably not accounted for by a simple model of the plasticity of a two phase structure, as used by Davies, but must also involve consideration of the fracture processes.

Very little so far has been done to study the return of the yield point and the behaviour of these steels under complex and reverse loading conditions as well as the other material parameters influencing formability such as R value and strain rate sensitivity, and some of these aspects are studied here.

To aid our understanding of the micromechanisms, a literature review has been carried out in Chapter 3 on the yield point and its conventional method of suppression, and some other related topics concerning two phase metals.

Chapters 4, 5 and 6 deal with the present work, which has shed some light on a number of the qualities of Dual-Phase steels relevant to their application. One of the most interesting aspects of the steel's behaviour, a strong strength differential effect has been revealed in this work and a full understanding of this effect has yet to be obtained.

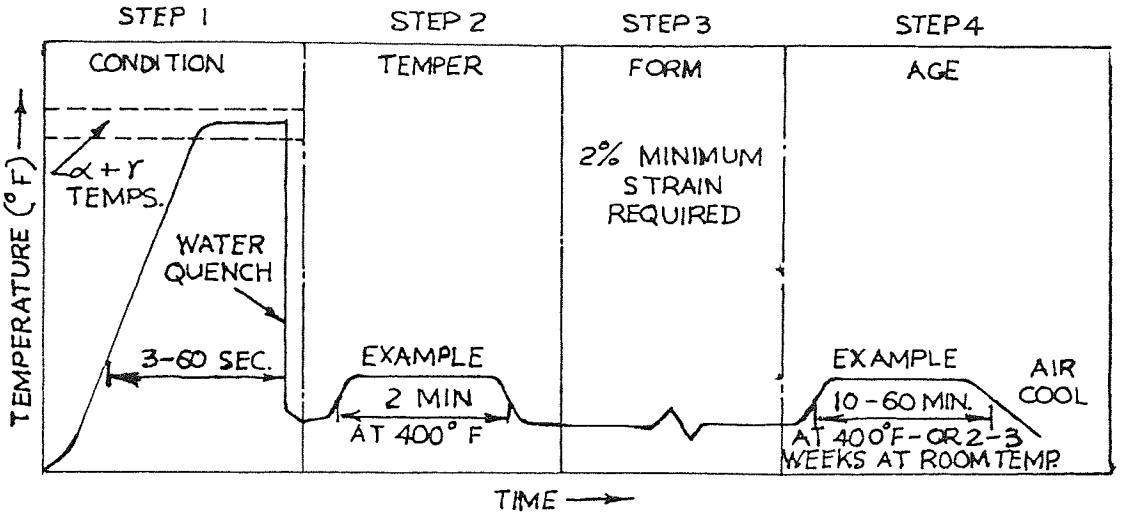

FIGURE 2.1a Thermomechanical Route employed by D.J. Bailey (2.4)

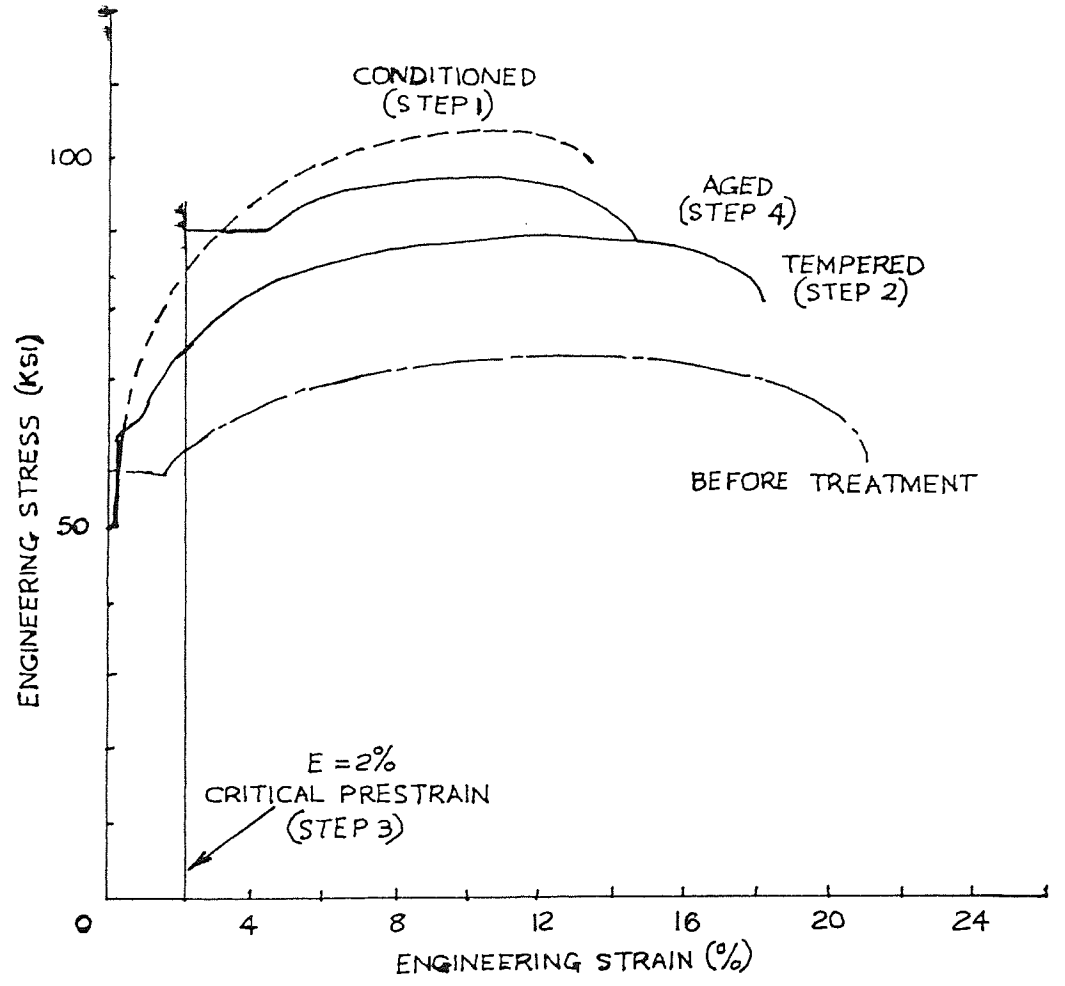

FIGURE 2.1b Nominal Stress/strain Curves obtained by D.J. Bailey at each stage of his treatment (2.4)

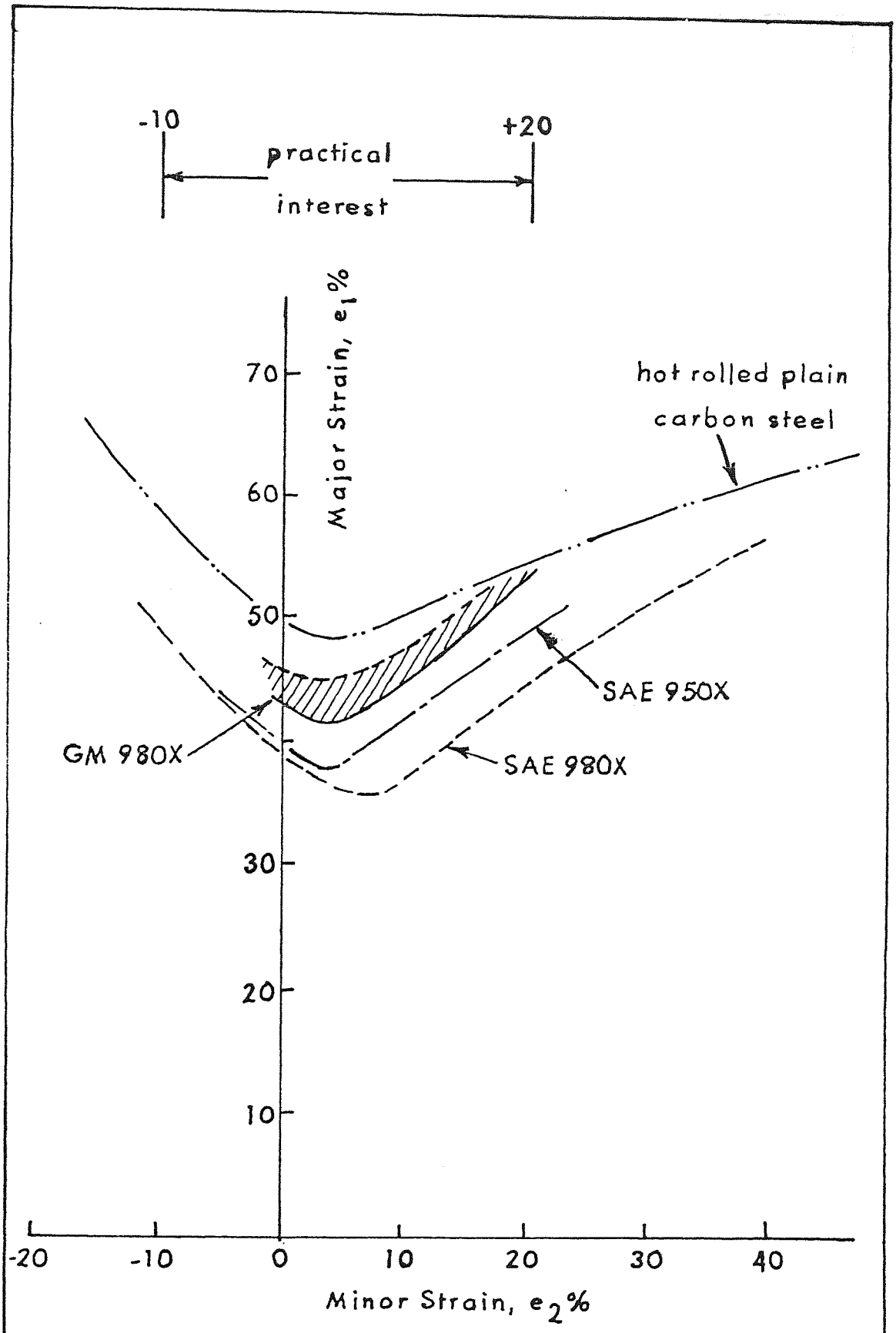

FIGURE 2.2 The range of the Forming Limit diagram (FLD) of GM980X compared with that of Plain Carbon steel and SAE950X and 980X. The GM980X was obtained by heat treating a SAE980X steel (ref. 2.7)

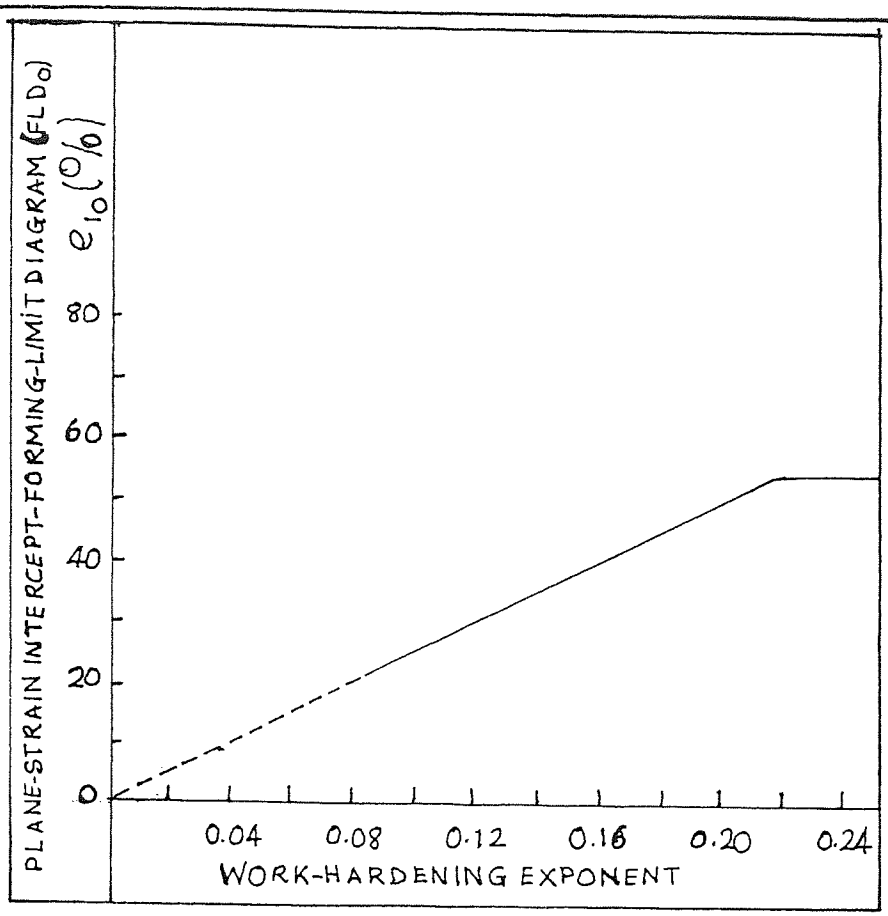

FIGURE 2.3 The relationship between the plane-strain intercept (FLD_0) and work-hardening exponent n for Dual-Phase steels (ref. 2.6)

LITERATURE REVIEW

3.1 Yield Point and Ageing Phenomena in Low-Carbon Steels and their Control

A yield point (Y.P.) is the occurrence of a sudden maximum in the tensile stress/strain curve at the onset of large-scale plastic flow. Ageing on the other hand covers the changes which occur with time in the properties of materials during storage.

There are two types of ageing that are of interest here which affect the mechanical properties of steel. These are:

1. Strain Ageing
2. Quench Ageing

The former is particularly detrimental in deep-drawing steels because ageing increases the yield strength and it is accompanied by loss of ductility. This gives rise to buckling and tearing during drawing as a result of the occurrence of a sharp yield point and the formation of Luders bands during pressing operations. To control it would be of great value.

Considering the yield point and strain ageing first, Figure 3.1.1a illustrates the type of stress/strain curve commonly obtained for mild steel. After the sharp yield point (U.Y.P. in Fig. 3.1.1a) deformation continues at a lower stress level for some strain up to as much as 6% strain followed by work hardening. This lower stress level is called the lower yield point (L.Y.P.) while the initial yield stress is called the upper yield point (U.Y.P.). The plastic strain without appreciable increase

in stress level at the lower yield point is referred to as the Luders strain or yield point elongation. This is a localized plastic flow of the material which originates at stress concentration centres and spreads through the entire cross-section of the tensile specimen to form a band. It is believed that dislocations in steels are pinned (or locked) by clusters of nitrogen and carbon atoms, and in some cases by boron, in solid solution after cooling from the hot rolling or annealing temperatures. This is because there are changes in interatomic spacing around an edge dislocation causing electrons to concentrate in the expanding side of the dislocation and leave the compressed side, leaving the dislocation as a line dipole with effective negative charge on the dilation side. This dipole field will then interact with the electronic structure around a solute atom thus pinning the dislocations to it and will have to be overcome before the dislocation can be free to contribute to plastic deformation.

The existence of the upper and lower yield point can be understood in terms of the dislocation dynamics. During deformation the plastic strain rate of metals is given by:

$$\dot{\epsilon}_p = pbv \qquad \text{.....(3.1.1)}$$

where $\dot{\epsilon}_p$ = plastic strain rate

b = Burgers vector

v = dislocation velocity

p = dislocation density

The upper yield point corresponds to a stress of which many dislocations are unpinned or new ones are formed at sources such as grain boundaries. Also the dislocation velocity is strongly stress dependent such that:

$$v = \left(\frac{\sigma}{\sigma_o}\right)^n \qquad \ldots\ldots\ldots (3.1.2)$$

n = constant ~ 35 in 3% Si-Iron

σ_o = stress for unit speed of dislocation in the lattice

v = velocity of dislocation under stress σ

As there is a sudden steep increase in dislocation density ρ at the upper yield point with the on set of plastic deformation, the same rate of elongation can be maintained by a lower dislocation velocity which implies lower σ thus the yielding stress drops to the lower value at (L.Y.P.)

The microstructure of the steel has an influence on both the upper yield point and the yield elongation in that their magnitude is increased by decreasing the grain size (d). This is obvious from the wellknown Hall-Petch relation for plastic flow stress in poly-crystalline metals.

$$\sigma_y = \sigma_i + k_y d^{-\frac{1}{2}} \qquad \ldots\ldots\ldots (3.1.3)$$

σ_y = Tensile stress necessary to propagate yield from one grain to the next

σ_i = lattice friction stress opposing the dislocation motion

k_y = Petch constant or grain size dependence constant

Observations on polycrystalline 3% silicon iron by N.J. Petch (3.1.1) and J.P. Worthington (3.1.2) have shown that at very large grain sizes most of the grains have deformed before the (U.Y.P.) is reached, so that no macroscopic yield drop occurs. This has led Petch (3.1.1), taking into consideration equation (3.1.2), to derive an expression for the magnitude of the yield drop as:

$$\sigma_{U.Y.P.} - \sigma_{L.Y.P.} = \Delta\sigma_o \, \text{Log}_{10} \frac{1}{Nd^3} \quad \ldots\ldots(3.1.4)$$

$\Delta\sigma_o$ = stress increase when the strain rate is increased ten-fold.

N = number of grains per mm^3 deforming plastically

d = grain size

For very large grain size mild steel (3.1.4) and 3% Si-Fe (3.1.2) this theory has been shown to give very accurately the grain size at which the yield drop disappears but for very fine grained steel there is a marked error in the prediction.

If an annealed low-carbon sheet steel is strained to a level between AB (Fig. 3.1.1a) it will exhibit stretcher strains. If strained beyond the point B of the curve the stretcher strains will become diffused. This is of

special interest in shallow drawing operations, particularly in the pressing of automobile door panels, where forming of steel which exhibits a yield point may lead to a rough surface on the drawn part. When the sample is loaded beyond U.Y.P. but strained to between A and B and then unloaded, upon immediate reloading it will start to deform only at the L.Y.P. level but if some time has elapsed between unloading and reloading, the sample may require a load greater than the L.Y.P. to deform if plastically. If it is strained beyond point B it will not show discontinuous yielding behaviour but with sufficient time the yield point and its associated Luders strain will re-emerge. The return of the yield point with consequent increase in strength is termed Strain-Ageing. When a decrease in strength accompanies it it is called Recovery (Fig. 3.1.1e).

The phenomena of yielding and strain ageing have been known since the 19th century and it was not until the early part of this century that some explanation of its occurrence started to emerge.

The theories put forward so far can be categorized into two types:

1. Static, and
2. Dynamic

The dynamic theory attributed the sharp drop in stress level to the rapid generation of large numbers of

mobile dislocations (3.1.3); while the static theory attributes it to the breakaway of dislocations from their solute atom atmospheres as mentioned above (3.1.4) (3.1.5).

Prior to these theories Dalby (1913) (3.1.6) and Kuroda (3.1.7) proposed that the yield point was due to grain-boundary cementite formed during the production of the steels which prevents the individual ferrite-grains from deforming until it has given way, under the applied load, with a pile-up of dislocations at the boundary, triggering dislocation movements, resulting in the creation of Luder band nucleus in each of the other ferrite grains and spreads across the specimen. This clearly, in the light of present day knowledge, cannot be so because of the thinness of the carbide films and this has been rightly criticised by Cottrell (3.1.4) above.

The theory which has the widest applicability and that is most appropriate here is that static theory of Cottrell and Bilby (3.1.5).

Although it does not take account of the rapid dislocation generation which takes place after yielding (3.1.8) and the immobilization and remobilization of these dislocations and their interactions with the Forest dislocation (3.1.9) (3.1.10), it still has the widest acclaim for explaining the yield phenomena in low-carbon steels.

In their theory they proposed that, because as little as 0.02% C has a pronounced effect on this phenomena, carbon atoms in solution in ferrite segregates to dislocations, locking them in position as a result of their interaction strain energy with the solute atoms. The driving force for segregation comes from the strain energy released by the movement of carbon from interstitial sites where they cause lattice dilation to the tensile side region around an edge dislocation. This energy was estimated by Cottrell and Bilby to be of the order of 0.5 eV per atom plane and they also estimate that approximately 10^{-6} wt % C is needed to put a carbon atom on each dislocation per atom plane given that the average dislocation density in annealed mild steel is about 10^{8} line/cm^{2}. Nitrogen and boron have been shown to have a similar effect (3.1.12). Locking by nitrogen is stronger than by carbon whilst boron locking is the strongest.

For carbon then, yield occurs when the mechanical work done on the metal plus the thermal fluctuation energy is greater than the above energy. At this point the dislocations break away from their pinning position, multiply and form the first Luders band. This binding energy is given by

$$U = 4\mu b\varepsilon' r^{3}\left(\frac{\sin\theta}{R}\right) \qquad \ldots\ldots\ldots (3.1.5)$$

where U = shear modulus

b = Burgers vector of the dislocation

~ 2.48 Å in Fe

$\varepsilon' = \left|\frac{r'-r}{r}\right|$ is a misfit parameter of the lattice

R and θ are polar co-ordinates of the solute atom with respect to the dislocation core.

The equilibrium concentration of the solute atoms around a dislocation was assumed to be given by a Maxwell-Boltzman distribution Law so that

$$C = C_o \exp\left(\frac{U}{KT}\right) \qquad \ldots\ldots\ldots (3.1.6)$$

C_o = average concentration of solute in the lattice.

A more appropriate distribution law should have been a Fermi-Dirac one as the dislocations have an electric charge associated with them and unless the charge energy is within U/kT of the Fermi surface no escape will be possible.

Using the above distribution law when C = 1

$$U = T_{crit} K \, Ln\left(\frac{1}{C_o}\right)$$

$$\text{or} \quad T_{crit} = -\frac{U}{K}\left(LnC_o\right)^{-1} \qquad \ldots\ldots\ldots (3.1.7)$$

Equation (3.1.7) represents a critical temperature when yield point phenomena should disappear. Using known values of U and C_o ($\sim 2.5 \times 10^{-3}$ wt%) it was estimated that T_{crit} is of the order $700^{o}C$ (3.1.11).

Strain ageing then is when the solute atoms migrate by diffusion to the freed dislocations and relock them giving rise to the reappearance of yield point and yield elongation.

Cottrell and Bilby and lately Bergström (3.1.10) via a different route based on the work of Wilson and Russell (3.1.13), (3.1.14) have shown that the number of solute atoms that condense out of solution in α-iron after a time t is given by

$$n(t) = 3\left(\frac{\pi}{2}\right)^{1/3} n_o \left(\frac{ADt}{kT}\right)^{2/3} \quad \ldots\ldots (3.1.8)$$

where n_o = initial concentration

A = elastic constant

D = diffusion coefficient

t = time in seconds

T = Temperature in ^oK

k = Boltzmans constant

Although this expression has been confirmed by Harper (3.1.16) using internal friction measurements on steel it is not always found to be true. McLennan (3.1.16) has observed a time exponent varying from 1.5 at early stages of ageing and 0.5 at a later stage. Newman (3.1.18) has criticised Cottrell and Bilby's theory because they did not take cognisance of the effect of back diffusion of the solute atoms so that their derivation will yield a more rapid approach to equilibrium.

A significant contribution to the understanding of yield point strain ageing and the subsequent plastic flow of metals was provided by Wilson and Russell (3.1.13, 14). Their work shows that there are two stages of strain-ageing. Stage I is characterised by an increase in Luders strain and yield stress with formation of interstitial solute atmospheres on the pre-strained introduced dislocations while in stage II there is an increase in flow stress and rate of strain hardening due to the growth of dislocation-nucleated precipitates. This behaviour is depicted in figure 3.1.1b-e. There can also be a decrease of flow stress shown in 3.1.1e called recovery. This work, and several others (3.1.8, 3.1.9, 3.1.10), have shown that during yielding large numbers of new dislocations are generated hence the theory has been largely modified to take cognisance of this fact (3.1.10).

There is another ageing phenomenon worthy of mention here called Quench Ageing, that may aid us in understanding the behaviour of Dual-Phase steel. This arises as a result of the increase in solubility of carbon and nitrogen in α-iron at elevated temperature. Upon rapid cooling to room temperature, the solute atoms are frozen in, in their high temperature randomly distributed positions throughout the α-iron matrix; there are more dislocations free of solute locking atmosphere, therefore in some cases the initial yield point may be absent.

On ageing the excess solute in the super-saturated matrix are precipitated and the dislocations become locked again. The solubility of carbon varies from 0.02% at 723^{o}C to 10^{-7}% at ambient temperature while that of nitrogen varies from 0.10% at 585^{o}C to 2×10^{-5} at ambient temperature and even though they have very low solubilities at room temperature their diffusion is sufficiently rapid to give rise to appreciable precipitation during storage giving rise to an increase in hardness with storage time. This was extensively studied by Davenport and Bain (3.1.18).

The degree of quench ageing depends on the rate of cooling; lower cooling rate gives low quench-ageing.

From the work of Davenport and Bain (3.1.18) and Cottrell and Leak (3.1.19) it is clear that the increase in hardness experienced comes from the imposed lattice strain from the formed precipitates which are initially coherent with the matrix but later grow and become incoherent with subsequent softening of the lattice taking place. Thus is termed "Overageing".

The first formed precipitates are known as ε-carbides and have the chemical formula $Fe_{12}C_5 \equiv Fe_{2.4}C$. Later these transform to cementite, Fe_3C. Nitrogen has the same effect as carbon except that it exhibits two hardness peaks. The first is due to the formation of Fe_8N which later overages and dissolves to form Fe_4N above

175°C as this does not form below this temperature. Carbon is soluble in Fe_8N and likewise nitrogen is also soluble in ε-carbide. Wert (3.1.20) has shown that the rate of precipitation of carbon from an Fe-C-N alloy system at 110°C was faster than it is in ordinary Fe-C system as a result of this effect. His work further shows that the rate of removal of carbon and nitrogen from solution is independent of the rate of nucleation rather than on diffusion rate.

It is therefore apparent, from all the above, that since nucleation and growth of precipitates are major factors which govern the increase in hardness with time during quench ageing and these depend on the availability of carbon and nitrogen, and since, further, these two elements are responsible, among other things for the existence of yield points and strain ageing any factor which will influence the availability of these two elements in solution can be used to control them. It is further clear that any process which makes available mobile dislocations in the lattice will help to suppress the yield point. Therefore alloying additions which have an affinity for carbon and nitrogen can be expected to affect the rate of diffusion as well as the rate of nucleation of precipitates. Other factors which affect this will be the presence of localised strained regions within the material which will impede the migration or precipitation of these solutes.

Elimination and Suppression of Yield Point and Strain Ageing

To achieve this it will be necessary, from the aforementioned factors contributing to yield points and ageing, either to make available in the material large supply of mobile dislocations (suppression since the solute may still migrate to these dislocations to tie them down again given sufficient time and temperature) or to remove as nearly as possible all the carbon and nitrogen in solution. This latter can be done by heating the steel in wet hydrogen or by alloying with strong carbide and nitride formers such as Al, V, Nb, Cr and Ti. The former method could be achieved by slight plastic deformation before testing. It could come by either a deliberate plastic work or from residual stresses generated from cooling from high temperature or rolling or from phase transformations. However the yield point and stretcher strains will return with time and there will be a reduction in the ductility of the metal. The deformation can be effected either by stretching to about 5% strain or cold rolling 1-2%. This latter case is known as Temper Rolling, Fig. 3.1.2a. The effect of temper rolling is to leave the surface of the sheet in a state of residual tension so that yielding can start from the surface and spread inward with rising applied stress without the formation of a Luders band. On the other hand the residual stresses set up cannot effectively explain the behaviour of temper rolled sheets. The rate of return of the sharp yield point, when the sheet thickness is reduced by three-quarters of its

initial thickness, is not affected even though the residual stress level has been considerably reduced. It is commonly observed that when the reduced sample is given different residual stress level (reduced by etching) it has different behaviour, illustrated in Figure 3.1.2b.

Hundy (3.1.21,22) and Wilson et al (3.1.23) have obtained similar behaviour. Wilson further found that in samples treated to remove the effects of prior plastic deformation, the presence of elastic residual stresses influenced the number of Luders band formed in such a way that the number of bands nucleated increased with increasing internal stress level. This they attributed to inhomogeneous deformation due to localised stress zones set up during temper rolling which produce a pattern of alternating bands of deformed and undeformed metal spaced about 10 to 20 to the inch transverse on the specimen along the rolling direction.

Since the yield strain in annealed mild steel is about 3%; if the material is given a total cold reduction of about 1%, the plastic strain will not be uniformly distributed but will occur in zones in which the strain is about 3% separated by zones experiencing little or no plastic deformation at all. These zones will then act as yield nuclei at the surface during subsequent loading. The way residual stresses act to retard the return of the yield point have been studied by Tardiff and Ball (3.1.24). They showed that it does not alter the migration rate of the interstitial elements to the dis-

locations but that it merely acts to mark the return of the yield point by preventing the whole specimen from yielding simultaneously.

By assuming that a definite yield point will be evident only if during yielding the slope of the load/elongation curve becomes negative and accepting the findings of reference (3.1.25) R.L. Whiteley (3.1.25) has been able to put forward an expression that describes the way residual stresses retard the return of the yield point on ageing given by:

$$(\sigma_{UYP} - \sigma_{LYP}) > (x_o - x)\left[-\frac{dF(x)}{dx}\right] \quad \ldots\ldots\ldots (3.1.9)$$

Where σ_{UYP} and σ_{LYP} are the upper and lower yield stresses respectively in the absence of residual stress. While F(x) is a function which describes the residual stress pattern with x. x is a distance measured from the point of maximum tensile residual stress to the boundary between the plastically strained and elastically strained region and it increases to x_o as the load is applied. x_o is equal to the half the wavelength of the residual stress pattern. $(\sigma_{UYP} - \sigma_{LYP})$ increases as a function of the rate of segregation of carbon and nitrogen in the steel to dislocations.

The effectiveness of temper rolling is not uniform in all directions because of the alignment of the deformed and undeformed zones in the rolling directions in the sheet

plane and along the directions of maximum shear stress in the through thickness direction, so that the yield behaviour in the transverse will be different to that along the longitudinal direction. This will increase with

a. greater reduction
b. rougher roll surface
c. large grain size
d. small roll diameter (3.1.23)

It should now be apparent that if temper rolling is employed on a sheet steel any forming operation to be carried out with it must be done within a short space of time. If however this is not feasible roller levelling may be employed, so long as ageing has not progressed to a stage where the yield point elongation is greater than 1.5%, to suppress the yield point and yield elongation.

Therefore if the sheet steel microstructure can offer some internal complex residual stress system this might help in masking or eliminating the yield point phenomenon and its associated stretcher strains. This perhaps can be done by imposing a large coherent stable precipitate of different thermal coefficients within the matrix of the sheet steel from which large numbers of free mobile dislocations can be rapidly generated or as a result of quenching from high temperature due to different thermal contraction and transformation induced strains. This

type of stress system is present in dual-phase steels.

Returning now to the use of alloying elements as a means of controlling ageing and the yield point. This has led to extensive use of Al-killed steel in the press shops. It has been shown (3.1.26) that Al-killed steel shows no ageing after 1 hour at 100°C but that ageing increases above this temperature. This is perhaps due to uncombined carbon or the dissolution of the AlN particles formed. Edwards (3.1.26) result could also be because he used too high a normalising temperature (950-1050°C) coupled with too high an ageing temperature (1 hour at 250°C). Later Leslie et al (3.1.27) showed that Al-killed steel does show ageing at 100°C and that Al by itself does not eliminate strain ageing at 100°C except when added in concentration with Si. Laxar et al (3.1.28) have further shown that aluminium in steel less than 0.08% decreases ageing while above 0.30% ageing is again on the increase. This perhaps is because silicon can form a nitride readily at temperatures between 600-650°Cwhich is isomorphous with AlN (3.1.29). Also Leslie et al, above, have shown that silicon, too, on its own cannot be used effectively to eliminate strain ageing except in combination with aluminium.

Another element that has been proposed to control ageing by Morgan and Shyne (3.1.30-32) is boron which forms BN. They showed that a significant reduction can be achieved provided the additive level is kept between 0.007-0.02wt%

Outside this level strain ageing increases as boron can also act as an interstitial element in α-iron pinning dislocations.

The most effective alloying additions are the combined carbide and nitride formers namely Cr, V, Nb and Ti.

Chromium (Cr) is the weakest in this category. 6% Cr addition is needed in order to reduce ageing considerably at 250°C with the removal of the sharp yield point. Vanadium on the other hand is much more effective than Cr in eliminating strain ageing. Edwards et al (3.1.26) found that about 0.69% V was sufficient to eliminate strain ageing while Epstein et al (3.1.33) have found that about 0.03-0.05% Vanadium was adequate in reducing strain ageing at 100°C but the yield point still exists.

Niobium (Nb) too has been found to be of value (3.1.26). Only 0.36% Nb was needed to eliminate both strain ageing and the initial yield drop. However this requires an annealing treatment at 650°C after normalising (3.1.34) because at this temperature nitrogen (N) should be dissolved by the growing ε-carbides ($Fe_{2.4}C$).

By far the most effective element in this group is titanium (Ti). A ratio of 9:1 of titanium to carbon could remove both ageing and the initial yield point. Edwards et al (3.1.26) obtained a stress/strain curve

similar to that of a dual-phase steel for a fully annealed 0.095% C, 1.08% Ti steel.

At long ageing times vanadium carbide (VC) precipitates grow to form V_6C_5 and in combination with titanium, forms $(V,Ti)_6C_5$ at high temperature. While ageing at 725°C it was found by Dunlop et al (3.1.35) that TiC dispersions initially coarsened rapidly while (V,Ti)C coarsened very little. The tendency of (V,Ti)C to resist coarsening was attributed to its higher chemical-bonding energy.

Clearly the occurrence of these types of precipitates in an alloy steel will also add to its strength via the particle hardening effect as well as controlling its ageing characteristics by tieing up the interstitial solute atoms. However a premium might be paid in ductility. It should also be observed that from all the preceeding techniques for suppressing or eliminating the yield point in steel; the yield point in most of the commercially available dual-phase steels cannot be said to have been eliminated it has merely been suppressed by the nature of the processing technique as in some cases even though the majority of the carbon atoms are tied up in the martensite there is still an adequate supply of interstitial nitrogen to cause the yield point to be present but, by virtue of the transformation, residual stresses are set up which cause the yield point to be masked.

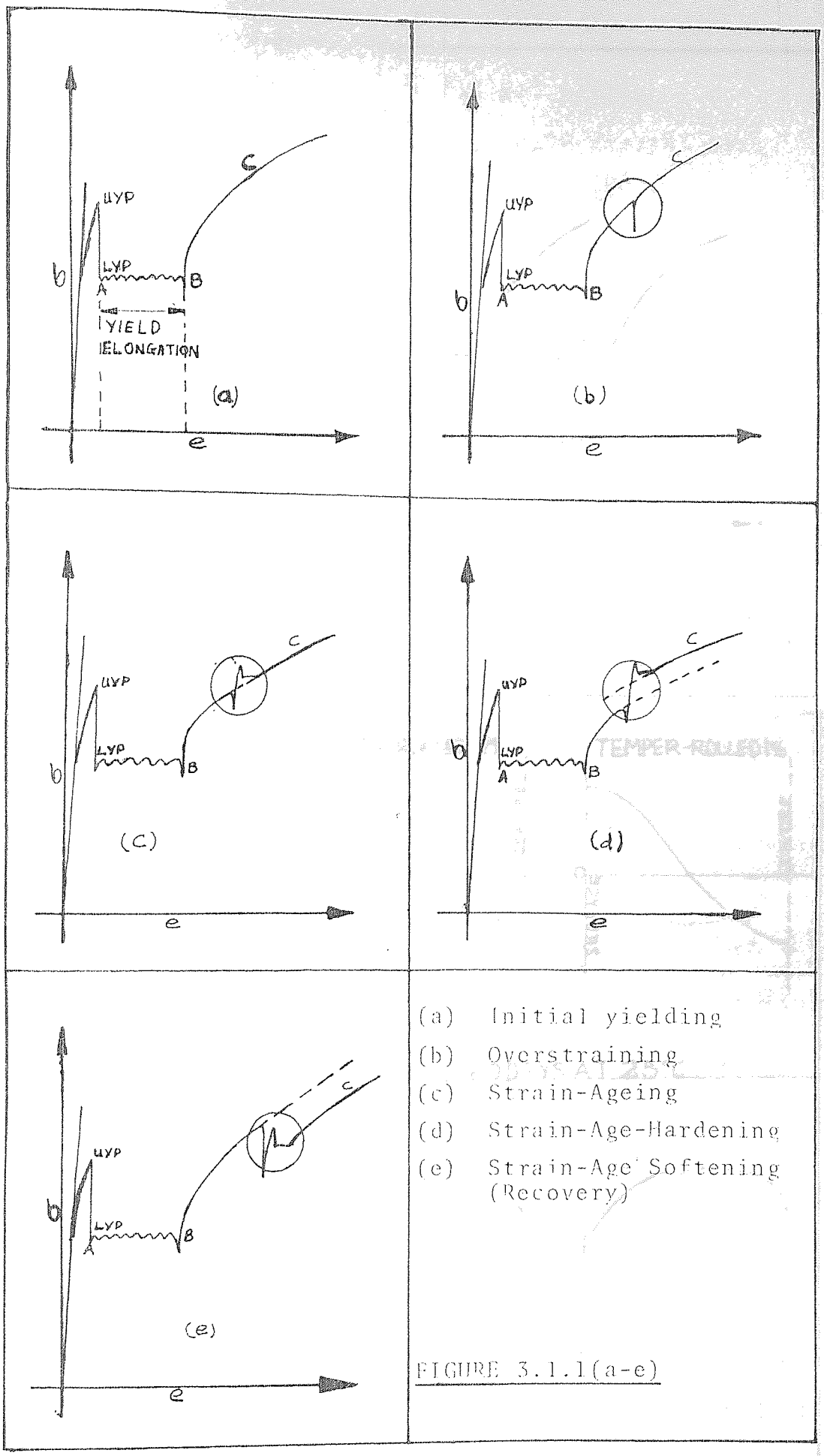

(a) Initial yielding
(b) Overstraining
(c) Strain-Ageing
(d) Strain-Age-Hardening
(e) Strain-Age Softening (Recovery)

FIGURE 3.1.1(a-e)

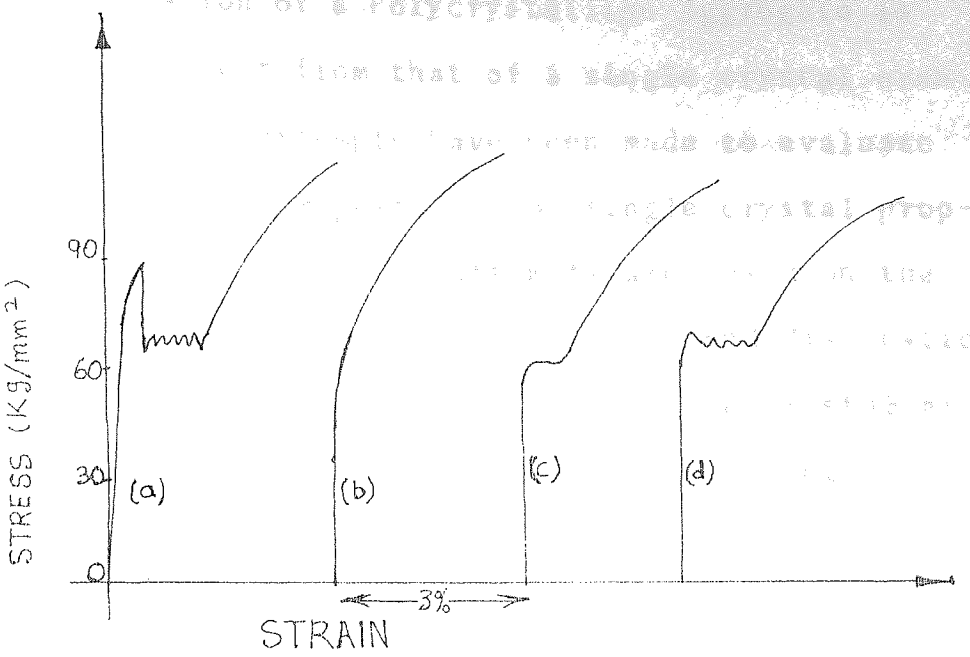

FIGURE 3.1.2a Illustrating σ/ε curves for mild steel in various conditions: a) annealing; b) temper rolled, 1.5% (suppression of yield point); c) Aged one week say; d) Aged one month say

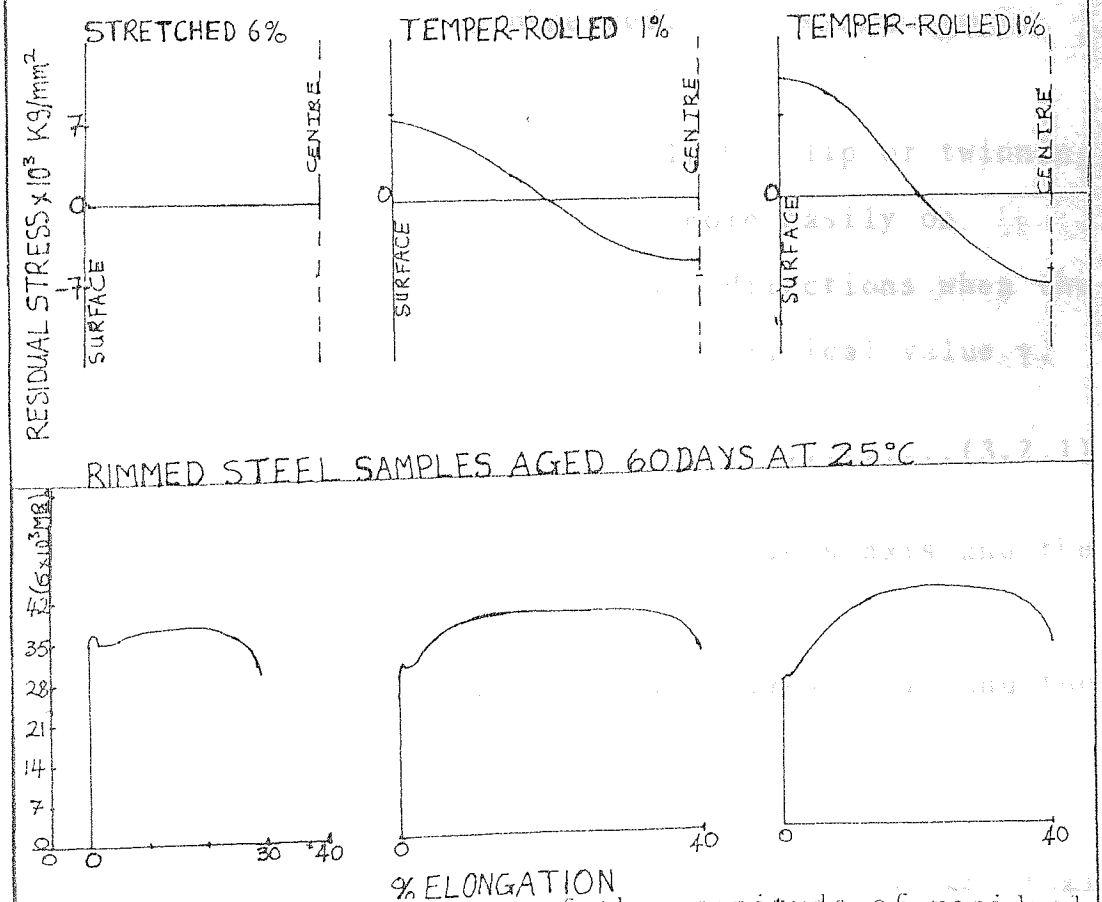

FIGURE 3.1.2b The effect of the magnitude of residual elastic stress in temper-rolled sheet on their plastic flow characteristics after ageing (ref. 3.1.31)

3.2 Plastic Properties of Polycrystalline and Two-Phase Aggregates

The deformation of a Polycrystalline Aggregate is vastly different from that of a single crystal even though several attempts have been made to evaluate polycrystalline properties from single crystal properties (3.2.1-5). These attempts are based on the assumption that the same slip systems and dislocation mechanisms which are operative in single crystals are also operative in polycrystals. This assumption is incorrect and much evidence has been produced against it (3.2.6 and 7).

In reference (3.2.6) they found that in a bicrystal of Al, slip occurred on the {110} planes whereas in single crystal Al only {111} is observed.

The mode of deformation is normally by slip or twinning. Slip is anisotropic and can occur more easily on certain crystallographic planes and directions when the shear stress acting on it assumes a critical value γ.

$$\gamma = M\sigma = \frac{\sigma}{\cos\phi\cos\lambda} \quad \ldots\ldots\ldots (3.2.1)$$

where ϕ = angle between applied stress axis and the slip plane normal

and λ = angle between applied stress axis and the slip direction.

The slip planes are usually the planes of closest atomic packing while the slip direction is that which has the

closest packing in that plane. The most common slip systems are {111}<110>, {110}<111> and {0001}<11$\bar{2}$0> in F.C.C., B.C.C. and H.C.P. metals and the other deformation systems that have been observed for most metals have been summarised by Dillamore et al (3.2.8)

From the above equation it can be concluded that the behaviour of a single crystal depends on its orientation relative to the tensile axis. In 1970 U.F. Kocks (3.2.9) further provided evidence showing that the stress/strain curve for single crystal aluminium depends on its oriented slip plane, shown in figure 3.2.1.

In polycrystals grain boundaries act as obstacles to dislocation motion which implies that the easy glide region observed in F.C.C., B.C.C. and H.C.P. metals cannot occur because the mean free path (L) of the dislocations cannot exceed the grain size (d) nor equal the specimen's dimensions. However, work hardening mechanisms acting in single crystals in stages II and III should also be operative in polycrystals since L<d. In single F.C.C. metal crystals at low temperature the work-hardening rate is controlled by the dislocation intersection mechanisms over stages I and II. It is only at high stress states in stage III that the stress assisted thermal activation of cross-slip has been reported to take place in single crystals (3.2.10). Therefore any attempt to evaluate the behaviour of poly-

crystalline aggregates from single crystal slip must be based on appropriate single crystal data which refer to the same mechanisms that are operative in the polycrystalline aggregate but in polycrystals individual grains can have a variety of randomly distributed orientations. However this might not necessarily be so; from solidification, there may be a preferred solidification direction and texture may also be present. The individual grains then would deform differently for a given stress were they not connected to each other.

During deformation of a polycrystalline aggregate some constraint must therefore be satisfied. These are:

1. Continuity of strains must be preserved across the grain boundary

2. Equilibrium of stresses must be preserved across the grain boundaries

3. Multiple slip systems must be operative.

It has also been shown by G.I. Taylor (3.2.1) that at least five independent slip systems must be operative in order to preserve continuity of strain. This is necessarily so because to preserve the grain/grain cohesion under an externally applied stress the polycrystal can only deform homogeneously if each of its grains can undergo large plastic shape change with constancy of volume. The lack of 5 independent slip

system then might give rise to lack of ductility in a polycrystalline material. This explains why polycrystalline H.C.P. metals exhibit little ductility at low temperature. In H.C.P. metals, at low temperature, slip occurs only on the basal plane which has two independent burgers vectors and this implies that they should show little plasticity in polycrystalline state although as a single crystal they may be very ductile. It has been confirmed experimentally that Zn, Cd, Mg, Be become ductile only at high temperatures when non-basal slip is activated.

For F.C.C. structures on the other hand there are 12 slip systems $\{111\}\langle 1\bar{1}0\rangle$ but only 2 out of the 3 slip directions are independent in each plane. The $\{111\}$ planes form a tetrahedron in the F.C.C. lattice, shown in figure 3.2.2. How the five independent slip systems arise can be visualised for F.C.C. metals, by following Thompson's tetrahedron notation and considering the condition for the Burgers vector in the slip planes α, β, γ and δ. These are:

$$(DB)_\alpha + (BC)_\alpha + (CD)_\alpha = 0$$ similarly for the other three

We can also have shears of the type

$$(CD)_\alpha + (DC)_\beta + (AB)_\gamma + (BA)_\delta = 0$$

which leads to rotation of the lattice about the line

joining the tetrahedron edges AB and CD about <100>. There are three such conditions; so that there are only 12-4-3 = 5 independent slip systems left to provide plasticity of a grain of the F.C.C. lattice. Thus F.C.C. polycrystals are very ductile and likewise so are B.C.C. metals.

According to Taylor's analysis the work done in tensile straining a polycrystalline aggregate an amount $d\varepsilon$ at a stress σ is equal to the work done by slip

$$\sigma d\varepsilon = \Sigma \tau_i d\gamma_i \qquad \ldots\ldots\ldots (3.2.2)$$

Where τ_i = critical shear stress slip and $d\gamma_i$ = the increment of shear strain due to slip on the i^{th} system.

Taylor further assumed that work-hardening was isotropic and took the average critical resolved shear stress to be the same over all slip systems as well as from grain to grain. Observations on single crystals have revealed that this is not so (3.2.11 and 12) but it can be taken to be an approximation over the range of various slip systems, and that the strains are not altogether uniform over a grain.

. . we can write that

$$\frac{\sigma}{\tau_i} = (\Sigma |d\gamma_i|)/d\varepsilon = m \qquad \ldots\ldots\ldots (3.2.3)$$

The five operative slip systems will contribute to $\Sigma|d\gamma_i|$ and they were taken to be those for which $\Sigma|d\gamma_i|$ was a minimum in Taylor's theory. He was able to show that the average value of $m \equiv \bar{m}$ for random orientation of F.C.C. metals was 3.06.

$$\therefore \quad \sigma = 3.06\ \tau_c$$

The average τ_c was determined from single crystal σ/ε curve where it was assumed:

$$\langle \tau_c \rangle \equiv \tau_i \{\int \Sigma |d\gamma_i|\} = \tau_c \{\bar{m}' d\varepsilon\},$$ but he neglected the influence of work-hardening.

He also predicted the occurrence of preferred orientation in tensile strained randomly orientated F.C.C. polycrystalline metals but his prediction in this wise has been shown to be inaccurate (3.2.13).

Later Bishop and Hill (3.2.2 and 3) and Bishop (3.2.14) presented a theory, using a principle of maximum plastic work to try and predict the σ-ε curve for polycrystal from that of a single crystal. They obtained the same result as Taylor but were unable to determine the actual preferred orientation that can result upon deformation, but Bishop showed that this might be achieved with slight modification and extrapolation of the theory. They further showed that the plastic potential which they calculated lies between the Tresca and Von Mises yield criteria under combined stresses as Taylor had also shown.

However the appropriate single crystal σ-ε curve that should be used to predict the polycrystalline σ-ε curve are those that are obtained from single crystals that are so oriented that slip can take place simultaneously on many slip systems.

There are several such orientations in F.C.C. metals, two of which are

1. Orientation with tensile axis aligned along [100] gives slip simultaneously on 8 systems.

2. Along [111] slip direction - has 6 systems.

It has been reported in (3.2.15) that the [100] orientation is an unstable one because small changes from this orientation lead to only two slip systems being operative. Therefore the most appropriate single crystal data for predicting polycrystalline behaviour are those from orientations where the tensile axis is in the [111] direction or perhaps according to Figure 3.2.1 a suitable combination of [111] and [100].

All the theories mentioned so far neglected the effect of work-hardening and grain size. An extensive review of the prediction of polycrystalline work-hardening from single crystals has been given by Thompson (3.2.15). In his conclusion it was noted that Taylor's theory still

gives a good approximation to polycrystalline behaviour but has discrepancies for materials of intermediate to low ease of cross-slip and small grain sizes.

Many observations have been shown that zones of complex slip are generated at grain boundaries. A dislocation in grain A moving towards the grain boundary does not usually find a plane matching its Burgers vector in adjacent grain B. Neither can it be absorbed by the high angle grain boundaries without seriously modifying the structure of the boundary. Therefore this dislocation and those following it on the same plane pile up at the grain boundary. This causes a stress concentration at the boundary, which eventually becomes so large that, at a critical shear stress τ_o dislocation sources in the neighbouring grain are activated. If λ is the distance of the source from the pile-up, then the excess shear stress set up above that in grain A will produce a stress concentration at this distance λ ahead of the band in the next grain given by (3.2.16).

$$(\tau_o - \tau_A)\left(\frac{d}{\lambda}\right)^{\frac{1}{2}} = \tau^1 M_{AB}$$

$$\text{or} \quad \tau_o = \tau_A + M_{AB}\,\tau^1 \left(\frac{\lambda}{d}\right)^{\frac{1}{2}} \qquad \ldots\ldots\ldots\ldots (3.2.4)$$

$$\equiv \tau_A + K_y d^{-\frac{1}{2}}$$

This is the wellknown Hall-Petch equation (3.1.1)

where τ_A = critical shear stress in grain A

τ^1 = minimum stress for activation of slip in grain B

M_{AB} transforms the shear stress from the slip system in grain A to that in grain B.

Another approach to this problem is that due to E. Kröner (3.2.5) which has been summarised by J.E. Dorn et al (3.2.7). Kröner noted that if a polycrystalline tensile specimen is loaded grains with a small M ($M = {}^1/\cos\phi \cos\lambda \equiv$ SCHMID FACTOR) begin to deform and exert stresses on other less favourably oriented grains, which then influence slip in the favourably oriented grains and a general stress state is set up which permits five slip systems to become activated. He therefore supposed that all grains of one orientation can be represented by an average spherical grain and its neighbours by an isotropic continuum matrix. Next the spherical grain is removed leaving a hole behind in the matrix and the specimen is subjected to stress in tension such that the surrounding matrix is prevented from collapsing into the hole left behind. To do this surface stresses are set up in such a way that, under the applied stress, the surrounding is unaware of the presence of the hole so that the hole and the matrix then deform plastically with the result that average deformation $\langle\varepsilon\rangle$ is

produced in the hole, while the spherical grain by itself would have suffered a different deformation ε. To reinstate the grain it must be first deformed elastically to the same shape. The stress needed to do this is given by $G(\varepsilon-\langle\varepsilon\rangle)$ approximately after (3.2.17). It is this stress which will activate the five necessary slip systems in the grain. This is similar to the macroscopic strain proposed by Taylor.

Kröners theory suffers from the same basic neglect as those before him. It does not take account of work-hardening, Bauschinger effect and single crystal orientation, whilst it also fails to note that during stage I work-hardening of a single crystal test, the dislocations can make an exi t from the crystal, whereas in a grain of a polycrystalline aggregate such dislocations can only pile up at the boundary though they may be relaxed by cross-slip and slip on secondary systems, thereby introducing barriers and increased density of the forest dislocations. It also neglects the grain size effect. Operation of several slip systems simultaneously leads to a strong interaction between dislocations, and hence work-hardening. From the above when trying to evaluate the σ-ε curve for a polycrystal the highly symmetric orientations like <111> and <100> of single crystals should be used. These directions should be able to express the σ-ε curve of polycrystals in all directions. In the x-direction the work done is given by:

$$\sigma_x d\varepsilon_x = dA$$

$$\sigma_x = \frac{dA}{d\varepsilon_x}$$

From Taylors theory $dA = \tau d\gamma$

$$\therefore \quad \sigma_x = \tau\frac{d\gamma}{d\varepsilon} \equiv M\tau$$

$$\therefore \quad M = \frac{\sigma x}{\tau} \rightarrow \text{Taylors factor} = \frac{d\gamma}{d\varepsilon_x}$$

Work-hardening for polycrystal in this direction is

$$\frac{d\sigma_x}{d\varepsilon_x} = \frac{d\gamma}{d\varepsilon_x} \cdot \frac{d}{d\gamma}(\sigma_x)$$

$$= M^2 \frac{d\tau}{d\gamma} = M^2\,\theta \qquad \text{.....(3.2.5)}$$

Two-Phase Aggregate

Any attempt to predict the behaviour of these alloys from the single crystal data of the constituent phases might prove formidable in the light of what has been said above.

There are generally two types that can be encountered:

a. both phases have comparable grain size,

b. the second phase is dispersed in the matrix. This is sometimes referred to as dispersion strengthened alloys.

The two types are depicted in Figure (3.2.3). The strengthening that is produced by the presence of the second phase is usually additive to solid-solution strengthening produced in the matrix and under equilibrium conditions it can ensure that there is a maximum solid solution. The presence of the second phase can cause localised internal stresses in the continuous matrix (3.2.18) which will modify the plastic deformation of the matrix. The factors which have been found to affect the strengthening from the introduction of the second phase are:

1. Strength of second phase
2. Ductility of second phase
3. Size, shape and number of second phase
4. The distribution and orientation of the second phase.
5. The work-hardening behaviour of both matrix and second phase.

Crystallographic fit between the phases, interfacial energy and interfacial bonding also contribute to the plastic properties of the composite as failure might occur by decohesion of the phases during working. Each phase then contributes to the overall properties of the aggregate. If the properties of each phase are independent of each other then the overall properties will be a weighted average of the two phases. If the presence of one influences the property of the other phase then it might be necessary to consider a convolution type approach to estimate the overall properties.

For the structure-sensitive properties a weighted approach cannot readily be used even though it might be dependent on the volume fraction of each phase.

Two assumptions are normally used to evaluate the properties of two-phase alloys, of coarse microstructure, from the properties of the individual ductile phases.

1. That the strain in each phase is equal. This gives the result that the average stresses will increase linearly with volume fraction of the stronger phase:

$$\langle\sigma\rangle = f_1\sigma_1 + f_2\sigma_2 \qquad \text{.....(3.2.6)}$$

and $f_1 + f_2 = 1$

2. That the two-phases are subjected to equal stress. This gives the overall average strain of the aggregate as:

$$\langle\varepsilon\rangle = f_1\varepsilon_1 + f_2\varepsilon_2 \qquad \text{.....(3.2.7)}$$

Usually the observed properties lie somewhere in between the two extremes. These assumptions also do not take into account the relative orientations of the phases to the tensile axis particularly for those of type 1. When this is done a misorientation term will have to be included in the above equations.

For a low alloy steel consisting of ferrite and pearlite Lizunov et al (3.2.19) have obtained the following equation for the UTS of the steel.

$$\sigma_b^{l} = \bar{\sigma}_c V_c \theta + \sigma_y^{l}(1-V_c-V_{sf}) + \sigma_y^{ll}(1-V_p) \quad ..(3.2.8)$$

where $\bar{\sigma}_c$ = average stress in carbide platelets

V_c = volume percent of carbide

θ = coefficient accounting for the mis-orientation angle of carbide phase in relation to the axis of deformation

V_{sf} = volume percent of structurally free ferrite

V_p = volume percent of Pearlite

σ_y^{l} = yield strength of Ferrite in Pearlite

σ_y^{ll} = yield strength of the structurally free ferrite

As is noted above, deformation will depend on the plasticity of each phase and on the volume fraction of the two phases. However not all second phase particles do produce strengthening. For there to be strengthening there must be a strong particle/matrix bond. During deformation slip will occur first in the weaker phase which might break the bond (3.2.20). M. Gensamer et al (3.2.21) have correlated the micro-structure of second phase and yield stress and they found that for Fe_3C in ferrite the flow stress for 0.2% strain was inversely proportional to the logarithm of

the mean interparticle spacing. This relationship has also been found to hold for fine Fe_3C in tempered martensite (3.2.22) and coarse particles in overaged Al-Cu alloys.

C.J. Lim et al (3.2.23) have also found such dependence for spheroidized steels, while Gurland et al (3.2.24) have also found it to be true for cobalt sintered carbides of tungsten (WC). The second phase particles block slip, so that plastic deformation is not uniform in the matrix, thus strain in the matrix will be localised and it will increase over the average strain of the specimen. We shall consider more fully the work-hardening behaviour of these two phase materials in the next section where some of the ideas of Ashby and Brown and Stobb will be discussed. However a good review of the properties and plasticity of the second type depicted in figure (3.2.3b) has been given by Ansell (3.2.25).

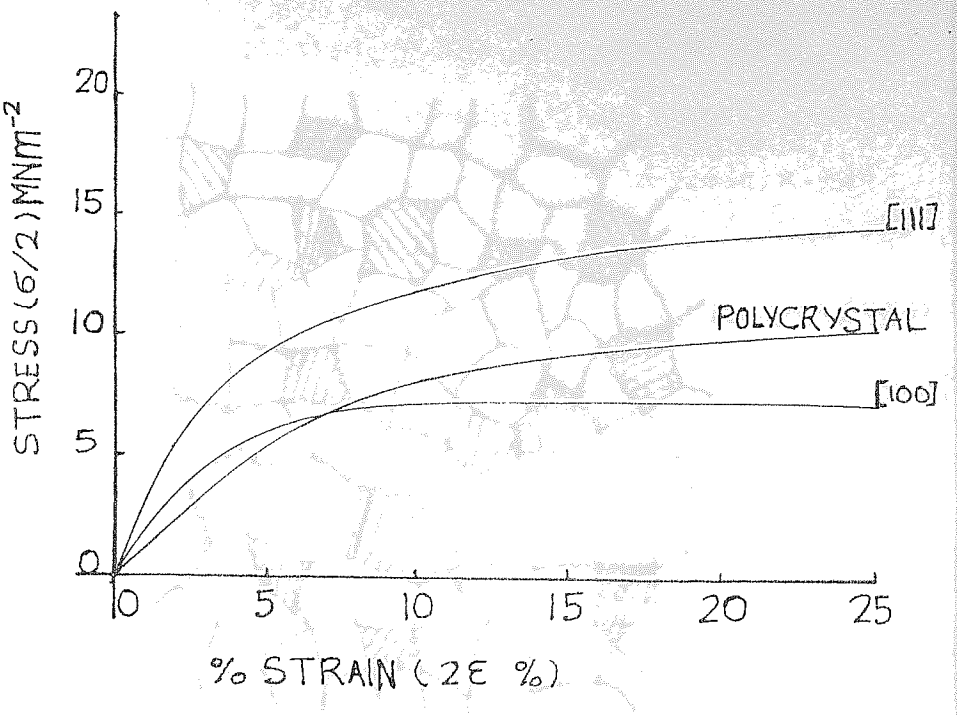

FIGURE 3.2.1 σ - ε curve for Al-single crystal of different orientation and a polycrystal of grain size 200 μm (from ref. 3.2.9)

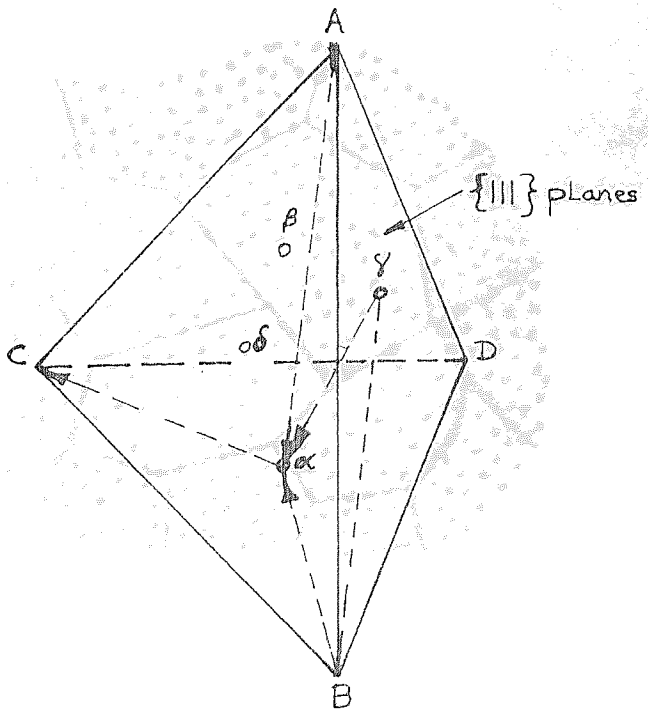

FIGURE 3.2.2 Thompson's Tetrahedron

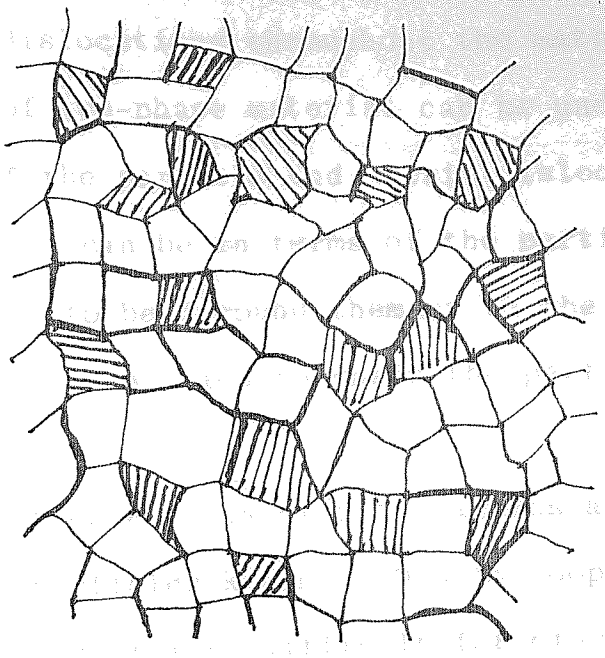

(a) Both phases have comparable sizes

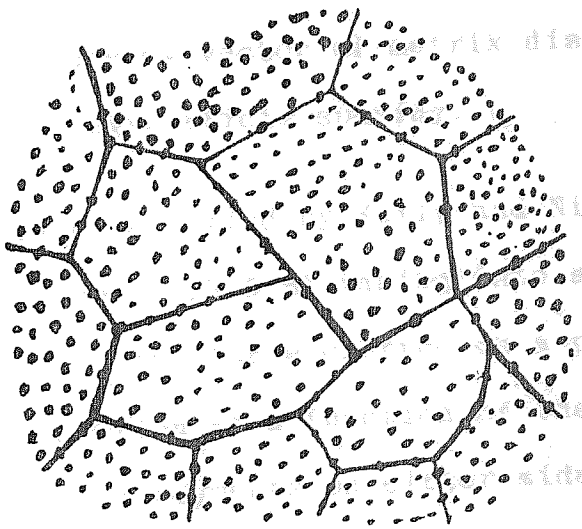

(b) Second phase dispersed in matrix

FIGURE 3.2.3

3.3 Work hardening and Fracture of Two-Phase Metals

Strengthening of crystalline metal is commonly achieved by the control of the nucleation and motion of dislocations throughout the matrix. The hardening of two-phase material can be understood in terms of the particle and matrix dislocation interaction. This can be in terms of the particles forcing dislocations to bend round them or to the work necessary for the dislocation to shear the particle.

In the first case loops of dislocations are left around the particles known as Orowan loops (3.3.1), thereby making it more difficult for other dislocations to pass through. The model proposed by Orowan (3.3.1) gave for the yield stress

$$\tau = Gb/\lambda$$

where G = matrix shear modulus

b = Burgers vector of matrix dislocation

λ = interparticle spacing.

This was later modified by Kelly and Nicholson (3.3.2) and Ashby (3.3.3) taking into account the particle diameter, the force exerted on a particle by a bowing dislocation as a function of the angle between the dislocation segments on either side of the particle and the random distribution of particles. Their expression for the yield stress can be written as

$$\sigma y = \sigma o + \frac{MGb}{2\pi(1-\nu)^{\frac{1}{2}}} N_S^{\frac{1}{2}} \text{Ln}\left(\frac{2r_s}{b}\right) \qquad (3.3.2)$$

$$N_S = \frac{3f}{2\pi r_s^2}$$

where r_s = Root mean square radius of particles intercepting the slip plane.

f = volume fraction of particle.

M = Taylor factor.

N_S = Number of particles per unit area intersecting a plane.

ν = Poissons ratio.

G and b have the same meaning as before.

Following Orowan's idea, Fisher, Hart and Pry (3.3.4) (often referred to as FHP theory) proposed a model to explain the work hardening of these types of metals based on the increase in the bypass stress necessary to pull a dislocation through an array of obstacles as a result of circular loops which previous dislocations have left by the obstacles. They assumed that these loops remain in the primary slip plane and exert a shear stress in the matrix which opposes further dislocation motion. They obtained for the increase in flow shear stress due to the presence of the particles.

$$\Delta\tau = \tau(\text{with particles}) - \tau(\text{without particles})$$

$$\Delta\tau = \frac{2f^{3/2} N G_m b c}{d} \qquad (3.3.3)$$

c = a constant of the order of 3

d = particle diameter on the glide plane

N = Number of Orowan loops around a particle

Gm = Matrix shear Modulus.

They also proposed that $\Delta\tau$ would reach a maximum at some strain because the stress built up around the particles that would eventually fracture them such that

$$\Delta\tau_{max} = 3f^{3/2}\tau_c \qquad (3.3.4)$$

where τ_c is a limiting stress which corresponds to the ideal strength of either the matrix, the particle or the particle/matrix interfacial strength. The above equation for $\Delta\tau$ predicted an increase in work hardening with decreasing particle size for a constant volume fraction and with increasing volume fraction for a constant particle size. Most of their predictions have been verified experimentally by several workers (3.3.5) - (3.3.7). D.V. Wilson (3.3.7) has found that the residual stresses in a plastically deformed two-phase alloy were compressive in the matrix and tensile in the particle as expected from the dislocation loop arrangement proposed in the FHP model. However this model did not take into account the fact that as the number of dislocations increase on the primary slip plane, work hardening of the primary slip plane occurs and the introduction of further dislocations becomes difficult. Further deformation can thence only be achieved if other secondary slip systems can be activated ie if cross-slip can

occur. Neither could their model explain the type of complex dislocation structures that are observed in these alloys by Transmission electron microscopy (3.3.8) - (3.3.11). The observed value of the limiting stress τ_c for Al-Cu and Cu-Cr alloys (3.3.5) are approximately 0.07E and 0.03E respectively (E = elastic modulus) which for the Cu-Cr alloy implies that about 50-100 Orowan loops surround each particle when maximum hardening occurs. This high number of primary loops are never observed in practice. Also the elastic modulus of the matrix is usually lower than that of the particles, thus the theoretical strength of the matrix would in general be exceeded prior to that of the particle thereby resulting in secondary dislocations being generated rather than the particle shearing or the interface splitting. When the particle modulus is lower than that of the matrix, hardening occurs resulting from the fact that the line energy of a dislocation depends on the shear modulus of the media through which it lies. Russell and Brown (3.3.11), Kocks et al (3.3.13) and Melander (3.3.14) have considered the contribution from this effect to the strengthening of two-phase alloys. Russell and Brown obtained the following expression for the yield strength taking into account the critical angle at which a dislocation can cut an obstacle ϕ.

$$\tau = \frac{0.8l\ Gb}{\lambda}\left(1-\frac{E_1}{E_2{}^2}\right)^{\frac{1}{2}} \quad \text{for } \sin^{-1}\frac{E_1}{E_2} \leq 50^{\circ} \qquad (3.3.40)$$

$$\tau = \frac{Gb}{\lambda}\left(1-\frac{E_1{}^2}{E_2{}^2}\right)^{3/4} \quad \text{for } \sin^{-1}\frac{E_1}{E_2} \geq 50^{\circ} \qquad (3.3.46)$$

The above equation gives a strength which depends inversely on the particle spacing λ and decreases as the particle radius increases for a constant volume of precipitate.

E_1 = Line energy per unit length of dislocation in precipitate.

E_2 = Line energy per unit length of dislocation in matrix.

Similar equations have been obtained by references (3.3.13) and (3.3.14) above. When a dislocation cuts through an ordered coherent precipitate or particle, an antiphase boundary is formed with surface energy γ_{APB}. The dislocations tend to move in pairs; the second dislocation removing the disorder created by the first. The equation for the increase in shear stress has been given by Horbogen (3.3.15) as

$$\Delta\tau_S = \frac{0.28\ \gamma_{APB}{}^{3/2}\ d.d^{\frac{1}{2}}}{\sqrt{2}\ G^{\frac{1}{2}}\ b^2\ D}$$

$$\frac{d}{D} = f^{1/3}$$

$$\therefore \quad \Delta\tau_S \simeq \frac{0.2\ \gamma_{APB}^{3/2}\ f^{1/3}}{b^2}\left(\frac{d}{G}\right)^{\frac{1}{2}} \qquad (3.3.5)$$

D = effective particle spacing.

Several attempts have been made to modify the FHP model of work hardening in the light of the observed facts (3.3.16 - 19). Two general approaches have been put forward. One based on continuum mechanics (3.3.16a and b), followed the work of Eshelby on the theory of elastic inclusions (3.3.20), and the experimental observations of deformation of two-phase metals. The other approach is based on the physics of dislocation interaction involving the self-hardening of a slip line by rows of loops generated by glide dislocations the second phase particles (3.3.17a and b) and (3.3.19).

Hart's (3.3.18) attempt assumed that work hardening of the matrix proceeds in the same manner regardless of whether particles are present or not and that the presence of the particle merely traps the loops of dislocations which raised the critical bowing stress and this increase in stress is super-imposed on the matrix flow stress. He however corrected for non-uniform particle size and he obtained the following expression

$$\tau_h = \tau_y \left[1+6C^{\frac{1}{2}} f_{eff}^{3/4} \left(\frac{G}{\tau_y}\right)^{\frac{1}{2}} \varepsilon^{*\frac{1}{2}} + 18cf^{3/2}\left(\frac{G}{\tau_y}\right)\varepsilon^*\right] \quad (3.3.6)$$

ε^* = Tensile strain discontinuity about a particle $\simeq \varepsilon$ for $\varepsilon < \varepsilon_c$.

ε_c = strain at maximum hardening stress

f_{eff} = effective volume fraction of particle

$C = 0.509\{1+\frac{\nu}{2(1-\nu)}\}$

This equation predicts a parabolic relationship. The stress/strain curve of single crystals is approximately parabolic after an initial short region of low work hardening. Harts treatment did not take account of recovery effects and hence $\varepsilon^* = \varepsilon$ is an approximation. Jones (3.3.21) has shown that this theory leads to very large error between calculated and observed values of stress/strain data and the value of f_{eff} has to be adjusted to fit the data. Further this theory did not explain the temperature dependence of work hardening and recovery effects in these materials. This will, however, not be laboured here but we note that there is some controversy about the micromechanisms by which this takes place. A detailed consideration of the different views has been presented by Hirsch and Humphreys (3.3.22).

The theories propounded in references (3.3.16, 17 & 19) all agree that with increasing deformation Orowan loops, primary prismatic loops and secondary prismatic loops of various types are formed in this order with the Orowan loops being formed below a certain critical plastic strain ε_{cp}. When the number of Orowan loops exceeds a certain critical value with further deformation the

innermost Orowan loops collapse to form prismatic loops by a double cross-slip process (two prismatic loops are formed per each Orowan loop converted, an interstitial loop and a vacancy loop are formed on opposite sides of the particle). The dislocation then glides past the particle, restoring an Orowan loop, and then interacting with the second (vacancy) prismatic loop, to form a double jog, which is then swept away from the particle. The secondary prismatic loop generation is supposed to be accompanied by cavitation at the particle/matrix interface. The smaller the particle size the larger the strains at which the relaxation mechanisms of secondary prismatic punching and captivation begin to operate.

The Orowan loops left around a particle exert a force on it called the image stress leaving a mean internal stress in the matrix (3.3.16) which is given by (3.3.23):

$$\langle \tau \rangle_m = 2\mu f \, \varepsilon^*_p \, \gamma \left\{ \frac{\mu^*}{\mu^* - \gamma(\mu^* - \mu)} \right\} \qquad (3.3.7)$$

μ^* = shear modulus of nondeformable particle

μ = shear modulus of matrix

γ = a shape factor = $\frac{7-5\nu}{15(1-\nu)}$ for a sphere (3.3.24)

and (3.3.25)

f = volume fraction of particle

ε^*_p = measures the incompatability between the matrix and the particle and it is related to the number of Orowan loops around the particle by

$$\varepsilon_p^* = \frac{nb}{4r_o}$$

where r_o = radius of particle and n = number of Orowan loops.

The elastic shear stress near the particle is given approximately by $\gamma_{es}=2\mu\varepsilon_p^*$. Tanaka and Mori (3.3.24) have shown that the image stress is equal to the derivative with respect to ε_p^* of the elastic strain energy stored in the system. In the absence of plastic relaxation for small plastic strain $\varepsilon_p^* = \varepsilon_p$; at large strain relaxation will occur and $\varepsilon_p^* < \varepsilon_p$. In addition to this image stress in the matrix the particles produce a local elastic stress field inversely proportional to the cube of the distance from each particle and its average value throughout the matrix is zero thus producing no hardening on a rigid dislocation but it can act on a flexible one to reduce the effective interparticle spacing i.e. the Orowan loops around the particle cause successive dislocations to stand off them resulting in an increase in work hardening called Source-Shortening. This source-shortening stress has been estimated to be given by (3.3.16):

$$\sigma_{sst} = \frac{\mu bf}{r_o}\left\{\left(\frac{4r_o\,\varepsilon_p\,\mu^*}{b\left[\mu^* - (\mu^*-\mu)\right]}\right)^{\frac{1}{2}} - 1\right\} \qquad (3.3.8)$$

This equation is valid after a critical strain ε_p when the bracketed terms equal zero.

$$c\varepsilon\rho = \frac{2\mu\ f\ \varepsilon_p^{*2}}{n} = \frac{2\mu\gamma f n b^2}{4r_o} \qquad (3.3.9)$$

Above about ten per cent deformation the equation is found to be no longer valid due to plastic relaxation. On the basis of transmission electron microscopic observation it has been suggested that ε_p varies parabolically with plastic strain ε_p.

Ashby's (3.3.19) and Hirsch and Humphrey's (3.3.17) theories do not differ too seriously with each other except in the nature and distribution of the dislocations they assumed. They also derived a parabolic relationship as mentioned earlier which can be described by the equation of the form

$$\sigma = \sigma_y + M^{3/2}CG(bf\varepsilon/\bar{D})^{\frac{1}{2}} \qquad (3.3.10)$$

M = Taylor factor

C = a constant of the order 0.2 to 0.4

All other symbols have the usual meaning.

Ashby (3.3.26) further showed that this type of relationship occurs if it is assumed that work hardening is due to the interaction of geometrically necessary dislocations nucleated at the particle/matrix interface due to the relaxed strain (secondary dislocations) along with the primary ones moving on the primary slip plane. These dislocations are introduced

into the matrix to relieve the stress due to slip on the primary plane caused by the incompatible deformation between the two phases. The strain gradient occuring during deformation will depend on the type and shape of the hard second phase particle. He derived equations for the density ρ^G of these geometrically necessary dislocations for the different particle shapes.

For an equiaxed particle

$$\rho^G_{equi} = (\frac{2f}{b})\frac{4}{b} \qquad (3.3.11)$$

where D = diameter of particle

γ = shear strain imposed on the matrix

f = volume fraction of particles

For a plate like particle

$$\rho^G_{pL} = \frac{4}{bL} \qquad (3.3.12)$$

where L = distance between plates.

For a single phase polycrystalline metal the dislocations emanate from the grain boundaries and

$$\rho^G_{gb} = \frac{\bar{\varepsilon}}{4bD} \qquad (3.3.13)$$

$\bar{\varepsilon}$ = plastic strain

D = mean grain diameter

b = Burgess vector as before.

The stress/strain curve is then described by

$$\tau = \tau_o + CGb\sqrt{\rho T} \qquad (3.3.14)$$

where $\rho^T = \rho^G + \rho^S$

ρ^S = density of statistically stored dislocations.

ρ^G will dominate when geometric slip distance λ^G is sufficiently small up to very high shear strain i.e. when $\lambda^G < 10\mu m$. λ^G is a characteristic of the microstructure which does not change with strain.

$$\left.\begin{array}{ll} \text{For equiaxed} & \lambda^G = (2f/D)^{-1} \\ \text{For plate} & \lambda^G = (1/L)^{-1} \\ \text{For grain boundary} & \lambda^G \simeq \left(\frac{M}{16D}\right)^{-1} \end{array}\right\} \qquad (3.3.15)$$

So that we can write that

$$\rho^G = \left(\frac{1}{\lambda^G}\right)\frac{4\gamma}{b} \qquad (3.3.16)$$

The corresponding λ^S for the statistically stored dislocations does vary with strain. Ashby's theory predicts that ρ^G increases linearly with strain and hence the flow stress increases parabolically.

However, it is generally observed that alloys to which this theory is applicable exhibit double n value (3.3.27 - 29). Reasonable correlation is observed for strains up to 3.5%, but above this value the work hardening no longer increases parabolically for some alloys. This discrepancy has been ascribed to the formation of

dislocation cell structures (3.3.28) approximately equal to the mean interparticle spacing.

When the microstructure becomes very coarse, of the order 1 to 100 μm, the above theories cannot readily be applied. The less deformable inclusions entail a concentration of plastic strain in the softer matrix which can be cared for by the idea of geometrically necessary dislocations if the soft phase is continuous.

In the section on plastic properties of polycrystalline aggregate it was stated that equal strain or equal stress models are often used to evaluate the overall property of this class of metals. In general it will be necessary to employ these ideas as well as that of Ashby's geometric dislocations to get a clearer view of what is going on. However no concrete understanding of their behaviour has yet emerged. A number of researchers, notably in Sweden, have addressed themselves to these problems (3.3.30-32). Several factors have been identified to have an effect on the mechanical properties of such coarse two-phase micro-structure. They are

1. The volume fractions f_1 and f_2 of the constituents
2. The surface per unit volume of grain boundaries (S_{11}, S_{22}) and of the phase boundaries (S_{12})
3. The continuity of the constituents

$$C_{11} = \frac{2\,S_{11}}{(2S_{11}+S_{12})} \qquad (3.3.33)$$

4. The hardness ratio of the constituents

$$k = \frac{(HV)_1}{(HV)_2} \cong \frac{\sigma_{y1}}{\sigma_{y2}}$$

In a structure consisting of isolated inclusions of phase 2 in a continuous matrix of phase 1, the specific surfaces are related to the mean free path between grain boundaries (λ_{11}) and to the mean size of phase 2 (d_2) by

$$S_{11} = 2f_1/\lambda_{11}$$

$$S_{12} = 4f_2/d_2 \qquad (3.3.30)$$

It has been suggested in reference (3.3.30) that the density of the geometrically necessary dislocations could be written as

$$\rho^G = \frac{1}{b}\left[C_1 . S_{11} . E_1 + C_2 \frac{f_2}{f_1} S_{12} . \Delta\bar{\varepsilon}\right] \qquad (3.3.17)$$

where C_1 and C_2 are constants.

ε_1 = plastic strain in phase 1.

$\Delta\varepsilon = \varepsilon_1 - \varepsilon_2$

When the second phase does not deform plastically $\Delta\varepsilon \simeq \varepsilon_1$.

It has been shown (3.3.30 & 32) that the difference in strain ($\Delta\varepsilon$) between the two constituents increases with their relative hardness ratio k and decreases with increasing overall strain. For a ferrite-pearlite

microstructure both the ferrite grain size and the second phase particle morphology have been shown to have an effect on the property. The Hall-Petch relation is obeyed with a lower k_y value (k_y as in $\sigma = \sigma_o + k_y d^{-\frac{1}{2}}$) than for a pure polycrystalline ferrite at large strain and $\Delta\varepsilon$ goes to zero. The work hardening is found to be independent of the cementite morphology (pearlite or spheroidite) but it increases with the volume fraction of pearlite. Similar studies on a Cu-Al eutectoid alloy gave the opposite effect. Small grain size gave higher flow stress as well as higher work hardening and a marked change in the Hall-Petch slope. This was explained on the basis of the coherent precipitate giving better ability to transfer load from the matrix to the hard second phase.

Ductile Fracture

The ductile fracture of two-phase alloys has been shown to be due to the voids nucleated at the second phase particles which subsequently grow until local instability sets in by coalescence of the voids and failure occurs. Fracture processes then involves strain localization with accompanying local strain gradients. The resulting strain gradient is accelerated by void growth but is retarded if the matrix material has a work hardening capability or if the flow stress can increase with increasing strain rate. The strain will gradually concentrate into a small region in the neck until almost only that region is deforming. Finally the volume fraction of

voids becomes so large in a thin slice in the neck that a crack is formed leading to fracture.

From what had been said on the role of the second-phase particle on work hardening it is then apparent that two mechanisms by which voids can be generated at a second phase particle are:

1. The particle can fracture under the induced stress system (3.3.35).
2. The normal stress on the interface with the particles may be sufficient to cause a breakdown of the particle/matrix interfacial bond strength (3.3.36 & 37).

A number of points have been observed on factors governing the initation voids. They are:

1. At ambient temperature alloys of copper, internally oxidised to contain strongly bonded equiaxed non-deforming particles of SiO_2, AL_2O_3 and BeO, produce voids after a uniform elongation of about 0.1 to 0.2 (3.3.38).

2. For a given alloy system there is a critical strain ε_c to cause void nucleation and for a given particle diameter, this void nucleation strain does not depend markedly

on the volume fraction of particles nor on interparticle spacing.

3. Within a given specimen larger particles tend to form voids at lower strains than the smaller ones. However, if a particle size effect does exist it is smaller than the effect of the strain limit of 0.1 - 0.2 (3.3.38). Rogers (3.3.40 & 41) has shown that some alloy systems do not show marked size dependence and he further observed that ductile fracture of poly-cryptalline metals tested in tension occurs by formation of voids at approximately the necking strain and that these voids would grow with increasing strain with crack growth taking place by the concentration of strain at the tip of the static crack. He also found that cracks at large particles need not coalesce but they may be linked by sheets of very small voids which form in shear bands between the large inclusions. This has been observed also by others (3.3.42, 43 and 44). In reference (3.3.44) they observed that void growth proceeds more rapidly from larger inclusions and the presence of hydrostatic pressure does

not affect the void nucleation process whereas it greatly enhanced the rate of void growth.

4. Lowering the temperature tends to reduce the void nucleation strain (3.3.46).

5. Solid solution additions have a drastic effect on the void nucleation strain, they can even reduce it to zero. This is because adhesion between particle and matrix depends sensitively on impurity additions and the void nucleation strain depends on the inter-facial strength. Also impurity elements can lower the stacking fault energy and produce a tendency towards planar slip and high stress concentrations (3.3.45).

6. The critical strain at which voids are nucleated depends strongly upon the shape and orientation of the particles (3.3.46 & 47).

Several theories have been put forward to explain ductile fracture (3.3.36, 17, 20, 48-53). Most of them paid more attention to cavity formation than to void growth. Many of them have been reviewed by Goods and Brown (3.3.54). However, the theory of

Brown and Stobbs (3.3.17) and Tanaka et al can be used more readily to explain the above observations with that of Ashby (3.3.20) being less successful.

For void growth McClintocks theory (3.3.50) is more widely used. However he did not consider the effect of strain rate sensitivity on ductile fracture. He assumed that voids pre-exist before the start of deformation and that they subsequently grow during deformation until they coalesce. For a material obeying the Ludwig-Hollomon equation $\sigma = KE^n$ and obeying a von Mises type of yield criterion, McClintock derived an expression for the rate of void growth with strain given by

$$\frac{dn}{d\varepsilon} = \frac{\text{Sinh}\left[(1-n)(\sigma_a+\sigma_b)\sqrt{3}/2\sigma\right]}{(1-n)\ \text{Ln}\ F^f} \qquad (3.3.18)$$

where $dn = \text{Ln}\ F/\text{Ln}F^f$

$$\sigma = \left[(\sigma_1-\sigma_2)^2+(\sigma_2-\sigma_3)^2+(\sigma_3-\sigma_1)^2\right]^{\frac{1}{2}}$$

σ_a and σ_b are the transverse stress components.
For voids of initial radius b_o and separation $2L_o$

F^f = critical growth factor = L_o/b_o

$F = bL_o/b_oL$

The fracture strain is then given by

$$\varepsilon_f = \frac{(1-n)\ \text{Ln}\ (L_o/b_o)}{\text{Sinh}\left[(1-n)\sqrt{3}(\sigma_a+\sigma_b)/2\sigma\right]} \qquad (3.3.19)$$

The above operations explain the fact that void growth leading to fracture is much more rapid in the neck portion of tensile specimen following instability than during stable deformation because the stress system in the neck changes such that the condition of instability becomes only half that for Considére.

Invariably most materials harden to some stress level σ' before voids are nucleated. The extent of the strain occurring after void formation depends both on the density of voids formed and the remaining matrix material capability to continue to deform in a uniform manner i.e. to continue to work harden. If it can, then fracture cannot occur but usually new voids as well as the growth of the old ones takes place. This was not considered by McClintock. Void formation is a softening process and if we assume that a volume fraction f_v of voids is formed at the stress level σ' then the remaining material will carry a stress

$$\sigma_m = (1-f_v)\sigma'$$

The net hardening then depends on the growth of the voids with strain and strain rate plus initiation of new voids plus the strain hardening of the matrix.

Filipovic et al (3.3.56) took note of this fact and they derive a condition for the matrix resistance σ_m to continue to increase given by

$$\frac{\partial \sigma_m}{\partial \varepsilon} = (1-f_v)\frac{\partial \sigma^v}{\partial \varepsilon} - \frac{\sigma' \partial f_v}{\partial \varepsilon} \qquad (3.3.30)$$

This expression does not show the dependence of stress on strain rate and only considers the partial derivative of the stress with strain. Further, this equation implies that σm ceases to increase when

$$\mathrm{Ln}\sigma' = \mathrm{Ln}\,(1/(1-f_v))$$

which appears to be constant for a given volume fraction of voids for all materials, which is clearly not correct. The fracture strain and the strain at which voids are nucleated are different from one metal to another.

For a two-phase material where voids are nucleated at particles, assuming that voids are nucleated at a critical strain ε_c we could write the volume fraction of voids, for a spherical void as

$$f_v = f_{vo} + f_p\left[e^{(\varepsilon_{\alpha p}-\varepsilon_c)} - 1\right] \qquad (3.3.21)$$

or as $f_v = f_p\left[e^{(\varepsilon_{\alpha p}+\varepsilon_o-\varepsilon_c} - 1\right]$

where f_{vo} = volume fraction of pre-existing void.

f_p = volume fraction of particles without void.

ε_o takes account of f_{vo} in the second equation.

A model of ductile fracture taking into account the influences of work-hardening rate, strain rate sensitivity and the presence of pre-existing voids has been presented by Melander (3.3.57 and 58). His model

presents a fracture criterion based on the assumption that strain localization occurs when the energy to deform a material by unit strain starts to decrease.

a. The strain in a tensile bar can localize to a thin sheet of material with a higher volume fraction of particles than the surrounding material and that the strain localization occurs at first gradually but later proceeds very fast until the volume fraction of voids becomes very large in the sheet of materials so that a microcrack is generated.

b. The fracture strain increases with increasing strain rate exponent m.

c. The fracture strain increases with increasing strain hardening exponent n.

d. The fracture strain in a material with small strain hardening exponent is more sensitive to the value of m than in a material with large strain hardening exponent.

e. The fracture strain decreases with increasing volume fraction of voids.

The influence of hydrostatic pressure is taken into consideration through the utilisation of the result of the work of

Gurson (3.3.59) on the influence of voids on the flow properties of a material.

Gurson's result showed that the flow stress is given by

$$\sigma_{eq} = \sigma_o \left[B_o - B_1 \cdot \frac{P}{\sigma_o} + B_2 \left(\frac{P}{\sigma_o}\right)^2\right]^{\frac{1}{2}} \qquad (3.3.22)$$

σ_{eq} = equivalent microscopic stress

$B_o = 1.06 - 3.45 f_v$

$B_1 = -0.38 + 0.021/(f_v + 0.05)$

$B_2 = -0.09 - 0.3 f_v$

P = Hydrostatic pressure $= -\sigma_{nn}/3$

σ_o = microscopic flow stress.

f_v = volume fraction of voids

The simplest of the models so far to explain void growth and coalesence is that due to Embury and Brown (3.3.53). They assume that after the voids have been nucleated, they grow by plastic extension even though the ductile matrix between voids cannot suffer very large deformations because it is plastically constrained by the surrounding material. As the voids grow from spherical to ellipsoidal and elongate, a condition is reached when the length of the voids becomes equal to the spacing of neighbouring voids, which, in a two phase material are centred on the particles. When this happens further plastic

deformation occurs along a single slip plane, the plastic constraint preventing local deformation is lost and ductile fracture ensues immediately. They derived an expression for the fracture strain given by

$$\varepsilon_T = \mathrm{Ln}\left[\left(\frac{\pi}{6f}\right)^{\frac{1}{2}} - \left(\frac{2}{3}\right)^{\frac{1}{2}} + \varepsilon_n\right] = \mathrm{Ln}\ A_o/A_f$$

where ε_n = strain to nucleate void, f = volume fraction of particles, A_o and A_f are the initial and final cross-sectional areas. The model did not take into account the formation of a neck and its effect on void growth and the presence of hydrostatic pressure, the work hardening and the strain rate sensitivity and therefore it is not very accurate but it does explain the dimple appearance of fracture surfaces of two-phase metals.

3.4 Plastic Instability in Metals

This section is intended to point out the various instabilities that can occur during metal deformation in particular during uniaxial tension, and the conditions under which they arise and further to highlight some of the factors which governed their onset, in so far that they will help us to understand the behaviour of Dual Phase steels, rather than to carry out an extensive literature survey on plastic instabilities. This has been done elsewhere (3.4.1, 2). Although the discussion shall be more pertinent to tensile deformation some mention of what happens in other modes of deformation will be given.

The first type of plastic instability likely to be encountered during metal deformation in uniaxial tension is that associated with discontinuous yielding at the yield point and its associated Luders extension. At this point the load drop is associated with a large increase in the mobile dislocation density. Cottrell (3.4.3) has considered this phenomena in detail.

The most familiar plastic instability in a tension test is that concerned with the load maximum. The point at which this occurs is of considerable interest as it signifies the onset of failure of materials during straining. The strain at which it starts depends on a number of variables like the state of the material

whether it contains mechanical or geometric defects, the stress state, local elongation or local strain rate and the prior history of the material.

However this form of instability is more amenable to mathematical analysis and several investigators have attempted this (3.4.4 - 11).

The condition for a load maximum for a homogeneous and isotropic material can be shown to be first reached when

$$\frac{1}{\sigma}\frac{d\sigma}{d\varepsilon} \leq \frac{1}{Z} \quad \ldots\ldots\ldots\ldots\ldots\ldots\ldots\ldots (3.4.1)$$

where Z is the subtangent to the (σ-ε) curve in tension.

σ = true stress and ε = true strain.

Z is equal to unity at load maximum; this is known as the Considere criterion (3.4.12). At this stage a gradual thinning (or necking) of the material develops, called diffuse necking, over a length much larger than the width or diameter of the test specimen. Later, the deformation becomes more localised into a thin strip with little lateral in-plane contraction forming a localised neck. A triaxial stress state exists in this neck and it has been shown that this only happens when Z = 2 (3.4.13) or when $\frac{1}{\sigma}\frac{d\sigma}{d\varepsilon} < \frac{1}{2}$ ..(3.4.2).

For Biaxial stretching Z is given by (3.4.14)

$$Z = \frac{4(1-x+x^2)^{3/2}}{(1+x)(4-7x+4x2)} \qquad (3.4.3)$$

where $x = \frac{\sigma_2}{\sigma_1} = \frac{\varepsilon r + 2\varepsilon_\theta}{2\varepsilon r + \varepsilon_\theta}$

The above equations do not tell us the effect of the various material parameters such as the workhardening rate, the strain rate sensitivity and the state of anisotropy together with the influence of temperature.

There are evidences in the literatures purporting that the stress can be represented by a function of the form

$$\sigma \equiv \sigma(\varepsilon, \dot{\varepsilon}, r, T) \qquad (3.4.4)$$

where $r = \frac{\varepsilon_2}{\varepsilon_1}$ = strain ratio

$\dot{\varepsilon}$ = strain rate, T = temperature

The condition if instability then becomes:

$$\frac{1}{\sigma}\frac{d\sigma}{d\varepsilon} \equiv \frac{1}{\sigma}\left(\frac{\partial\sigma}{\partial r}\right)_{\dot{\varepsilon}} + \left(\frac{\partial\sigma}{\partial \dot{\varepsilon}}\right)_{r}\frac{d\dot{\varepsilon}}{d\varepsilon} + \frac{\partial\sigma}{\partial r}\frac{dr}{d\varepsilon} + \frac{\partial\sigma}{\partial T}\frac{dT}{d\varepsilon} < \frac{1}{Z} \qquad (3.4.5)$$

under isothermal conditions $\frac{\partial T}{\partial \varepsilon} = 0$

Therefore equation (3.4.5) becomes after some rearrangement $\frac{\varepsilon}{\sigma}\frac{\partial\sigma}{\partial\varepsilon} + \frac{\varepsilon}{\sigma}\frac{\partial\varepsilon}{\partial\varepsilon}\frac{d\dot{\varepsilon}}{d\varepsilon} + \frac{\varepsilon}{\sigma}\frac{\partial\sigma}{\partial r}\frac{dr}{d\varepsilon} < \frac{\varepsilon}{Z}$

by letting $\gamma = \frac{\partial \mathrm{Ln}\sigma}{\partial \mathrm{Ln}\varepsilon}$ a measure of work-hardening rate

and $M = \frac{\partial \mathrm{Ln}\sigma}{\partial \mathrm{Ln}\dot{\varepsilon}}$ a measure of the strain rate senstivity.

We have $$\gamma + \frac{m d\mathrm{Ln}\dot{\varepsilon}}{d\mathrm{Ln}\varepsilon} + \frac{\varepsilon}{\sigma}\frac{\partial\sigma}{\partial r}\frac{dr}{d\varepsilon} < \frac{\varepsilon}{Z} \quad \ldots\ldots\ldots\ldots (3.4.7)$$

If we assumed that the contribution from anisotropy is negligible then equation (3.4.7) becomes

$$\gamma + \frac{m d\mathrm{Ln}\dot{\varepsilon}}{d\mathrm{Ln}\varepsilon} < \frac{\varepsilon}{Z} \quad \ldots\ldots\ldots\ldots\ldots\ldots\ldots\ldots (3.4.8)$$

For a strain rate insensitive, isotropic material $m = 0$ and the equation reduces to

$$\gamma < \frac{\varepsilon}{Z} \quad \ldots\ldots\ldots\ldots\ldots\ldots\ldots\ldots (3.4.9)$$

This is Considère's condition. If the material obeys the constitutive relation $\sigma = k\varepsilon^n$ then instability occurs when $\varepsilon = n$. This is the main reason why the uniform elongation is often equated to n, the work hardening exponent.

For a homogeneous strain rate sensitive isotropic material

$$\gamma + m\frac{d\mathrm{Ln}\dot{\varepsilon}}{d\mathrm{Ln}\varepsilon} < \frac{\varepsilon}{Z} \quad \ldots\ldots\ldots\ldots\ldots\ldots (3.4.10)$$

For constant extension rate test $\frac{d\dot{\varepsilon}}{d\varepsilon} = -\dot{\varepsilon}$ or

$$\frac{d\mathrm{Ln}\dot{\varepsilon}}{d\mathrm{Ln}\varepsilon} = -\varepsilon$$

Then we have

$$\gamma - m\varepsilon \leq \frac{\varepsilon}{Z}$$

or $$\gamma \leq \varepsilon\left\{m + \frac{1}{Z}\right\} \quad \ldots\ldots\ldots\ldots\ldots\ldots (3.4.11)$$

If one employes Harts condition for the onset of instability, that when the cross section at a pre-

exiting imperfection site begins to decrease at a faster rate than the rest of the specimen (3.4.4) then

$$\gamma < 1 - m \quad \ldots\ldots\ldots\ldots\ldots\ldots\ldots\ldots (3.4.12).$$

Hart showed that the amount of post uniform elongation in the steady state deformation of a tensille bar is strongly influenced by the magnitude of the strain rate sensitivity m.

It has been shown by Ghosh (3.4.5) that this instability criterion is not valid for geometric imperfections and that the criterion should read

$$\gamma < \frac{1 - m}{1 - \frac{\partial \mathrm{Ln} A_o}{\partial \mathrm{Ln} A}} \quad \ldots\ldots\ldots\ldots\ldots\ldots (3.4.13)$$

where A_o = initial cross-sectional area

A = current cross-sectional area

and ∂ refers to fluctuations between the imperfection and the material outside it.

However it has been shown (3.4.1) that neither criterion is wrong it is just a matter of definition used by each to describe what is happening. Harts equation refers to a mechanical defect whereas Ghosh's equation refers to geometric defects.

Later, Jonas et al (3.4.15) took into consideration the effect of compressive stress on mechanical and geometric defects. They were able to show that the

greater the rate sensitivity of a material the earlier the flow localisation will start in compression but it will be delayed in tension for mechanical defect while the geometric defect is different in that it is unstable from the onset of plastic flow.

Jones and Baudelet (3.4.16) have extended the argument of reference (3.4.15) to include the pre-existence and generation of cracks developed during straining. Their analyses showed that both processes increase the chance of tensile instability by their negative contribution to work hardening and rate sensitivity. They also show that when the crack or cavity generation rate varies along the specimen axis, initial defects are not required to initiate flow localisation and in the presence of several incipient necks, a defect generation rate gradient can lead to flow localisation at a single site.

A number of investigators have examined the influence of both n and m values both qualitatively and quantitatively (3.4.17-22) and their results show conclusively that both parameters influence the limit strain with n contributing to uniform strain while m has a marked influence on necking strain by retarding the growth of the neck once it is formed. In some cases it may retard the appearance of significant necking by many times the strain it takes to start a neck.

However, there are at least two recognisable forms of rate sensitivity:

(i) The first is obtained by the instantaneous rate change in a tensile experiment and it describes the dependence of the flow stress at any particular state of the material on the current strain rate.

(ii) The second describes the rate of evolution of the structure of the material with strain on the imposed strain rate (it describes the dependence of the strain hardening coefficient on the rate sensitivity).

The above facts have been taken into consideration in a recent analysis by Kocks et al (3.4.23) and they showed that the critical strain for catastrophic necking to occur is approximately given by

$$\varepsilon_c = \varepsilon_u + 1ON \quad \ldots\ldots\ldots\ldots\ldots\ldots \quad (3.4.14)$$

where $$N = \left(\frac{\partial \mathrm{Ln}\ \sigma}{\partial \mathrm{Ln}\ \dot{\varepsilon}}\right)_{\gamma} \quad \ldots\ldots\ldots\ldots\ldots\ldots \quad (3.4.14)$$

ε_u = Uniform elongation

Another recent approach which was formulated to explain the occurrence of shear banding in the neck is called bifurcation theory (3.4.24-26). The condition for this requires that corners be developed on the yield locus. However Melander (3.4.27) has shown that, based on the work of reference (3.4.25) the correction to be made to the uniform elongation

strain is very small for a material obeying

$$\sigma = K\varepsilon^{n} \quad \text{of the order of } 2\%$$

A more easily understood theory put forward to explain shear banding have been presented by I.L. Dillamore et al (3.4.28).

They assumed the following:

1. A flow rate given by $\tau = K(\gamma)^{n}$

   γ = shear strain k = constant

2. $\tau = \tau_{o}\left(\frac{v}{v_{o}}\right)^{m}$ where v = dislocation velocity

3. $\dot{\gamma} = Nbv$ where N = density of mobile dislocation

4. $\dot{\varepsilon} = \dot{\gamma}/M$ where M = Taylor factor.

They derived an instability condition given by

$$\frac{1}{\sigma}\frac{d\sigma}{d\varepsilon} = \frac{n}{\varepsilon} + \frac{m}{\dot{\varepsilon}}\frac{d\dot{\varepsilon}}{d\varepsilon} + \frac{1 + n + m}{M}\frac{dM}{d\varepsilon} - \frac{m}{N}\frac{dN}{d\varepsilon} \leq 0 \quad \ldots\ldots (3.4.15)$$

The last term being negative conforms to the situation at the yield point because of the negative contribution of any increase in mobile dislocation density with strain. In Dual Phase steels the increase with changes in strain should be large and hence large negative contributions ensue. Dillamore et al (3.4.28) used the contribution from $\frac{dM}{d\varepsilon}$ to explain the shear band formation as a case of $\frac{dM}{d\varepsilon}$ being negative (Geometric Softening).

In a forming operation, however, additional factors come into play contributing to unstable deformation. They are:

(a) Failure of the draw piece caused by exceeding its strength in a site located outside the area of forming e.g. tearing of the bottom of a draw piece during deep drawing operation.

(b) Galling on the tool - material interface

(c) Wrinkling of sheet metal during stamping (Compression Instability)

(d) Fracture of tools - caused by exceeding their strength

(e) Occurrence of an inhomogeneity such as a groove along which strain and stress gradients may exist.

(f) The contact pressure between the tool surface and the material and the friction on the tool surface.

The strain rate sensitivity of the material, the change in the stress ratio in the groove, the gradient of strain along the length of the groove, the contact pressure and the friction on the tool surface have all been shown (3.4.29) to stabilize the process of straining after the loss of stability of the sheet metal and to delay the concentration of strain. Whereas the initial inhomogeneity of the sheet metal, pressure concentration on the tool surface as well as unfavourable direction of frictional forces can accelerate the localization of strain.

3.5 Properties Required for Sheet Forming

The formability of sheet metals depends to a large extent on the materials mechanical properties. In particular its ability to distribute strain. This is characterised by the work hardening parameter $1/\sigma \; d\sigma/d\varepsilon$ which decreases in successive stages, as the strain state advances, in such a way that the material becomes progressively unable to spread the strain to less deformed parts. The strain eventually concentrates into small localised regions, as has been mentioned in the prece ding section (3.4), until it breaks. This shows itself by the appearance of a neck during testing. Therefore, apart from frictional effects between the die and the sheet metal surface, which will depend on the surface quality of the metal as a result of mode of production, the material properties which strongly influence the formability of sheet metals are:

1. Its work hardening behaviour which can be estimated through its work hardening coefficient n.

2. Plastic anisotropy.

3. Strain-rate sensitivity, ductility and of course temperature of forming but here we are only concerned with cold formability.

Any metallurgical factors which influence these properties can be used to improve or control the forming characteristics of a sheet metal.

We shall now consider each in turn.

1. Work Hardening: This can be observed from a tensile stress-strain measurement. In section 3.4 it was shown that at maximum load, according to Consideres Condition $\frac{d\sigma}{d\varepsilon} = \sigma$ and $\varepsilon = n$ for a material obeying $\sigma = k\varepsilon^n$. Thus for most metal the plastic instability strain, under tension, has a numerical value equal to n. At strains greater than n, the rate of increase in tensile strength due to strain hardening is less than the rate of stress increase due to the diminution of cross-sectional area. This coefficient then can be used to measure the degree to which a material can distribute strain or work harden effectively. High n value material will be able to sustain work hardening more and will prevent localised strain concentrations within the material. This n value can also be related to the tensile strength/yield stress ratio such that high n value means a greater TS/YS ratio. The effect of this on hydraulic bulging of circular diaphragms has been studied by Wang et al (3.5.1). They showed that the polar thickness strain is lowered with increasing n value

Any metallurgical factors which influence these properties can be used to improve or control the forming characteristics of a sheet metal.

We shall now consider each in turn.

1. Work Hardening: This can be observed from a tensile stress-strain measurement. In section 3.4 it was shown that at maximum load, according to Considere's Condition $\frac{d\sigma}{d\varepsilon} = \sigma$ and $\varepsilon = n$ for a material obeying $\sigma = k\varepsilon^n$. Thus for most metal the plastic instability strain, under tension, has a numerical value equal to n. At strains greater than n, the rate of increase in tensile strength due to strain hardening is less than the rate of stress increase due to the diminution of cross-sectional area. This coefficient then can be used to measure the degree to which a material can distribute strain or work harden effectively. High n value material will be able to sustain work hardening more and will prevent localised strain concentrations within the material. This n value can also be related to the tensile strength/yield stress ratio such that high n value means a greater TS/YS ratio. The effect of this on hydraulic bulging of circular diaphragms has been studied by Wang et al (3.5.1). They showed that the polar thickness strain is lowered with increasing n value

for a given ratio of bulge height/radius of free diaphragm. Therefore it is clear that a high n value material will be desirable. However, this cannot be improved upon indefinitely. Investigations of work hardening of metals has revealed that there is a correlation between deformation and dislocation arrangement orientation of tensile axis, temperature, rate of deformation, twinning and stacking fault energy and indeed it has been suggested (3.5.2) that better sustained work hardening, through the control of stacking fault energy, mechanical twinning or strain-induced phase transformation can be exploited to enhance stretching properties.

Grain size also has influence on n value as well as decreasing the upper yield point and the yield elongation (section 3.1). It has been shown that it obeys an equation of the form (3.5.3, 3.5.4)

$$n = \frac{\alpha_1}{\alpha_2 + d^{-\frac{1}{2}}} \qquad \ldots\ldots\ldots (3.5.3)$$

where $\alpha_1 = 6.7$ and $\alpha_2 = 17$

For sheet metals when the grain size is such that the number of grains across the sheet thickness is less than 20-100 the ductility is impaired (3.5.2). At this stage polycrystalline constraints become insufficient to diffuse strain localisation

in the softer grains and this will lead to early failure. This limitation leads to what is called the orange peel effect; that is on straining, a coarse grained material develops a grainy surface texture.

Temper rolling which is used to suppress the yield point and yield elongation and strain ageing both lower the n value; this has been shown by Baren and Levy (3.5.5 and 6) and their results are quoted by P.L. Dillamore (3.5.7). Most methods of strengthening do lead to reduction of n value. Texture hardening like precipitation hardening and other methods of hardening also leads to reduction of work hardening. This has been shown by Dillamore et al (3.5.8) for a decarborised rimming steel.

Therefore to improve work hardening it will be necessary to remove sources of strain ageing and to have high dimensional accuracy of specimen. Thus the interstitial free steel (IF steel) which has good ductility and no strain ageing tendency because of the large addition of titanium and/or niobium to tie up the carbon and nitrogen can be useful for difficult pressings. They do not require temper rolling and they have high r values.

2. Anisotropy: Reduction of metals from the Ingots into sheets and its subsequent fabrication creates various types of directionability (or anisotropy) in its properties. It is regarded as undesirable in the case of earing in deep-drawn cups. The tendency to have certain crystallographic planes or directions aligned with prior working implies that oriented slip systems are operative which allow easier deformation in some directions than others. This implies that if we can create plastic anisotropy in which properties in the rolling direction are different from those along the transverse directions we might be able to improve the overall shape of the stress/strain curve, the yield stress, tensile strength and the rate of work hardening.

The directionality of properties is characterised by the R value which was originally suggested by Lankford et al (3.5.9) and it is defined by

$$R = \frac{\varepsilon_w}{\varepsilon_t} = \frac{\mathrm{Ln}(w_t/w_o)}{\mathrm{Ln}(w_t L_t/w_o L_o)} \quad \ldots\ldots(3.5.4)$$

The R value averaged over all directions in a sheet $\bar{R}$ has been shown to be related to the maximum size of blank that may be drawn to form a flat bottom cup (3.5.10). If the R value is greater than 1 then the material has resistance to thinning and therefore has increased through-thickness strength. If the

R value is less than 1 the opposite is true. For Dual Phase steels the R value is approximately 1. Sometimes there is a variation of anisotropy within the plane of a sheet; this is termed planar anisotropy and denoted by ΔR and it is responsible for earing in deep-drawn cups.

The average normal R value $\bar{R}$ is then defined as:

$$\bar{R} = \frac{R_o + 2R_{45} + R_{90}}{4}$$

whereas ΔR is defined as: .....(3.5.5)

$$\Delta R = \frac{R_o + R_{90} - 2R_{45}}{2}$$

Thus $\Delta R = R_o + R_{90} - 2\bar{R}$ .....(3.5.5)

For a completely isotropic material $\bar{R} = 1$ and $\Delta R = 0$. It is desirable to have a sheet metal with high $\bar{R}$ but $\Delta R = 0$. The degree of anisotropy in sheet metals is related to the crystal structure. Anisotropy develops more readily in H-C-P metals (Be, Ti, Zr) than in the B.C.C. or F.C.C. metals. The type and amount of alloying elements also influence the nature of the anisotropy, e.g. Al increase $\bar{R}$ in Al-killed steel over that obtained for Rimming steel and this is influenced by its processing history. Of importance are; the finishing temperature, coiling temperature, amount of cold reduction and the annealing cycle. The

range of $\bar{R}$ obtained for different metals are shown in table below (3.5.11).

$\bar{R}$ value	Metal
1.00	Normalised low carbon steel
1.00-1.35	Rimmed steel
1.35-2.00	Al-killed steel
0.80-1.00	Cu, Brass
0.2	Pb
3.00-6.00	H.C.P. metals (Ti)

The major influence of $\bar{R}$ value on metal forming is in cup drawing. With high $\bar{R}$ value the cup wall is strengthened relative to the deforming flange such that the cup wall can support larger loads without failure. This is what was referred to as Texture hardening above. The influence of $\bar{R}$ value has been shown by Atkinson (3.5.12) to increase LDR as $\bar{R}$ value increases. Variations of $\bar{R}$ value with angle determines the amount of earing and lower $\bar{R}$ value implies poorer drawability. This has been studied in copper strips by Richards (3.5.13) and in annealed deep-drawing quality steel sheet by Wilson et al (3.5.14). They showed that UTS, YS, percentage elongation and $\bar{R}$ value at 20% strain all vary with angle to the rolling direction.

In biaxial stretching $\bar{R}$ value also influences the strain state. Dillamore (3.5.7) has pointed out that it is desirable, according to Hill's theory, to have a high biaxial strength for pressings so that strain distribution can be shifted away from unconstrained region of biaxial stress to the constrained region under uniaxial or plane-strain state. Hill's theory gave

$$\frac{\sigma_b}{\sigma_u} = \left(\frac{1+R}{2}\right)^{\frac{1}{2}}$$

This implies that the greater the value of $\bar{R}$ the greater will this difference be. In fact, $\bar{R}$ can be made to approach infinity in cubic metals by having (111) plane oriented grains in the plane of the sheet. However the textured strength observed for such arrangement under biaxial tension is only 1.2 times that for isotropic material. Thus we cannot make σ_b/σ_u approach infinity as well as implying that the influence of $\bar{R}$ on biaxial stretching is not of great significance. Dillamore further assessed this point by comparing his calculated values of $\bar{R}$ and σ_b/σ_u to the experimental observation of Held (3.5.15). He was able to conclude that, within the R value range of 1.0-2.0 Hill's theory can be assumed to be upheld.

Horta et al (3.5.16) and Pearce (3.5.17) have found that the σ-ε curve obtained for bulge tests, on a number of steels, was greater than that found for tensile testing

with the larger differences being recorded for high $\bar{R}$ valued materials and that there is a reduction of limit strain. They also found that the strain was more uniformly distributed over the surface of the bulge in the high $\bar{R}$ value material.

Altogether then the two parameters n and $\bar{R}$ together can give a good measure of the performance of a sheet steel under complex loading conditions. n value dominates the performance under stretching whilst the $\bar{R}$ value dominates under deep drawing conditions.

3. Strain rate Sensitivity and Ductility: The flow stress of metal also depends on the strain rate $\dot{\varepsilon}$ ($\sigma = K\dot{\varepsilon}^{m}$). Localisation of strain after maximum load has been attained during tensile testing should be less severe in a material which exhibits high strain rate sensitivity as has been pointed out in section (3.4) of this thesis. This has been suggested by Cantalejos et al (3.5.18) to be the reason why a relatively high post maximum load strain is obtained during tensile testing of mild steels. The precise influence of strain rate sensitivity on formability is not yet clear, but it can be expected that the amount of forming depth which occurs after the onset of instability may depend on the strain rate sensitivity. However there are some conflicting reports which suggest that the strain rate sensitivity during a particular pressing operation is a function of

the process path rather than of the material being deformed. Wilson's result (3.5.19) for punch stretching of temper rolled stabilised steel with oil lubricant shows less uniform strain with increasing punch speed while the work of Mellor et al (3.5.20), in oil stretching, no evidence of changes in strain distribution was observed. It is however known that lubricants are more rate sensitive than metals and they can break down under non-uniform loading which can lead to local adiabatic heating and consequently results in strain localisation. It has also been suggested that dislocation strengthening during tensile testing reduces strain rate sensitivity (3.5.2) and likewise precipitates can have a detrimental effect on it.

Ductility is a measure of the extent of the materials ability to undergo plastic deformation and it is measured in a tensile test by the total elongation of the material. Product failure occurs when the level of material ductility attainable is less than that required in the forming operation. In particular the material performance under bending and in hole expansion is controlled by the factors that governed its ductility. It is now well known that these factors are largely a function of its degree of cleanliness and the shape and distribution of its inclusions (3.5.22). Fracture processes can be started at these inclusion sites by particle cracking or the interface between the particle and matrix split creating voids.

Butler et al (3.5.23) have shown that the most important of these factors is the shape of the inclusion particles which can be controlled by Rare-Earth metal additions (Ce). They further showed that omission of these inclusion shape controlling elements was detrimental to bending in plane-strain and it gave a reduction of hole-expansion of about 50% in Van-60 range of steel. Davison et al (3.5.24) have also shown that inclusion shape control gave improvement on the limit strain. Likewise Lee and Hiam (3.5.25) found a significant rise in FLD_o for a niobium treated steel, inclusion modified by Zr, when the major strain is transverse to the rolling direction but not when it is along the rolling direction. The sheet thickness too can influence the FLD shape by shifting the limit strain upward. This has been confirmed in (3.5.25).

3.6 Development of Sheet Steels for Forming Applications

In the preceding section on the properties required for sheet formability it has been highlighted that the properties which strongly influence the formability of sheet metal are: its work hardening ability characterised by n_{value}, its plastic anisotropy measured by the R_{value}, its strain rate sensitivity index m and its ductility. With industrial advances towards increased mass production of goods such as motor vehicles, refrigerators and tin cans for the packaging industry, the need for high strength easily formable steels arises. The industrial need together with social demands gave the impetus for the development of these steels in the early sixties when the demand for more light weight articles became more prominent. Theproperty required of the steels depends on the job they are to be employed for and they can be divided into two categories:-

(a) Low strength cold formable steels; used for car body panels and for packaging

(b) High strength formable steels; used for structural and safety related purposes, e.g. car roof pillars, side impact bars and bumper face bars. They require high yield strength, low impact transition temparature, minimum cost, easy weldability and good formability.

The first type normally contain very low carbon and are in flat rolled sheet strip form, less than about

6mm thick, and produced in the cold-rolled and annealed conditions with often final temper rolling to eliminate the yield phenomenon. Their compositions are usually approximately 0.05%C with 0.3 - 0.4% Mn and at times very small additions of Al, Ti and V are made. These can be further divided into two types:-

1. Extra-deep drawing type (EDD steels) where cold formability is of prime importance rather than strength (commonly used for car body pressings),
2. Steels where high strength is required, but without much formability, e.g. high strength tinplate steels which can be used to reduce weight in products by using thinner gauges. Normally produced by continuous annealing at high speed (700 M/min.) to prevent grain growth. They have strengths about twice the EDD steels (400 N/mm^2) and a composition in the range of 0.07%C, 0.3 - 0.4% Mn with occasionally small addition of Nitrogen, Phosphorus or Silicon. Hot shortness is prevented by the small addition of Mn just enough to prevent the formation of FeS by forming MnS instead.

Grain refinement is achieved by cold working, rapid heating and cooling rates. At times a steel may be annealed above the Ac, followed by rapid quenching

to lath martensite to give added strength in the range 900N/mm^2 with less directionality than those steels in which added strength is achieved by cold working after annealing. The mechanical properties required for optimum press performance from the EDD type steel are;

(i) high R value
(ii) high uniform elongation
(iii) high n-value (i.e. well sustained work hardening)
(iv) high elongation at fracture
(v) low yield strength
(vi) low but uniform rate of strain ageing.

They are traditionally produced as Rimming steel as high Ingot yield can be obtained and because a uniform smooth surface is required in the end product to permit defect-free coatings to be applied.
A typical production flow chart has been given by D.J. Blickewede (3.1.25) and is reproduced in figure 3.6.1). It is commonly found that R_{value} greater than 1.3 cannot be achieved in Rimming steels. The connection between R_{value} and deep drawability was first provided by Whiteley and Wise (3.6.1) when it was also known that Al-killed steel gave better R_{value} than Rimmed steel. High R_{values} are desirable for deep-drawing of cups giving increased through thickness strength in the sheet

metal. Higher R values than that for Al-killed steel are found in the interstitial free steels (IF steel). The reason for this perhaps can be ascertained from the work of Takahashi and Okamoto (3.6.22). They showed that decreasing both the carbon and nitrogen content of Rimmed low-carbon cold rolled sheet steel increases their R value substantially. It has previously been held that the improvement in R value of Al-killed steel to that of Rimmed steel was due to the presence of ALN in these steels. Raising the strength usually causes a decrease of R value and it has been shown (3.1.25) that by increasing the ferrite grain size the R value can also be increased, governed by the relation:

$$R = R_o - kN$$

Where R_o and k are constants and N is ASTM grain size number. Better combinations of strength and R value are obtained through P addition or in Cu containing steels (3.6.3) and by box annealing or continuous annealing.

For the low strength steel to improve the strength severe cold reductions are employed which impair the ductility thus reducing its forming ability. To recover some ductility annealing is employed which causes high production costs and loss of strength.

Because of this and the desire to reduce weight of vehicles the high strength steels emerged. To produce the strength was simple enough; the various methods of strengthening metal have been well-documented. The grain size was known to increase the strength linearly with $d^{-\frac{1}{2}}$ and likewise precipitation strengthening increases with volume fraction of non-deformable precipitate ($\sigma \propto f^{\frac{1}{2}}$). Alloying additions are also known to control the grain size as well as cold reduction and heating rate. The various methods of achieving the desired strength are summarised in Table 3.6.1. These steels are produced either as high strength low alloyed hot rolled sheet steel (HSLA steel) or as high strength low alloyed cold rolled sheet steel (HSCR). A review of the structure - property relationship of the steel has been provided by Gladman et al (3.6.4) and Pickering (3.6.5) and will not be dwelt upon here. Carbon was initially used to obtain the strength but because of the material requirements during fabrication, for welding of these steels, apart from being formable, ductile and fracture resistant, it has been found necessary to lower the carbon content. Carbon as low as 0.03wt% has been used to date. This implies that something must be done to regain the strength lost by removing carbon. It is found that in contrast to all the other strengthening mechanisms precipitation hardening

and grain refinements seems the most effective and practicable means of improving strength. To refine the ferrite grain size produced by austenite transformation in the HSLA steels, rapid heat treatment and microalloying additions of elements such as Al, Nb, V or Ti either singly or in combination along with renitrogenisation are employed. Renitrogenised steel are of course cheaper than the microalloyed varieties. They offer the advantage of increasing strength through forming and ageing but their strengths are generally lower than those of microalloyed steels. The strengthening mechanisms of microalloyed steels are: grain refinement, precipitation hardening, solid solution hardening (addition of P, Si, and Mn) and dislocation strengthening. The strength levels depend strongly on hot rolling temperature, the percentage reduction per pass and the cooling temperature. Nb, V and Ti are all carbo-nitride formers whereas AL is a nitride former and Nb can be used in a balanced steel with economic advantage. However its precipitates are formed only after heating to very high austenitizing temperatures because of its limited solubility. V on the other hand forms more soluble carbo-nitrides, but there is a danger of over-ageing with V alloyed steel (3.6.6), and therefore it can produce precipitation hardening in the conventionally normalised condition.

Controlled rolling to a low finishing temperature, even down into the ($\alpha + \gamma$) phase field, from high solution treatment temperatures ($\sim$ 1250^{o}C) is often employed in most high strength low alloyed steel to provide maximum precipitation and dislocation hardening and to obtain the finest possible austenite grain size. The lower the finishing temperature the more dislocations are left behind in the matrix as recrystallization will be prevented to a degree. Mn can be used to depress the transformation temperature of austenite but there is a danger of producing an acicular structure. If this can be avoided refinement of the polygonal ferrite grain size will be achieved which may be increased by controlled cooling on rolling mill runout tables. The reduction of carbon leads also to improved toughness as it reduces the amount of pearlite formed but this can cause the formation of embrittling carbide filaments on the ferrite grain boundaries (3.6.7) if accompanied by low Mn contents or slow cooling rates from austenite. Most present day HSLA steels now employ high hardenability in order to achieve very high yield strength of the order of 600MPa and low impact transition temperatures of the order of -70^{o}C (3.6.8 and 9). The acicular ferritic steels having bainitic structure stem from the realisation that to develop good toughness in the bainitic structure low carbon content together with very fine prior austenite grain size is a necessity but the inclusions must be controlled (3.6.10 and 11). This has been done

by the addition of Zr, Ca, Ce or Ti. They decrease the anisotropy in these steels and give rise to improved toughness and ductility. Calcium additions alter the constitution of Al_2O_3 preventing the formation of stringers but it must be kept below 0.1% otherwise charpy-shelf energy will decrease. Zr also form $Zr_4C_5S_2$ while Ti forms $Ti_4C_2S_2$ which are small and spherical in structure. They reduce the MnS. Zr, Ca, and Ti all also combine with oxygen and therefore can only be added to fully killed steels. The effect of modifying inclusion shape can be seen in hot-rolled steel strengthened with either Nb or Ti carbide precipitation. Nb does not form a sulphide in steel whereas Ti does and evidence shows that a Ti steel having modified sulphide inclusions maintains its transverse ductility much better than the unmodified Nb steels as the strength is increased (3.6.12). Zr can, however, not be used in steels which derive their properties from high nitrogen contents to modify the sulphides, in such a case Ce is used. For the HSCR steels the main idea is to obtain high strength by mechanical hardening such as cold rolling and temper rolling followed by annealing to recover some ductility. The starting material can either be the high yield strength hot band steels (HSLA) or low carbon mild steels. Their strengthening mechanisms are also summarised in table 3.6.1. For precipitation strengthening Cu, too can be added. Cu has high solubility in α-iron at high temperature. Little precipitation

hardening is achieved during hot rolling and coiling because of this and hence they have relatively low yield strength after hot rolling so that low rolling load is required during cold rolling. They are continuously normalised between 870^{o} to 927^{o}C to take the Cu into solution and recrystallise the steel. Increased strength is achieved by subsequent low temperature ageing at approximately 500^{o}C for (2-40) hours to precipitate ε-Cu phase which strengthens the steel. However there is an attendant problem of surface hot shortness associated with Cu containing steel which produces surface and edge cracking and poor surface finish. This problem is solved by the addition of Ni.

A newcomer into the field of cold formable steels are the dual phase steels, the production and properties of them together with their applications will be discussed in the next three sections.

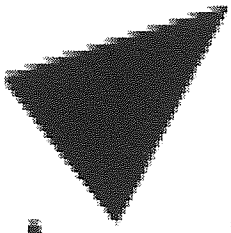

Aston University

Illustration removed for copyright restrictions

Figure: 3.6.1 Simplified Flow Chart of the Production of Low-Carbon Sheet Steel (From Reference 3.1.25)

TABLE 3·6·1

Conventional Methods of raising the strength of Low Carbon Steel

3.7 Development and Production of Dual-Phase Steel

The development of Dual-Phase steels stemmed from the early work in the mid-1960's on the development of high strength formable steels. These were either hot-rolled or cold-rolled types and were in thick gauges. They have the same composition as plain carbon steels with micro-alloying additions V, Nb, or Ti plus AL, Mn and Si and are thermo-mechanically or mechanico-thermally treated but they are less formable compared to mild-steels.

By the early 1970's industrial demand for high strength thick gauge formable steels became prominent as a result of social demands. This lead to a lot of developmental work being undertaken by the steel industries of Europe, United States of America and Japan which led to the accidental discovery of the Dual-Phase process by Bailey (2.4). His work was quickly followed up by M.S. Rashid (3.5 and 6) also at the General Motors. Since then a large volume of published works have emerged mainly from the U.S. and Japan. The steel has also gained wide acclaim from the automobile industry as it promises a large reduction in vehicle weight (3.7.1).

One of the earliest Japanese reports on Dual-Phase steel was by S. Hayami et al. (3.7.2). They were able to produce these steels by batch and continuous

annealing with strength between 400-800 Mpa. The Japanese have since developed the continuous annealing method to production line level and steels produced in this way are termed CAPL-Dual-Phase Steels (CAPL ≡ Continuous Annealing and Processing Line). They are produced by cooling, at about 10^{o}C/sec, after heat treatment at temperatures in the Ferrite + Austenite phase field. The shape fixability, after press-forming of these steels has been assessed (3.7.3) and are found to be superior to that of conventional HSLA steels because of their lower yield strength.

Several Dual-Phase steels are now commercially available in the U.S. and in Japan and are beginning to emerge into the U.K. market. They contain about 10-20% volume fraction of hard second phases in a polygonal Ferrite matrix.

The required microstructure can be produced by a number of routes, discussed below:

Production

The microstructure required can be obtained by the following ways :-

(1) By rapid cooling after intercritical annealing in the $\alpha + \gamma$ region.

(2) Controlled cooling after annealing

(3) Balancing alloy content with cooling cycle and starting with a fully Austenitic heat treatment.

Each route has its merit but they all require a

a balance of strip thickness, cooling rate and hardenability.

The first method transforms most, if not all, of the Austenite formed at intercritical annealing temperatures to martensite. Very lean alloying can be used in 1 and 2 such that the percentage of martensite can be controlled by changing the carbon content and alloying with elements that will stabilize the Austenite or by varying the inter-critical annealing temperature. However, modifying the carbon content can have an adverse effect on weldability of the steel. Some steels with different compositions have been found to develop Dual-Phase microstructure and properties after slow cooling following box-annealing (3.7.4) and after air cooling (3.5.2, 5 and 6). High hardenability is essential in these steels because the intercritical anneal treatments always produce high carbon Austenites. Manganese, silicon and vanadium are popular elements for doing this. The commercially available steel called VAN-QN derived its properties from alloying addition of 1.4% Mn, 0.5% Si, and 0.1% V. Vanadium has the dual property of contributing to hardenability as well as producing fine microstructure and as has been shown in section 3.1 it can aid the control of steel ageing properties.

Its close neighbour elements Niobium and Titanium, which can also be used to increase strength by their propensity to form carbide and nitride, have been found to be incapable of playing this dual role.

It has been further suggested that intercritical annealing in the $\alpha + \gamma$ range is more beneficial to producing Dual-Phase microstructure (3.7.7) because annealing in this range followed by slow cooling tends to decrease the hardenability with respect to ferrite formation while there is a retardation of pearlite formation compared to annealing above A_3. This view has been further reinforced by the work of Holmström et al. (3.7.8). They made a comparison of the properties of several commercially available hot rolled and annealed Dual-Phase steels. The annealed steels show better properties than hot-rolled steel. However, the validity of their observation should be taken with caution. The annealed steels examined have finer mean grain sizes of 3.85 μm compared to that of the hot-rolled ones of 4.23 μm. Further the percentage of martensite in the annealed steels is higher than that of the hot-rolled steels. The hot-rolled steels have both acicular ferrite and bainite in their micro-structure. The percentage of martensite in the annealed steels has been very closely controlled around the peak for good n_{value} (19 -22%M). Previous work has shown that n_{value}

increases gradually along a curve, it reaches a maximum at about 20% Martensite after which it deteriorates. This being one of the reasons why G.M. specify 20% martensite for this type of steel. The hot-rolled steels have the martensite occurring as large separated islands while the annealed steel has its martensite as small closely spaced islands along the ferrite grain boundaries. The former distribution should be more favourable for better mechanical properties. Although the n_{value} for annealed Dual Phase steels examined are greater than those of hot-rolled, giving better uniform elongation and ultimate tensile strength, their yield strengths are comparable. It will have been better to have a comparison of the steels with the same grain size, the same percentage of martensite and polygonal ferrite.

The other method of controlled cooling starting from the Austenite region has been used to produce inter-critical continuous annealed sheet in hot-rolled steel coils (3.7.9). This method has been pursued by steel manufacturers in the United States and Canada and is pioneered by work at Climax molybdenum company research laboratory. It requires very little expense to be incurred in the production line modification. Typical cooling rates being used at present are less than

$100^{o}C$/sec. $28^{o}C$/sec has been reported in reference (3.7.9). It has, however, been shown recently that to get the best properties from Dual Phase Steel produced by this route, called ARDP steels, (ARDP ≡ As Rolled Dual-Phase) it is necessary to maintain their composition within the following ranges of alloying addition for good reproducibility of properties from one run out mill to another (3.7.10).

0.4 - 0.7 wt %C, 0.8 - 1.0 wt % Mn, 1.2 - 1.5 wt % Si, 0.4 - 0.5 wt % Cr, 0.33 - 0.38 wt % Mo, 0.02 wt % AL (minimum value) with sulphur and phospherous kept as low as possible but if more than 0.003 wt % then rare-earth or zirconium should be added for inclusion control. At the same time the ratio of the time of cooling from the Austenite region for the start of pearlite formation to that for 75% polygonal ferrite to have been formed should be kept between 10 and 20.

Attainment ofDual-Phase microstructure does not inevitably give excellent ductiblity. The agglomerates property depends on the properties of its individual constituent phases namely ferrite/ martensite or low bainite or as it has been reported, retained-austenite (3.7.11). It also depends on the volume fraction, size and distribution of the phases and since it is desirable to eliminate as much carbon as possible from the high-temperature ferrite, by diffusion, for optimum ductility and control of

yield point, steel with high alloying content that will produce ferrite-martensite at slow cooling rates are more desirable for good properties.

Davies (3.7.12-14) has shown that the mechanical properties of the ferrite matrix controls the ductility of Dual-Phase steels as well as influencing its strength. The best results are obtained with very fine grained polygonal ferrite that is strengthened by substitutional alloying elements like Si. This tends to improve the UTS/Uniform elongation ratio due to its propensity for enhancing the strain hardening rate of ferrite.

However Repas (3.7.15) has shown that Si additions will not necessarily produce the desired increase in strength except in combination with a fast cooling rate. He further found that increased Si content does eliminate the yield point and produces the continuous yielding characteristic of Dual-Phase Steels and that at low Si levels and slow cooling rates the Austenite formed at intercritical annealing temperatures transforms to ferrite, pearlite and grainboundary cementite which is detrimental to formability. When the Si level and cooling rate were simultaneously increased he found that ferrite and pearlite formation are suppressed and bainite and martensite formation are favoured and that the tensile

strength of Dual-Phase steel is improved as a result of strengthening effect of Si on the ferrite phase. This result is in line with that of Davies (3.7.10) and it is not surprising that Si in conjunction with AL can eliminate strain ageing and also in ternary Fe-Si-C alloys carbon tends to diffuse away from silicon (3.7.16). Since Si is in solid solution with ferrite it will not be easy for the carbon to redistribute to form pearlite while cooling.

H. Masui et al (3.7.17) studied the hardening mechanism most conducive to getting the best properties in ferrite. Generally the higher the strength the lower is the ductility and it has been found (3.7.18) that in low interstial content iron, the ductility is independent of grain size. This is rather surprising as the flow stress of metal obeys Hall-Petch relation. Intercritical annealing reduces the interstial content in ferrite and this segregates into the Austenite region. Masui et al (3.7.17) have found that solid solution hardening by Si or Mn gave the best combination of strength and ductility; precipitation hardening by Tic was worst and grain boundary hardening was intermediate. It has also been shown (3.7.19) and (3.7.20) that there is a good combination of tensile strength and uniform elongation with increasing amount of Si in the range 1.0 - 2.0 wt % but that the addition of phosphorous singly from 0.20 - 0.40 wt % has a deleterious effect.

Further Davies (3.7.20) showed that ferrites containing 2.0 % Si plus 0.2% P exhibit greater uniform elongation with tensile strength comparable to conventional HSLA steels. Increasing the tensile strength by grain size reduction will lead to loss of ductility and as has been said in the preceding sections the inclusion shape also has an effect and therefore they must be modified.

it is therefore apparent, from the above that for good properties to be achieved in Dual-Phase steels stringent control of alloying additions must be adhered to. Addition of Si in the range of 1 - 2% and high Manganese with Al or V to tie up the nitrogen and some of the carbon together with Mo and Cr to delay the pearlite formation and stabilize the austenite are necessary. However it has also been shown in (3.7.11) that silicon content greater than 1.5 wt % is undesirable, in the case of ARDP steels, as it speeds up the formation of ferrite and pearlite during coiling in such a way that the range of acceptable cooling rate on a run out table is made narrower when the weight percent is more than 1.5.

3.8 Mechanical Properties and Fracture of Dual-Phase Steel

The stress-strain curve of a Dual-Phase steel is characterised by a low yield strength, continuous yielding and a large strain-hardening from low strain state to high strain states together with a high tensile strength comparable to conventional HSLA steels. Thus a high tensile stress/yield stress ratio is observed. The high n value and uniform elongation provide exceptional ability to distribute strain during forming and allows relatively complex shapes to be formed successfully. However, the observed n values are not single valued, the value at low strain may be slightly higher or lower than that at high strain depending on the volume fraction of martensite present. The yield strength in cold formed components can reach a level comparable to that of conventionally treated HSLA steels. A good combination of strength and ductility is needed to achieve optimum properties and as has been discussed in the last section, solid solution hardening with Si, gave the best combination of strength and ductility.

Figure 3.8.1 gives a comparison of the stress-strain curve obtained for Dual-Phase steel with mild steel and a conventional HSLA steel while in Figure 3.8.2 its work hardening characteristics in relation to the other steels is given by $^{1}/\sigma \frac{d\sigma}{d\varepsilon}$ is shown.

Investigations have been carried out to find out the various properties of the two phases that give control of optimum property of the Dual-Phase steel (3.8.1, 2 and 3). These works showed that the flow stresses are a function of the percentage of martensite independent of its carbon content but depend upon the ferrite grain size as well. They also show that the uniform elongation decreases with increasing tensile strength and that the work hardening parameter n value increases with annealing temperature (increasing % martensite) up to about 850^{o}C then subsequently decreases. The product of UTS and uniform elongation (ε_u) has also been found to be approximately constant up to 20% martensite and then decreases with increasing martensite (3.8.4). Nakaoka et al (3.8.5) have also obtained the same result, explaining this on the basis that above 20% martensite void formation occurs so fast that fibrous fracture supersedes necking thereby impairing the total elongation. Lagneborg (3.8.4), on the other hand, thinks that the observed relationship between UTS x ε_u versus % martensite content results from a linear relationship between UTS and elongation which leads to a parabolic decline of UTS x ε_u with increasing martensite content. His argument can be seen as follows:

Since UTS is proportional to elongation we can say that

$$UTS = \phi \times \varepsilon_u$$

where ϕ is a constant

then since it has been observed that UTS x ε_u is also dependent on % martensite. We could also write

$$UTS \times \varepsilon_u = \phi_2 \times \%M$$

Then substituting we get

$$\frac{(UTS)^2}{\Gamma} = \%M$$

$$\therefore \quad UTS = (\Gamma \%M)^{\frac{1}{2}} \equiv \text{Constant} \times (\%M)^{\frac{1}{2}}$$

a parabolic relationship; where Γ and ϕ_2 are both constants of proportionality.

However it is not quite correct for one to assume as he did that there is an absolutely linear relationship between uniform elongation and UTS. It might be more correct to assume that the relationship between UTS and ε_u is parabolic. Also his assumptions did not take cognisance of the approximate constancy of UTS x ε_u for percentage of martensite up to 20%.

Other experiments have been carried out to compare the influence of V, Nb and Ti in Dual-Phasing HSLA steel (3.8.6, 7 and 8). Their results show that Vanadium steels only have the Dual-Phase characteristics after annealing and air cooling. The strength of Dual-Phase steel is increased if the air cooling after annealing is interupted at low temperature, about 350^{o}C and quenched, as compared to air cooling all the way to room temperature. Better elongation at a constant UTS has also been obtained by

annealing above A_3 as compared to annealing below it (3.8.9). Uniform elongation remains relatively constant with decreasing grain size in pure iron. A small ferrite grain size is considered favourable for good combination of UTS and elongation, and has been observed to have marked effect on the properties. When coarse grain ferrite/martensite microstructures (50 - 100 μm) are used it was found that they gave inferior UTS/ elongation to typical fine-grained (∿10 μm) Dual-Phase steels (3.8.10). It has also been reported that when this steel was alloyed with Si and P together the constancy of n value with grain size disappeared (3.8.11).

The independence of flow stress on the carbon content of the martensite, that were earlier observed by Davis (3.8.1) and Rashid (3.8.2), is an unexpected result since it was known that the martensite strength depends linearly on its carbon content (3.8.12). The martensite present in these steels as a result of annealing in the $\alpha + \gamma$ region has a carbon composition approaching the eutectoid value.

Laterly careful experimentation and analysis based on Jaoult and Crussard plot (3.8.13) by several workers (3.8.14-18) have revealed that the martensite carbon content does have an influence on the work hardening rate at low strain but the effect disappears at high strain for all percentages of martensite. For a particular

volume fraction of martensite grain size was also shown to have a similar effect. These observations are shown in Figures 3.8.3 to 5.

Further, the work of reference (3.8.17) showed quite clearly that an inhomogeneous band of deformation, similar to that of Luders band, passed through the sample during deformation, with the exception that strain hardening prior to the passage of this band, is observed, with a positive slope much greater than zero.

Several earlier attempts have been made to give a quantitative explanation to the tensile properties of Dual-Phase steel (3.8.19, 3, 4 and 20). The first attempt was due to Davis (3.8.1). He applied a theory of a composite based on the Law of Mixtures (3.8.21). With this he predicted a linear variation between the tensile strength of the Dual-Phase steel and its volume fraction of martensite. However, it did not determine why the strength should be independent of the martensite carbon content over the range of carbon concentrations Davis studied. Also this theory gave a slightly higher overall strength than was observed. Recently, Koo et al (3.8.22) have attempted to introduce the variation of strength of martensite with its carbon content into this theory and found again that the observed UTS is lower than the calculated one.

This theory, as well as Davies' own, assumed that there is an equal partitioning of both stress and strain between the more ductile ferrite matrix and the harder martensite

and that the two phases obey the equation $\sigma = k\varepsilon^n$. These assumptions are unrealistic. They neglect the different work hardening rate of the phases, the interfacial bonding and interfacial energy between the two phases and the fact that slip will occur first in the weaker phase. They also neglect the possibility of residual stress and relaxation effects in the lattice of the matrix. It is more likely that there will be a non-equal partitioning of both the stress and the strain among the two phases. Later Lagneborg (3.8.4) has attempted to partition both the stress and the strain non-equally but in accordance with the observed stress-strain curves for each phase such that the strain is lower in the martensite than in the ferrite. He too was able to predict a linear relationship between the tensile strength and the volume fraction of martensite and he further deduced that it is better for the martensite strength to be increased rather than that of the ferrite, which is in opposition to what Davies has earlier concluded. He suggested that

a. Uniform elongation increases with Ultimate Tensile Strength of the ferrite

b. Uniform elongation increases with Ultimate Tensile Strength of the martensite

c. Marginal increases in uniform elongation are obtained if the ferrite strength are increased while maintaining the strength of the martensite constant.

Even if the predictions of Lagneborg are correct, much more can be done to strengthen ferrite than can be done with martensite.

Another two very similar approaches to explain the work hardening characteristics of these steels have been proposed by Araki et al (3.8.20) and Tomota et al (3.8.23). Continuum mechanics are used in these models to describe the stress-strain curve of Dual-Phase steel which was built up from the stress-strain curves of each composite phases. Araki et al considered the problem in terms of the increase in internal stored energy due to plastic deformation, taking into account the interaction energy between the two phases via the Eshelby transformation strain tensor. Tomota et al on the other hand divided the deformation progress into 3 stages

i) when only the softer phase alone deforms plastically,

ii) when the internal stress accumulated in the hard phase as a result of the previous deformation of the soft phase just causes it to undergo plastic flow, and finally

iii) when both the soft and the hard phase are deforming together.

At each stage stress equilibrium conditions are derived.

Bhadeshia et al (3.8.24) have examined the applicability of Tomota et al's theory to a high silicon Dual-Phase steel and found that it gave a better result than Mileikos theory of composite used by Davies above. However, its success depends critically on the strain distribution assumed between the two phases. Araki et al made allowance for strain partition between the two phases and took account of relaxation effects resulting from grown-in dislocations close to the hard second phase. A comparison between their theoretical results and experimental data gave good agreement only for volume fractions of martensite below 20% and they too concluded, like Davies, that the way to improve the ductility of high strength Dual-Phase steels is to improve the tensile strength - uniform elongation relationship of the softer phase (ferrite) and to strengthen the hard phase as much as possible, but to control the level of martensite to not more than 20%. The commercially available alloys fall within this range.

Recently Rigsbee et al (3.8.3) have attempted to explain the high initial work hardening rate by suggesting that it is due to the existence of retained austenite, which they showed to be present along with the martensite in their oil quenched steels. Their explanation was that the retained austenite transforms into martensite during straining to provide an increase contribution to strength. Although they showed a correlation of the work hardening exponent n with retained austenite and with the mean austenite interparticle spacing, this idea was not too convincing in that the retained austenite was about 10%

of the total volume fraction of the second phase and it decreased to less than 3% of this amount within the first 10% strain. Therefore any later contribution to hardening rate would not be from this sourse and so its regime of influence is therefore restricted to low strain levels. It will contribute to raising σ whilst not sustaining a high $d\sigma/d\varepsilon$ to compensate at high strains.

In the range of 1-7% plastic strain Rigsbee et al concluded that work hardening is primarily due to strengthening of the ferrite matrix by dislocation structures generated during the continuous transformation of the retained austenite to martensite while from 8% strain onwards the material behaves like a composite and work hardens by the developed non-homogeneous internal stress fields, which effectively restrict dislocation motion. The increase in plastic stability then will give an attendant increase in uniform elongation.

A suggestion has also been put forward (3.8.1) that the sustained work hardening is due to the high purity polygonal ferrite formed in Dual-Phase steels. This suggests that, according to the findings above and those of (3.7.17), that the limit to work hardening is due to the advent of fracture processes. The nucleation of voids contributes negatively to work hardening in a metal.

The two mechanisms of crack initiation by second phase particles that are generally encountered in steel have been discussed in section 3.3 (internal fracture or decohesion of particle). One or both mechanisms may operate for a specific particle in a matrix. For low carbon steels it has been observed that the crack initiation sites are the iron carbide particles and for elongated carbide particles the fracture initiation mode is by internal fracture (3.8.25 and 26). Gladman et al (3.8.27) have also reported evidence of negative contribution to work hardening from voids nucleated at sulphide inclusions in steel. Also internal fracture has been observed in spherical carbides (3.8.28) but some decohesion has also been reported (3.8.29). It is therefore necessary to have stringent control of cleanliness and to modify the shape of the inclusions present in Dual-Phase steels, to have good properties. Ferrite free of hard inclusions will also harden considerably further while the martensite present in Dual-Phase steel will offer additional resistance to deformation and the stress generated across the martensite/ferrite interface might eventually either crack the martensite (this is more likely to happen with as quenched martensite) or open up the interface (tempered martensite).

Stevenson (3.8.30) has observed that, in the as quenched TMT Dual-Phase steel, fracture is initiated by internal fracture of the martensite colonies which then progress through the ferrite as a very sharp crack. When the steel is tempered the cracks are initiated by decohesion of the

propagating through the ferrite are blunted. He also observed a similar effect of dissolved carbon content on the sharpness of the propagating crack in the same material, which he conditioned below the eutectoid temperature. Therefore, tempering both increases the martensite fracture stress and decreases the martensite/ferrite interfacial energy. This is because at the beginning of tempering martensite redistribution and segregation of carbon atoms occur with little precipitation taking place. Segregation will most likely occur at the twin boundaries, lath boundaries and martensite/ferrite interface. This will reduce the interfacial energy between martensite and ferrite with the result that the low interfacial energy will lead to martensite particle being resistant to fracture.

The plastic failure of Dual-Phase steel is characterised by little diffuse necking compared to mild steel, suggesting that they do not become unstable prior to fracture, i.e. the limit strain is not determined by the work hardening behaviour but rather by the intervention of fracture. The amount of diffuse necking is governed by the material's strain-sensitivity index m, as has been discussed in section (3.4). Since m influences the advent of a neck and thus the development of a triaxial strain in the neck which will also influence the propagation of the crack it is therefore evident that this effect of tempering is to reduce the dissolved carbon content which increases the m value, thereby assisting the propagating crack to blunt. From the above it can be inferred that no thorough understanding of the mechanical

behaviour of Dual-Phase steels has yet emerged and that it is imperative for good properties in Dual-Phase steel to make the martensite tough enough to resist fracture to high stresses and that elements which can segregate to, and weaken, the interfaces be strictly controlled, if not eliminated completely.

FIGURE 3.8.1 Nominal stress-strain curve for a dual-phase steel (D.P.), a mild-steel and a conventional hot-rolled HSLA steel (HSLA) (reference 3.6.10).

FIGURE 3.8.2 $\frac{1}{\sigma}\frac{d\sigma}{d\varepsilon}$ as a function of strain for the three materials represented in Figure 3.8.1. Instability in uniaxial tension occurs when $\frac{1}{\sigma}\frac{d\sigma}{d\varepsilon} = 1$ (reference 3.6.10).

FIGURE 3.8.3 Engineering stress-strain curves of Fe-C-Mn-Si steels with dual-phase structure. Martensite carbon contents and martensite volume fractions as shown. Constant grain size = 100 μm.
Steel composition HT.1: 0.052 C; 0.9 M; <0.01 Si; 0.02 S; <0.002 V; 0.005 Ti; 0.013 P; 0.006 Al; 0.0038 N.
HT.6: 0.11 C; 0.78 Mn; 0.28 Si; 0.015 S; <0.002 V; 0.003 Ti; 0.012 P; 0.074 Al; 0.0049 N
(reference 3.8.18).

FIGURE 3.8.4 Stress-strain curve of steel HT.1 according to Jaoult-Crussard analyses (reference 3.8.18).

FIGURE 3.8.5 Jaoult-Crussard analysis of a series of stress-strain curves for steel HT.1 showing the effect of grain size on the Initial Yielding (reference 3.8.17).

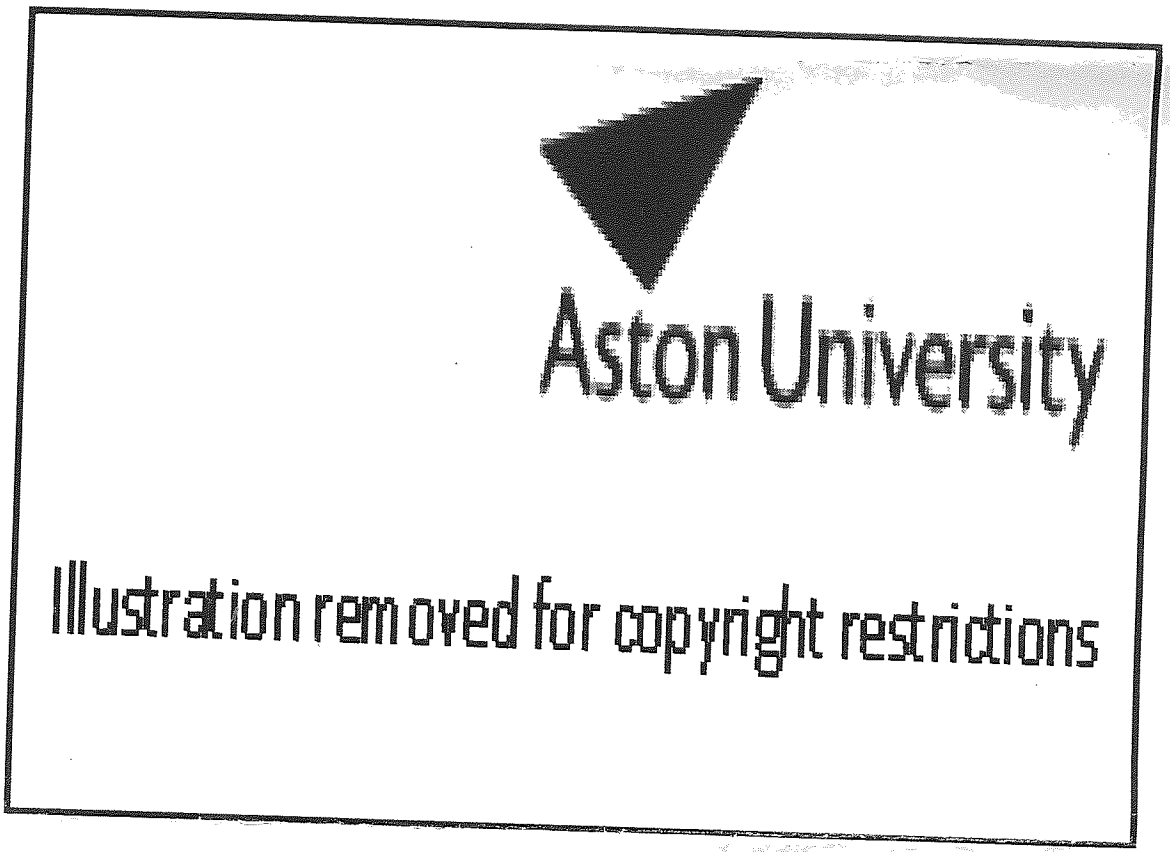
Aston University
Illustration removed for copyright restrictions

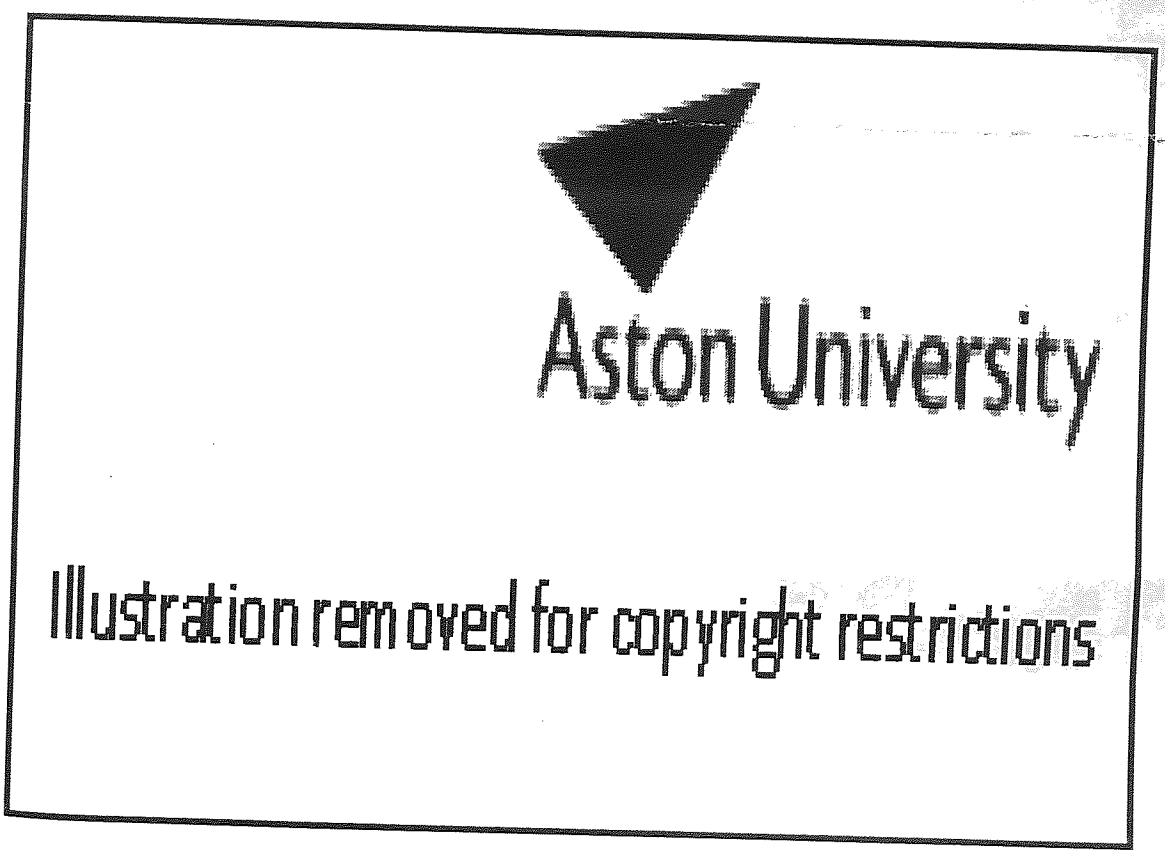
Aston University
Illustration removed for copyright restrictions

3.9 Current Applications of Dual-Phase Steels

Formability of most High Strength steels is poor compared to mild steel and therefore they have limited use in automobile applications. The superior formability resulting from Dual-Phasing them has enhanced their utilisation potential for auto parts considerably. A few investigations have been carried out to evaluate the performance of these steels in forming auto parts such as:

a. wheel discs and rims
b. bumper reinforcements
c. face bars and jack posts
d. pulleys
e. steering coupling reinforcements

and in recent years some General Motors' cars have been fitted with them. The majority of the work done in this arena has been carried out by M.S. Rashid (3.9.1, 2 and 3) on the GM980X series of steel. These are Vanadium strengthened Dual-Phase steel which is an offspring of the SAE980X series, a product of Jones and Laughlin Steel Corporation called VAN-80.

The trials were carried out using existing production tools and methods that were designed for plain carbon steels. A total of 25% weight reduction has been achieved using these steels in an average sized car. Formability was assessed by visual inspection of the formed components for wrinkles, surface cracks, thinned areas or necking at high strain regions together with

measurement of the main outline of the components to check for dimensional accuracy. The strength developed in the formed parts was also evaluated by standard tensile tests to failure. The results so far have been satisfactory.

In a recent comparative study, reported in (3.9.3), of formability of SAE950X, SAE980X and GM980X (3.9.4) it was concluded that SAE950X and SAE980X do not have enough formability to make discs unless parts and tooling design modifications are made, whereas a trial with GM980X was successful without modification of production tools as well as using the same lubrication and manufacturing procedure that is used for mild steel. Kary (3.9.5) has also observed the same result in an attempt to reduce weight of automobile bumper systems. In his work the weight reduction in the bumper system was achieved by increasing the face bar strength and stiffners to eliminate reinforcement. It was shown that using SAE955X and altering the shape of the face bar, allowed a gauge reduction of the face bar without reducing the impact strength of the bumper system in a 1135 kg bar. The work indicated that steel with high formability is needed and hence existing HSLA steels like the SAE980X cannot be used whereas the GM980X proved successful but spring back was found to be higher compared to plain carbon steel. The bumpers were found to perform better than current production components in an 8 km/hr barrier and pendulum impact test. The face bars are generally polished flat after

forming in a plating solution. Two plating systems are currently in use, i) Cu-Ni-Cr, ii) Ni-Cr. The latter requires a smooth final surface finish while the former can tolerate some surface roughness to a degree. Any slight roughness will be levelled out in this system. GM98OX bumpers have been successfully plated in both systems with satisfactory results but occasional surface roughness is observed in the Ni-Cr system.

In wheel rim forming trials, Rashid (3.9.3) has found that with HSLA steels large numbers of rims failed usually during flaring and the final expansion operations. Fracture occurs in the weld heat affected zone (HAZ) a few millimeters from the weld centre line. The weld area was found to be harder than the base metal in all steels with higher hardness being recorded for high strength steels. Examination of SAE98OX rims at different stages of manufacture showed that a small volume of HAZ may have been annealed during welding to a lower yield stress than the base metal yield stress. These annealed areas formed narrow parallel zones at about 4 to 5 mm on either side of the weld line. Therefore during roll forming operations these annealed zones will work-harden to the yield stress of the starting metal but will have to suffer larger plastic deformation before the starting metal will yield; hence localised neck systems often form in this area leading to rejects. However, the forming trials of the GM98OX were much more

successful. He also performed some fatigue tests on samples of this steel at a load 50% higher than normally specified for mild steel and found that GM980X had double the fatigue life of the heavier plain carbon steels even at this higher load. A recent survey (3.7.6 and 7) shows that by 1984 something in the region of 0.9 million tons of Dual-Phase steels will be required by the United States automobile industries.

3.10 The Strength Differential Effect in High Strength Steels

When high strength martensitic steels are tested in tension and compression it is found that their strength in compression is considerably greater than that in tension. This phenomena, now known as strength differential effect (S-D effect for short), is found to persist up to very high strain level, as high as 0.6 in some steels, and therefore cannot be accounted for by the normal Bauschinger effect.

It has been reported in the literatures that the effect was observed as early as 1927 by Siebel and Pomp (3.10.1) and by Polakowski (3.10.2) in 1951. It is only recently that its occurrence has been widely studied and some attempts made to find an explanation for it. However, the S-D effect found in ferrous-martensite steel should not be confused with the pseudo-S-D effect that is found in T-D nickel by Olsen and Ansell (3.10.3) which can be ascribed to the relative ease of void formation at the Thoria-Nickel interface in tension as compared with compression. The reason why this should be can be ascertained from the work of Goodier (3.10.4) who showed that a spherical non-deforming particle embedded in a deforming matrix acts as a stress concentrator, such that in tension the stress acting around its interface with the matrix is raised by approximately 1.93 times the applied stress while the same stress under compression loading is only 0.21 times the applied stress. For such material both the compression and tension (σ-ε) curve merge after some plastic

strain (∿1%) whereas for a genuine S-D effect the difference in stress level persists to high plastic strain.

It is now known that the effect does not only occur in regular quenched and tempered martensitic structure (3.10.5) but also it exists in bainitic, widmanstatten (or accircular) ferrite-pearlite structures, ultra-fine grained martensite, maraging steels (3.10.1), (3.10.6) and 3.10.7) and in a ferrite/martensite micro-structure (Dual-Phase steel) (3.10.8). Observations so far show that, with the exception of some maraging steels, all ferrous structures with a high dislocation density after transformation seem to show an (S-D) effect (3.10.1).

The following factors have been found to influence the magnitude of the (S-D) effect:

1. At a given plastic strain the (S-D) effect decreases with increasing tempering temperature and does not disappear until the tempering treatment is done above 650°C (3.10.9) and (3.10.6)

2. The magnitude of S-D increases with carbon content in the martensite such that: (3.10.5) and (3.10.1)

$$\Delta\sigma_{(S-D)} = |\sigma_{COMP}| - |\sigma_{TEN}| = 131.1 \text{ (wt percent C) } MP_a.$$

even though Spitzig et al have found no dependence of S-D on carbon content (3.10.10).

3. The S-D increases appreciably with decreasing temperature (3.10.11) below room temperature down to $77^{o}K$.

4. The (S-D) is insensitive to hydrostatic pressure (3.10.11).

5. During plastic deformation under atmospheric condition there is a measurable plastic volume expansion which is larger for materials showing high (S-D) effect than for those showing small (S-D) effect (3.10.10).

6. The (S-D) effect can be separated into athermal and thermally activated components with both being superimposed on each other at lower temperature. The possible sources of the athermal component being due to perhaps non-linear dislocation/carbon atom interaction or non-linear elastic effect.

The above observations have prompted a host of hypothesis to be put forward, trying to explain the origin of the S-D effect. They are:

1. Effect of friction between the platten of the testing machine and material interface during compressive loading. This idea has been dismissed by the work of Rauch and Leslie (3.10.1) and Chait (3.10.6).

2. Residual stresses arising from quenching and phase transformations deformation. This is not likely as any effect of residual stress will be destroyed after some plastic strain and it has been shown that rolling by as much as 25 percent did not remove the (S-D) effect (3.10.7).

3. Bauschinger effect arising from the compressive stresses set up in the hard-phase as a result of the matrix accommodating the volume expansion of the austenite → martensite transformation. This too, as in 2, should disappear with strain.

4. Internal microcracks arising from the hardening quench treatment of high strength steels. Possible, but tough ultra-fine-grained martensitic steel as well as fine-grained ferrite/martensite structure have been shown to exhibit (S-D) effects.

5. Non-linear elastic interaction effect between interstitial carbon solute and grown in dislocations (3.10.9).

6. Difference of elastic moduli in compression and tension (3.10.13).

7. Volume expansion occurring during plastic deformation.

8. That the thermally activated component arises from a dilatation which occurs during the activation process for dislocation motion causing an increase in the

activation energy under compressive loading and a decrease under tensile loading. This idea is supported by the observations of Fletcher et al who put forward the idea.

A review of the ideas 1 to 5 and 7 have been given by Hirth and Cohen (3.10.9) and their shortcomings pointed out. They themselves offered the non-linear elastic interaction hypothesis. Though their idea is able to account for about 3-6 percent of the observed (S-D) effect it does not explain the temperature dependence. They believe however that their idea should be taken as a plausible one requiring further refinement in the assumed interatomic potential energy of the iron/carbon bonding and also the dislocation strain field among other things.

A not too dissimilar hypothesis to that of Hirth and Cohen is that of Pampillo et al (3.10.13) based on the fact that the internal stress contribution to the flow stress of metals σ_i is proportional to the shear modulus μ (i.e. $\sigma_i = \alpha\mu$, where α = constant) and that the elastic modulus at large strains is not constant but depends on strain in such a way that it is smaller in tension than in compression because of the asymmetry of the interaction potential between atoms. Their hypothesis gave a reasonable explanation of the observed carbon and dislocation density dependence of S-D effect and of increase

at low temperature. It has, however, been critisised by W.C. Leslie (3.10.4) on account of the difficulty in separating the yield or flow stress σ into its two components of internal stress σ_i and thermal effective stress σ^* ($\sigma = \sigma_i + \sigma^*$) and the fact that the hypothesis of Pampillo et al predicted an (S-D) effect in titanium-gettered iron where non is detected. They have given an explanation of how the separation of σ into σ_i and σ^* can be achieved and gave a correction factor to their earlier derived formulae (3.10.15) and further explained that the S-D observed in titanium-gettered iron may very likely be due to friction effect at the platten.

An (S-D) effect can also occur from an odd dependence of the yield condition on either of first and third stress invariants defined by

$$J_1 = \sigma_1 + \sigma_2 + \sigma_3$$

$$J_2^1 = ({\sigma_1}^2 + {\sigma_2}^2 + {\sigma_3}^2)/2$$

$$J_3^1 = ({\sigma_1}^3 + {\sigma_2}^3 + {\sigma_3}^3)/3$$

$$\sigma_i^1 = \sigma_i - \frac{\sigma_1 + \sigma_2 + \sigma_3}{3} = \sigma_i - \frac{J_1}{3}$$

$$= \sigma_i - P \text{ (hydrostatic pressure)}$$

σ_i = Principal stresses in the i^{th} direction,

and the yield function f is a function of J_1, J_2^1 and J_3^1; $f = F(J_1, J_2^1, J_3^1)$

The signs of J_1 and J_3^1 depends on the sign of the stress components and therefore could be different in tension and compression. Furthermore according to the normality flow rule of Von Mises;

$$\frac{d\dot{\varepsilon}_i^p}{dt} = \dot{\varepsilon}_i^p = \lambda \frac{\partial f}{\partial \sigma_i}$$

the plastic volume change during deformation must be zero unless yielding depends on the mean stress J_1. This is obvious from

$$\dot{\varepsilon}_i^p = \lambda \frac{\partial f}{\partial \sigma_i}$$

The rate of plastic volume change $\dot{\delta}^p = \dot{\varepsilon}_1^p + \dot{\varepsilon}_2^p + \dot{\varepsilon}_3^p$

$$\therefore \dot{\delta}^p = \dot{\lambda}\left[\frac{\partial f}{\partial \sigma_1} + \frac{\partial f}{\partial \sigma_2} + \frac{\partial f}{\partial \sigma_3}\right] \equiv 3\dot{\lambda}\nabla.f = 3\lambda \frac{\partial f}{\partial J_1}$$

$$\nabla \equiv \left(i \frac{\partial}{\partial \sigma_1}, \; j \frac{\partial}{\partial \sigma_2}, \; k \frac{\partial}{\partial \sigma_3}\right)$$

$\dot{\varepsilon}_i^p \equiv$ a vector normal to the yield surface

$=$ the three principal plastic strain rate

So that unless $\frac{\partial f}{\partial J_1} \neq o$, $\dot{\delta}^p \neq o$ either

This idea of Drucker (3.10.12) have been examined by Spitzig et al (3.10.10) while they found an (S-D) effect in the steel tested under hydrostatic pressure, the predicted plastic volume change according to the normality flow rule is considerably higher than what they are able to measure (predicted = 0.075; measured 0.005).

Another possibility for the occurrence of an (S-D) effect in an isotropic material is that that may arise if the internal shear mechanism of plastic deformation is directionally sensitive (3.10.16) (i.e. sensitive to the sign of the shear stress). For example, twinning in an F.C.C. metal occurs by $\{111\}\langle 11\bar{2}\rangle$ shear but not by the reverse $\{111\}\langle \bar{1}\bar{1}2\rangle$ shear and for B.C.C. iron it is easier to slip in the forward $\{112\}\langle \bar{1}\bar{1}1\rangle$ twinning direction than in the opposite. Hosford and Allen (3.10.16) have used this idea to calculate the yield locus for randomly oriented F.C.C. metals deforming by $\{111\}\langle 11\bar{2}\rangle$ twinning and they concluded that an (S-D) effect should be expected in any material deforming in this mode. However, their calculation for B.C.C. shows a result in opposition to what have been reported in literatures and they concluded that the reported (S-D) effect in this type of metal must be due to a pressure sensitivity of yielding in accordance with the idea of Drucker (3.10.12).

From the foregoing it is then apparent that no proper explanation of the S-D effect can be said to have emerged even though some of the ideas do predict an S-D effect. However it is likely that several of the above processes 5 to 8 might combine together to give an effective S-D effect of the correct magnitude. The magnitude of the volume change measured in tension and compression are the same and therefore indicate that the volume expansion and (S-D) effect did not arise from internal preferential

microcracking in tension. Another way in which volume change (or density change) can occur is if vacancies or dislocations are generated during plastic deformation. Spitzig et al (3.10.10) have used this idea to show that, for the 4310 and 4330 martensitic steel they studied, this is quite another plausible cause as only an increase of about 15% in the dislocation density at 4% plastic strain will be necessary to account for the observed S-D effect. This idea, too, might go with the ferrite/martensite structure where the introduction of geometrically necessary dislocation during plastic deformation is expected.

PRESENT WORK

Chapter 4 Experimental Procedure.

4.1 Material Used:

The major part of this work was carried out on a steel supplied by Dofasco steel corporation of Canada which was manufactured according to the specifications of Climax Molybdenum Company. The compositions of this steel are given in table 4.1 while its production schedule and continuous cooling curve are shown in figure 4.1 and 4.2 respectively.

A second steel, an (Al-Si) killed cold rolled annealed steel was also used to determine the influence of dual-phasing on its R value. This steel came as a strip of 0.56 mm thickness while the Dofasco steel was supplied in the as hot rolled dual-phase condition in the form of a sheet approximately 3.40 mm in thickness.

Two other steels, a Ti HSLA steel and a mild steel were also used to compare the as-received dual-phase steel property to conventional steels. The chemical compositions of these are also given in table 4.1.

4.2 General Preparation and Heat Treatment of Specimens

4.2.1 Cold Rolling

Three rolling schedules were employed in this work, All to reduce the initial thickness of the Dofasco steel to 0.75 mm; approximately 78% reduction.

The starting materials were first of all cut into wide parallel strips, parallel to the as-received rolling direction, before the rolling schedules which were:

1. Some strips were cold rolled 50% after which they were annealed at 675^{o}C and air cooled. They were subsequently descaled and then finally cold reduced further to 0.75 mm. At each stage of cold rolling passes whenever the temperature of the sample became too hot to touch, it was kept under running water for some time, then dried, before continuing rolling.

2. Same as in 1 but the annea.ling temperature was 700^{o}C.

3. No intermediate anneal was given otherwise the same procedure as in 1 was used.

After the cold working standard 165.1 mm (6½ inches) tensile specimens were machined from them. Small metallographic samples were cut along with the tensile for subsequent metallographic work or alternatively a small piece was eventually cut from the tensile grip end of the samples after they had been heat treated. These were then used for optical metallography.

4.2.2 Heat Treatment

Apart from the tensile samples that were cut from the cold rolled materials some tensiles were also cut from the as-received sheet steels. The heat treatments employed were chosen to give a variety of ferrite grain sizes and percentages of martensite. The materials were all coated with BERKATEKT 204 paint, supplied by Steetley Minerals Ltd., of Manchester, to prevent severe oxidation during high temperature heat treatment. The entire materials were then divided into two groups for heat treatment as follows:

Group 1: These were subdivided into two further groups a and b both of which had the same final means of obtaining dual-phase microstructure given to them. This involved inter-critical annealing at 780°C for two minutes followed by water quenching.

Sub-group 1a: were Austenitised at 950°C for two minutes then held at various temperatures below AC_1 [700°, 620° and 540°C] for either 4 or 10 minutes and then slowly cooled to ambient temperature before the final dual-phasing treatment above. These treatments gave different ferrite grain sizes in ferrite-pearlite structures.

Sub-group1b: were Austenitised at the same temperature followed by rapid water quenching to full martensite. These were then tempered for 24 hours at 700°, 620°

and 540°C the same temperatures as above, and air cooled to room temperature before dual-phasing at 780°C. These treatments too permitted various degrees of grain growth to occur to give different final grain sizes.

These above treatments also altered the carbide distributions in the samples thus even though the same final intercritical temperature (780°C) was employed for dual-phasing them the same percentage of martensite was not obtained.

Group 2: These were also subdivided into two groups a and b.

Sub-group 2a: were Austenitised at 970°C for 5 minutes followed by water quenching. They were then heated into the $\alpha + \gamma$ phase field and held there at different temperatures ranging from 740°C to 850°C for holding times of 5 minutes, 10 minutes and 30 minutes followed by water quenching. They were then held at 200°C for 10 minutes and air cooled.

Sub-group 2b were again Austenitised at 970°C for 5 minutes then transferred to a salt bath held at various temperatures in the $(\alpha + \gamma)$ range, from 740°C to 850°C for the same duration as for sub-group 2a, followed by water quenching and subsequently held at 200°C for 10 minutes and air cooled. The Austenitising

treatments were done in either a tube furnace with argon gas flowing through it or in a muffle furnace also with argon flowing. The intercritical anneals were done in a neutral salt bath while the tempering treatments at 700, 620 and 540°C were also carried out in a salt bath. The 200°C treatments were either carried out in a low temperature salt bath or in an air circulating furnace. Extra precautions were necessary when using the high temperature salt baths; specimens that have been previously quenched were carefully dried by blowing air over them to remove excess water and kept in a pre-heating furnace, beside the salt baths, at approximately 120°C for 10 minutes before transferring into the salt baths. These specimens that were given long tempering treatments were wrapped in a mild steel sheet before heat treatment to prevent corrosion of the specimens by the salt.

The small samples for metallographic work were also heat treated along with the tensiles. They were strapped to the middle of the specimens. A chromel-Alumel thermo-couple attached to the centre of the specimens was used to monitor their temperatures at all stages of the heat treatment. The Al-Si sheet steel used for the R value measurement was treated the same way as those of sub-group 2a to get various percentages of martensite and approximately similar

grain sizes to the order ~ 25 μm.

4.2.3 Mechanical Testing

Along with the tensile specimens cut from the as-received material some compression specimens were also cut along the rolling direction. They were 8 mm x 4 mm x 3 mm in dimensions. These were to be used to compare the behaviour of the dual-phase steel under tensile and compressive loading.

The tensile tests were carried out in an Instron machine model 1192 at a cross-head speed of 5 mm/min with a 50 mm gauge marked on them. An Instron type strain gauge was also used to measure the extension. This has a 50% total extension capability. The compression tests were carried out with the same machine but at a cross-head speed of 0.5 mm/min. During this test the specimen height reduction was monitored via a strain transducer attached to the Compression Jig. The jig is shown in figure 4.3. From the load extension curve obtained, values of 0.2% offset yield stress, tensile strength and total elongations were obtained using the relations

$$\sigma = \frac{P}{A_o}(1+e)$$

$$\varepsilon = (\text{true strain}) = \ln(1+e)$$

σ = true stress

P = load

e = engineering strain

A_o = original cross-sectional area

The uniform elongation was taken to be the elongation at the limit of maximum load.

Before testing, the samples were descaled and polished down with a 1200 grade silicon carbide paper. The dimensions of the specimens were measured after the treatment at three places and the average taken. During the compression test a molybdenum disulphide grease (Castrol M3) was used as lubricant between the platte ns and the specimen interface. This was found to be better behaved than PTFE tapes. The layers of PTFE are critical; if too thin a layer is used it is punctured during test and the lubrication breaks down; if on the other hand it is too thick, the specimen tends to rotate in the jig, therefore since this effect was easily overcome by spraying a film of the molybdenum disulphide and brushing on a smear of the grease, that also was used throughout the tests.

To check for thickness effect in the mechanical properties some as-received samples were mechanically ground to different thicknesses and chemically polished after grinding to remove any grinding damage before testing. The chemical polishing solution used was 5%

sulphuric acid saturated with oxalic acid, mixed in the ratio of 3:2 with 40% hydrogen peroxide. The tests were also carried out at a cross-head speed of 5 mm/minutes.

4.2.4 Strain Rate Sensitivity Index

For this the tensile test was started at a cross-head speed of 0.5 mm/minute and then changed to 5 mm/minute at strain intervals (tenfold jump in strain rate). The change in load when this upward change is effected is noted from the load extension curve and the strain rate sensitivity index m calculated from

$$m = \frac{Ln10(\sigma_2/\sigma_1)}{Ln_{10}(\dot{\varepsilon}_2/\dot{\varepsilon}_1)}$$

since $\dot{\varepsilon}_2/\dot{\varepsilon}_1 = 10$ in this test the denominator equals unity.

4.2.5 R Value Measurement

This too was done in a tensile test at various intervals up to strain levels close to the strain at maximum load previously determined for each specimen.

The samples were strained at a head cross speed of 0.5 mm/minute and stopped at each stage to take the width dimensions with a micrometer. A caliper set fixed to the required gauge extension was used to monitor when the gauge marks have reached the required level to stop the progress of the machine cross-head

for measurements to be taken. Again three measurements are recorded and the average observed. From these measurements the R value was calculated using Lankford's relation

$$R = \frac{\varepsilon_w}{\varepsilon_\tau} = \frac{-\varepsilon_w}{\varepsilon_w + \varepsilon_L} = \frac{Ln(w_o/w_i)}{Ln(\frac{L_i w_i}{L_o w_o})}$$

where ε_w, ε_t and ε_L are the true strains in the width, thickness and length directions respectively.

w_o and L_o are the original width and gauge mark spacings respectively, while w_i and L_i stand for the same measurements at the chosen strain levels.

The gauge lengths were measured accurate to $\pm$ 0.02 mm using a sliding vernier caliper while the widths were measured accurate to $\pm$ 0.005 mm with a micrometer.

4.2.6 Strain Hardening Coefficients (n) and Hardening rate

The n value was determined by plotting a log true stress versus log true strain curve for values of true stress/true strain above 8% plastic strain, determined previously by the procedure of section 4.2.3 and taking the gradient. This measurement assumes that the material obeys the equation $\sigma = K\varepsilon^n$. The strain hardening rate $1/\sigma \, d\sigma/d\varepsilon$ was determined for the as-received material from the converted true stress/ true strain curve, at different strain levels from very low

strain to high strain. A log ($d\sigma/d\varepsilon$) versus log (ε_p) curve was also drawn to emphasise the double n behaviour of some dual-phase steels.

4.2.7 Punch Test

A Hille machine was used for this purpose. Circular blanks 70 mm in radius were cut from the as-received Dofasco steel. The blanks were descaled in a xysk-alene mixture for 7 minutes, washed thoroughly under running water and later degreased with inhibisol before they were electrochemically gridded. The grids were 2.54 mm in diameter. To get various positive minor strains in the Hille machine, two conditions were used:

a) Two layers of polythene sheet (0.08 mm thick) plus a machine oil lubricant were used to simulate equibiaxial tension.

b) No lubricant but degreasing the specimen was employed in order to shift the failure site away from the pole of the punch.

The forming limit diagram was plotted by plotting locus of safe points obtained from a graph of major and minor strains across the failure. This gives the failure limit and from the equivalent opposite point technique the fracture locus was determined. The method has the advantage that fewer specimens are

needed than in most other techniques. This technique has been described in reference (4.1). After grid marking the blanks they were rubbed with mineral oil to prevent corrosion until they were ready for testing then they were degreased.

4.3 Metallography

Optical Metallography

The small samples of each specimen were taken after the heat treatments and mounted in bakelite for optical examination. They were mechanically polished on silicon carbide papers down to 1200 grade of paper, then on to diamond pasted wheels where they were further polished down to 6 μ and 1 μ. Final polishing was done on a soft cloth impregnated with 0.3 μ gamma alumina powder and 0.05 μ powder in succession before etching to reveal the microstructure. Various etchants were tried:

1. 2% Nital solution; this does not give very good contrast between the phases. It tinted martensite brown and ferrite remains bright, bainite just slightly darkened but cannot distinguish retained austenite from the rest of the phases.

2. 5% Sodium metabisulphite ($Na_2 S_2 O_5$) solution etch followed by etching in 2%

Nital. The sodium metabisulphite darkens both martensite and bainite but leaves ferrite white. The nital etch reveals the ferrite grain boundaries. Retained austenite is coloured light grey.

3. A mixture of 2 gm $(NH_4)_2 S_2 O_8$
   2 ml HF
   50 ml $CH_3 COOH$
   and 150 ml H_2O.

   It etches martensite and bainite black, colours retained austenite grey and leaves ferrite bright but must be followed with a short immersion in 2% nital to highlight the ferrite grain boundaries, (5 seconds immersion).

4. A solution of 1.4 gm Picric Acid,
   1 gm sodium tridecylbenzene - sulphonate in
   100 ml of distilled water.

   It whitens the martensite, leaves bainite dark grey and ferrite is tanned. It reveals the prior austenite grain boundaries and leaves retained austenite greyish.

5. 1% sodium metabisulphite ($Na_2 S_2 O_5$) in distilled water and 4% picric acid $[C_6 H_2 (NO_3) OH]$ in ethyl alcohol prepared as a 50:50% solution.

It etches martensite white, bainite black and ferrite tanned. Grain boundaries are not strongly etched. A 2 seconds immersion in 2% nital sharpens the ferrite grain boundaries.

However good this etchant may be in showing up the phases more clearly, if present, it requires a lot of careful sample preparation and the solutions should be mixed fresh just before use.

The specimens should be polished down to 1/4 μ first, thoroughly rinsed and washed with tee-pol under a stream of luke warm water then etched first in 4% picric acid solution, then polished with 0.3 μ gamma alumina to remove all the frosted material from the picral etch. Again thoroughly wash under a fast flowing stream of water clean with a soft cloth. Repolish again with 0.05 μ gamma alumina, repeat the washing and dry with meths (not isopropyl alcohol nor acetone; they tend to leave a whitish film on the sample after etching). After this the solution is blended and the sample etched in it for 12 seconds. The prior polishing and etching should be done at least twice. If not a frosted film is again left on

the surface of the specimen.

Etchant number two was used more often. The others were tried to attempt to identify the phases that are present more clearly. No retained austenite was visible is the as-received material not in those processed for mechanical testing. A separate 0.3%C steel was used initially to study the properties of these etchants. The specimens were examined under a Vickers desk microscope or a Vickers projection microscope to check the phases present before tensile testing; where the desired microstructure is not obtained the tensiles were discarded and reprocessed. This procedure was adopted initially to ascertain the effectiveness of the heat treatment methods in getting the required microstructures, so that materials, which were limited in quantity were not wasted. The heat treatment procedures were found to be quite effective. Photomicrographs were taken where necessary to show typical microstructures that are obtained as a result of the heat treatments and that of the as-received materials.

4.3.2 Volume Fraction of Second Phases

These were determined by the point counting technique. A grid 10 cm by 10 cm with lines ruled at 1 cm intervals both vertically and horizontally was used for this purpose. The Vickers projection microscope was set at magnification of 1000x so that 1 μm at this

magnification equals 1 mm. The magnification was checked with a standard graticule, with 1 mm sub-divided into 100 equal parts, supplied with the microscope. At least 25 measurements were taken for each sample made up of 5 fields coming from the long edge of the specimens to the centre, a movement of about 1.7 mm in the as-received material then having reached the centre 10 fields are chosen to either side. For the processed specimens, because they were very thin 5 fields were taken across the specimen and the remainder taken along the central region. This procedure ensures that on the average a large enough number of points are counted to limit the error to around ± 4% using Hilliards and Cahns formula (4.2):

$$\text{Relative error} \equiv \frac{\sigma_{vf}}{v_f} = \sqrt{\frac{1}{P\alpha}}$$

where σ_{vf} = estimated error in determining the volume fraction v_f

$P\alpha$ = number of grid points falling on the α phase.

4.3.3 Grain Size and Mean Interparticle Spacing

The mean linear intercept method was used to determine the grain size, The same grid and magnification was used as above. The mean intercept along both the vertical and horizontal directions were determined and the mean value of the two was taken. For these, too, 5 fields of measurements were taken. In each field 10 lines

measurements were recorded in both directions. Thus a 100 line measurement was taken limiting the relative error to approximately 7% for a 95% confidence limit

$$\text{relative error} = \frac{0.7}{\sqrt{n}} \quad \text{from reference (4.3).}$$

where n = number of measurements.

To determine the mean interparticle spacing, that is the mean surface distance between the hard phases, the procedure of Humphreys and Hirsch (4.3) was adopted. The number of the second phase islands, without discriminating between the phases, per unit area N on the gridded area was counted. By assuming that the islands are spherical, the mean surface interparticle spacings are given by

$$\lambda \text{ in micron} = N^{-\frac{1}{2}}(10^{-4})\mu m$$

4.3.4 Strain Distribution

The method of T. Malkienewicz and S. Rudnik (4.4) was adopted. This method assumes a spherical or ellipsoidal shaped second phase. The ratio of the major and minor axis b/a was determined for the islands.

The same grid as above was used with lines drawn as before horizontally and vertically. Polished specimen etched as before were viewed at a magnification of

1000x. Samples were cut from tensile specimens which had been previously deformed to various strain levels in tension, parallel to the tensile axis. The tensile axis was aligned parallel to the longitudinal axis of the grid. The major and minor axes were measured by positioning a vertical or horizontal line just touching the edge of an island and moving across it to the other side. The position of the vernier scale on the microscope was noted at each step, the subtraction of which gives the distance moved. Five fields were used in each case, each field covering at least 68 islands, thus a total of at least 340 islands are covered for each specimen. The mean of the rates for the as-received Dofasco material, λ_o, was found to be approximately 1.002 so that to all intents and purposes the polygonal structure can be regarded as spherical. The mean strain in the second phase islands after subsequent straining are given by:

$$\varepsilon: \quad (\text{second phase}) = \frac{2}{3} \text{Ln} \left(\frac{\lambda_i}{\lambda_o}\right)$$

That in the ferrite was obtained by subtracting this measured value from the originally imposed strain. This method is preferred because it eliminates the influence of microscope magnification and as long as the particles are fairly spherical it can also eliminte any particle rotational effect. The method has also been successfully utilized by T. Inoue and S. Kinoshita (4.5)

to determine the strain partitioning in a ferrite-pearlite steel deformed in tension.

4.3.5 Electron Microscopy

To examine the structures at higher magnifications, carbon replicas were taken of the as-received specimen polished and etched surface. The specimen was electropolished in a solution of 35.7 gm CrO_3 + 190 ml glacial acetic acid (CH_3COOH) + 10 ml of water, using 25 volt and a current density of 0.1 ampere per cm^2 in a stainless steel electrode beaker. The solution was kept cool by running water constantly through a glass spiral tube immersed in the solution. About 7 minutes polishing time was adequate. It was washed clean under water and dried with meths. The replicas were examined in a JEOL 100B electron microscope at 12 kv and 45 kv. These correspond to a magnification of 4000x and 15000x respectively.

The internal structures were also examined at different strain levels under transmission high voltage electron microscope. For this thin wafers of the materials were cut from the tensile specimens already strained to different levels about 1 mm thick in the longitudinal direction (i.e. parallel to the tensile axis), with a diamond cutting wheel. These were further thinned down first with the chemical polishing solution already described in section 4.2.3. Final thinning was carried out in a Struers electropolishing unit using a polishing

solution containing 8% perchloric acid in glacial acetic acid plus a few drops of H.F. or 6% perchloric acid in 2-butoxyethanol. The resulting thin foils were examined in a high voltage electron microscope at Birmingham University at a magnification of 25,000x and 50,000x.

4.3.6 Fracture Surface Observations

After tensile testing to failure the as-received materials, the fracture face of one half of the specimen was cut and mounted on an aluminium stud for examination in a Cambridge SEM 150. The other half was coated with nickel in an electro-plating solution consisting of 85.5 gm of $NiSO_4 - 7H_2O$, 16.7 gm $(NH_4)_2 SO_4$, 10 gm (H_3BO_3) and 1000 cc of distilled water. A current density of 0.1 amp/cm^2 was passed for 6 hours. Nickel plate was used as anode while the specimen forms the cathode. The solution was continuously stirred with a magnetic stirrer. A length of about 1 cm was cut from the fractured end and sectioned longitudinally. This was then polished both mechanically and by electro-polishing in the chromium trioxide solution above, section 4.3.5. It was then etched in sodium meta-bisulphite solution followed by a few seconds in 4% nital solution. The specimen was then examined in the scanner from the fracture inwards to observe the voids formation and distribution.

4.3.7 X-Ray Diffraction

Pole Figure Determination

A square specimen 25.4 mm^2 (1 inch square) was cut from the as-received Dofasco steel for pole figure determinations. One side of the specimen was surface ground flat to remove about 0.70 mm of material and then chemically polished to remove altogether a 1/4 of its original thickness (to remove 0.85 mm of material). The other side was lacquered during the chemical polishing process.

Pole figures were determined by a counter technique with a Siemens texture goniometer and a Phillips x-ray machine and counting equipment using a scintilation counter at 900 volts.

{200} and {222} pole figures were determined using a molybdenum tube running at 50 kv and 20 MA with a Zr filter.

Schulz reflection method was adopted (4.6). The sample was simultaneously rotated about the rolling plane and the normal to the rolling plane in steps of 5^{o}/minutes. In this way the centre of the pole figure was covered outward spirally up to approxi mately 80^{o}. The peripheral regions of the pole figure, which require a transmission technique, were not covered by the scan.

Checking for Retained Austenite

The presence of retained Austenite was checked for by quantitative x-ray diffractometric technique. The same x-ray filter and conditions that were used above were also used here. The sample, a small strip of the as-received steel which has been previously cleaned by pickling in xyskalene mix to remove surface contaminants was scanned at a rate of 1^{o}/minutes. This technique is accurate to the order of 0.5 volume %.

Chapter 5 Experimental Results and Observations

5.1 Optical Microstructure

The microstructure of the as-received material is shown in Figure 5.1. The as-received material comprises 20% second phase of which 14% is martensite and 6% bainite. The heat treatment of group 1 materials gave two distinct microstructures; in one of which the martensite appears as discrete separate islands, called the disconnected microstructure. This came largely from group 1a heat treatment and it is shown in Figure 5.2.

The second microstructure is one in which the martensite islands extend to join each other in places and this was denoted as connected microstructure and is shown in Figure 5.3. This came largely from group 1b heat treatment. However, there were a few samples from this group that showed a disconnected microstructure. These came from the batches that were tempered at 620^{o}C and 700^{o}C. The remainder of the heat treatment gave disconnected microstructures.

5.2 Tensile Results

All the materials tested gave a continuous stress/strain curve. In figure 5.4, the stress/strain curve for the as-received materials is compared to that of Ti HSLA

and mild steel whose compositions are given in Table 4.1. Figure 5.5 shows the work hardening characteristics of the dual-phase steels while Figure 5.6 depicts the double work hardening behaviour via a Jaoul-Crussard plot. Table 5.1a and b shows the mechanical properties obtained from the processed steels. Figure 5.7 shows the variation of the yield and tensile strength for the connected and disconnected microstructure of Table 5.1a, with grain size. Figure 5.8 shows their variation with percentage martensite. No special distinction was considered to exist in their tensile strength versus percentage martensite behaviour in Figure 5.8 and therefore a single line was drawn through the points. The connected microstructure did not show any variation of yield strength with percentage of martensite but it does with grain size while the disconnected ones show a gradual increase in yield strength with percentage of martensite. Because the range of grain sizes covered for the connected microstructure is not sufficient to justify extensive comment these results were not considered further.

In order to separate the effect of martensite content from that of the grain size the results of the disconnected microstructures in Table 5.1a and b were combined. These cover a range of martensite from 9.0 to 35.0 per cent and a grain size range from 3.0 μm

25 μm. Multiple regression analysis was carried out on these results using a computer program UA13 available from University of Aston Computer Centre. The following equations were obtained:

$$Y.S = (14.84 + 0.23\%M + 0.03d^{-\frac{1}{2}})kg/mm^2 \quad (5.1)$$

$$T.S = (30.98 + 0.07\%M + 0.09d^{-\frac{1}{2}})kg/mm^2 \quad (5.2)$$

$$e_u = (8.18 - 0.11\%M + 0.03d^{-\frac{1}{2}})\% \quad (5.3)$$

These equations were then used to plot the graphs of Figure 5.9 to 5.11 fixing the values of the grain size at 8 μm and the martensite at 20% in turn. The equations indicate that the grain size affects the tensile strength more than the percentage of martensite while the reverse is true for the yield strength. Increasing the martensite content can be seen to be detrimental to uniform elongation. The influence of the mean surface to surface island spacing (λ) is also shown in Figure 5.12. The yield strength does not appear to change significantly with variation in λ. It remained almost constant over the range of λ observed. The tensile strength on the other hand decreases much more rapidly with increasing λ over the range observed.

5.3 Effect of Cold Rolling on Tensile Deformation

To ascertain whether the deformation under rolling condition is the same as under tension, some as-received materials were cold rolled 10, 15, 20 and 25%

before being tensile tested. The resulting tensile stress/strain curves are plotted against that of the as-received material.

The prior cold reductions are converted to their equivalent tensile strain assuming uniaxial stress condition exists during tensile testing; therefore the reduction must be multiplied by $2/\sqrt{3}$ to get the equivalent strain in tension. The resultant curve is shown in Figure 5.13 and it suggests that the deformation under rolling is not different from that under tension.

5.4 Strain Distribution

The result of these measurements is shown in Figure 5.14 showing that very little deformation of the hard phases that are present in the as-received material took place during straining up to quite high levels.

However metallographic techniques are not sensitive enough to determine microstrains which may be important.

5.5 Effect of Straining on the Microstructure

Figure 5.15 shows the stress/strain curve obtained in tension and compression of the as-received material. The stress/strain curve obtained from compression testing after prior tensile strains are also shown on the same figure, curves A to E. Figure 5.16 shows the transmission electron micrographs of the as-received material and those given prior straining in tension

at 5%, 10%, 20% and 25% respectively. From the micrographs, it can be seen that very little deformation, if any, of the hard phases occurred until quite high strain levels corroborating the result of section 5.4.

Curves A and B are seen to still climb above the as-received tension curve even though they yielded at lower stress level than the tensile pre-stress. Curves C, D and E are backing off from the as-received tension curve showing permanent softening. In the necked region the hard second phase islands are seen to have elongated and aligned with the tensile axis. The load carrying capacity drops quickly after this has happened with subsequent rapid generation of voids at the hard phase/matrix interfaces.

Overall the results also show that a strength-differential effect characteristic of high strength martensite steels exists in this dual phase steel and it is further considered in the next section.

5.6 Strength-Differential Effect

The strength-differential effect was further investigated by taking both tensile and compression samples at $22\frac{1}{2}^{o}$, 45^{o}, $67\frac{1}{2}^{o}$, 30^{o}, 60^{o} and transverse to the rolling

direction in the plane of the as-received material and tested as before. The results of these tests are shown in Figure 5.17. In all cases the compressive strength is higher than the tensile strength. However, the $22\frac{1}{2}^{o}$, 30^{o} and the 60^{o} samples show distinctly higher (S-D) effect than the remaining angles particularly at low strain levels.

To further investigate this effect, as-received samples were annealed in the ($\alpha + \gamma$) phase field to have different percentages of martensite. This was to clarify whether the effect is due to residual stresses set up as a result of rolling schedule during production of the as-received material before coiling.

A dimensionless constant defined as

$$\Delta_{SD} = 2\left\{\frac{\sigma_c - \sigma_t}{\sigma_c + \sigma_t}\right\}$$

at 0.05 strain level was used to evaluate the results of this test. Figure 5.18 shows that the value of the $\Delta(S\text{-}D)_{0.05\varepsilon}$ increases linearly with increasing percentage of martensite and it is also found to be independent of grain size. Furthermore to ascertain whether the effect should be associated with the presence of the hard phase or not, samples were heated to $900^{o}C$ for 10 minutes and furnace cooled to ambient temperature over a 20 hours period by dropping the temperature gradually $50^{o}C$ every 90 minutes until it reached $500^{o}C$, when the furnace was switched off.

The samples were previously coated with Berkatekt 204 paint to prevent decarbonization during heating. The result of both the compression and tension test on these samples is shown in Figure 5.19. Clearly these results show the presence of the yield point in this material which has been masked before, and there was no strength differential present. This is the expected result and it gave a vindication of the testing technique employed in this study.

Carbon replica photomicrographs were taken at 4000x and 15,000x to show the microstructural features present after this treatment, apart from the ferrite.

These micrographs are shown in Figures 5.20a and b. The resultant microstructure is a ferrite mixture and no martensite is present in the material after this heat treatment.

5.7 Return of Yield Point and Ageing

The as-received dual phase steel has a rounded stress/strain curve. When it was aged at different temperatures, 100°C, 200°C, 220°C, 250°C and 300°C it developed a yield phenomenon after sometime at temperature. The time it took for the yield point elongation to reappear depended on the ageing temperature.

A plot of the logarithm of the ageing time for the return of the yield point versus the reciprocal of the

absolute temperature is shown in Figure 5.21. This shows an Arrhenius type of relationship. The gradient gave an activation energy for the process of return to be:

$$Q = 78.7 KJ/mol.$$

The value is comparable to the activation energy for carbon diffusion in pure-iron which is - 80.3KJ/mol. (5.1). The observation in this material is different to what has been observed for a Vanadium-bearing dual phase steel by Davies (5.2). He observed Q for that steel to be 138 KJ/mole. The explanation given for such a high value of activation energy was that it is due to the presence of V atom clusters in the Vanadium bearing dual phase steel. These V atom clusters are formed due to the dissolution of vanadium carbide precipitates during the intercritical anneal he employed 740-820^{o}C. This will not happen in the steel studied here and the ferrite prior to ageing should be clean. It was also noted in a preliminary study, that the higher the volume fraction of martensite at a constant grain size and also the longer it takes for the return of the initial yield phenomenon. An example of the dependence of percentage martensite on yield return is shown in Figure 5.21c.

In Figure 5.21b is plotted the yield and tensile strength for the different treatment temperatures versus treatment time. The points representing the 100°C treatment values show a gradual decrease of the yield strength but not very noticeable change in the tensile strength values. At the other temperatures the yield strength increased above the as-received value but for the tensile strength there was a large scatter of values. In particular the 220 and 250°C values stand much below these at 100, 200 and 300°C. This behaviour may be a reflection of the tempering processes of the martensite islands.

5.8 R value Measurements

The possibility of developing higher R values in dual phase steels than are obtainable in conventional HSLA steels, was investigated. The cold rolled and annealed AL-Si killed steel was converted to a dual phase microstructure by intercritical annealing followed by water quenching. The R value resulting from this treatment measured in the usual manner is compared to that of the as-received steel in Figure 5.22. The R value measured at about 10% elongation is very close to unity in all cases.

The initial values for the two samples starts at a high level comparable to the as-received material while the

third sample started below unity but soon approached the same level as the others as strain progresses. This observation suggests that very little can be done to improve the R value above unity.

The R value measured for the as-received Dofasco steel is also shown in Figure 5.23. This lies below unity through out. The value, after 15% strain, measured in the longitudinal and transverse directions are 0.77 and 0.89 respectively. There is a hump in this curve between 4.0 - 12.0% nominal strain. The reason for this is not clear.

5.9 Strain-rate Sensitivity

The observed strain-rate sensitivity index m is shown in Figure 5.24. The m value is rather low just like the R value. Clearly this cannot be responsible for the good tensile properties of dual-phase steel.

5.10 Forming Limit and Punch Stretching

In tensile tests fracture often occurs soon after the maximum load is reached therefore it may be expected that in sheet forming fracture may, under some circumstances, precede instability.

In Figure 5.25 is shown both the instability and fracture locii for as-received dual phase steel. It shows

that fracture follows instability closely for strain paths approaching equibiaxial tension. Figure 5.26 shows the effect of the meeting of fracture and instability locii for two 50 mm punch tests. Using good lubrication (A) (equibiaxial tension) the material fractures under a rising load with no apparent necking. In the second test (B), where no lubrication was used, the failure site was moved from the punch nose, away from equibiaxial tension, and the necking preceding failure is clearly seen in the photograph.

5.11 Pole Figure

The result of the {200} and {222} pole figures are shown in Figure 5.27 and 5.28. The pole figures show that the texture is not very pronounced. There is a spread about the {111} pole, fibrous in character. The components of the texture are mainly {111} <112>, {111} <110> {100} <011> {100} <130> and {100} <100>.

5.12 X-ray Determination of Retained Austenite

No retained austenite could be detected in the as-received material within the limit of detection of the technique used. Nor could any be observed optically with the different etchants that were prepared.

5.13 Thickness Effect

The total elongation measured for the processed steels were in the range of 14-25%, rather lower than that

found in the as-received Dofasco steel. This raises the question of the importance of the material thickness to the evaluation of properties, because the initial material, having a grain size of the order of 8 μm, has a similar initial flow stress to those given in Table 5.1a and b. The effect of the thickness on the properties are shown in Table 5.2. There does appear to be a genuine thickness effect, samples of approximately 1 mm thickness show significantly lower total elongations than those of greater thickness. There is also a change in the fracture appearance, as shown in Figure 5.29, only the thickest samples have fractures running transverse to the tensile axis.

5.14 Fracture Surface

Figure 5.30 shows the observed fracture surface, which is ductile in character. In figure 5.31 are shown longitudinal sections through the fracture surface. The occurrence of voids emanating from the interface between the ferrite/martensite interfaces are evident in the picture. The volume fraction of voids increase one as one approaches the fracture surface. The voids run together to form cavities on the fracture surface.

CHAPTER 6 DISCUSSION AND CONCLUSIONS

The approach used in this work has been of a general nature to get a broad view of the formability and mechanical properties of Dual-Phase steel and consequently the discussion will be on the same level. We shall first of all consider the stress/strain curve starting with the initial yielding and work-hardening characteristics.

6.1 Initial Yielding and its Suppression

The result shown in the preceding chapter showed a continuous stress/strain behaviour, Figure 5.5, with lack of the initial yield phenomenon similar to that obtained for a temper rolled mild steel.

The curve also shows a high initial rate of work-hardening, characterised by $^{1}/\sigma \; d\sigma/d\varepsilon$, up to about 7% strain. From the discussions of section 3.1 it is observed that in general it is claimed that the discontinuous yielding in α-iron and steel is due to a shortage of mobile dislocations. The shortage of mobile dislocations may be due to either the immobilisation and locking of prior dislocations by Cottrell's atmosphere formation and precipitation effects or by their total absence. The previous history of the material will determine whichever is the case. The lack of yield point perhaps can be attributed to the transformation stress set up in the ferrite matrix as a result of the formation of martensite plus additional stresses due to the fact that the coefficient

of thermal expansion of the phases, austenite, martensite and ferrite differ from each other and also the fact that there is a relative difference in the cooling rate between the outer surfaces and the interior of the samples during cooling from the ($\alpha + \gamma$) intercritical annealing temperature. This latter effect will be more prominent for a very thick specimen but for the sizes dealt with in this work this aspect may be considered negligible.

We would like to get an insight into the nature and extent of these transformation stresses. The problem of ascertaining the value of the misfit strain and stresses developed by the above processes have been the subject of consideration for many researchers (6.1-5).

Following Weatherly (6.1) these stresses can be represented by

$$\sigma = \left(\frac{2K^*}{2K^* + K}\right) \mu e^T \qquad \ldots\ldots\ldots (6.1)$$

Where μ = Shear Modulus of the ferrite matrix; K and K* are the bulk modulii of the ferrite and the hard second phase respectively. e^T = dilatation strain of the particles $\equiv$ 3 x linear strain. For the case of thermal expansion $e^T \equiv 3(\alpha - \alpha^*)\Delta T$. Where α and α^* are the coefficient of linear thermal expansion of ferrite and hard second phase respectively.

From transforming from austenite to martensite e^T will be given by the fractional volume change during the transformation. The expansion of austenite to martensite involves a volume change of the order of 4% (6.6) (i.e. a linear strain $\sim$0.0133). This however depends on the percentage of carbon and the alloying elements in the martensite but generally a value of 3 to 5% is quoted for low carbon steels (6.6).

If the combined effect of the above stresses exceeds the theoretical stress necessary to create dislocations in the lattice then dislocations will be punched into the ferrite matrix surrounding the martensite islands. This will create a local plastic zone of length λp say, around the islands. The length of the zone, or the radius of the punched out dislocations depends on the particle radius and the matrix yield stress and it has been given by Lee et al (6.2) to be

$$\lambda p = a \exp\left(\frac{\sigma}{2\sigma_y} - \frac{1}{3}\right) \quad \ldots\ldots\ldots (6.2)$$

Furthermore, by adopting the Von Mises yield criterion they derived the result that yielding will start at the matrix particle interface when the pressure exerted on the misfitting particles reaches a critical level σ_c given by:

$$\sigma_c = \frac{2\sigma_y}{3}$$

Where σ_y = The matrix yield stress.

An exact estimation of the number of dislocations generated by the above means is made difficult by the fact that the thermal coefficient of expansion is a function of temperature, and possibly will be affected by the cooling rate, and that dislocations of like character exerts a repulsive force on each other. Hence after the first dislocations have been punched subsequent ones will be opposed and plastic relaxation effects will occur.

The plastic zone sizes observed, are of the order 2 to 4 particle sizes, by Ashby et al (6.7) and 1.5 to 1.8 particle size in reference (6.2). If we neglect this for the present and assume that the dislocation loops are of the order of the radius of the martensite islands, we could get a rough estimate of the dislocations that will be introduced into the matrix. The stress needed to expand a loop of dislocation of radius λ_p, equivalent to the particle radius is: $\sim$

$$\frac{\mu b}{2\lambda_p}$$

The number of dislocations that will be punched into the matrix by an island of radius λ_p is

$$n = \left(\frac{\sigma_{trans} + \sigma_{them} - {}^{2}/_{3}\,\sigma_y}{\mu b}\right) 2\lambda_p \quad \ldots.(6.3)$$

Where b = burgers vector of B.C.C. ferrite $\sim$2.48Å. In this material $\lambda_p \sim 5 \times 10^{-7}$m

If we assume that $\sigma_y \sim \mu/1000$ for mild steel and that $\alpha = 2\alpha^*$; $\alpha^* = 0.65 \times 10^{-5}$; $K = 2K^*$; $\Delta T = 800^oC$ and $e^T = 0.0133$; we arrive at a value of $n \sim 56$.

If on the otherhand we employ a modified form of Brooks Criterion (6.5) to take account of the fact that there is a threshold particle radius below which no dislocation can be punched into the matrix, then, we have

$$\lambda_p \, e_c > nb \qquad \ldots\ldots\ldots(6.4)$$

Where λ_p is the particle radius and e_c is the misfit strain generated from the above transformation processes, then we have $n \sim 30$.

For a sample with mean interparticle spacing of ~ 10 μm, there are approximately 350 particles per unit volume giving a dislocation loop density of the order of 10^4, due to these transformation stresses, in addition to the normal density found in an annealed mild steel $\sim 10^8$ line/cm^2. This additional dislocation density is not very significant compared to that existing by normal annealing.

However, these dislocations will form high density clusters around the martensite islands as is evident in the transmission micrographs of Figure 5.16. The above estimate will not be correct because of the relaxation processes mentioned earlier and the fact that it will depend on the threshold radius of the particle but the calculation is

intended to show that the important consideration here is not the density of the mobile dislocations, as has been purported by others, but the stress gradient introduced into the matrix by the inhomogeneous distribution of dislocations in the matrix lattice with a high density around the martensite islands and a lower density at the grain interior.

It has also been shown (6.1) that the dislocation punching effect is particle size dependent and Brown et al (6.3) have shown that it will only be energetically favourable for particles with a radius $r>r^*$ to nucleate dislocations such that

$$\frac{r^*}{b} = \frac{1}{8\pi\varepsilon(1-\nu)} \left\{ \text{Ln} \frac{8r^*}{b} - 1 + \frac{3-2\nu}{4(1-\nu)} \right\} \quad \ldots\ldots\ldots (6.4)$$

Where ν = Poissons ratio ($\nu \sim 0.3$)

ε = imposed misfit strain

For a typical strain of $\sim 7.3 \times 10^{-3}$ in iron $r^* \sim 120$Å which is much less than the martensite island sizes found in the dual phase steel used in this work ($dm > 1\ \mu m$). In any event it is not envisaged that many more dislocations can be punched into the matrix than has been estimated above even though this is not accurate. The stresses set up will be high at the martensite/ferrite interface and will tail off with respect to the cube root of the distance ($\sim r^{-3}$) from the interface into the ferrite matrix. When the spacings between the martensite islands are too close

they will interact with each other to reduce the gradient of these stresses between the interior of a grain and the interface. The punched dislocations will themselves exert a back stress on the martensite island which should lead to a strong Bauschinger effect.

In section 3.1 it was stated that the total number N(t) of interstitial atoms arriving at the dislocations in time t seconds is given by the Cottrell-Bilby relation

$$n(t) = 3\left(\frac{\pi}{2}\right)^{\frac{1}{2}} n_o \left(\frac{ADt}{KT}\right)^{2/3} \quad \text{.....(2.1.5)}$$

Where $D = 3.94 \times 10^{-3} \exp\left(\frac{-19160}{RT}\right) \text{ cm}^2/\text{s}$

$n_o \simeq 0.022\%$ at 723°C

$A \simeq 3 \times 10^{-11} \text{ Nm}^2$ (or 3×10^{-20} dyne cm^2)

The time required to form an atmosphere of three atoms per atom plane is at 700°C, $\sim 1.0 \times 10^{-6}$ sec

at 300°C, $\sim 2.0 \times 10^{-3}$ sec

All these times are much shorter than the time taken to cool the specimens from the $(\alpha + \gamma)$ intercritical annealing temperatures. In the as-received Dofasco material there is approximately 0.26% C in the hard second phases leaving on average about 0.005% C in the ferrite. The solubility of C in ferrite at room temperature is $\sim 10^{-7}$% while at 300°C it is $\sim 1 \times 10^{-3}$. Thus the above value of 0.005% C is higher than that to be expected from normal equilibrium conditions at room temperature. Cottrell and Bilby further showed that approximately 10^{-6} wt% C is needed to put one carbon atom on each dislocation per

atom plane for an average dislocation density of $\sim 10^8$ lines/cm^2. Thus it is apparent that the dislocations in dual-phase steels are most probably locked strongly.

The observed microstructures of dual-phase steels is heterogeneous with a preponderance of high dislocation density around the martensite islands and a lower density in the grain interiors. The plastic zones around the particles as a result of the high dislocation density may act as a source of dislocations during the initial stages of yielding creating an inhomogeneous band of deformation akin to the Luders band of deformation through the matrix. This acts to mask the yield phenomenon. The degree of masking depends on the value of the residual stress and the initial volume of material affected by the residual stress. This volume of material will decrease as strain progresses until the residual stress itself is wiped out after some applied strain. The stress/strain behaviour then results from a combination of these dislocations (or residual stresses) produced by the martensite formation and quench ageing because of the supersaturation of interstitial solutes in ferrite grain emanating from the rapid cooling from the ($\alpha + \gamma$) intercritical annealing region.

On ageing the as-received material, in the temperature range of 200-300^{o}C, the yield point returned after a while (Figure 5.21).

It has also been shown, for a dual-phase steel containing P and Si (6.8) and for a vanadium bearing dual-phase steel (5.2) after straining and ageing at temperatures in the range 150-350°C, that the yield point returned. The time of return being dependent on the amount of prestain at a given temperature. If we assume for the present that the return is due to the diffusion of C atoms to dislocations to relock them; an estimation of the diffusion distance in the Dofasco steel at 200°C from $\bar{x} = 2\sqrt{Dt}$ gave $\bar{x} \sim 2.8$ μm, which is reasonable compared to the grain size of ∿8 μm we have in the as-received states. This treatment, however, was not carried out with any prestraining in tension but only on the as-received condition. On the otherhand Tomo Tanaka et al (6.9) have observed that the masking effect of the yield point elongation in the annealed steels was not affected by a 1% temper - rolling but that the return is speeded up by a 1% straining in tension. They also observe that the magnitude of the delay is larger for an annealed dual-phase steel than for a 1% temper rolled ferrite-pearlite steel and that decreasing the grain size reduces the time required for the re-emergence of the yield phenomenon. It is also found here that increasing the volume fraction of martensite at a particular grain size delays the return of the yield point at a particular ageing temperature (Figure 5.21c).

The higher percentages of martensite require a higher annealing temperature for a given %C steel. As the annealing temperature in the $\alpha + \gamma$ region is raised, the carbon concentration in the ferrite decreases as does that of the austenite islands.

Temper rolling will produce a substructure of alternate regions of inhomogeneously deformed and uniformly deformed material as discussed in section 3.1, whilst tensile straining will destroy any inhomogeneous deformation zones in the material in a diffused manner. To what extent this will be accomplished depends on the initial distribution of the residual stresses and to what strain level they are effective in masking the yield phenomenon. The dislocations around the particles will be spread out so that they are no longer a preferred site for nucleation of bands of deformation, i.e. the residual stress pattern in the lattice will be more diffused if not totally destroyed. Suppose initially that every small volume element has a local yield stress $\bar{\sigma}_{yL}$. If some volume element is at a stress level $\bar{\sigma}_R$, the residual stress will depress the initial yield stress by an amount equal to its value and it may mask the yield point if there is no correlation between $\bar{\sigma}_R$ and $\bar{\sigma}_{yL}$. On straining all the small volume elements which have residual stresses associated with them may not experience the same local flow processes so that with increasing strain the effective volume fraction of material that has had the residual

stresses removed will be gradually reduced. Because of this the range of effectiveness of the residual stresses will be extended with respect to strain.

A pre-strain may homogenise the residual stress pattern in the sense that it leaves a pattern of residual stresses such that on subsequent loading all points in the material come to their local yield stress at the same value of the external applied load together. On ageing a sample homogenised in this way may show the return of the yield point. Dislocation sources will be easily locked by the short-range diffusion of carbon atoms available locally and hence only a short ageing time is needed for the yield point return after straining in tension. When no pre-tensile strain if given the dislocations in the high density region will not be easily locked because the locally available solute atoms can be easily exhausted before enough atmosphere is formed and long range diffusion of the carbon atoms from the grain interior will be needed to accomplish total pinning. Thus long ageing times will be needed in such a case.

However, the yield may also return through relaxing the residual stresses that have masked the yield point. This would be a recovery process, involving glide and climb of dislocations. The activation energy for recovery may coincide with that for carbon diffusion since the migrating dislocations will be accompanied by their carbon atmosphere which has been shown above to be associated with them.

In a material with no sharp yield point it is not clear why temper rolling should give the blocky yielding pattern found in low carbon steels. Thus the observation of Tomo Tanaka et al (6.9) needs some explanation. There may be long-range residual stresses, through the thickness due to the skin effect which could retard the return of the yield point.

6.2 Work-Hardening

Considering Figures 5.5 and 5.6 it is clear that the stress/strain curve cannot be described by a Ludwig-Hollomon type equation $\sigma = K\varepsilon^n$. There is a rapid increase in work-hardening at low plastic strain which drops down to a lower value after about 5% strain.

In formulating ideas about the work-hardening characteristics it will be pertinent to draw from our knowledge of the deformation of polycrystalline alloys containing large second phase inclusions that do not deform during plastic deformation. The dual-phase steel work-hardening characteristics will have contributions from:

a. Residual stresses accrueing from the austenite to martensite transformation and from quenching σ_R.

b. On straining, the dislocation in the ferrite will be increased by both the statistical and geometrically necessary dislocations with the statistical ones coming from normal work-hardening of the ferrite while the geometrically necessary ones arise as a

result of the need to maintain compatibility between the soft and the hard phases.

However, this plastic compatibility cannot be totally maintained by punching dislocations. Some dislocation loops are left behind around the hard phase and these increase in number with strain. They exert a pressure on the martensite islands which in turn gives rise to long range back stresses in the ferrite and further impedes dislocation movement in the ferrite. The residual stresses help us to mask the initial yield phenomenon by providing a local plastic zone around the martensites. This will be saturated after a small plastic deformation in tension wiping out the inhomogeneous distribution of dislocations between the interior of the grains and the ferrite/martensite interfaces. An inhomogeneous band of deformation akin to the Luders band will sweep through the lattice but unlike the Luders band in annealed mild steel this will occur with rising stress level. This inhomogeneous band of deformation has been observed by Matlock et al (3.8.17) and Cribb and Rigsbee (3.8.14). They also showed that both the grain size and volume fraction of martensite has effect on work-hardening.

In addition to the back stresses there is also the source shortening stress discussed in section 3.3 which reduces the effective interparticle spacing. The contribution from this source is additive to the others after some

plastic strain given by equation 3.3.9 and hence not much manifested at very low strains. This will explain why the U.T.S. shows a dependence on the mean inter-particle spacing, Figure 5.12 and not much by the yield strength. Figure 5.14 also shows that very little deformation of the hard second phases took place during straining until very high strains in agreement with the above ideas. The flow stress of a dual-phase steel will therefore have a contribution from the following:

1. Normal lattice friction stress σ_i, and contribution from the extent of the microstructure and alloying.
2. Residual stress σ_R.
3. Image stress or back stress σ_{im} (or σ_B)
4. Source shortening stress σ_{sst}
5. Geometrically necessary dislocations σ_g, and
6. Statistically stored forrest dislocations σ_{for}

The first two can be added together to give an initial yield stress σ_o while 4, 5 and 6 must be added in a root mean square manner because they will all be felt jointly by a moving dislocation through the lattice. Thus we could write for the flow stress of dual-phase steels:

$$\sigma_{flow} = \sigma_o + \sigma_B + \{\sigma_{sst}^2 + \left[c\mu b \left(\frac{2f}{d_m}\right)^{\frac{1}{2}} \left(\frac{4\varepsilon p}{Mb}\right)^{\frac{1}{2}}\right]^2 + \sigma_{for}^2\}^{\frac{1}{2}} \quad ..(6.5)$$

From section 3.3 σ_{im} is proportional to $(\frac{f}{r_o})$ and directly to strain at small plastic strains

$$\therefore \quad \sigma_B = \alpha_1 \mu f \epsilon_p^* \qquad \ldots\ldots\ldots(6.6)$$

σ_{sst} is dependent inversely on the particle radius and directly on the volume fraction of particles in the matrix but parabolically on strain. The contribution from σ_g is dependent on the square root of the volume fraction directly and on $d_m^{-\frac{1}{2}}$, where d_m is the mean particle diameter, while the forrest hardening depends on the geometric slip distance λ_G to the power of minus a half. λ_G is proportional to the grain size and so is d_m. When the volume fraction of particles are small the contributions of σ_{im} and σ_{sst} are small. Thus when all these are put together we could write equation 6.5 simply as:

$$\sigma_{flow} = \sigma_o + \sigma_B + K^1 \mu \left\{\left[\left(\frac{f}{\theta}\right) + 1\right] \frac{\epsilon_{pb}}{D}\right\}^{\frac{1}{2}} \qquad \ldots\ldots\ldots(6.7)$$

Where D = grain size, K^1 is a constant and involves the effect of all other constants combined, μ = shear modulus and θ is a constant of proportionality between the grain size and the particle radius.

The above equation 6.7 implies that to enhance the rate of work-hardening of the steel we can either refine the grain size and particle size or we can increase the volume fraction of hard phase. But this latter recourse would be detrimental to ductility as is evident from section 5.2. The regression equation for uniform

elongation has a negative contribution from the volume fraction of martensite.

However, it should also be realised from our earlier discussion on dislocation punching that, in refining the grain and particle size, the particle size should not be too small either, otherwise no dislocations will be punched into the ferrite lattice due to the transformation from austenite to martensite and only an elastic strain field might be left behind. The masking effect of the initial yield phenomenon due to the presence of residual stresses might then be lost.

6.3 Strength and Fracture

The results of the 0.2% off-set yield stress and U.T.S. on grain size and percentage of martensite depicted in Figures 5.3 to 5.11 shows a stronger dependence of the U.T.S. on grain size than the off-set yield stress for a given % of martensite. Conversely there is a greater dependence of the martensite volume fraction on the off-set yield stress than on the U.T.S. in line with what has been said above in section 6.2. This variation of the grain size dependence of strength with increasing strain is contrary to that which is known for single phase polycrystalline metals and it implies that the Petch relation for the flow stress, $\sigma_f = \sigma_o + K_f d^{-\frac{1}{2}}$, of the material has an increasing value of K_f with increasing strain. This can be understood in terms of the long range back stresses set up by the pile up of

dislocations against the particle/matrix interface. Therefore it may not be the Petch relation concerning plastic deformation of the ferrite which is dominating the U.T.S. but the Cottrell-Petch relation for the fracture stress of the martensite or martensite/ferrite interface suggesting that voids leading to ductile fracture are formed by pile up of glide dislocations against the particles. When the stresses set up by this pile up reach a critical value to create voids or cracks, determined by surface energy considerations, and these voids or cracks are able to grow fast and fracture ensues.

A pile up of n dislocations of Burgers vector b at the base of a wedge shaped crack will produce a plastic displacement equal to nb. The effective shear stress giving rise to this displacement will be the applied shear stress minus the friction stress $(\tau - \tau_i)$. If the shear modulus of the matrix is μ then this is equal to $\frac{\mu nb}{\lambda}$. Where λ = slip band or pile up length. The work done is the applied stress multiplied by the plastic displacement, i.e. $\sigma \times nb$. For the crack to propagate plastic relaxation processes much be absent and the above work must be greater than the effective surface energy of fracture and since two surfaces are created when fracture occurs this is equal to $2\gamma_{surf}$.

$$\therefore \quad 2\gamma_s \leq \sigma nb \leq \sigma \left\{\frac{(\tau-\tau_i)\lambda}{\mu}\right\} \qquad \ldots\ldots\ldots(6.8)$$

The pile up length will be proportional to the grain size and hence $\lambda = \theta^1 d$. Where θ^1 is a constant of proportionality.

$$\therefore \quad 2\gamma_s \leq \sigma \left\{ \frac{(\tau - \tau_i)\theta}{\mu} \right\} \qquad \ldots\ldots\ldots (6.9)$$

But $\sigma = m\tau$, $m \equiv$ Taylor factor ~ 2.8

$$\sigma_y = \sigma_i + K_y d^{-\frac{1}{2}} \quad \text{or} \quad \tau_y - \tau_i = \frac{K_y d^{-\frac{1}{2}}}{m}$$

On yielding $\tau = \tau_y$ subsequently $\tau = \tau_f$

$$\therefore \quad \sigma = \frac{2\gamma_s \mu m \theta^{1} d^{-\frac{1}{2}}}{K_y}$$

$\therefore$ The critical growth stress is

$$\sigma_{\text{growth}} \simeq \left(\frac{5.6\ \gamma_s \mu}{K_y}\right) d^{-\frac{1}{2}}$$

Thus when work-hardening increases the flow stress above that for the voids to grow and all relaxation processes are blocked fast fracture will occur. The problem of continuity of plastic deformation at the martensite/ferrite interface gives rise to a resistance to the further deformation which increases with strain. When this resistance reaches a limiting value determined by the fracture stress of the martensite or martensite/ferrite interfacial energy then voids are opened up which will grow on further straining. To improve the value of equation 6.10 we can do either of the following:

a. increase γ_s

b. decrease d

c. lower K_y

K_y is a measure of the local resistance to nucleation of slip ahead of a pile up of slip dislocations at

grain bounaries and it is given by

$$K_y \simeq 2\tau_p r_p^{\frac{1}{2}}$$

Where τ_p = unpinning stress at a distance r_p from the tip of the slip band.

Our transmission micrographs show that there is a high density of dislocations surrounding the martensite islands which can be easily activated, aided by the residual stresses during yielding to cause a lowering of K_y. As straining progresses; work-hardening raises the stresses in the matrix and a competition between further work-hardening and fracture comes into play. Eventually instability sets in when the material can no longer work-harden at the expense of fracture through ductile voiding and here the grain size is important as it controls both work-hardening and fracture stress and as the grain size is decreased more strain hardening is required to reach the fracture stress. We must also make sure that solid solution additions which can reduce the void nucleation strain are avoided.

This behaviour has implications for the formability of these steels and it will be discussed further latter.

6.4 Thickness Effect

The result of the thickness effect on strength presented in the preceding chapter has implications from the work-hardening behaviour of dual-phase steel point of view since slip modes in individual grains of a polycrystalline

solid are strongly affected by the interaction of its adjacent grains. On yielding this interaction will spread into a wide region across the first nearest-neighbour grains so that the flow stress markedly decreases with decreasing specimen thickness when the number of grains contained along the thickness direction becomes smaller than a critical value commonly taken to be 5 (6.10-13). This long-range interaction is a function of the slip mode in each individual grain, and hence it is very sensitive to both grain size and the stacking fault energy of the specimens. The grain size determines the mean free path of dislocations which in turn depend on the distribution of obstacles to its motion developed during straining. The mean free path of dislocations in high stacking fault metals is determined at high strains by the cell walls developed. In dual-phase steels this will be determined by the interparticle spacing. The long range stresses set up will be relaxed at the specimen surface because there is no other particle ahead for the last particle to the surface to interact with. Hence as the specimen thickness decreases the number of these obstacles giving rise to the long-range stress diminishes. Further, if the number of active slip systems is limited, the relaxation will not occur isotropically and the elastic strain energy in the affected zone cannot be relieved homogeneously with the first nearest-

neighbour grain alone, so that a wider region is necessary for the relaxation. Hence stresses due to some other particle further inside the specimen up to some distance can be relaxed at the surface. S. Miyazaki et al (6.12) have shown by a theoretical argument that the extent of the affected zone decreases with increasing stacking fault energy and increasing grain size and that the radius of the affected region at the upper yield stress of Fe is different from that at the lower yield stress. Further they conclude that in a textured material the critical ratio of $^{t}/d$ will be increased when the material is elongated normally to the extended direction of the affected zone because the strain cannot be easily relieved in certain directions.

6.5 Formability

Some simple methods of evaluating the formability of sheet steels have been used in studying the behaviour of dual-phase steels. These are the R_{value}, the work-hardening exponent n already discussed with the work-hardening above and the forming limit diagram. Together they provide information on the drawability, stretchability and limit strains for both instability and fracture and thus cover most of the circumstances encountered in steel forming.

a. R_{value}

These results are presented in section 5.8. The amount of the ferrite in the as-received Al-Si killed steel used in this study converted to martensite is less than 20%. The initial ferrite had already been endowed with a favourable crystallographic texture before the heat treatment. There are two possible explanations for the reduction of the R_{value} from the initial value of 1.6 to about 1.0 by dual-phasing. The first of these is that the martensite forms from a particular range of ferrite orientations, leading to weakening of the texture, which is unlikely. The second is that the presence of the martensite so modifies the deformation of the ferrite as to make textural effects unimportant. As we have seen in the previous sections long range back stresses are set up in the ferrite which controls its work-hardening.

Some insight into this idea is furnished by the results of Figure 5.22. It is interesting to note that the initial strain ratio in two of the heat treated samples starts in the same range as for the as received material but then decline rapidly with strain towards a value of $\sim$1.0. One sample showed an initial low R_{value} less than 1, the reason for this is not quite clear, but what is significant is that the incremental strain ratio also tended

towards unity with increasing strain for this specimen. Also we should note that on the yield surface R is a measure of the angle between the strain vector and the tensile direction such that

$$\tan \theta = \frac{R}{1+R}$$

For isotropic material $R = 1$, $\theta = \tan^{-1}\frac{1}{2} \simeq 26.6^{o}$. If $R > 1$ this implies that the through thickness strength is greater than the strength in the other two orthogonal directions $[\sigma_{y(3)} > \sigma_{y(1,2)}]$. If on the other hand $R < 1$ then $\sigma_{y(3)} < \sigma_{y(1,2)}$. This implies, that in the light of the observation of Figure 5.22, for a dual-phase state, then, that the specific work of plastic deformation is not isotropic until at higher strain levels when the R_{value} approaches 1. This will be due to the constraint deformation of the ferrite matrix by the martensite and is tied up with the long range back stress relaxation at the surface. Along the thickness direction there are less particles to interact with each other than along the width. Thickness specimen might have only shown a constant R_{value} with strain where the surface relaxation effect will be masked.

The above results clearly suggests that the influence of the martensite on ferrite deformation increases with strain and progressively over-rides the minor effects of ferrite texture and that there is very little that can be done to improve the R_{value} above 1 in these steels.

b. Forming Limit

The result shows that fracture follows instability closely for strain paths approaching equibiaxial tension consistent with the grain size dependent strength observed earlier. The forming limit of dual-phase steel is shifted upwards from that of conventional HSLA steel, as shown in Figure 2.2 in the introductory section. But it is still not as good as that of mild steel. However the fracture limit is down and clearly it may be undesirable as it means that small increases in strain beyond the forming limit can lead to fracture. This decreases the reliability of the forming limit diagram and may lead to damage of the tooling employed by sudden release of stored energy in the part. From this aspect conventional HSLA steels are better than dual-phase steels and therefore it is not envisaged that dual-phase steels will completely replace mild steel and HSLA steels, in particular where difficult parts to form are involved. The current success of dual-phase then emanate from their superior work-hardening capacity and lack of initial yield phenomenon.

6.6 Strength Differential Effect

This is the most interesting aspect of this work and one that is not easily understood. Most of the possible reasons that have been covered in section 3.10 can be ruled out. Residual stress effects can be rejected on the ground that they would disappear after some deformation, leaving a strain difference of the order of the elastic limit or will give rise to a permanent softening

following the work of Wilson (6.14), on reversal stress direction.

Furthermore from the observations of Figure 5.15, curves A and B, after the initial pre-strain in tension, though yielding at a stress below the tensile pre-stress, still work-hardened to meet the as-received compression curve. Whereas curves C, D and E remained below the tension curve suggesting some degree of permanent softening has taken place and that whatever mechanism gave rise to the (S-D) effect has now been modified. The initial rate of work-hardening of curves 1 and 2 (as-received tension and compression curves), up to about 2% strain can be seen to be slightly different but subsequently the two curves remain practically parallel. The observed magnitude then cannot be due to a normal Bauschinger effect because the compressive strength is higher than the tensile strength. That the effect must be due to the presence of the martensite in the matrix is borne out by the results of Figures 5.18 and 5.19.

The retained austenite hypothesis is improbable since no retained austenite has been detected in all the processed samples neither can the loss of strengthening due to particle/matrix interface decohesion in tension because the effect is too large.

In section 3.10 it was stated that the magnitude of the normal (S-D) effect increases with increasing percentage of carbon in the martensite. In the dual-phase steel it is observed that increasing volume fraction of martensite gave an increase in magnitude of (S-D) effect, Figure 5.18. As the volume fraction of martensite increases the carbon content of the martensite decreases. Further since no deformation of the hard second phases are observed until very high strain levels then the observed effect cannot be due to large plastic deformation of the martensite. But since the effect is clearly associated with the martensite the answer for it must be sought elsewhere.

The idea of the odd dependence of the yield condition on the stress invariants of Drucker will require further test under hydrostatic pressure to clarify it, and it has been suggested as a topic of future research. However, we must bear in mind that the (S-D) effect exists not only in martensitic steels but it has been observed in bainite, Widmanstatten ferrite-pearlite as well as in ferrite-martensite microstructures (3.10.1). Thus suggesting that the interaction of the transformation dislocations in this type of microstructure with the matrix lattice might have something to do with the S-D effect.

When all the above has been considered the only other plausible reason for the observed (S-D) effect in this steel is that due to directionality of the martensite strength and directionality of slip mode in the ferrite. It has been reported (3.10.1) that tempering of martensite, does not eliminate the (S-D) effect, even at temperatures as high as 650^{o}C for short periods, though it was lessened. It has also been reported that, for iron, easier slip occurs in the forward $\{112\}\langle\bar{1}\bar{1}\bar{1}\rangle$ twinning direction than in the reverse direction (6.15) and Hosford et al (3.10.16) have shown that twinning and directional slip can lead to an (S-D) effect. Their calculation gave 28% (S-D) effect for F.C.C. metals but a reverse effect for B.C.C. metals and of smaller magnitude and they suggest that in B.C.C. metals the effect must be due to a pressure sensitivity of yielding. This can arise if vacancies or interstitials are generated during plastic deformation.

However, pursueing the idea of directional slip further; Figure 5.17 a, b and c, presents the results of the directional dependence of tensile and compressive stress/strain curves. It is evident that there is a more marked anisotropy effect in compression than in tension and a plausible explanation will be, judging from the results of the transmission micrograph, Figure 5.16a in particular, based on the twinned character of the martensite. The twinning resulted from the processing

deformation of the F.C.C. austenite lattice which subsequently transformed to B.C.T. martensite. The twins will be of the {111}<112> type and must be terminated in the ferrite since ferrite does not twin on this system. Twins in B.C.C. ferrite occur on {112}<111>. On transforming the austenite to martensite the twins are carried over and there is a concentration of strain energy at the tip of the twin and around the martensite island. The twin interface consists of a series of $^{a}/_{6}$ <111> partial dislocations on successive {112} planes. If the motion of the leading partial at the tip of the twin is resisted, those behind it will pile up against it under the action of an applied stress. If the barrier is impassable the concentration of strain energy at the head of the pile up may be relieved by a dislocation reaction like

$$^{a}/_{6}\,[111] \longrightarrow {}^{a}/_{3}\,[\bar{1}\bar{1}\bar{1}] + {}^{a}/_{2}\,[111]$$

(see references 6.16 and 6.17).

Slip in the B.C.C. structure occur on {110}<111> or on any available plane containing the <111> direction, i.e. (112) and (123). Hence the dislocation $\frac{a}{2}\,[111]$ is a lattice dislocation in the ferrite and it is called an emissary dislocation (6.18). The incorporation of the emissary glide dislocations $^{a}/_{2}\,[111]$ into the ferrite lattice deformation gives rise to a back stress for compression only (6.19 and 20). That is to say, since the other partials $^{a}/_{6}\,[111]$ and $^{a}/_{3}\,[\bar{1}\bar{1}\bar{1}]$

cannot move away from the tip of the twin band they are trapped there. Under tensile stress they give rise to more emissary dislocations in the ferrite which can move away from them but on reversal of stress the emissary is pushed against them but since they cannot run into the martensite (i.e. by untwinning the martensite which is not likely to happen for a hard martensite such as that in the present study) they present higher resistance to their backward motion. This resistance or back stress has the strongest effect in the <110> direction (resolved shear stress 0.24) and a smaller effect in the <112> direction (resolved shear stress 0.32) (6.20), which is in accord with the anisotropy of the compression results.

After some straining other sources of dislocations in the lattice will have been adequately activated so that the initial effect of these emissaries will no longer be noticeable - they will now be part and parcel of the normal forrest dislocations and the rate of work-hardening in compression is seen to level up with that in tension. In the same manner a certain amount of prestrain in tension will have produced enough of other dislocations in the ferrite lattice so as to make the emissary dislocations no longer paramount when re-tested in compression and a normal Bauschinger type of effect is observed. The effect of these emissary glide dislocations coupled with the elastic modulus effect on the

strength of the martensite, together with the stress invariant pressure sensitive yielding is most probably responsible for the strength differential effect observed here. Subsequent heat treatment in the (α + γ) range will not destroy this effect because of the memory effect of austenite to martensite transformation. The effect will only be destroyed when the martensite is prevented from forming and probably if other dislocation punching processes are prevented as well, as is evident in Figure 5.19.

It is, however, not intended that the last has been said about this phenomenon and future research might reveal the true nature of the (S-D) effect to give us a better understanding of it.

6.7 Conclusions

In conclusion then it can be said that the lack of a yield point in dual-phase steels is due to the masking effect of the residual stresses set up during the austenite to martensite transformation and in quenching. The return of the yield point though appears to be due to diffusion of carbon atoms to repin the punched out dislocations surrounding the martensite islands, it could also be viewed in terms of the relaxation of the residual stresses through recovery processes involving dislocation rearrangement. The level of carbon concentration in the lattice suggests that the dislocations are most probably pinned from the start. The material

shows a grain size dependent strength with $K_y < K_f$. Finer grain sizes are better for improving the strength and work-hardening of the steel than increases in volume fraction of martensite. Martensite volume fraction has a negative effect on ductility and for dislocations to be punched out into the lattice as a result of the transformation and quenching strains the martensite islands must not be less than about 120 Å.

The performance of dual-phase steel in the press shop is due to its better work-hardening capacity rather than its strain-rate sensitivity or its R_{value}. Hence a small, but nevertheless significant, post-uniform elongation is found for dual-phase steel unlike the extensive one normally found for mild steel.

While their forming limit is good compared to conventional HSLA steels their fracture limit is not so good because it decreases towards the forming limit on approach to balance biaxial tension. Thus great care must be exercised in the press shop to avoid damage to tooling when they are being formed. On this note it is envisaged that their use as a potential vehicle weight reducer will be limited to certain parts. For severe deep drawing mild steels will still be a better bet than dual-phase steels. The observed R_{value} is low and lies around 1.0, and there is very little scope for improvement of this R_{value}. There is also a

thickness effect on the strength and elongation, this is attributed to the relaxation effect, at the surfaces, of the long-range stresses set up in the lattice as a result of dislocation/particle interaction taking place in the lattice.

There is also another very interesting effect; the strength-differential effect [(S-D) effect] in which the compressive strength is higher than the tensile strength. This effect probably is due to the introduction of emissary type of dislocation into the ferrite lattice as a result of the twins present in the martensite. These emissaries give rise to an added initial rate of work-hardening in compression which is directional in character. Along with this effect, the elastic modulus effect and the stress invariant pressure sensitive yielding effect might also contribute to account for the magnitude of the (S-D) effect.

7 Suggestions for Future Research

(1) To observe by electron transmission microscopic technique the distribution and dislocations in dual phase steels when aged at temperature range from 50 - 400°C after quenching from the ($\alpha + \gamma$) range.

(2) To check the grain size effect on strength against the number of grains transversing unit thickness of a dual phase sample and compare to available observations on low carbon steels, Cu and Cu-AL alloys.

(3) To observe their fracture and mechanical behaviour from about 100°C down to very low temperatures say -100°C to evaluate their use under cryogenic conditions.

(4) To study the corrosion and errosion (wear) properties of these steels and to check the effect of their exposure to service condition on their strength and fracture behaviour.

(5) In as much as the strain distribution measurement did not reveal any deformation of the martensite until quite high strain levels, it will be inter-

esting to know how the strain distribution varies with increasing percentage of martensite and also the variation of mean interparticle spacing with strain. X-ray techniques might also be employed to find out the nature of the residiual microstresses set up in the lattice with strain.

(6) To develop a method either computational or otherwise for quick estimation of the amount of transformational residual stresses set up in a material during rapid cooling and to evolve ideas about the plastic relaxation and thermal relaxation of these stresses around the particles.

(7) Further work on the (S-D) effect to ascertain whether it is a characteristic of all dual phase steels irrespective of processing history and to check whether the strength can be recovered by low temperature treatment without return of the yield phenomenon.

(8) To further check the effect of hydrostatic pressure on the (S-D) effect.

(9) To check the effect of different percentage of martensite on strain distribution and fracture stress. This can be tied up with suggestion 6 above.

(10) To study the fatigue and impact properties of dual phase steels with variation in temperature and environmental conditions.

Acknowledgement

The work reported in this thesis was carried out in the Department of Metallurgy and Materials of the University of Aston in Birmingham.

The author wishes to thank the Dofasco Steel Corporation of Canada for their help in supplying the steel used in the major part of the work.

I am particularly indebted to Dr. W. B. Hutchinson and my supervisor Prof. I. L. Dillamore for their help, advice and encouragements throughout this work.

Thanks are also due to Dr. R. K. Ray of the Indian Institute of Technology, Kanpur-India for his help, while visiting Aston in summer 1979, with the transmission micrographs and also to Prof. C. A. Verbraak of the Technical University Twente Enschede/The Netherlands for his interest and helpful discussions on the strength differential effect.

Finally I wish to express my gratitude to the Technician members of the department and the Workshop Staffs for their help at one stage or other and to the University of Benin, Nigeria for their financial support. Along with them I must also thank Miss G.C. Adiele-Nmasso,

Mrs. M. O. McKone and Mr. B. A. Shitta for their financial assistance and encouragements during the last 9 months of this work and to the typists, Mrs. H. Howell and Miss Sharon Ellis for their effort in typing the thesis.

3.5 REFERENCES

3.5.1 N. Wang and M.R. Shammamy, J.Mech.Phys.Sol., 17, 43, 1969

3.5.2 I.L. Dillamore, R.E. Smallman and D.V. Wilson, 9th Commonwealth Mining and Metallurgy Conference, 1969, Paper 10

3.5.3 W.B. Morrison, Trans. ASM, 59, 824, 1966

3.5.4 J.H. Woodhead, "Effect of Second Phase particles on the Mechanical Properties of Steel", I.S.I. Conference, p.130, 1971

3.5.5 M.R. Barren, "Mechanical Working and Steel Processing, Vol. VII", A.I.M.E. Conference, p.16, 1969

3.5.6 B.S. Levy, B.H. Levine and J.L. Golding, ibid

3.5.7 I.L. Dillamore, B.S.C. Report MG/16/72

3.5.8 I.L. Dillamore, P. Mella and R.J. Hazel, J.Inst. Met., 100, 50, 1971

3.5.9 W.T. Lankford, Trans. ASM, 42, 1197, 1950

3.5.10 R.L. Whiteley, Trans. ASM, 52, 154, 1960

3.5.11 S.P. Keeler, Sheet Metal Industries, July 1971

3.5.12 M. Atkinson and I.M. Maclean, Sheet Metal Industries, 44, 167, 1965

3.5.13 H. Richards, Progress in Metal Physics, Vol. Pergamon Press

3.5.14 D.V. Wilson and R.D. Bulter, J.Inst.Metals, 201, 16, 1963

3.5.15 J.F. Held, "Mechanical Working and Steel Processing IV", A.I.M.E. Conference, 1966, p.3

3.5.16 R.M.S.B. Horta, W.T. Roberts and D.V. Wilson, Int. J. Mech.Sci, 12, 231, 1970

3.5.17 R. Pearce, Int. J. Mech. Sci., 10, 995, 1968

3.5.18 N.A. Cantalejos and R.A. Maynard, 3rd International Conference on strength of Metals and Alloys, Paper 76, I.S.I., I.M., London 1973

3.5.19 D.V. Wilson, Sheet Met. Ind., 43, 929, 1966

3.5.20 P. Mellor and A.N. Bramley, Int. J. Mech. Tool Des. Res., 5, 43, 1965

3.5.21 I.L. Dillamore, R.F. Dewsnap and R.A. Maynard, "Control Processing of HSLA Steels", B.S.C. York Conference, 1976

3.5.22 R. Dewsnap, D.M. Keane and R. Bramson, B.I.S.R.A. Open Report, MG/34/71

3.5.23 J.F. Butler, Vanitec Seminar, Oct. 1978

3.5.24 R.M. Davison and J.F. Morrow, Met. Eng. Quart, 16, 10, 1976

3.5.25 J. Hiam and A. Lee, Sheet Metal Ind., May 1978, p. 631

SECTION 2 REFERENCES

2.1 T. Gladman, D. Dulieu and I.D. McIvor, in Microalloying 75, p. 32, Union Carbide Corporation, New York, 1977

2.2 D.P. Koistein, U.S. Patent No. 3461002, August 1969, and 3490957, January 1970

2.3 D.J. Bailey and D.P. Koistein, Paper 124, Proceeding of the 3rd International Conference on the Strength of Metals and Alloys, Cambridge, England, Vol. 1, p. 586, 1973

2.4 D.J. Bailey, United State Patent No. 3,930,907, Jan. 1976, 3,928,086, Dec. 1975

2.5 S.P. Keeler, Sheet Metal Industries, May-Oct, 1971

2.6 S.P. Keeler and S.S. Hecker, "Relationship between Laboratory Material Characterisation and Press-Shop Formability", Microalloying 75, published by Union Carbide Corporation, New York, 1977

2.7 M.S. Rashid, "Relationship between Steel Microstructure and Formability", General Motor Report No. GMR-2647

2.8 M.S. Rashid, "Manufacture of Automobile Components from Dual-Phase Steels", Vanitec Seminar on Vanadium Cold-Pressing and Dual-Phase Steels, West Berlin, Oct. 1978, Paper 4.

3.1 REFERENCES

3.1.1 N.J. Petch, Acta Met. 12, 59, 1964

3.1.2 P.J. Worthington, Acta Met. ±5, 1795, 1967

3.1.3 R.J. Arseneult, Trans. A.I.M.E. 230, 1571, 1964

3.1.4 A.H. Cottrell, Physical Society Report, p.30, 1948

3.1.5 A.H. Cottrell and B.A. Bilby, Proc. R. Soc. A62, 104, 1949

3.1.6 W.E. Dalby, Proc. R. Soc. 488, 281, 1913

3.1.7 E.O. Hall, "Yield point phenomena in metals and alloys", Macmillan Publishing Company, 1970

3.1.8 W.G. Johnson and J.J. Gilman, J.Appl.Phys., 30, 129, 1959

3.1.9 H. Conrad, Acta Met. 15, 147, 1962

3.1.10 Y. Bergström, Mat.Sci. & Eng., 9, 101, 1972

3.1.11 R.W.K. Honeycombe, "The Plastic deformation of Metals", Edward Arnold Publishing Company, 1968

3.1.12 I. Codd and N.J. Petch, Phil. Mag. 14, 30, 1959

3.1.13 D.V. Wilson and R. Russell, Acta Met. 8, 36, 1960

3.1.14 D.V. Wilson and R. Russell, ibid, 8, 468, 1960

3.1.15 S. Harper, Physics Rev., 83, 709, 1951

3.1.16 J.E. McLennan, Acta Met., 13, 1299, 1965

3.1.17 R.C. Newman, Acta Met., 10, 971, 1962

3.1.18 E.S. Davenport and E.C. Bain, Trans. ASM, 12, 1047, 1935

3.1.19 A.H. Cottrell and G.M. Leak, J.I.S.I., 11, 301, 1952

3.1.20 C.A. Wert, J.Appl.Phys., 20, 943, 1949

3.1.21 B.B. Hundy, J.I.S.I., 178, 127, 1954

3.1.22 B.B. Hundy, ibid, 179, 23, 1955

3.1.23 D.V. Wilson, ibid, 201, 16, 1963

3.1.24 H.P. Tardiff and C.S. Ball, ibid, 182, 9, 1965

3.1.25 R.L. Whiteley, Reported by D.J. Blickwede, Trans. ASM, 61, 653, 1968

3.1.26 C.A. Edwards et al, J.I.S.I., 142, 199, 1940

3.1.27 W.C. Leslie et al, Trans. A.I.M.E., 197, 1021, 1953

3.1.28 F.A. Laxar et al, Trans. ASM, 53, 683, 1961

3.1.29 J.M. Arrowsmith, J.I.S.I., 201, 699, 1963

3.1.30 E.R. Morgan and J.C. Shyne, ibid, 185, 156, 1957

3.1.31 E.R. Morgan, Proceeding International Symposium on Annealing of low carbon steel, Oct. 30, 1957, Case Institute of Technology, U.S.A.

3.1.32 E.R. Morgan, Trans. A.I.M.E., 209, 65, 1957

3.1.33 S. Epstein et al, ibid, 188, 830, 1950

3.1.34 W.B. Morrison, J.I.S.I., 201, 317, 1963

3.1.35 G.L. Dunlop and R.W.K. Honeycombe, Metal Science, 8, 367, 1978

3.2 REFERENCES

3.2.1 G.I. Taylor, J.Int.Met. 62, 307, 1938

3.2.2 J.F.W. Bishop and R.Hill, Phd.Mag. 42, 414, 1951

3.2.3 J.F.W. Bishop and R. Hill, Phd.Mag. 42, 1298, 1951

3.2.4 U.F. Kocks, Acta. Met. 6. 85, 1958

3.2.5 E. Kröner, Acta Met. 9. 155, 1961

3.2.6 J.D. Livingston and B. Chalmers, Acta Met. 5, 322, 1957

3.2.7 J.E. Dorn and J.D. Mote, "On the Plastic Behaviour of Polycrystalline Aggregates"

3.2.8 I.L. Dillamore, R.E. Smallman and D.V. Wilson, "Physical Metallurgy of Sheet Metal Forming" 9th Commonwealth Mining and Metallurgy Congress 1969.

3.2.9 U.F. Kocks, Trans. A.I.M.E., 1, 1121, 1970

3.2.10 S.K. Mitra, P.W. Osborne and J.E. Dorn, Trans. A.I.M.E., 221, 1206, 1961

3.2.11 W. Boas and M.E. Hargreaves, Proc. Roy. Soc. A193, 89, 1948

3.2.12 W.L. Wain et al, J. Inst. Met. 13, 241, 1940

3.2.13 C.S. Barrett, Trans. A.I.M.E. 137, 112, 1940

3.2.14 J.F.W. Bishop, J.Mech. and Phys. Solid, 3, 130, 1954

3.2.15 A.W. Thompson, "Polycrystal Hardening", T.M.S.-A.I.M.E. Sumposium on Advances in Understanding of Work-hardening, Cinncinati, U.S.A., Nov. 11 1975

3.2.16 R. Armstrong, I. Codd, R.M. Douthwaite and N.J. Petch, Phil. Mag. 7, 45, 1962

3.2.17 J.D. Eshelby, Proc. Roy. Soc., A241, 376, 1957

3.2.18 M.F. Ashby, Phil.Mag. 21, Nos. 170, 139, 1970

3.2.19 V.I. Lizunov et al, Metalov, No. 11, 41, Nov. 1976

3.2.20 B.I. Edelson et al, Trans. A.S.M. 55, 230, 1962

3.2.21 M. Gensamer, E.B. Pearsall, W.S. Pellini and J.R. Low Jr., Trans. A.S.M. 30, 983, 1942

3.2.22 A.M. Turkalo et al, Trans. A.S.M. 466, 1075, 1954

3.2.23 C.J. Lim et al, Trans. A.I.M.E. 242, 1535, 1968

3.2.24 J. Gurland et al, Trans. A.I.M.E. 203, 311, 1955

3.2.25 G.S. Ansell, "Mechanical Properties of Two-Phase Alloys in Physical Metallurgy" by R.W. Cahn.

REFERENCES.

3.3.1 E. Orowan,
Symposium on Internal Stresses in Metals and Alloys, p.481, The Institute of Metals, London. 1948.

3.3.2 A. Kelly and R. B. Nicholson,
Progress in Material Science,
10, p.336, 1963.

3.3.3 M. F. Ashby,
Physics of Strength and Plasticity, Edited by A. S. Argon, p.113, Published by M.I.T. Press Cambridge, Mass, U.S.A., 1969.

3.3.4 J. L. Fisher, E.W. Hart and R.H. Pry,
Acta Met. 1, 336, 1953.

3.3.5 W. R. Hibbard and E. W. Hart,
Trans. AIME 203, 200 1955.

3.3.6 A. M. Safdar and V. A. Phillips,
AIME 215, 340, 1959.

3.3.7 D. V. Wilson,
Trans. ASM 47, 321, 1955.

3.3.8 M. H. Lewis and J. W. Martins,
Acta. Met. 11, 207, 1963.

3.3.9 F. J. Humphrey and J. W. Martins,
Phil. Mag 16, 927, 1957.

3.3.10 R. S. Goodrich and G. S. Ansell,
Acta. Met. 12, 1097, 1964.

3.3.11 R. Ebelling and M. F. Ashby,
Phil. Mag. 13, 805, 1966.

3.3.12 K. C. Russell and L. M. Brown,
Acta Met. 20, 969, 1972.

3.3.13 U. F. Kocks, A. S. Argon and M. F. Ashby,
Progress in Material Science 19, 196, 1975.

3.3.14 A. Melander,
Scripta Metallurgica 11, 393, 1977.

3.3.15 E. Hornbogen,
3rd International Conference on the Strength of Metals and Alloys, Cambridge, England, 1973. Vol. 2, p.108.

3.3.16 L. M. Brown and W. M. Stobbs,
Phil. Mag. 23, 1185, 1971a.

3.3.16b L. M. Brown and W. M. Stobbs,
Phil. Mag. 23, 1201, 1971b.

3.3.17a P. B. Hirsch and F. J. Humphreys,
Proc. R. Soc. A318, 45, 1970.

3.3.17b P. B. Hirsch and F. J. Humphreys,
Proc. R. Soc. A318, 45, 1970.

3.3.18 E. W. Hart,
Acta. Met. 20, 275, 1972.

3.3.19 M. F. Ashby,
Phil. Mag. 14, 1157, 1966.

3.3.20 J. D. Eshelby,
Proc. R. Soc., A241, 376, 1957.

3.3.21 R. H. Jones,
Met. Trans. 4, 2799, 1973.

3.3.22 F. J. Humphreys and P. B. Hirsch,
Phil. Mag. 34, 373, 1976.

3.3.23 J. D. Atkinson, L. M. Brown and W. M. Stobbs,
Phil. Mag. 30, 1247, 1974.

3.3.24 K. Tanaka and T. Mori,
Acta. Met. 18, 931, 1970.

3.3.25 L. M. Brown and D. R. Clarke,
Acta. Met. 23, 821, 1975.

3.3.26 M. F. Ashby,
Phil. Mag. 21, 170, 1970.

3.3.27 D. V. Wilson and Y. A. Konnan,
Acta. Met. 12, 617, 1964.

3.3.28 L. Anand and J. Gurland,
Acta. Met. 24, 901, 1976.

3.3.29 T. Gladman, B. Holmes and F. B. Pickering,
J.I.S.I. N22, 172, 1970.

3.3.30 H. Fischmeister, J.O. Hjeslmered, B. Karlson,
G. Linden and B. Sundstrom,
3rd International Conference on the
Strength of Metals and Alloys, Cambridge,
England, Paper 131, Vol. 1, 1973.

3.3.31 B. Karlson and G. Linden,
Mat. Sci. Eng. 17, 153, 1975.

3.3.32 B. Karlson and B. O. Sundstrom,
Mat. Sci. Eng. 16, 161, 1974.

3.3.33 J. Gurland,
Trans. AIME 212, 452, 1958.

3.3.34 B. Karlson and G. Linden,
4th International Conference on Strength
of Metals and Alloys, Nancy, France, 1974.

3.3.35 C. T. Liu and J. Gurland,
Trans. ASM 61, 156, 1968.

3.3.36 J. Gurland and J. Plateau,
Trans. ASM 56, 442, 1963.

3.3.37 J. D. Embury,
Trans. AIME 239, 114, 1967.

3.3.38 I. G. Palmer and G. C. Smith,
in Oxide dispersion strengthening, p.253,
Edited by G. S. Anell, Published by Gordon
and Breach, New York.

3.3.39 T. Inone and S. Kinoshita,
3rd International Conference on the Strength
of Metals and Alloys, England, Paper 32,
Vol. 1, 1973.

3.3.40 H. C. Rogers,
"Ductility", ASM Publication, Ohio 1968,
p. 31.

3.3.41 H. C. Rogers,
Trans. AIME 218, 498, 1960.

3.3.42 H. Herφ K. D. Uko, A. Filipovic and
J. L. Duncan,
Scandinavian Journal of Metallurgy 6,
282, 1977.

3.3.43 A. Kozasu and K. Kubota,
Trans. I.S.I. Japan 11, 321, 1971.

3.3.44 T. B. Cox and J. R. Low,
Met. Trans. 5, 1457, 1974.

3.3.45 J. W. Hancock, I.L. Dillamore and
R. E. Smallman,
Paper 24, 6th Plansee Seimnar on High Temp-
erature Materials, Reutte/Tyrol, Austria,
June 24, 1968.

3.3.46 T. C. Lindley, G. Oates and C. E. Richards, Acta. Met. 8, 1127, 1970.

3.3.47 T. C. Lindley, G. Oates and C. E. Richards, "Effect of 2nd. Phase Particles on Mechanical Properties of Steel". The Iron and Steel Institute, London, 1972.

3.3.48 C. Tipper, Metallurgica 39, 133, 1959.

3.3.49 K. Puttock, Phil. Mag. 4, 964, 1959.

3.3.50 F. A. McClintock, International J. of Applied Mech., p. 363, June 1963.

3.3.51 J. R. Rice and D. M. Tracey, J. Mech. Phys. Solids 17, 201, 1969.

3.3.52 M. A. Nagumo, Acta. Met. 2, 1161, 1973.

3.3.53 L. M. Brown and J. D. Embury, 3rd International Conf. on Strength of Metals and Alloys, Cambridge, England, Paper33. Vol. 1, p.164, 1973.

3.3.54 S. H. Goods and L. M. Brown, Acta Met. 27, 1, 1979.

3.3.55 K. Tanaka, T. Mori and T. Nakamura, Phil. Mag. 21, 1970.

3.3.56 A. Filipovic, H. Herϕ and J. D. Embury, Scandinavian Journal of Metallurgy, Vol. 6, 89, 1977.

3.3.57 A. Melander, "The Influence of Work Hardening Rate on Ductile Fracture". Swedish Institute for Metals Research Report, Number IM-1427, Feb. 1980.

3.3.58 A. Melander, "The Influence of the Strain Rate Sensitivity on Ductile Fracture". Swedish Institute for Metal Research Report, Number IM-1443, March, 1980.

3.3.59 A. L. Gurson, Journal of Eng. Mat. and Tech. 99, 2, 1977.

3.4 REFERENCES

3.4.1 F.A. Nichols
Acta Met. 28, 663, 1980

3.4.2 A.S. Argon
"The Inhomogeneity of Plastic deformation"
p. 161
Edited by R.E. Reed Hill, A.S.M. Publications
1971

3.4.3 A.H. Cottrell
"The relation between the structure and mechanical Properties of Metals"
National Physical Laboratory Symposium
Number 15, January 1963.

3.4.4 E.W. Hart
Acta Met. 15 351, 1967

3.4.5 A.K. Ghosh
Acta Met. 25, 1413, 1977

3.4.6 J.D. Campbell
J.Mech.Phys. Sol. 15. 359, 1967

3.4.7 M.J. Hillier
J.Mech.Sci. 7. 531, 1965

3.4.8 M.J. Hillier
Ibid 7. 539, 1965

3.4.9 E. Duncombe
Ibid 14, 325, 1972

3.4.10 E. Duncombe
Ibid 10, 1445, 1974

3.4.11 M.Y. Okuda, M.C.C. Rodriquez and P.R. Cetlin
Scripta Met. 1, 101, 1977

3.4.12. G.E. Dieter
"Mechanical Metallurgy" McGraw-Hill

3.4.13 R.Hill
J.Mech.Phys.Sol. 1. 19, 1952

3.4.14 S.P. Keeler and W.A. Backofen
Trans ASM 56. 25, 1963

3.4.15 J.J. Jonas, R.A. Holt and C.E. Coleman
Acta Met 24. 911. -976

3.4.16 J.J. Jonas and B. Baudelet
Acta Met 25, 43, 1977

3.4.17 A. Melander and Kjell-Ole Husby
Swedish Institute for Metal Research Report
No. IM-1416 Nov. 1979

3.4.18 A.K. Ghosh
Met. Trans. 8A 1221, 1977

3.4.19 A.K. Ghosh
"Formability, analysis, modeling and experiment" Edited by S.S. Hecker, A.K. Ghosh and H.L. Gegel
T.M.S. Publications 1978

3.4.20 J.W. Hutchinson and K.W. Neale
Acta Met. 25, 839, 1977

3.4.21 D. Lee and F. Zavel Jr.
Acta Met. 28. 1415, 1980

3.4.22 J.M. Jalinier, N. Christodoulou, B. Baudelet and J.J. Jonas
"Formability, analysis, modelling and Experiment" edited by S.S. Hecker, A.K. Ghosh and H.L. Gegel
P.29. T.M.S. Publications 1978

3.4.23 U.F. Kocks, J.J. Jonas and H. Mecking
Acta. Met. 27. 419, 1979

3.4.24 J.P. Miles
J.Mech.Phys. Solids 19. 89. 1971

3.4.25 J.W. Hutchinson and J.P. Miles
J.Mech.Phys. Solids 22, 61, 1974

3.4.26 R. Hill
J.Mech.Phys.Solids 10, 1, 1962

3.4.27 A. Melander
"Scandinavian Journal of Metallurgy"
9, 51, 1980

3.4.28 I.L. Dillamore, J.G. Roberts and A.C. Bush
J. of Metal Sci. 2, 73, 1979

2.4.29 Z. Maciniack
"Mechanics of Sheet Metal Forming: material behaviour and deformation analysis"
Edited by D.P. Koistinen of N.M.Wang,
General Motor Symposium, 1978.

3.6 REFERENCES

3.6.1 R.L. Whiteley and D.E. Wise
Trans ASM 52, 154, 1960

3.6.2 M. Takahashi and A. Okamoto
5th International Conference on Texture
of Materials, AAchen 1978

3.6.3 T. Matsuoka and K. Yamamoti
"Metallurgical Aspects in Cold rolled High
strength steel sheets"
ASM/AIME Materials Engineering Congress

3.6.4 T. Gladman, D. Dulieu and I.D. McIvor
Microalloying 75

3.6.5 F.B. Pickering
The Metallurgist and Materials Technologist
July 1977 page 375

3.6.6. I.L. Dillamore, K.I. Nam and M.B.O.O. Shitta
"Formability in higher strength sheet steels"
3rd Congresso Brasileiro de Engenharia e
Ciencia des Materials, Dec. 1978 Brasil

3.6.7 N.P. Allen
J.I.S.I. 174, 108, 1953

3.6.8 A.P. Coldren
Trans AIME 163, 1973

3.6.9 M. Martenson
Met. Trans. 2, 3490, 1971

3.6.10 J.B. Balance
14th Mechanical Working and Steel Processing
Conference Met. Soc. AIME, 1972

3.6.11 L. Luyckx, J.R. Bell, A. McLean and M. Korchynsky
Met. Trans. 7, 3341, 1970

3.6.12 G. Glover and J. Havranek
J. Aust. Inst. Met. 18, 82, 1973

3.7 REFERENCES

3.7.1 A.M. Sage
"Dual-Phase Cold Pressing Vanadium Steels in the Automobile Industry"
Proceedings Vanitec Seminar, Berlin, October 1978

3.7.2 S.Hayami and T. Furukawa
Microalloying 75 p 311, 1975

3.7.3 H. Takechi and M. Usuda
10th Biennial Congress IDDRG, Warwick U.K. 1978, p.211

3.7.4 T. Matsuoka and K Yamaori
Met. Trans. 6A, 1613, 1975

3.7.5 M.S. Rashid
SAE Paper No.760206 Feb.1976

3.7.6 K. Araki, K. Nakaoka, M.Abe and N. Ohashi
Proc. 9th IDDRG Congress 1976, p.39.

3.7.7 R. Lagneborg
Vanitec Seminar Oct. 1978

3.7.8 A. Holmström, P. Öström, R. Lagneborg
Swedish Institute for Metal Research
Report No.IM-1423, Jan.1980

3.7.9 A.P. Coldren and G. Tither
J. of Metals 30, 6, 1978

3.7.10 A.P. Coldren and G.T. Eldis
J. of Metals 3, 41, 1980

3.7.11 J.M. Rigsbee and P.J. Vander Arend
"Laboratory Studies of Microstructures and Structure-Propety Relationships in Dual-Phase SLA Steels".
AIME Symposium on "Modern Development in HSLA Formable Steels" AIMEFALL Meeting, Chicago, 1977.

3.7.12 R.G. Davies
Met. Trans. 9, 41, 1978

3.7.13 R.G. Davies
Met. Trans. 9, 451, 1978

3.7.14 R.G. Davies
Met. Trans. 9, 671, 1978

3.7.15 P.E. Repas
Vanitec Seminar, Berlin, Oct. 1978

3.7.16 P.G. Shewman
"Transformations in Metals p. 61
McGraw-Hill Book Company

3.7.17 H. Masui
Trans. ISI Japan, 16, 69, 1976

3.7.18 W.B. Morrison
Trans. ASM 89, 824, 1966

3.7.19 R.G. Davies
Vanitec Seminar, Berlin, Octo. 1978

3.7.20 R.G. Davies
Met. Trans.ION, 113, 1979.

3.8 REFERENCES

3.8.1 R.G. Davies, Ford Motor Company Research Lab. Technical Report No. SR-77-51, 1977

3.8.2 M.S. Rashid, General Motors Research Publication GMR-2647

3.8.3 J.M. Rigsbee and P.J. Van Der Arend, A.I.M.E. Symposium on "Modern Developments in HSLA Formable Steels", A.I.M.E. Fall Meeting, Chicago, 1977

3.8.4 R. Lagneborg, Vanitec Seminar, Berlin, Oct. 1978

3.8.5 K. Nakaoka, K. Araki, and K. Kurihara, A.I.M.E. Fall Meeting, Oct. 1977

3.8.6 M.S. Rashid, General Motor Corporate Research Laboratory Report GMR-1044, Feb. 1976

3.8.7 J.W. Morrow, G. Tither and R.M. Buck, Climax Molybdenum Co. Research Lab. Report, L-176-182, March, 1978

3.8.8 J.F. Butler and J.H. Butler, Vanitec Seminar, Berlin, Oct. 1978

3.8.9 P. Ustrŏm, Swedish Inst. for Metal Research Report, IM-1308, August 1978

3.8.10 B. Karlson and B. Sundstrom, Mat. Sci. Eng., 16, 161, 1974

3.8.11 P.E. Repas, Vanitec Seminar, Oct. 1978

3.8.12 W.C. Leslie and R.J. Sober, Trans. ASM, 60, 459, 1967

3.8.13 B. Jaoult, J. Mech. Phys. Solids, 5, 45, 1957

3.8.14 W.R. Cribb and J.M. Rigsbee, In Structures and Properties of Dual-Phase Steels, Edited by R.A. Kot and J.W. Morris, A.I.M.E. Publication, 1979

3.8.15 J. Gerbase, J.D. Embury and R.M. Hobbs, ibid

3.8.16 G.R. Speich and R.L. Miller, ibid

3.8.17 D.K. Matlock, G. Krauss, L.F. Ramos and G.S. Huppi, ibid

3.8.18 L.F. Ramos, D.K. Matlock and G. Krauss, Met. Trans. 10A, 259, 1979

3.8.19 R.G. Davies, Ford Motor Co. Research Lab. Tech. Report, SR-77-50- August 1977

3.8.20 K. Araki, Y. Takada and K. Nakaoda, Trans. I.S.I., Japan, 17, 710, 1977

3.8.21 S.T. Mileiko, J.Mat.Sci., 4, 974, 1969

3.8.22 J.Y. Koo, M.J. Young and G. Thomas, Met. Trans. 11A, 852, 1980

3.8.23 Y. Tomota, K. Kuroki, T. Mori and I. Tamura, Mat. Sci. and Eng., 24, 85, 1976

3.8.24 H.K.D.H. Bhadeshia and D.V. Edmonds, J.Met. Sci., 2, 41, 1980

3.8.25 W.H. Bruckner, Welding Journal Res. Suppl. 29, 467, 1950

3.8.26 C.J. McMahon, Acta Met. 13, 591, 1965

3.8.27 T. Gladman, B. Holmes and I.D. McIvor, "Effect of 2nd Phase Particles on the Mechanical Properties of Steel", I.S.I. Report p. 68, 1971

3.8.28 J. Gurland, et al, Trans. ASM, 61, 1968

3.8.29 J. Gurland, Acta Met. 20, 735, 1972

3.8.30 R. Stevenson, General Motor Res. Lab. Report No. 2432

3.9 REFERENCES

3.9.1 M.S. Rashid, "SAE Preprint 770211", Feb. 1977

3.9.2 M.S. Rashid and G.D. Lawrence, SAE Paper No. 780138, Feb. 1978

3.9.3 M.S. Rashid, Vanitec Seminar, Berlin, Oct.1978

3.9.4 J.A. Lumm, G.M. Hughes and B.J. Bastian, SAE Preprint No. 740179, Feb. 1974

3.9.5 J.S. Kary, SAE Preprint No. 760012

3.9.6 R.G. Davies and C.L. Magee, Vanitec Seminar, Berlin, Oct. 1978

3.9.7 Vanitec Technical Committee Report, "Dual-Phase Steels in Automobile Industry", Vanitec Seminar, Berlin, Oct. 1978

3.10 REFERENCES

3.10.1 G.V. Ranch and W.C. Leslie, Met. Trans., 3, 373, 1972

3.10.2 N.H. Polakowski, J.I.S.I., 169, 337, 1951

3.10.3 R.J. Olsen and G.S. Ansell, Trans. ASM, 62, 711, 1969

3.10.4 J.N. Goodier, J.App. Mech., 55, 39, 1933

3.10.5 W.C. Leslie and R.J. Sober, Trans. ASM, 60, 459, 1967

3.10.6 R. Chait, Met. Trans., 3, 365, 1972

3.10.7 D. Kalish and M. Cohen, Trans. ASM, 62, 353, 1969

3.10.8 G.R. Speich and A.S. Keh, 1968 Research Report, U.S. Steel Corporation, Monroeville, Pa. U.S.A., Reported in reference (3.10.1)

3.10.9 J.P. Hirth and M. Cohen, Met. Trans., 1, 3, 1970

3.10.10 W.A. Spitzig, R.J. Sober and O. Richmond, Acta Met. 23, 885, 1975

3.10.11 F.B. Fletcher, M. Cohen and J.P. Hirth, Met. Trans. 5, 905, 1974

3.10.12 D.C. Drucker, Met. Trans. 4, 667, 1973

3.10.13 C.A. Pampillo, L.A. Davies and J.C.H. Li, Scripta Met., 6, 765, 1972

3.10.14 W.C. Leslie, Scripta Met., 6, 1145, 1972

3.10.15 C.A. Pampillo, L.A. Davies and J.C.M. Li, Scripta Met., 6, 1147, 1972

3.10.16 W.F. Hosford and T.J. Allen, Met. Trans., 4, 14, 1973

REFERENCES

4.1 A. Daglish, A. Duncan and M.B.O.O. Shitta, Paper presented by A. Daglish at a seminar of the IDDRG Liege, Belgium, 1979.

4.2 J.E. Hilliard and J.W. Cahn, Trans. AIME 221, 344, 1961.

4.3 P.B. Hirsch and F.J. Humphreys, Proc. Roy. Soc. A318, 45, 1970.

4.4 T. Malkiewicz and Rudnic, J.I.S.I., 1 33, 1963.

4.5 T. Inoüe and S. Kinoshita, Trans. I.S.I.J. 17, 245, 1977.

4.6 M. Hatherly and W.B. Hutchinson, "An Introduction to Texture in Metals", The Institution of Matallurgists, Monograph No. 5, 1979.

References

5.1 A. E. Lord and D. N. Beshers,
Acta. Met. 14, 1659, 1966.

5.2 R. G. Davies,
Met. Trans. 10A, 1549, 1979.

CHAPTER 6 REFERENCES

6.1 G.C. Weatherly, J.Met. Sci., 2, 237, 1968

6.2 J.K. Lee, Y.Y. Earmine, H.L. Aaronson and K.C. Russell, Met. Trans. 114, 1837, 1980

6.3 L.M. Brown, G. Woolhouse and U. Valdre, Phil. Mag. 17, 781, 1968

6.4 M.F. Ashby and L. Johnson, Phil. Mag. 20, 1009, 1969

6.5 H. Brooks, Reported in reference 6.2, Metal Interfaces, p.20, ASM Metals Park, OH, 1952

6.6 J.M. Moyer and G.S. Ansell, Met. Trans. 6A, 1785, 1975

6.7 M.F. Ashby, S.H. Gelles and L.E. Tanner, Phil. Mag, 19, 757, 1969

6.8 M. Nishida, 10th I.D.D.R.G. Congress Proceedings p. 211, 1978, Warwick, England

6.9 Tomo Tanaka, Minoru Nishid,Koichi Hashiguchi and Toshieyaki Kato, In structure and properties of dual-phase steels, page 221, edited by R.A. Kot and J.W. Morris, The Metallurgica Socient of A.I.M.E.

6.10 R.L. Fleishor and W.F. Hosford Jr., Trans. Met. Soc. A.I.M.E. 221, 244, 1961

6.11 A.W. Thompson, Scripta Metall, 8, 145, 1971

6.12 S. Miyazaki, K. Shibata and H. Fujita, Acta Met. 27, 855, 1979

6.13 S. Miyazaki and H. Fujita, Trans. J.I.M. 19, 438, 1978

6.14 D.V. Wilson, Acta Met. 13, 807, 1965

6.15 J.W. Christian, 2nd International Conference on the Strength of Metals and Alloys, ASM, 1970, p. 31

6.16 R. Priestner, Acta Met. 13, 564, 1965

6.17 A.W. Sleeswyk, Acta Met. 12, 670, 1964

6.18 A.W. Sleeswyk, Acta Met. 10, 705, 1962

6.19 A.W. Sleeswyk and C.A. Verbraak, Acta Met. 9, 917, 1961

6.20 C.A. Verbraak, Private Communications

TABLE : 4.1

STEEL	C	Mn	Si	Cr	Mo	P	S	AL	Cu	Ni	Ce	N	O	Ti
DOFASCO	0,04	1,25	1,10	0,57	0,38	0,021	0,010	0,18	—	—	0,010	0,009	—	—
AL-Si	0,07	0,31	0,045	—	—	<0,01	0,034	0,072	—	—	—	—	—	—
Ti-STEEL	0,10	0,84	0,10	0,11	0,03	0,018	0,022	0,17	0,13	0,13	0,13	0,13	—	0,17
MILD-STEEL	0,07	0,30	0,007	S/Tr	S/Tr	0,010	0,022	S/Tr	—	—	S/Tr	S/Tr	—	—

S/Tr = SLIGHT TRACE

FIGURE 4.1 Production schedule of as-received steel (ex Dofasco)

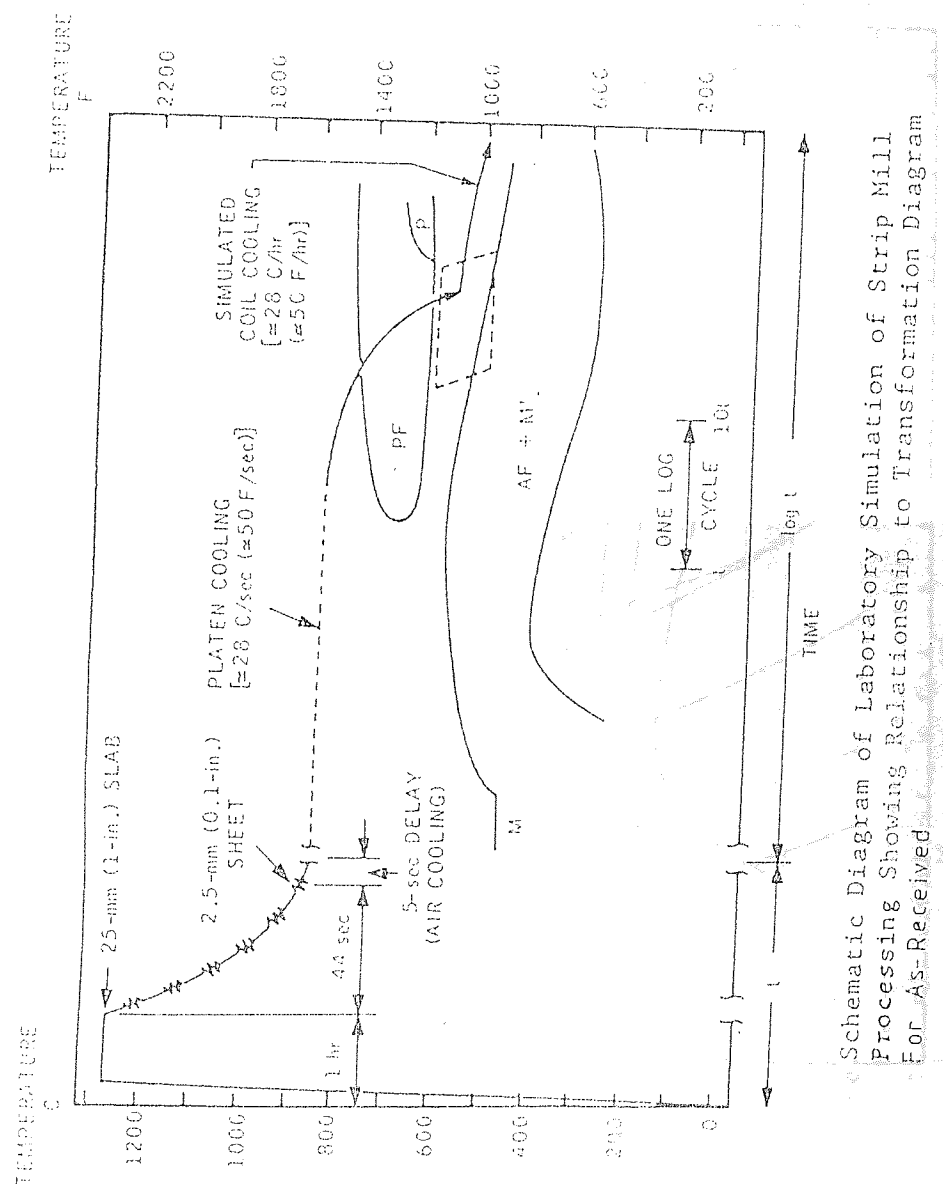

Schematic Diagram of Laboratory Simulation of Strip Mill Processing Showing Relationship to Transformation Diagram For As-Received

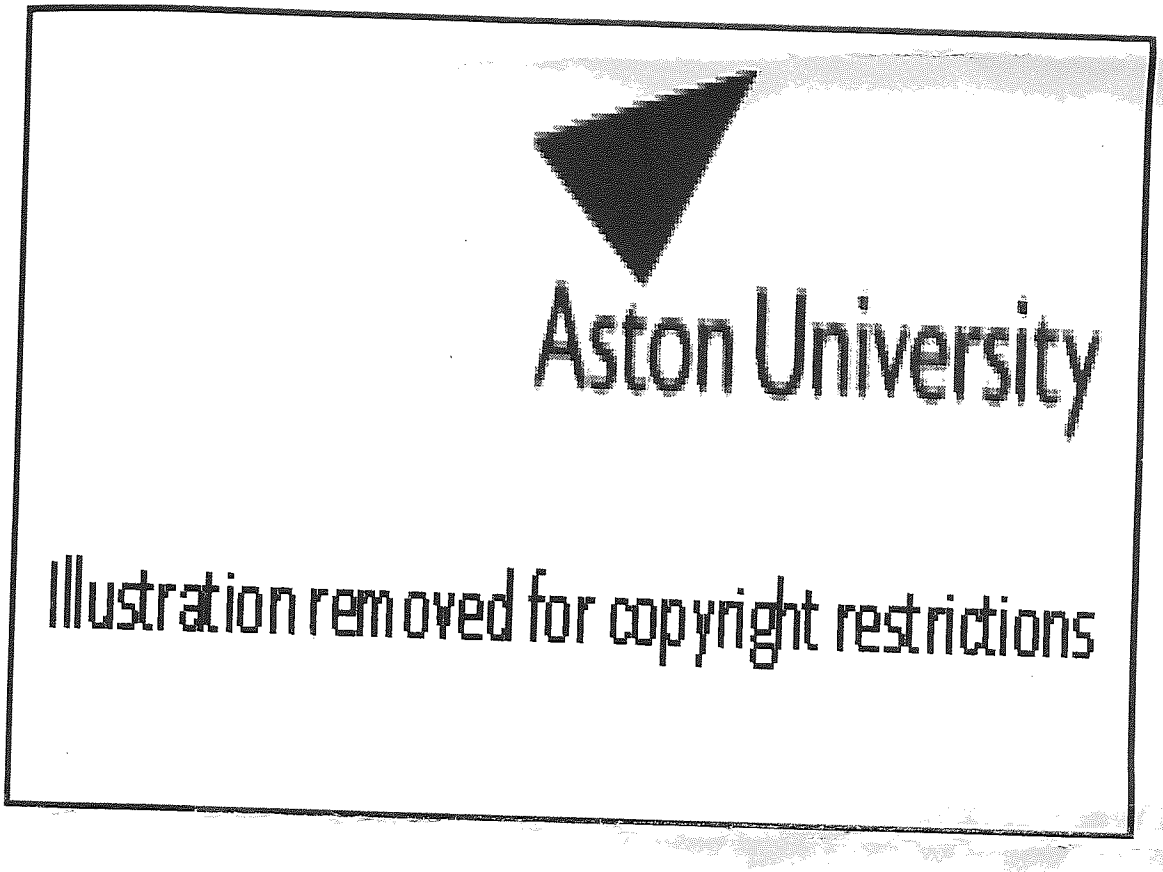
Aston University
Illustration removed for copyright restrictions

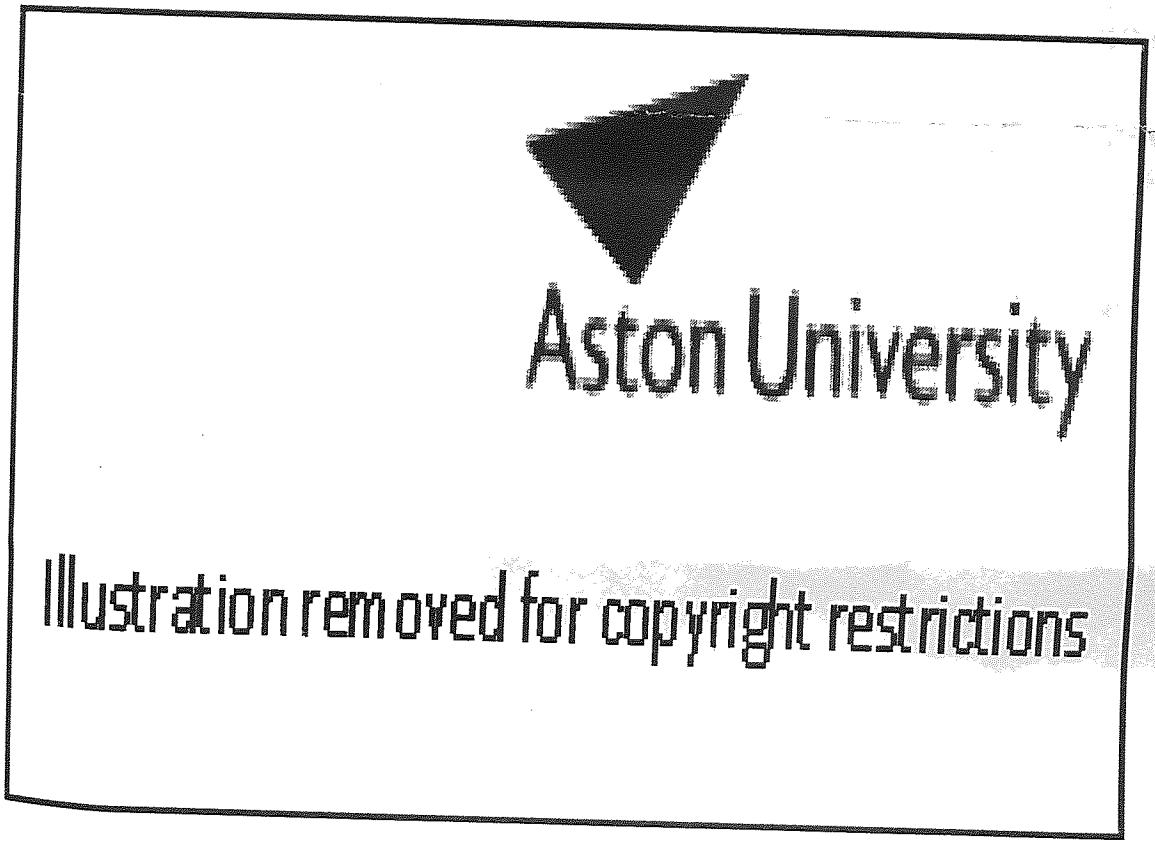
Aston University
Illustration removed for copyright restrictions

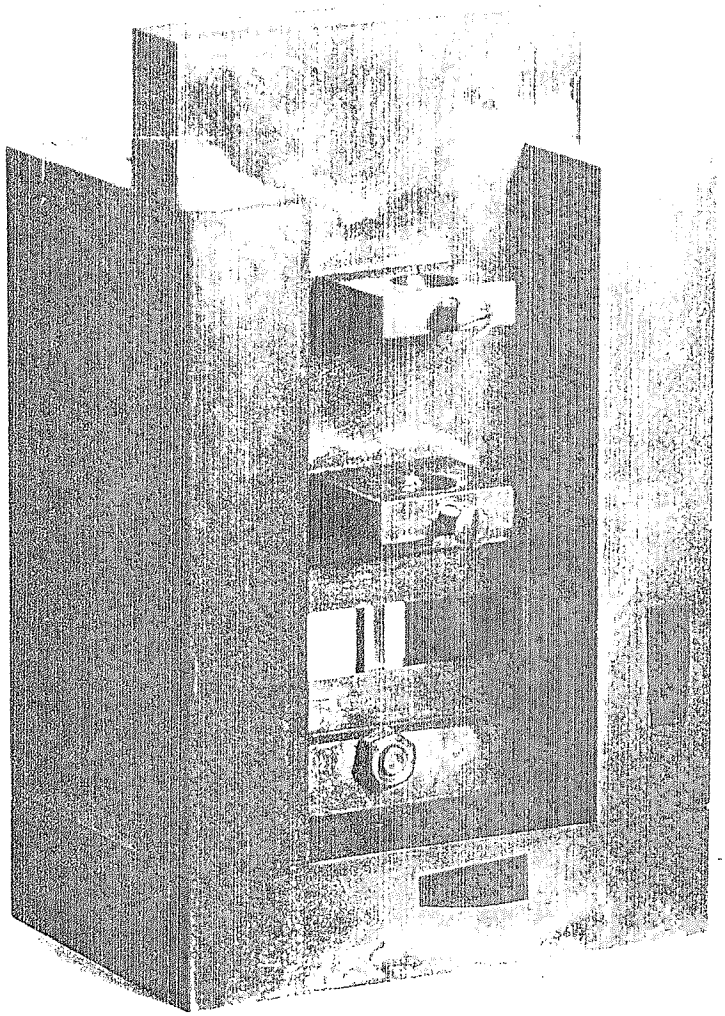

FIGURE 4.3 Showing the jig used for compression testing

CM = Connected Microstructure
DM = Disconnected Microstructure

TABLE 5.1a

No.	Treatment		Type	G.S. dμm	$d^{-\frac{1}{2}}$	% M	Y.S. (0.2% off set) Kg/mm^2	T.S. Kg/mm^2	$<n_{value}>$	e_τ %	ε_u %	λ
1	700°C	1a	DM	13	277.4	20.0	28.54	61.16	.165	18.5	12.4	
2	700°C	1a	DM	13.1	276.3	19.5	24.36	60.55	.160	21.5	13.5	
3	620°C	1a	DM	9.76	320.1	14.5	23.04	66.67	.165	21.5	15.7	
4	620°C	1a	DM	9.76	320.1	14.5	27.42	69.22	.175	18.5	14.0	
5	620°C	1a	DM	8.29	347.3	16.5	23.96	67.38	.200	20.5	17.3	
6	540°C	1a	DM	9.47	325.00	16.5	26.61	67.58	.185	19.0	14.2	
7	540°C	1a	DM	12.10	287.5	16.0	26.61	66.26	.195	20.0	15.0	
8	700°C	1b	DM	24.40	202.4	9.0	25.38	49.95	.190	21.3	16.5	
9	700°C	1b	DM	23.50	206.3	10.0	20.89	47.09	.170	17.3	13.4	
10	700°C	1b	CM	9.12	331.1	18.0	31.29	56.57	.170	25.0	18.5	
11	700°C	1b	CM	11.20	298.8	9.5	31.91	51.58	.200	20.5	17.1	
12	700°C	1b	CM	11.20	298.8	9.5	25.18	48.83	.210	21.8	17.3	
13	700°C	1b	CM	9.72	320.8	16.5	34.35	61.67	.170	22.5	17.4	
14	620°C	1b	DM	19.10	228.8	12.0	23.96	54.43	.180	18.5	13.9	
15	620°C	1b	DM	19.60	225.9	12.0	24.26	55.25	.220	17.0	14.0	
16	540°C	1b	CM	8.70	339.0	13.0	34.56	68.91	.215	22.5	16.5	
17	540°C	1b	CM	9.23	329.2	18.0	33.23	63.30	.175	17.4	13.3	
18	540°C	1b	CM	9.21	329.5	24.0	34.35	75.03	.150	21.0	15.4	
19	540°C	1b	CM	8.19	349.4	13.0	34.86	70.64	.180	22.5	16.0	
20	540°C	1b	CM	8.01	353.3	25.5	31.60	79.62	.160	22.5	16.2	
21	540°C	1b	CM	9.12	331.1	19.0	32.31	75.54	.170	23.0	16.6	

DM = Disconnected Microstructure

TABLE 5.1b

No.	Treatment		Type	G.S. dμm	$d^{-\frac{1}{2}}$	% M	Y.S. (0.2% off set) Kg/mm^2	T-S. Kg/mm^2	$<n_{value}>$	e_T %	ε_u %	λ
1	(α+γ)	2a	DM	3.33	548.00	24.00	31.41	82.37	.21	25.00	19.72	
2	(α+γ)	2a	DM	4.60	466.30	27.60	36.18	83.39	.20	23.00	19.22	
3	(α+γ)	2a	DM	4.39	477.3	23.10	35.38	84.70	.21	23.00	20.59	
4	(α+γ)	2a	DM	4.60	466.3	20.20	34.81	82.98	.20	22.50	18.12	
5	(α+γ)	2a	DM	6.04	406.9	27.80	33.65	84.10	.20	24.00	19.50	
6	(α+γ)	2a	DM	4.60	466.3	21.20	34.26	82.30	.20	24.50	20.07	
7	(α+γ)	2a	DM	4.83	455.0	27.00	30.80	76.45	.21	25.00	20.17	
8	(α+γ)	2a	DM	5.37	431.5	28.60	33.68	70.80	.20	21.00	17.33	7.20
9	(α+γ)	2a	DM	5.37	431.5	34.30	32.15	73.17	.20	22.00	18.26	6.90
10	(α+γ)	2a	DM	6.00	408.3	20.00	24.20	70.80	.23	21.00	17.78	8.28
11	(α+γ)	2a	DM	6.90	380.70	18.35	28.05	72.76	.22	25.00	19.70	8.44
12	(α+γ)	2b	DM	7.43	366.86	15.10	29.87	73.77	.25	24.00	20.4	8.35
13	(α+γ)	2b	DM	7.74	359.44	18.39	26.63	64.51	.24	20.00	16.17	9.25
14	(α+γ)	2b	DM	6.90	380.70	15.54	27.43	55.08	.19	14.50	11.96	10.24
15	(α+γ)	2b	DM	6.90	380.70	22.07	28.00	60.28	.20	19.00	14.91	9.38
16	(α+γ)	2b	DM	8.78	337.48	17.60	27.75	58.95	.22	14.83	13.20	10.61
17	(α+γ)	2b	DM	9.66	321.75	17.80	30.50	54.11	.20	16.32	14.08	11.60
18	(α+γ)	2b	DM	10.74	305.14	19.50	27.27	59.89	.21	20.00	16.50	14.25
19	(α+γ)	2a	DM	5.16	440.23	15.90	31.91	60.43	.20	26.00	25.00	
20	(α+γ)	2b	DM	19.60		12.00	24.00	55.30	.22	17.0	14.00	

FIGURE 5.1 Showing the microstructure of the as-received material

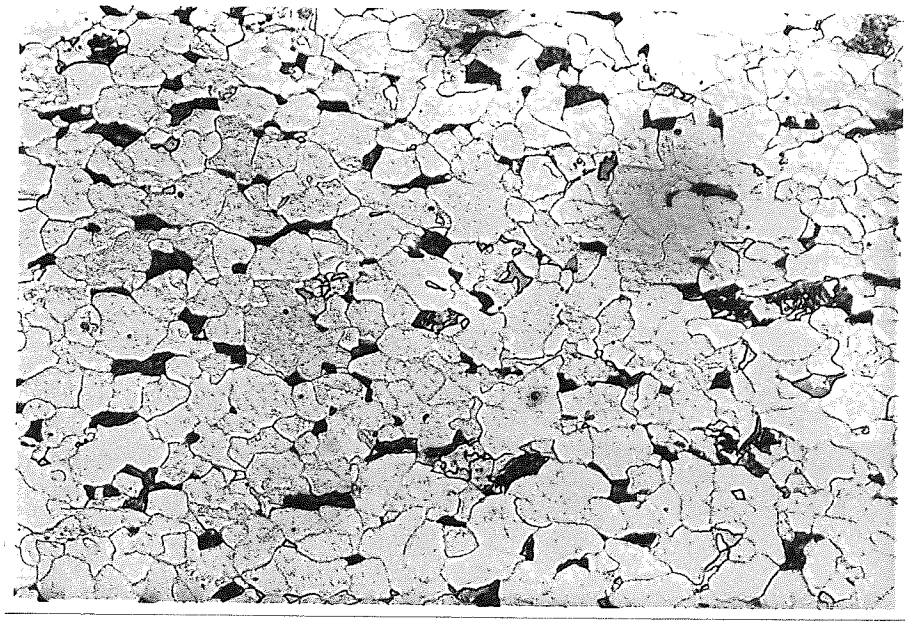

x 1000

FIGURE 5.1a Optical Micrograph of as-received Dofasco steel. Etch with 12 ml HNO_3, 7 ml HCl, 2 ml HF and 480 ml H_2O

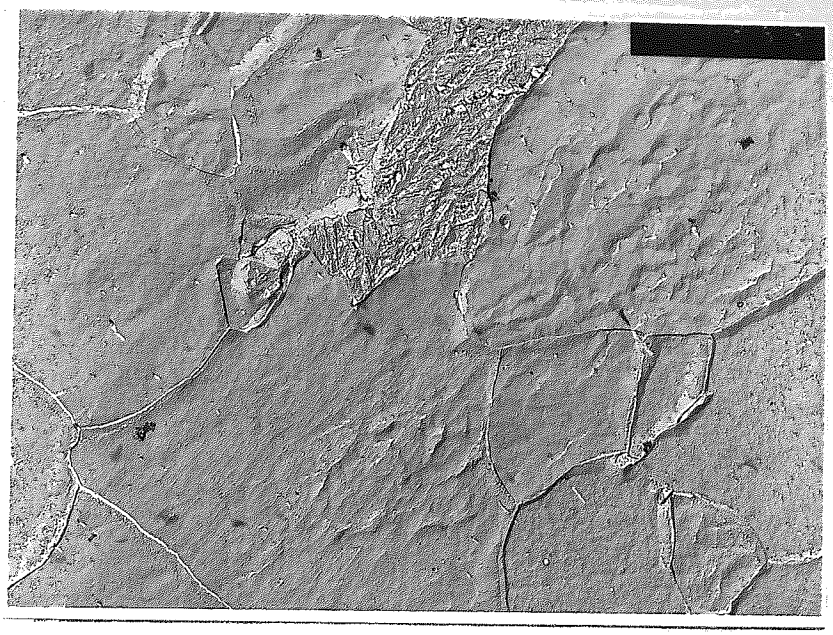

Martensite-Ferrite

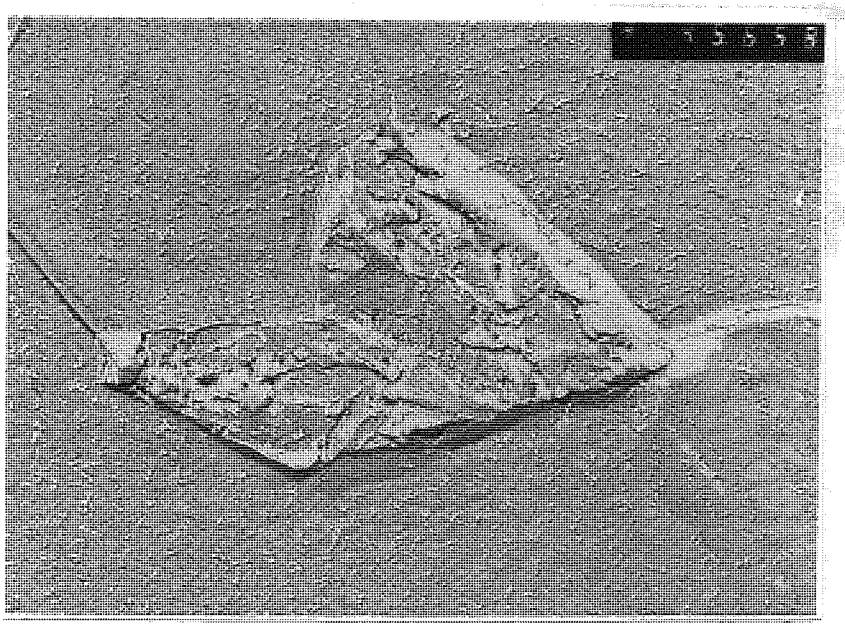

Bainite-Ferrite

FIGURE 5.1b Transmission electron micrograph of the replica of as-received Dofasco steel

FIGURE 5.2 Showing disconnected microstructure

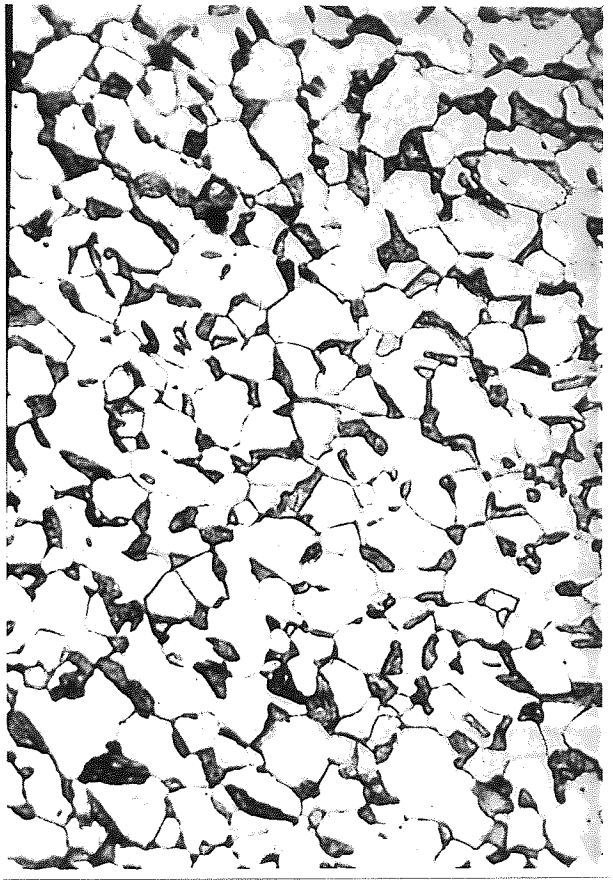

x 600

FIGURE 5.2 Showing disconnected microstructure

FIGURE 5.3 Showing the connected microstructure

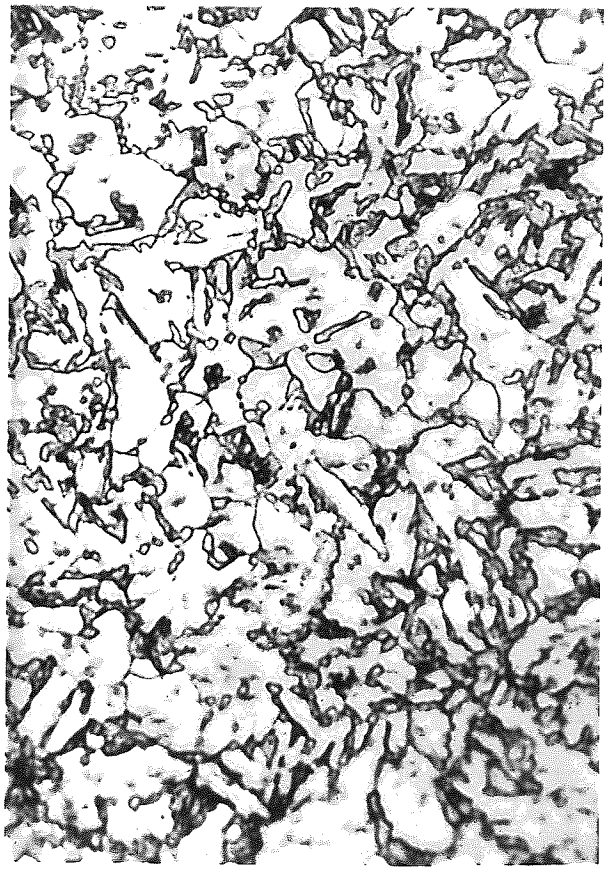

x 600

FIGURE 5.2 Showing the connected microstructure

FIGURE 5.4 Showing the stress/strain curve for as-received Dual-Phase steel compared to a Ti hot rolled steel and mild steel.

Chemical composition of these steels are shown in table 4.1

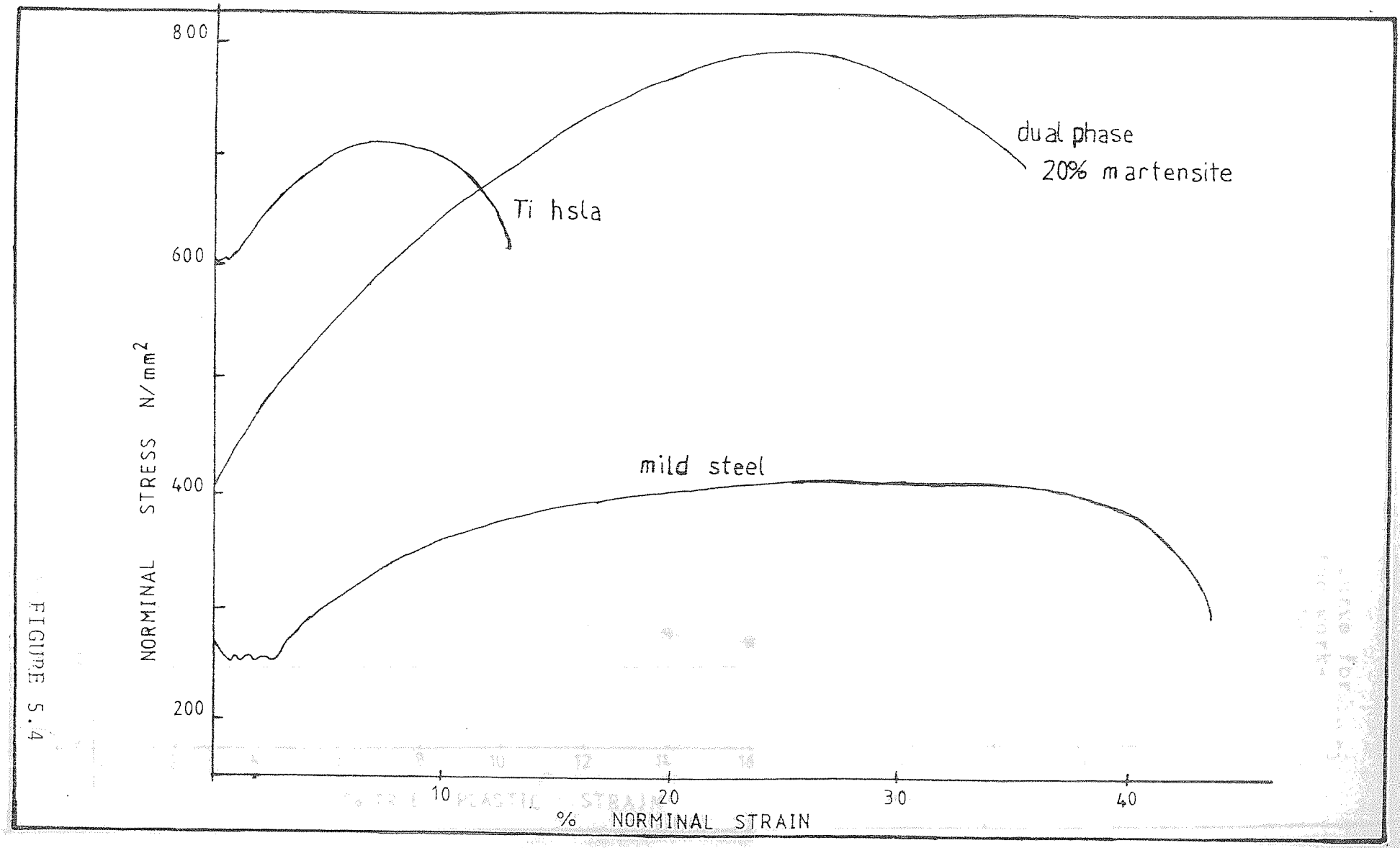
800
600
400
200
NORMINAL STRESS N/mm²
dual phase
20% martensite
Ti hsla
mild steel
10
20
30
40
% NORMINAL STRAIN

FIGURE 5.4

FIGURE 5.5 Showing stress-strain curve for Dual-Phase steel and the work-hardening rate described by

$$\frac{1}{\sigma}\frac{d\sigma}{d\varepsilon}$$

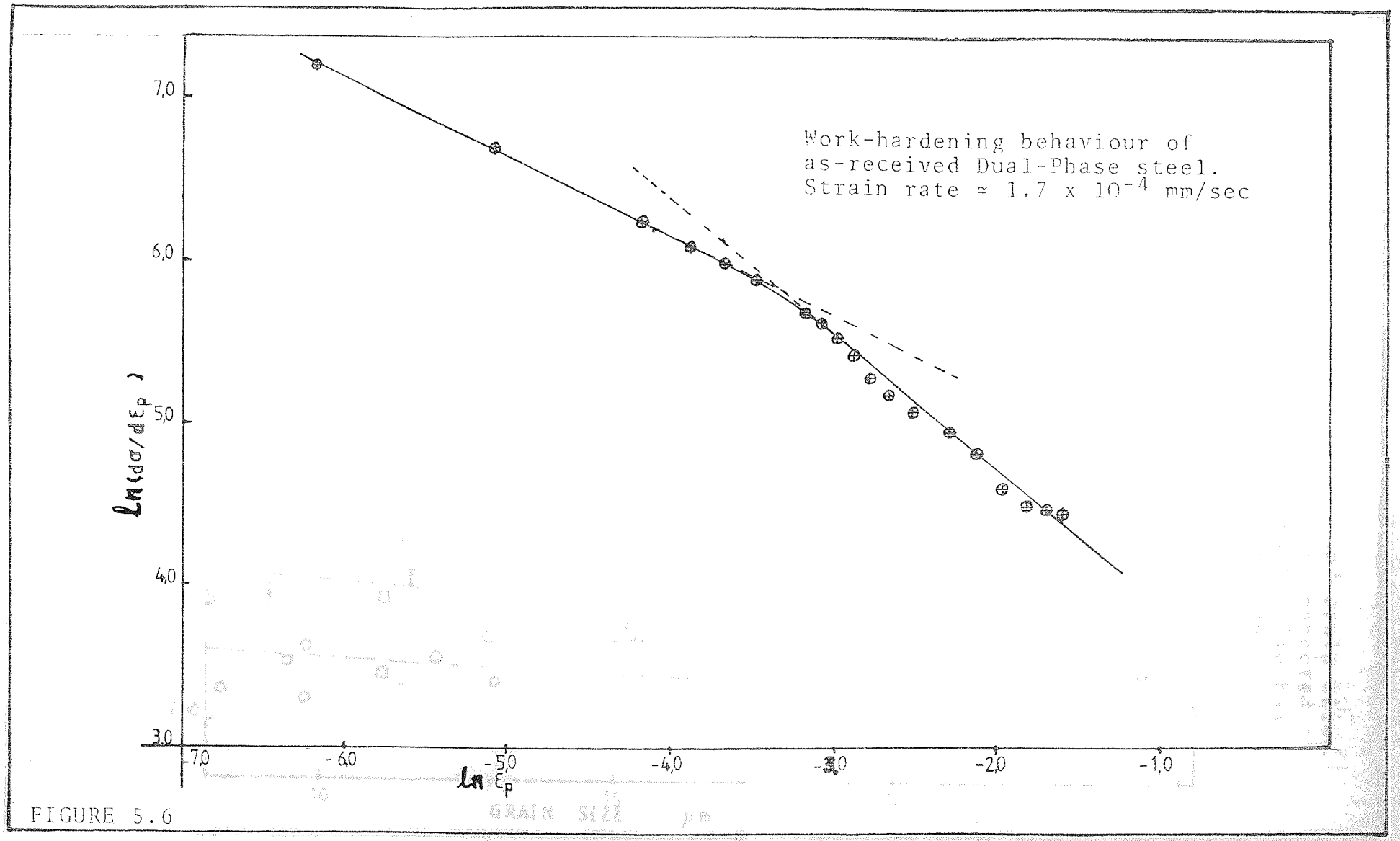
Work-hardening behaviour of
as-received Dual-Phase steel.
Strain rate ≈ 1.7 x 10^{-4} mm/sec
7,0
6,0
5,0
4,0
3,0
$\ln(d\sigma/d\varepsilon_p)$
-7,0
-6,0
-5,0
-4,0
-3,0
-2,0
-1,0
$\ln \varepsilon_p$

FIGURE 5.6

The relationship between strength and grain size for the two types of microstructures connected and disconnected. The effect of martensite has not been isolated from that of grain size

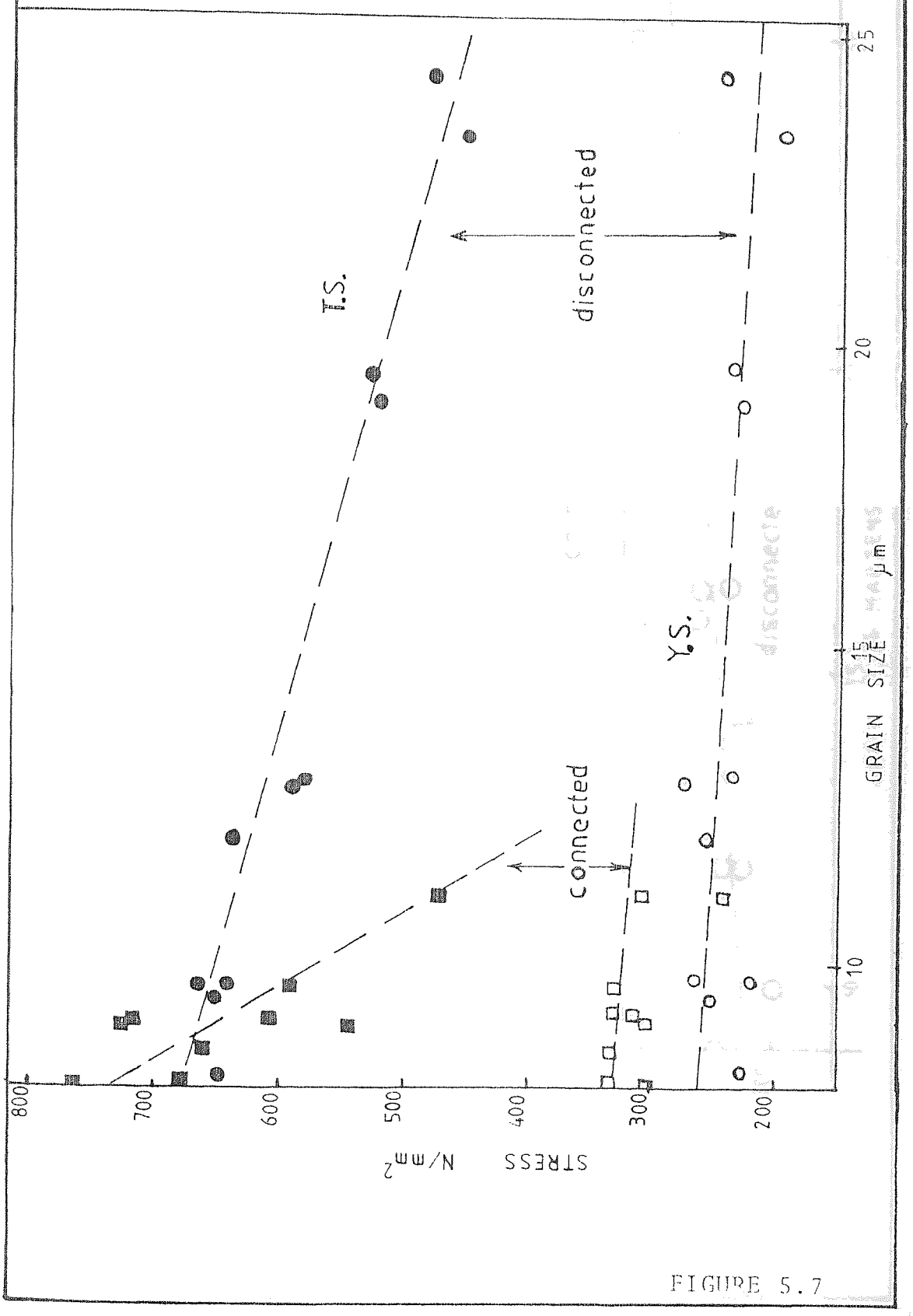

FIGURE 5.7

The relationship between strength and martensite content. The grain size effect is not isolated

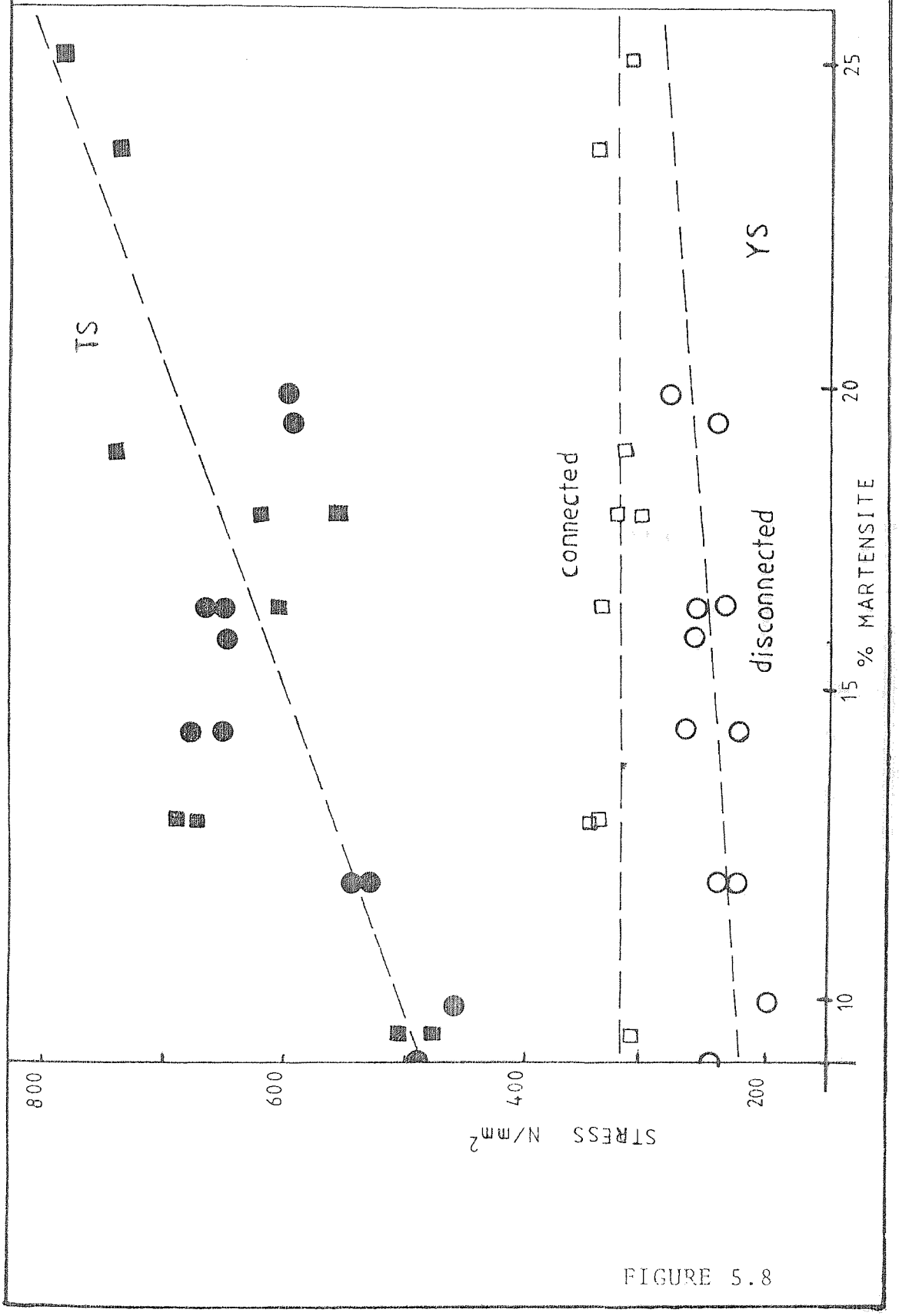

FIGURE 5.8

FIGURE 5.9 Showing graphs of yield strength vs $D^{-\frac{1}{2}}$ and yield strength vs % martensite plotted from the regression equations. Yield strength versus $D^{-\frac{1}{2}}$ is plotted by keeping the % martensite fixed at 20% while yield strength vs % M is plotted by keeping the grain size fixed at 8 μm.

It shows that both the grain size and % M affects the yield strength strongly, grain size slightly higher than % martensite

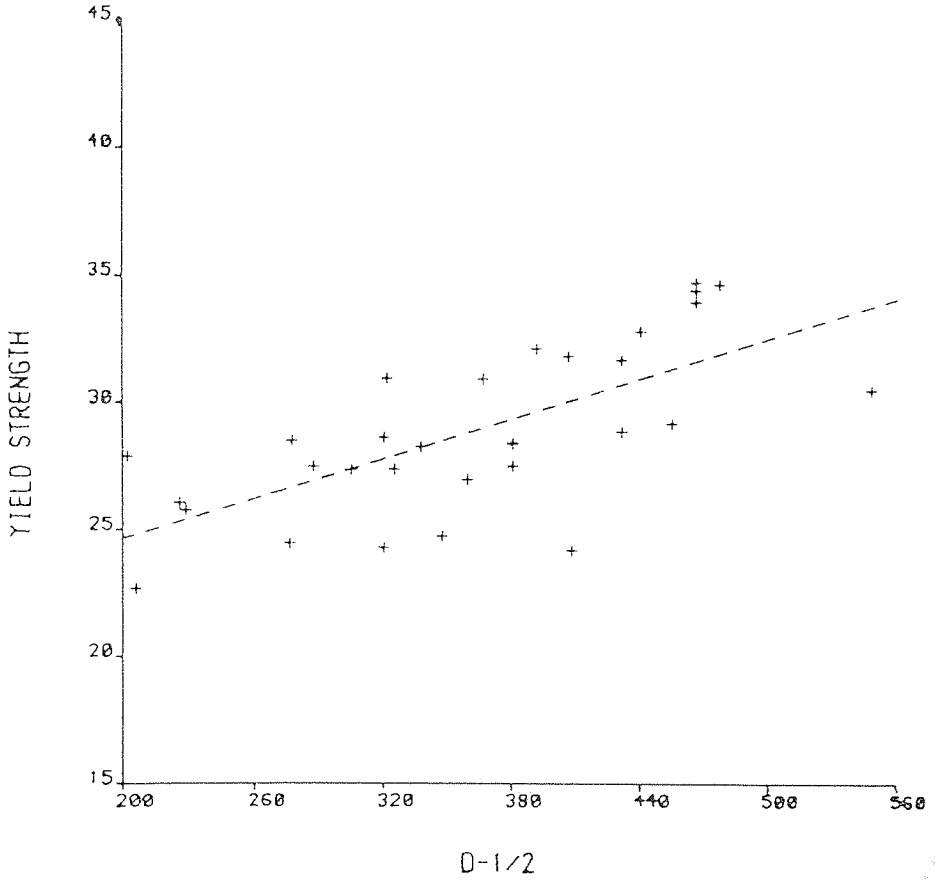

YIELD STRENGTH/D-1/2

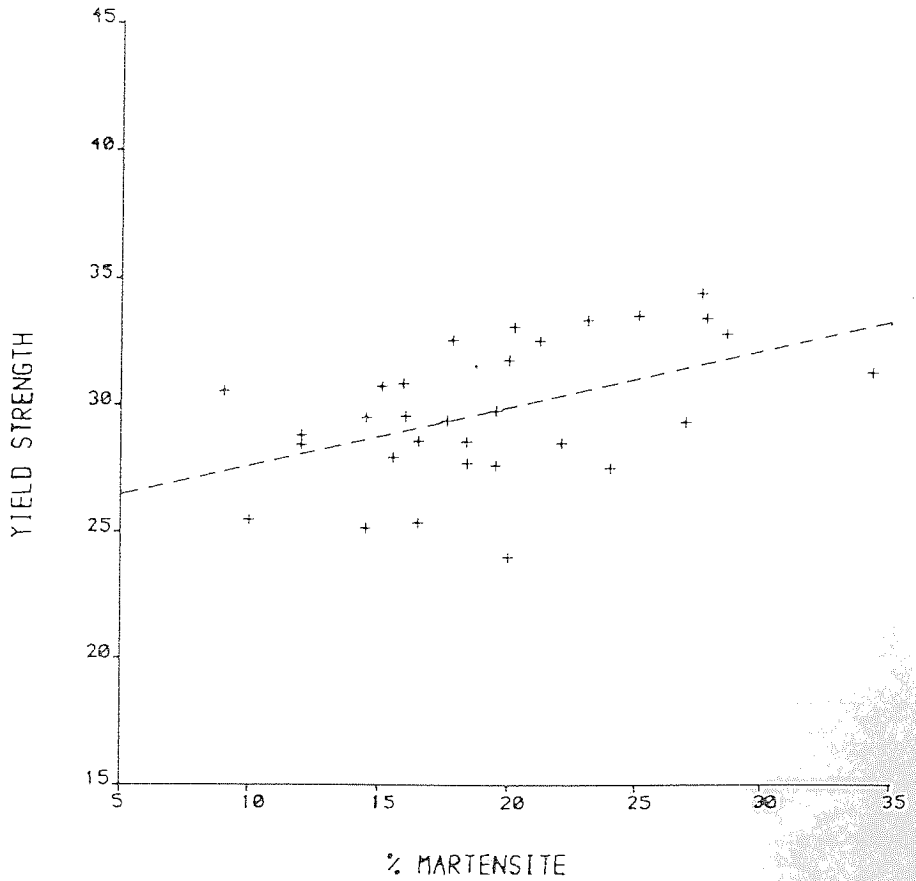

YIELD STRENGTH/%MARTENSITE

FIGURE 5.10 Showing graphs of tensile strength versus $D^{-\frac{1}{2}}$ and % martensite in turn plotted from the regression equation. The curves are plotted by keeping % martensite and grain size fixed at 20% M and 8 μm respectively.

It shows that the grain size influences the tensile strength much more markedly than % martensite through its effect on work-hardening.

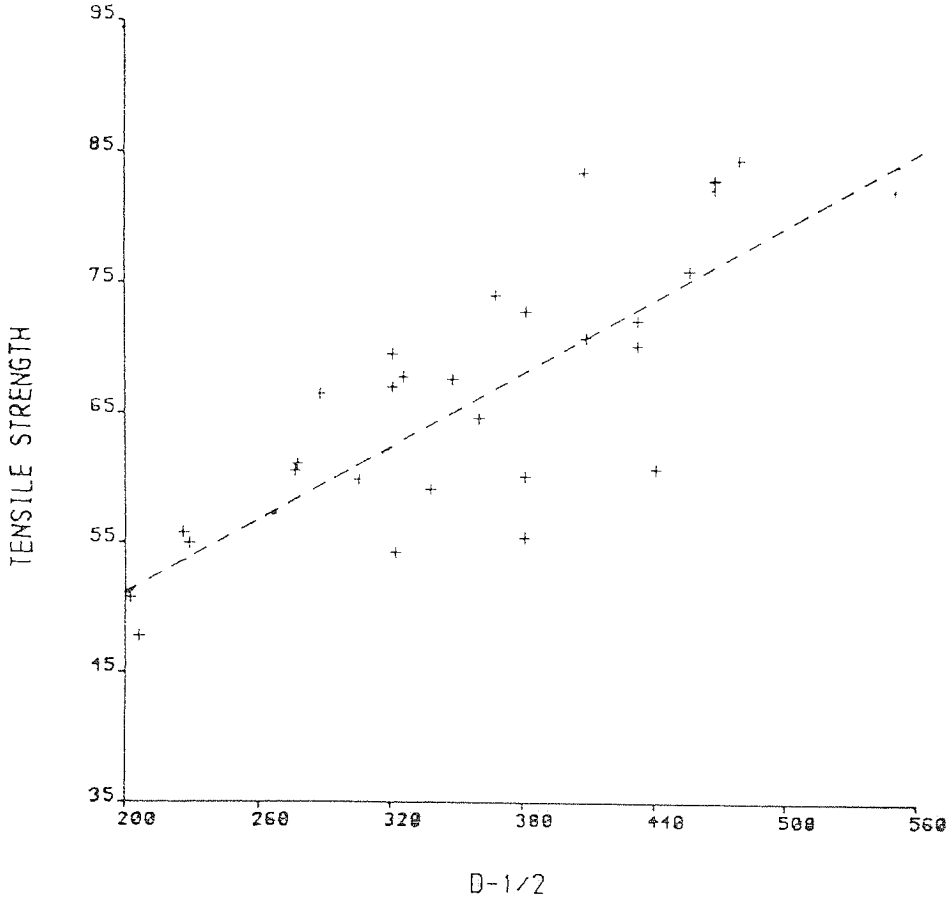

TENSILE STRENGTH/D-1/2

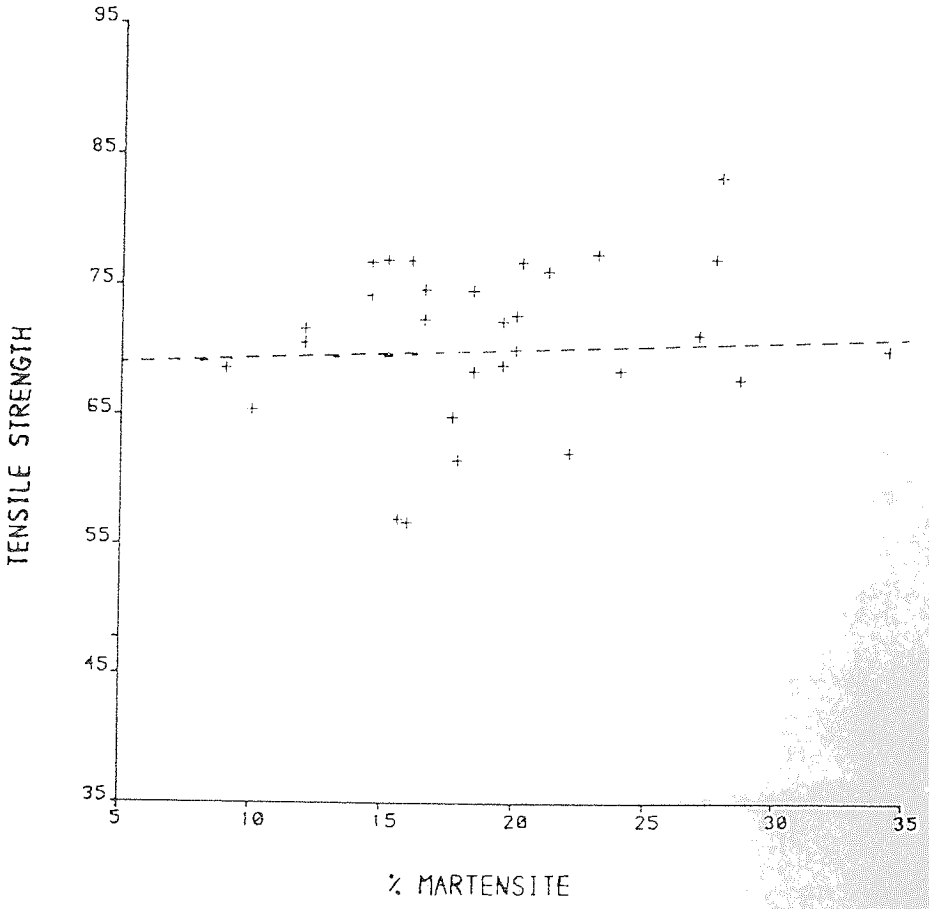

TENSILE STRENGTH/%MARTENSITE

FIGURE 5.11 Showing the effect of the two quantities $D^{-\frac{1}{2}}$ and % M on uniform elongation.

Increasing martensite has negative effect while decreasing the grain size has positive effect.

The curves were drawn from the regression equation keeping grain size at 8 μm and % M at 20% as before.

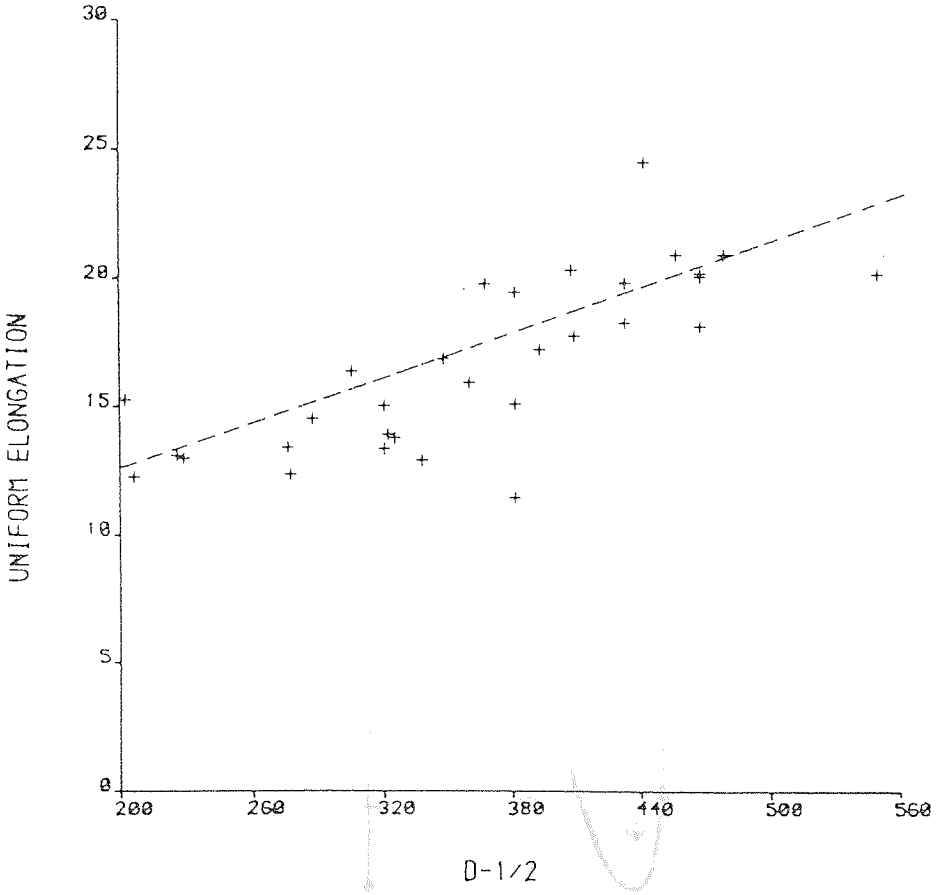

UNIFORM ELONGATION/D-1/2

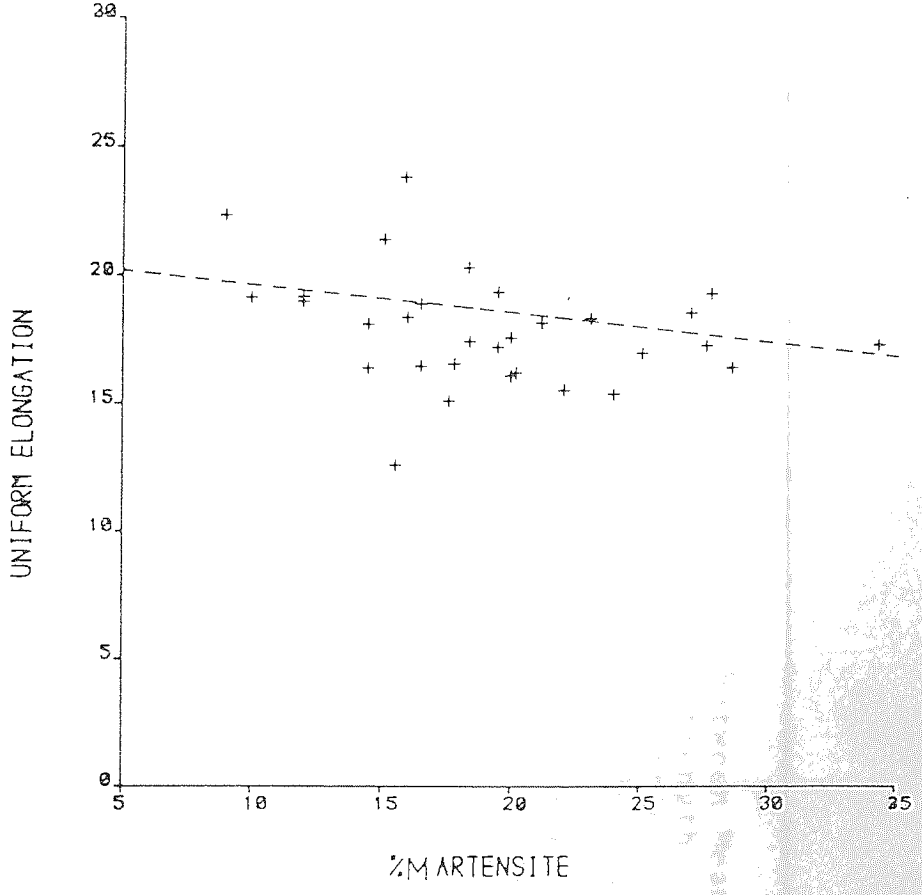

UNIFORM ELONGATION/%MARTENSITE

FIGURE 5.12 Showing the relationship between Mean Interparticle spacing and strength. The yield stress seems to show little dependence on mean interparticle spacing in agreement with the idea that initial yielding is controlled by mean ferrite grain size. The tensile stress shows a greater dependence on interparticle spacing suggesting this is controlled by work-hardening parameter.

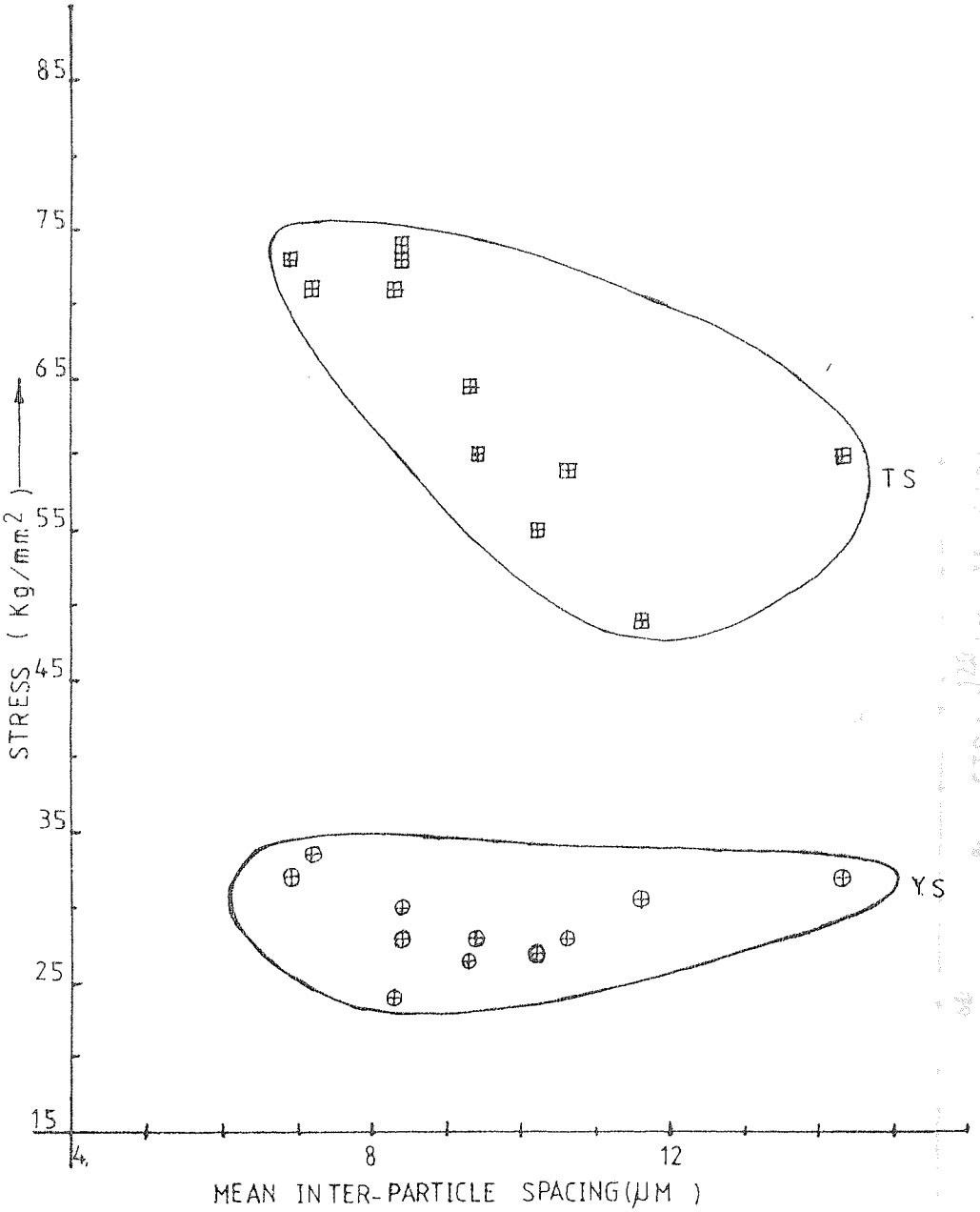

FIGURE 5.13 Showing the effect of Prior Cold Rolling on tensile properties. From which it can be inferred that the deformation process is the same under uniaxial as well as under rolling condition.

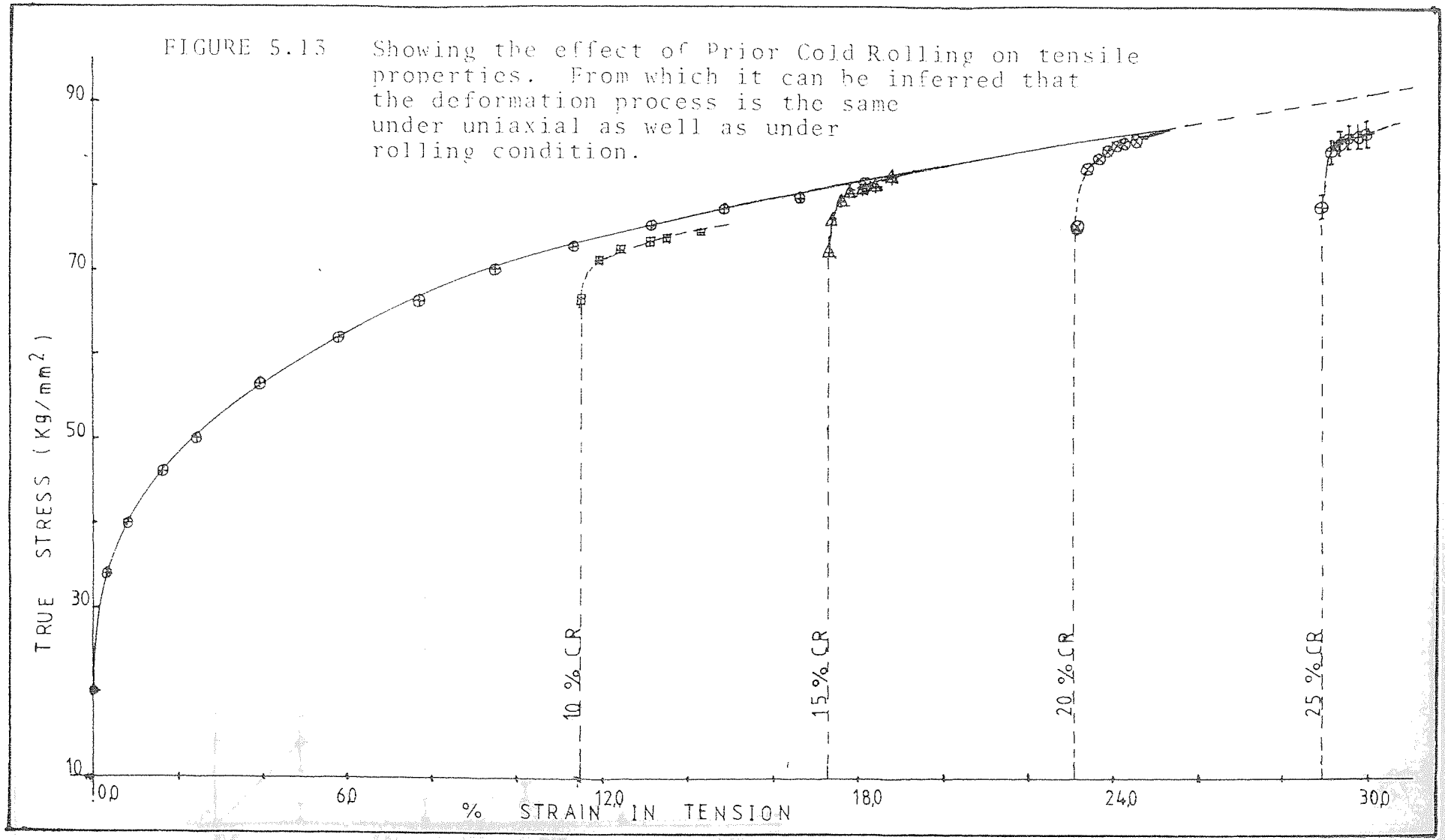

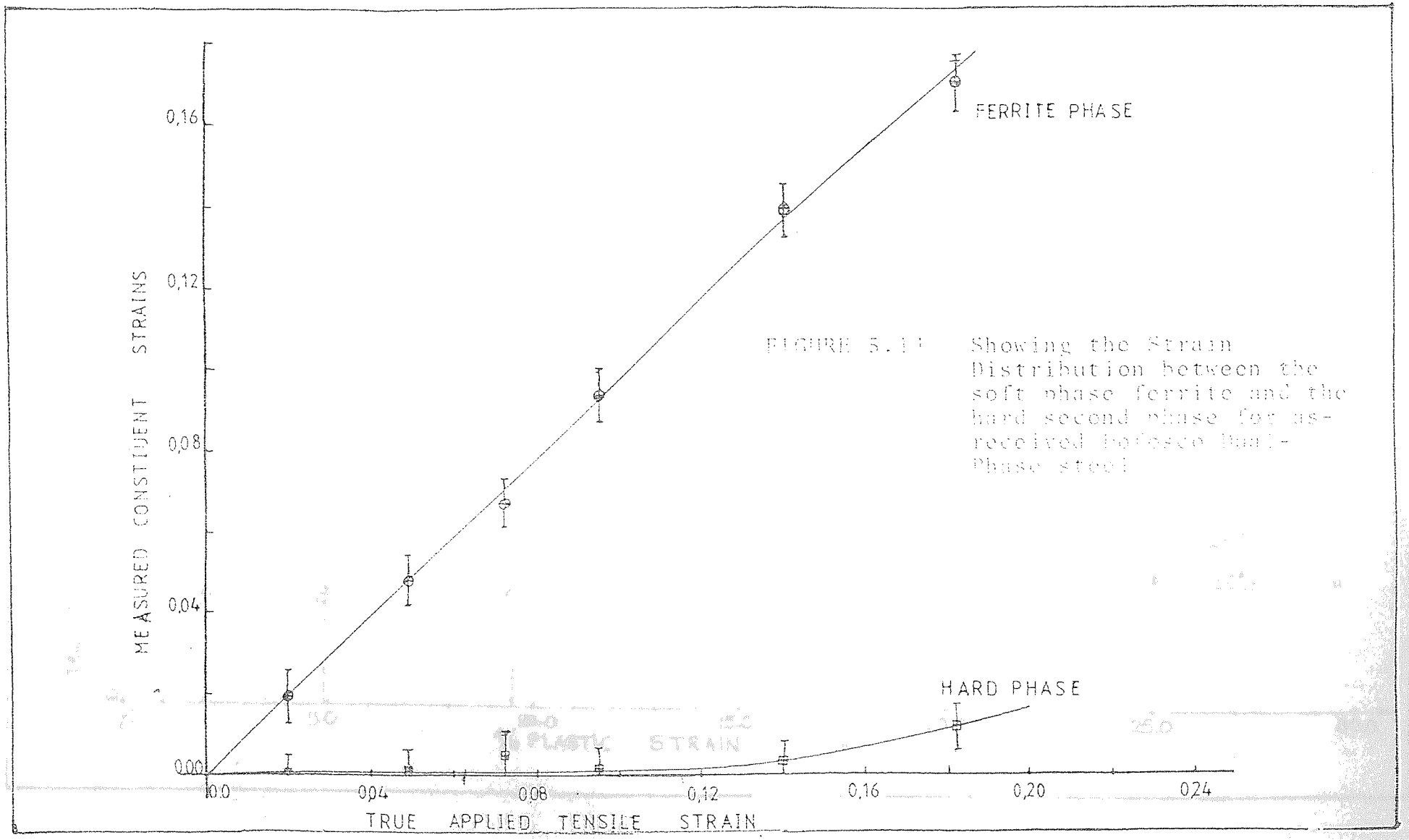

FIGURE 5.11 Showing the Strain Distribution between the soft phase ferrite and the hard second phase for as-received Bofesco Dual-Phase steel

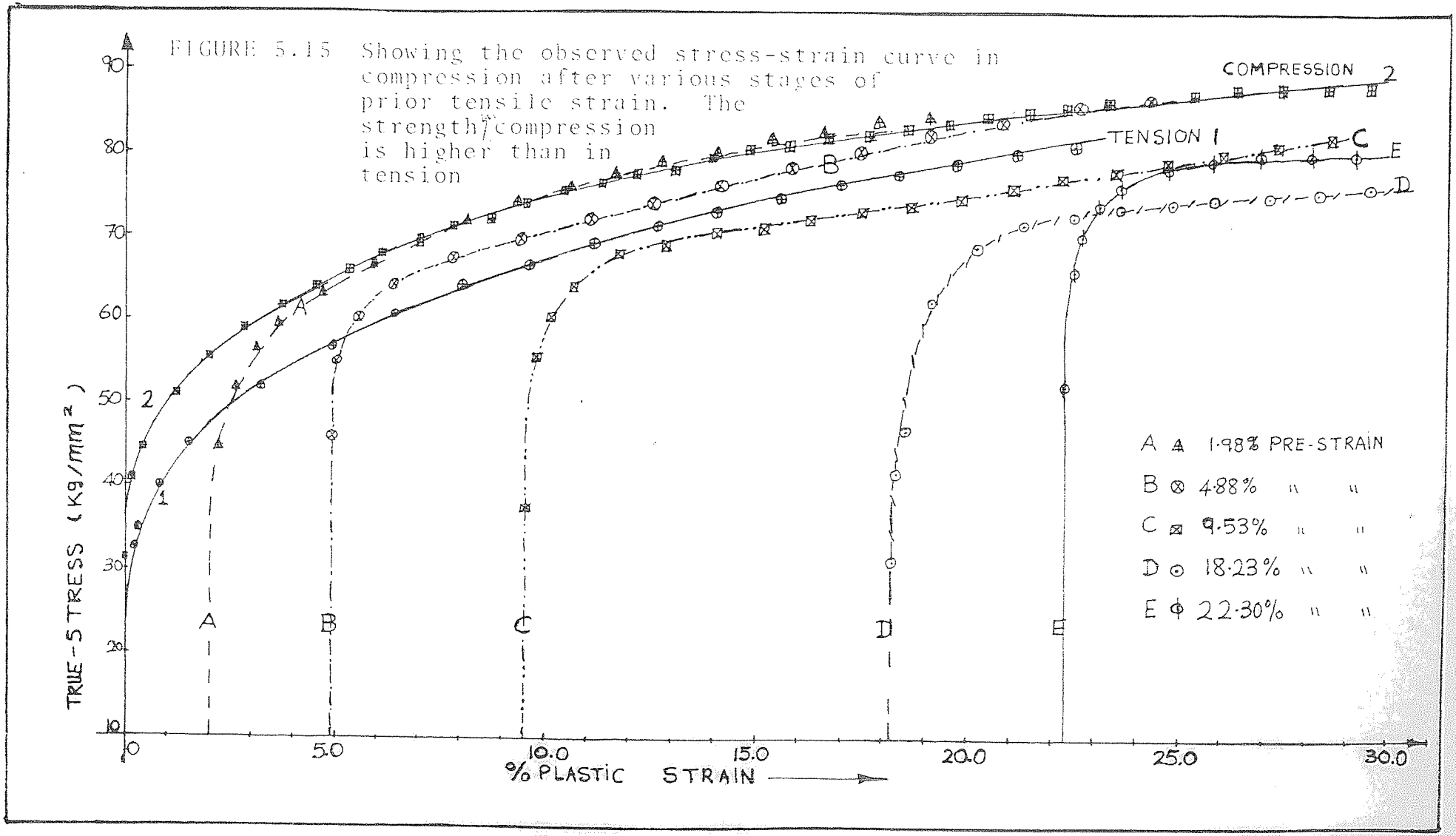

FIGURE 5.15 Showing the observed stress-strain curve in compression after various stages of prior tensile strain. The strength in compression is higher than in tension

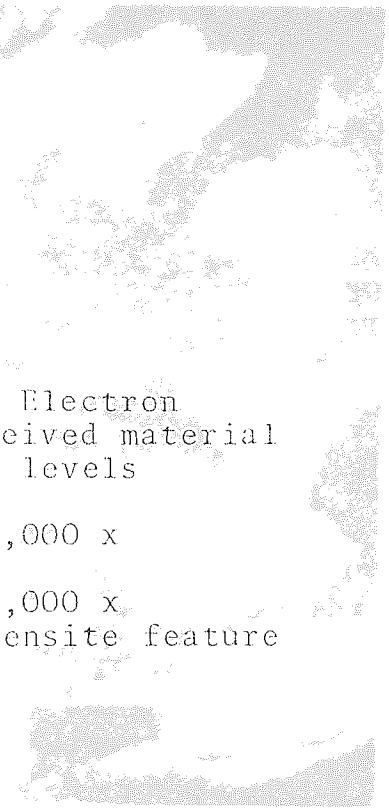

FIGURE 5.16 Showing Transmission Electron Micrograph of as-received material after various strain levels

a) as-received 25,000 x

b) as-received 50,000 x showing the martensite feature

c) 5% strained

d) 10% strained

e) 20% strained

f) 25% strained

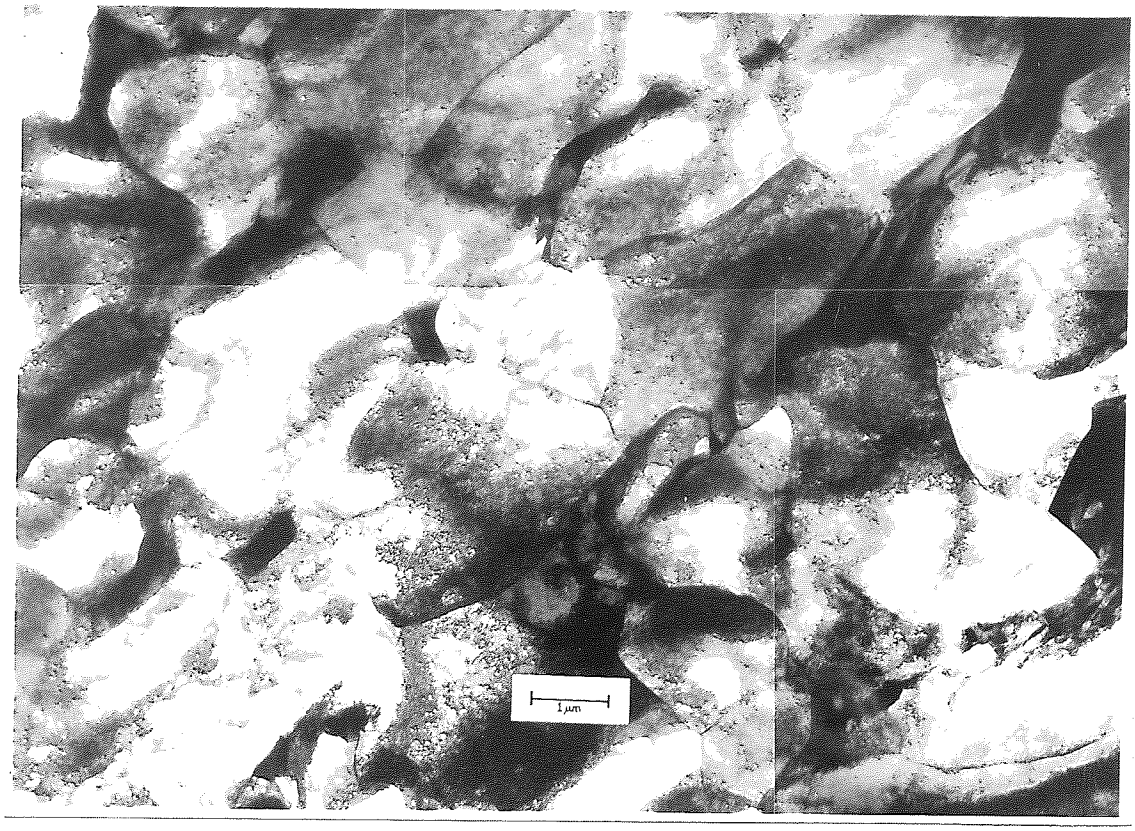

x 25,000

FIGURE 5.16a Showing Transmission Electron Micrograph of as-received material

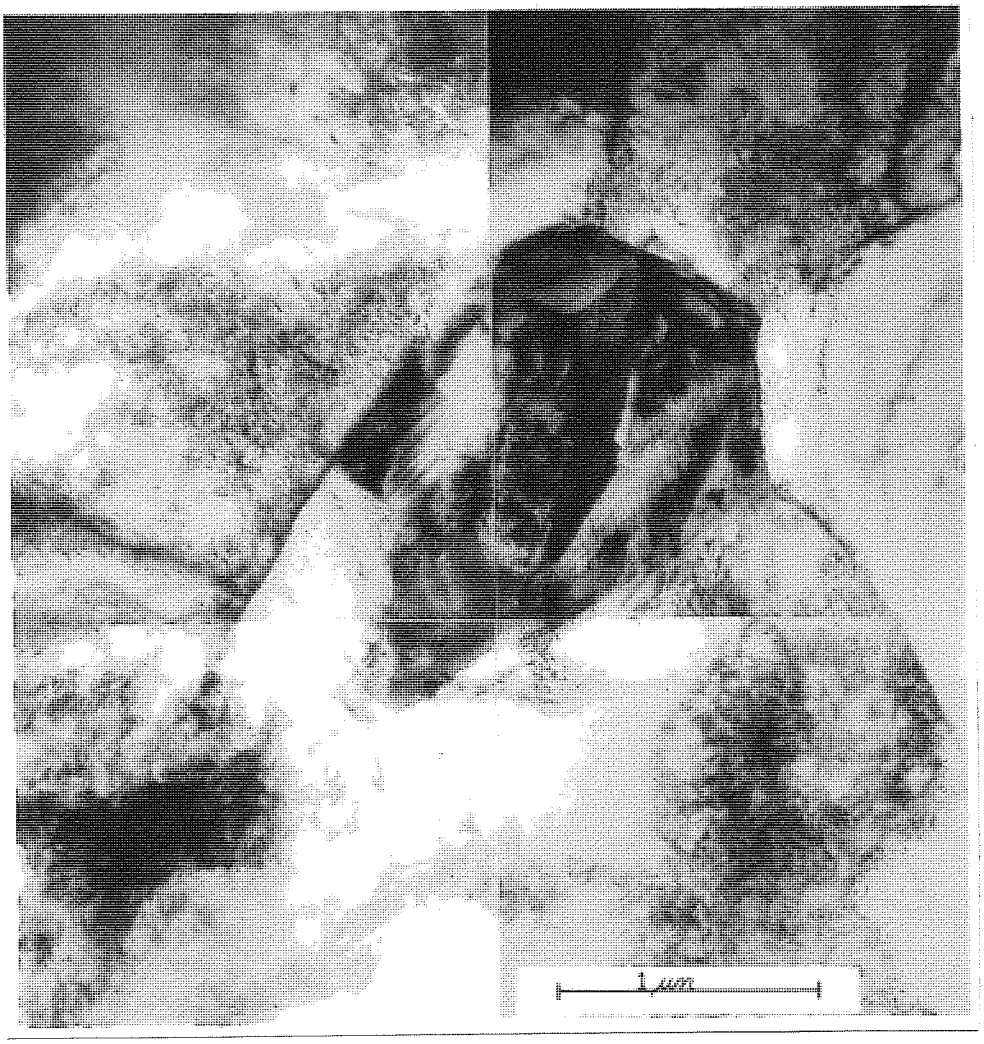

FIGURE 5.16: Showing Transmission Electron Micrograph of As-Received material showing the features of the martensite

b. As-Received, x 50,000

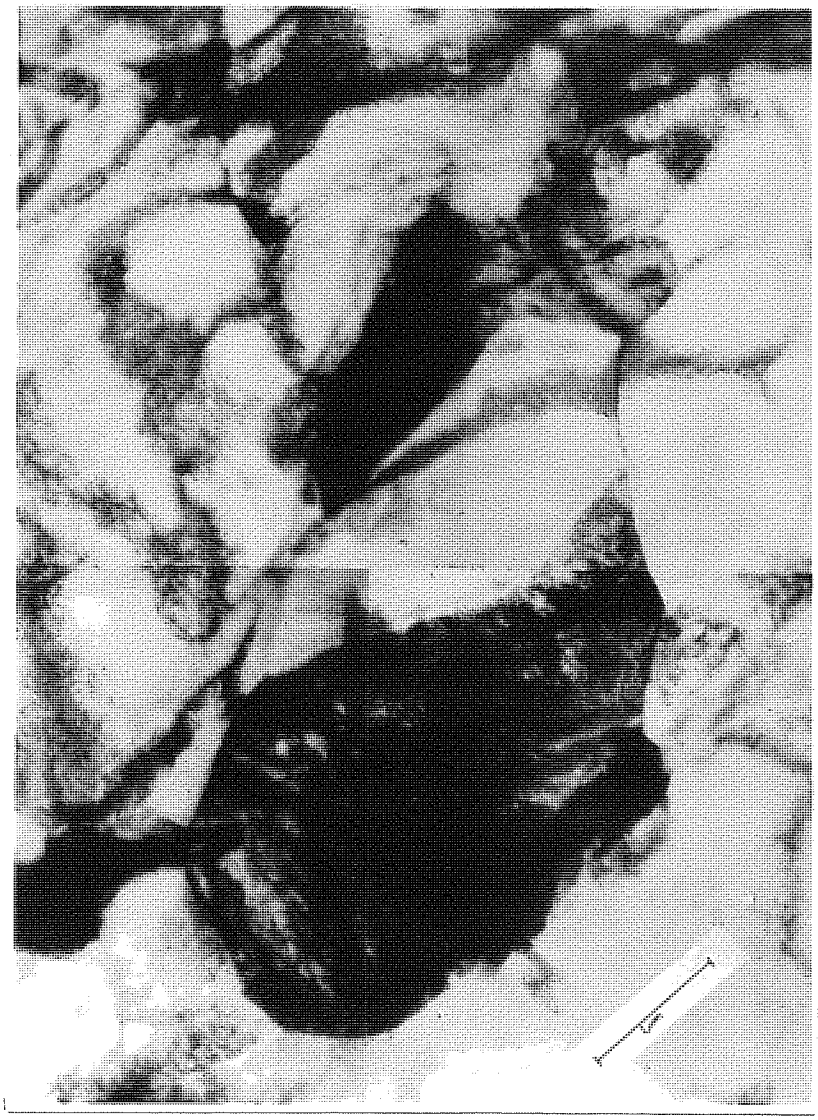

FIGURE 5.16c Transmission Electron Micrograph after 5% strain

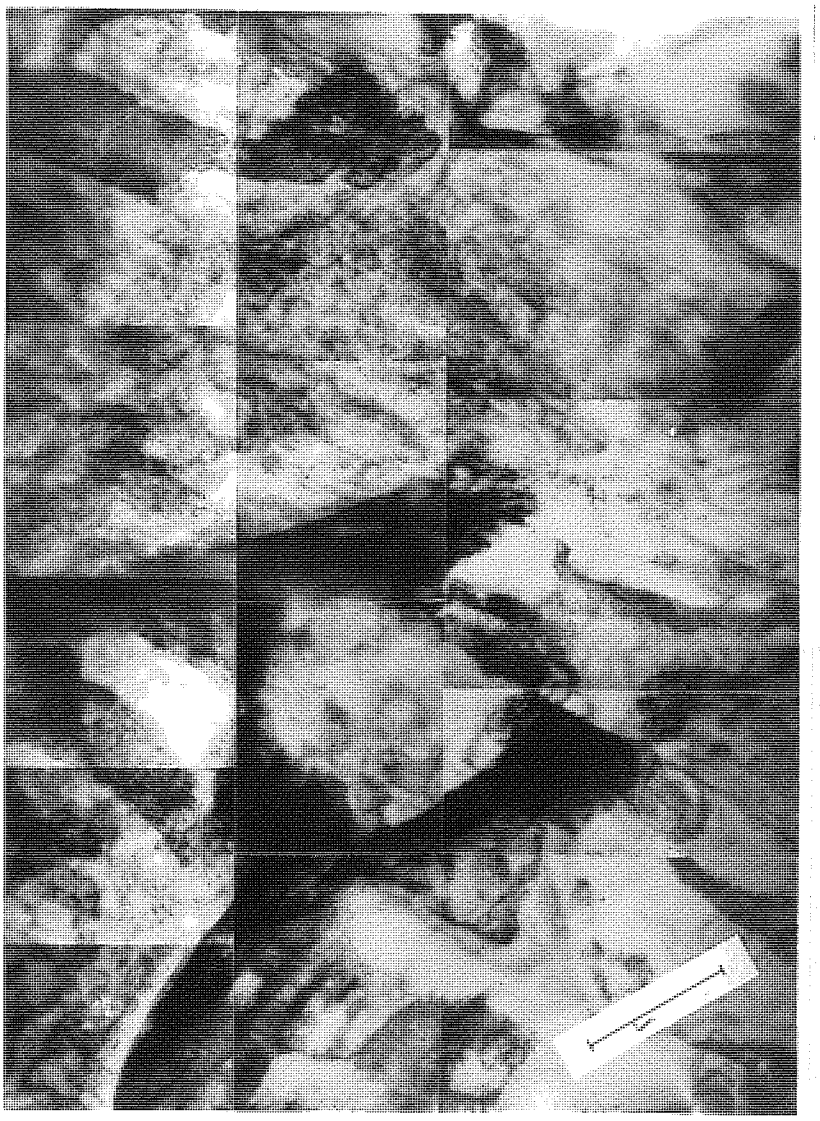

FIGURE 5.16d: Transmission Electron Micrograph after 10% strain

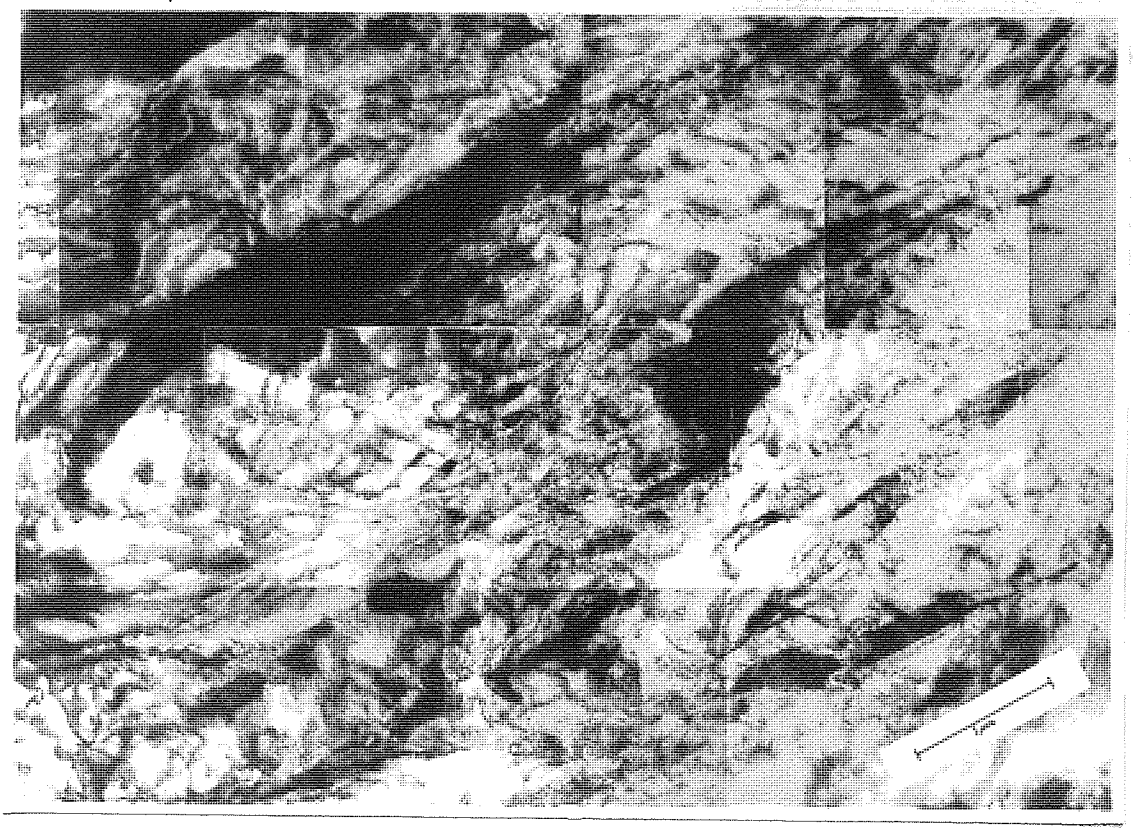

FIGURE 5.16é: Transmission Electron Micrograph after 20% strain

FIGURE 5.16f Transmission Electron Micrograph after 25% strain

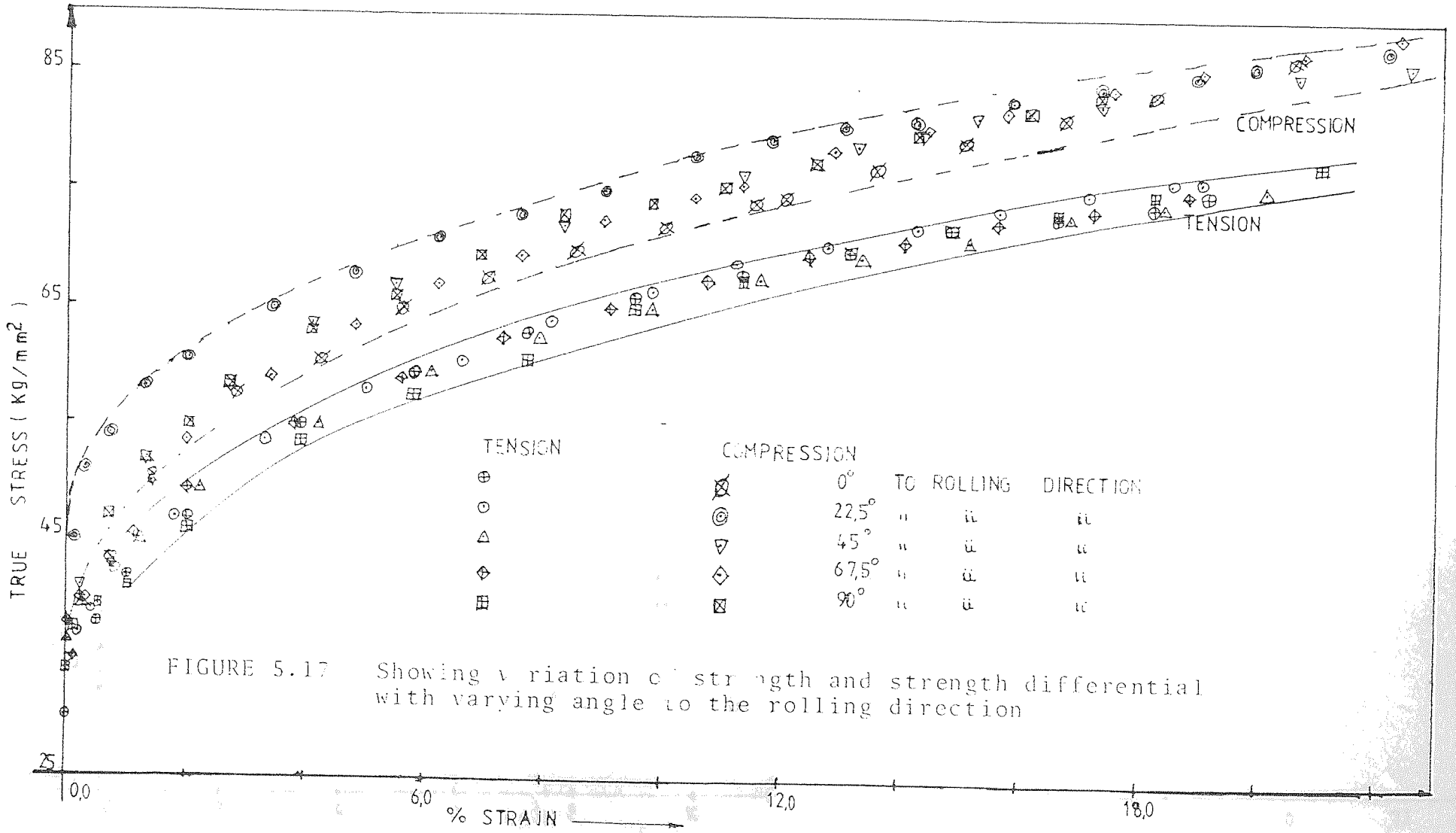

FIGURE 5.17 Showing variation of strength and strength differential with varying angle to the rolling direction

FIGURE 5.17b Showing variation of strength and strength-differential with varying angle to the rolling direction

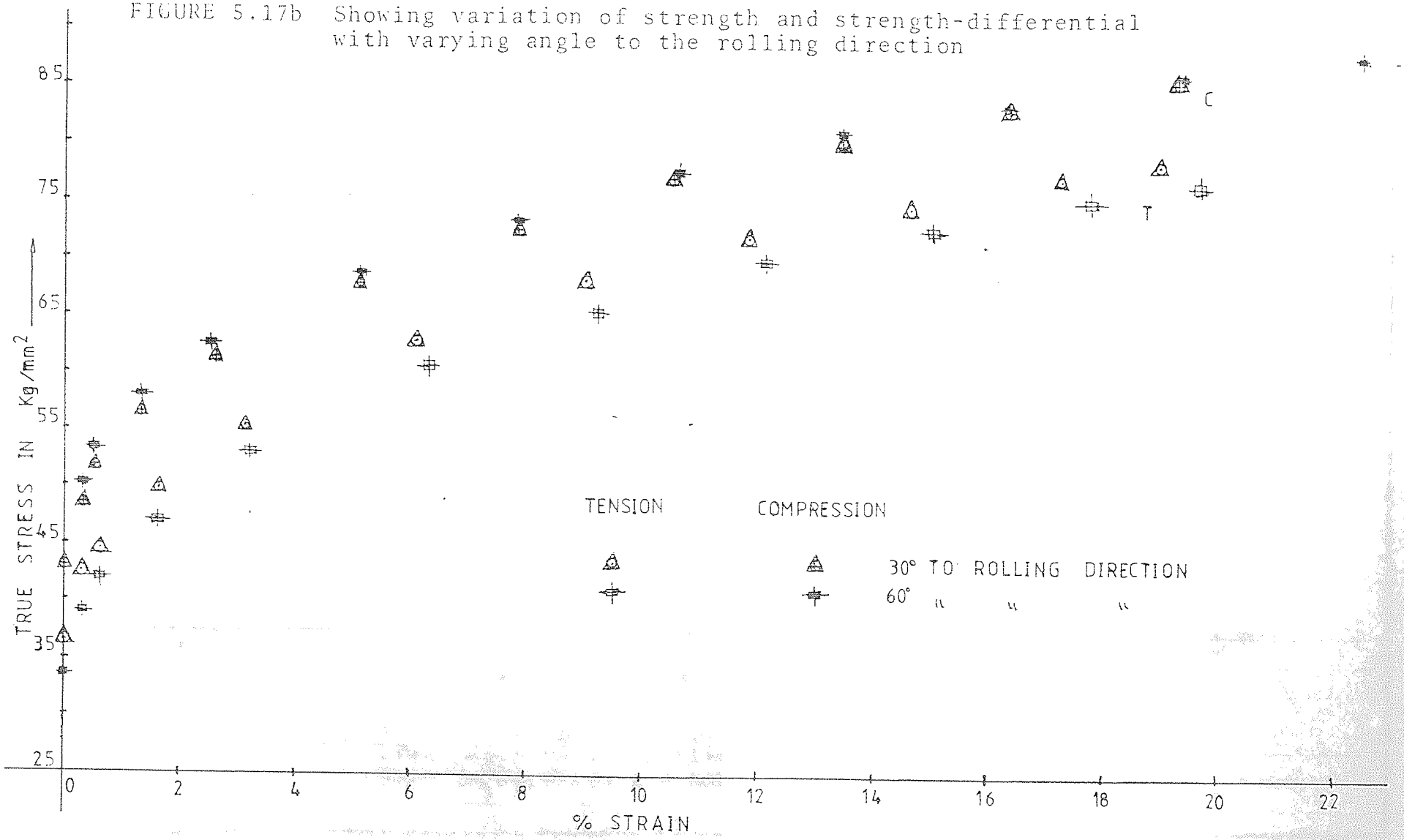

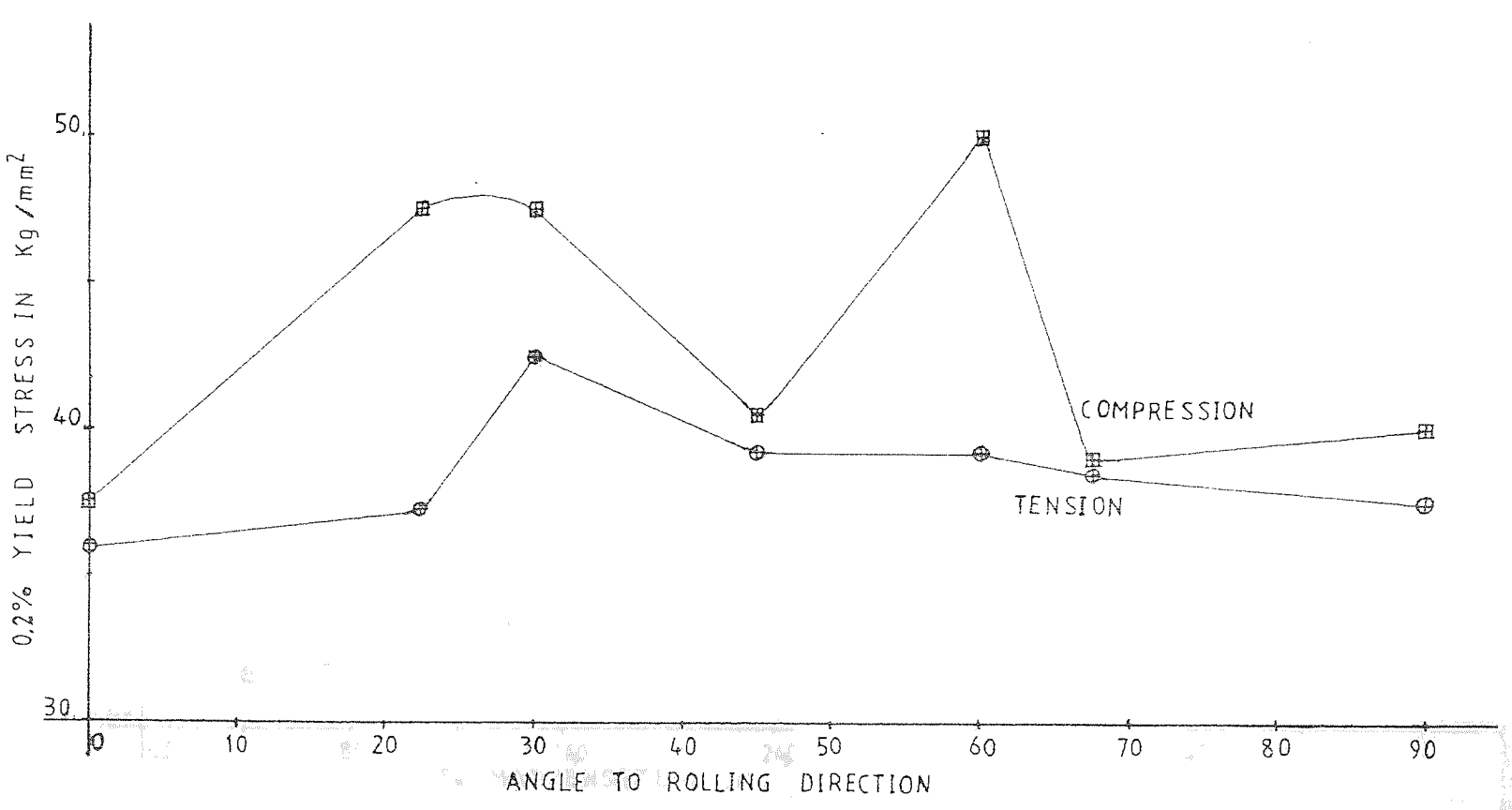

FIGURE 5.17c Showing variation of 0.2% off-set yield stress with angle to as-received rolling direction for both compression and tension

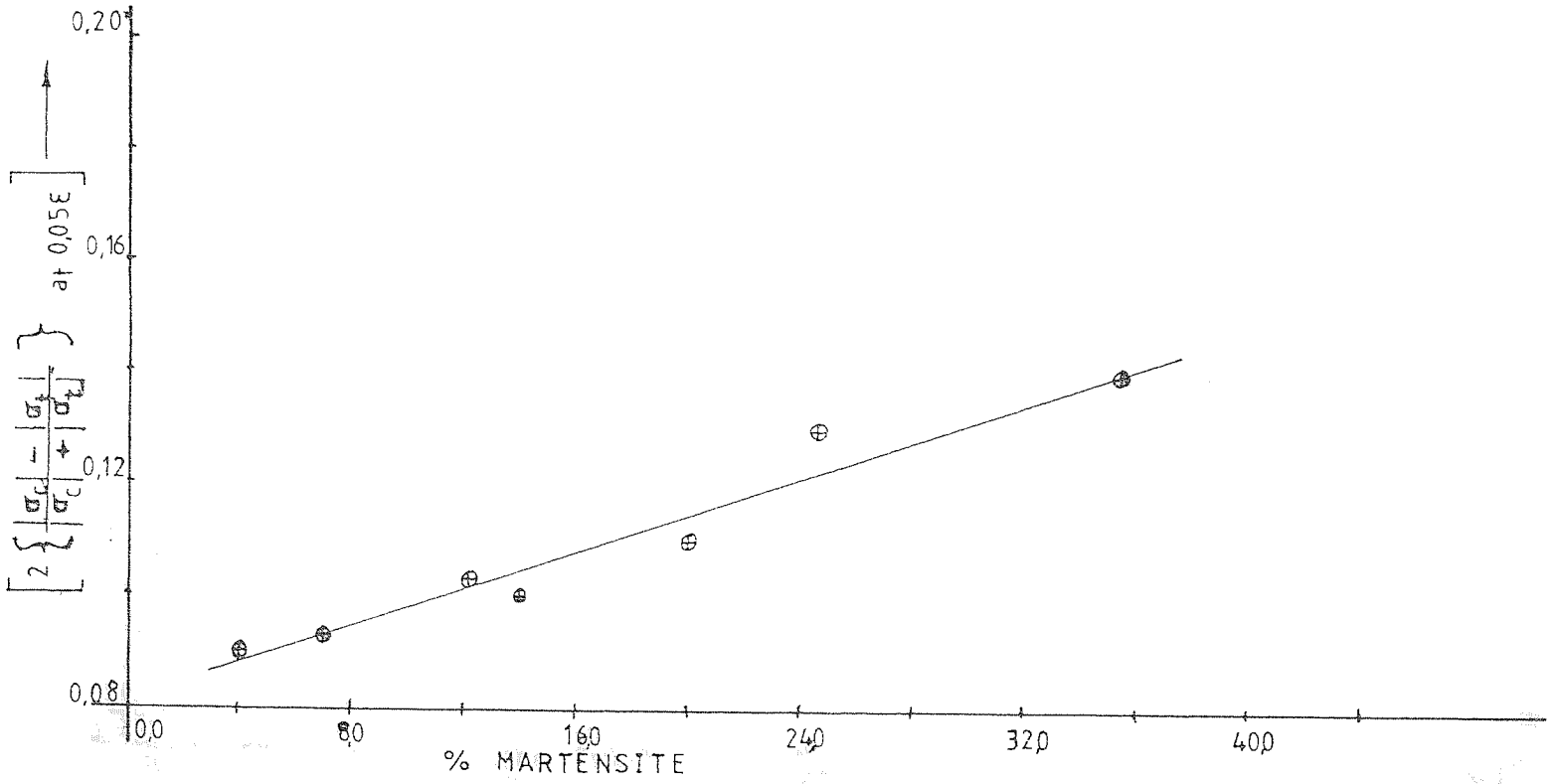

FIGURE 5.18 Showing variation of strength differential effect with % martensite

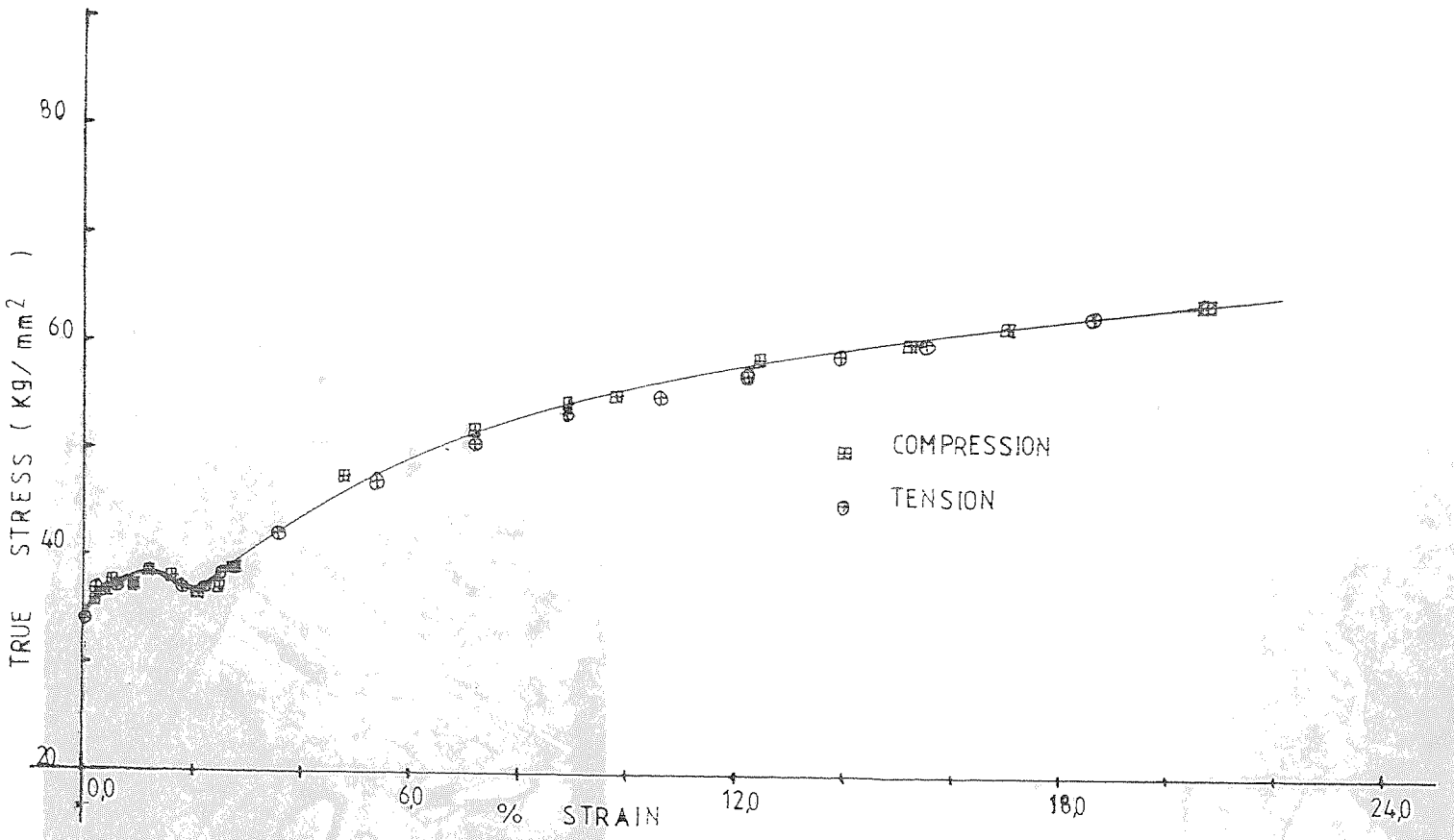

FIGURE 5.19 Showing the absence of strength differential after annealing at 900°C and furnace cooling to room temperature

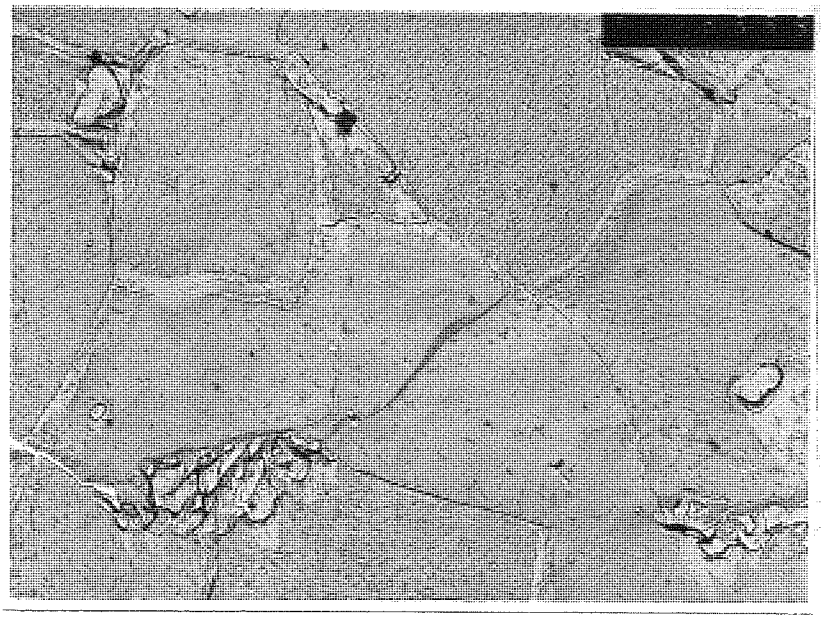

a. x 4000

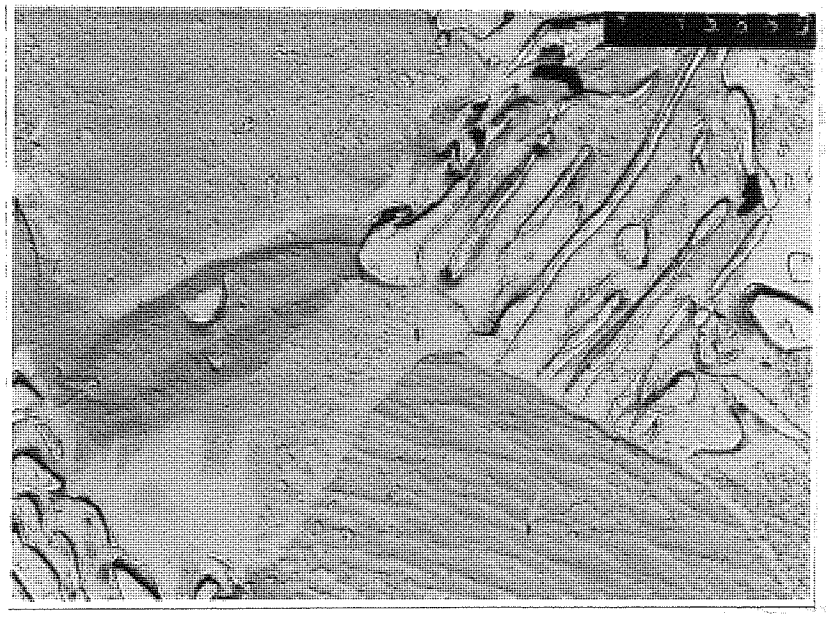

b. x 15000

FIGURE 5.20 Showing the features of the sample treated at 900°C and furnace cooling. No strength differential is present

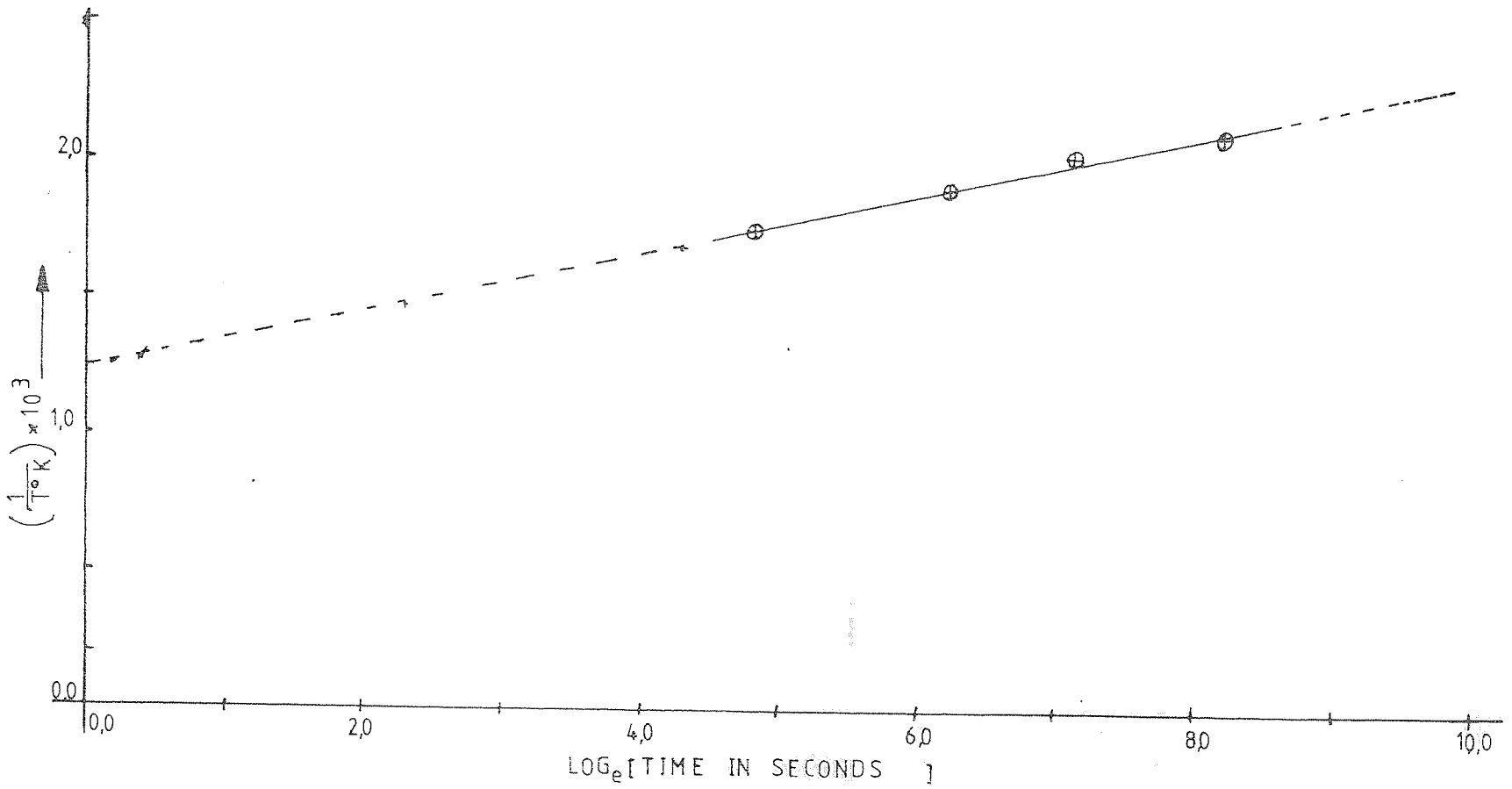
2,0
1,0
0,0
$\left(\frac{1}{T°K}\right) \times 10^3$
0,0
2,0
4,0
6,0
8,0
10,0
LOG_e[TIME IN SECONDS]

FIGURE 5.21a

FIGURE 5.21a Reciprocal of absolute temperature vs natural logarithm of time, in second, for return of yield point on as-received Dual-Phase steel

$$\text{Gradient } \frac{R}{Q} = \frac{0.75 \times 10^{-3}}{7.1}$$

Given $Q = 78.7$ KJ/mol

Normally $Q \simeq 80.22$ KJ mol^{-1} for diffusion of carbon in iron

FIGURE 5.21b Showing variation of tensile strength and yield stress versus ageing time at different temperatures of ageing

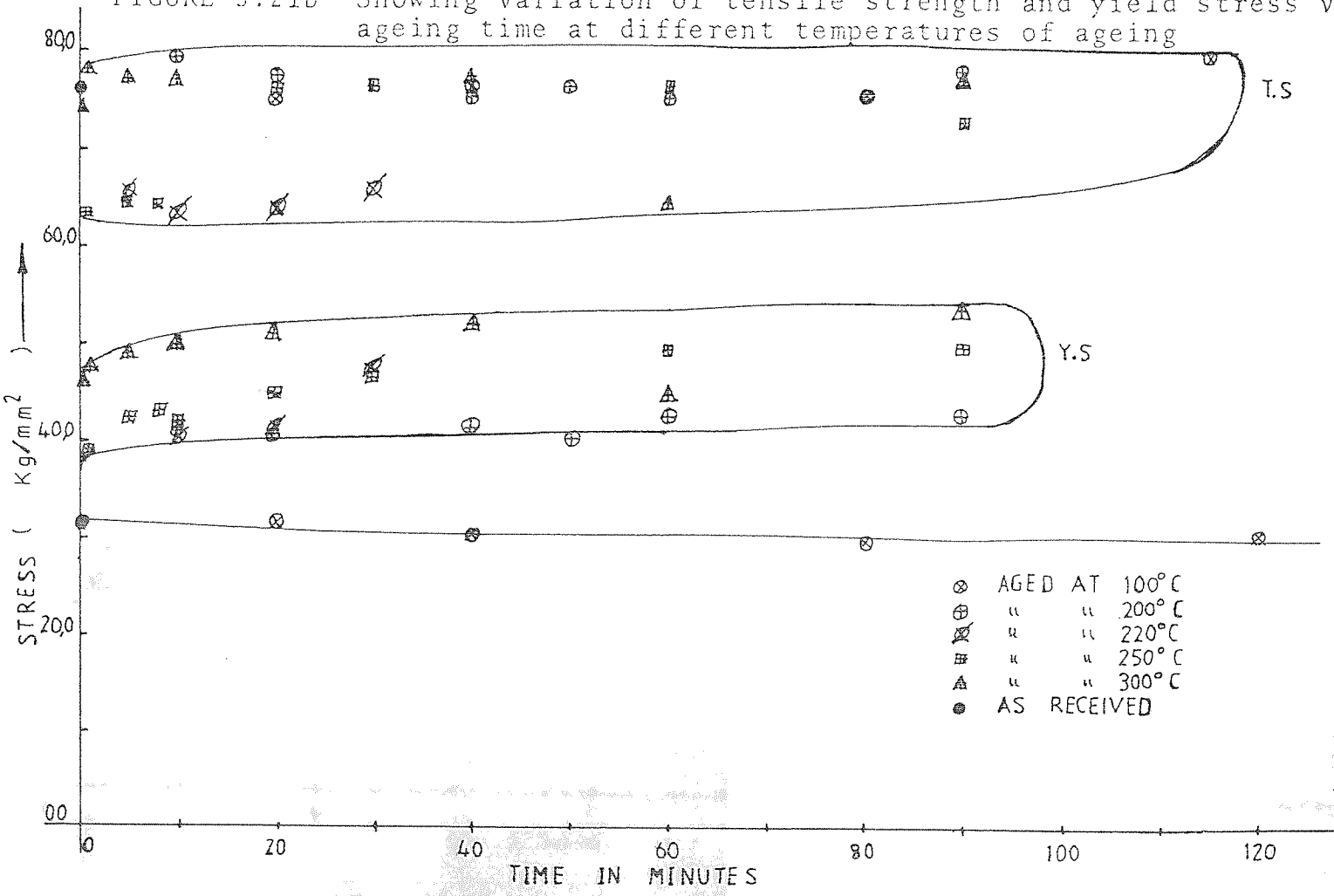

FIGURE 5.21c Showing the effect of percentage of martensite on return of yield point. Higher percentage of martensite delays return of yield point at the same ageing temperature

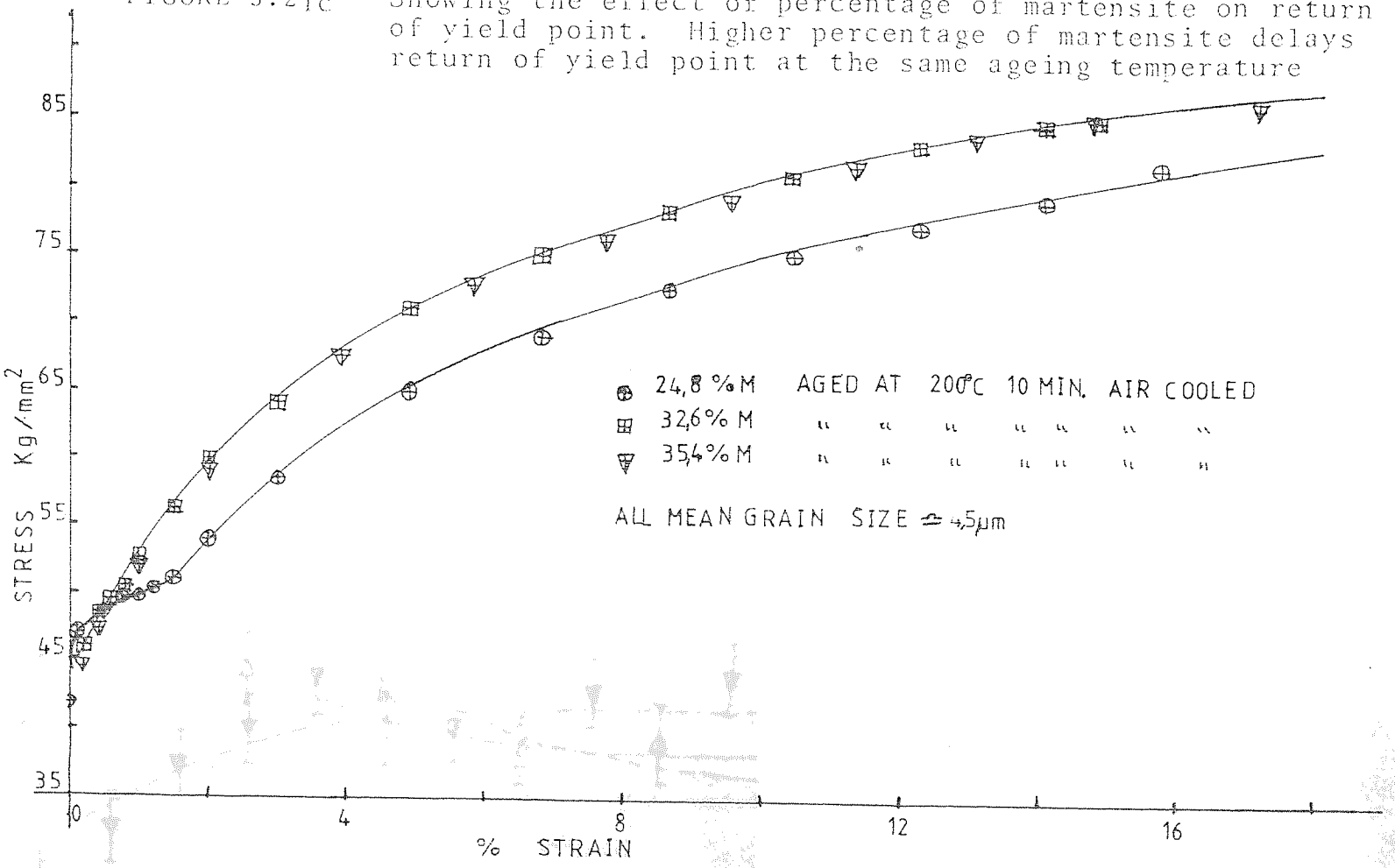

FIGURE 5.22 R_o values as a function of strain for Al-Si killed steel in the as-received and Dual-Phase condition showing the effect of percentage martensite on R_o value

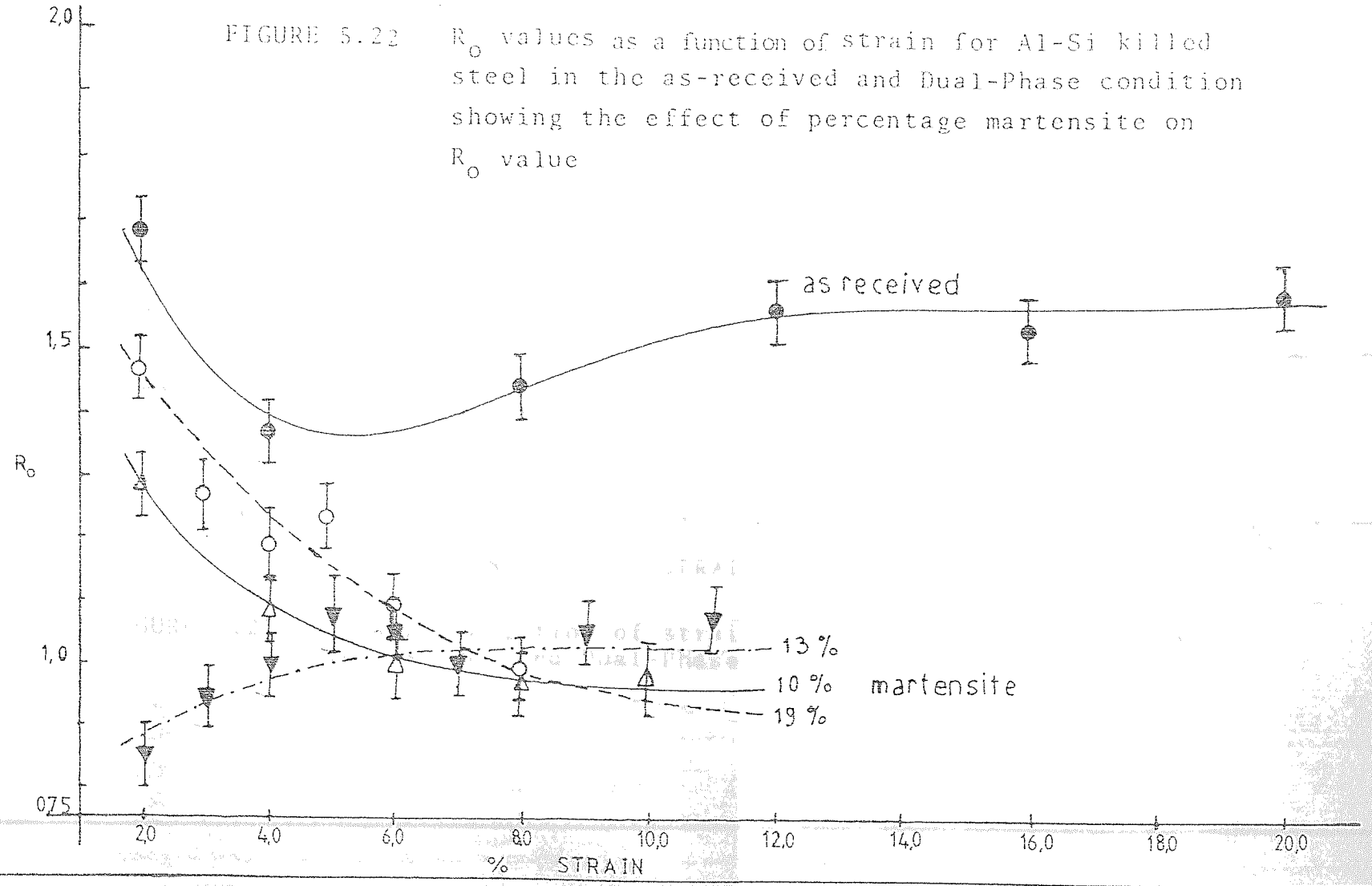

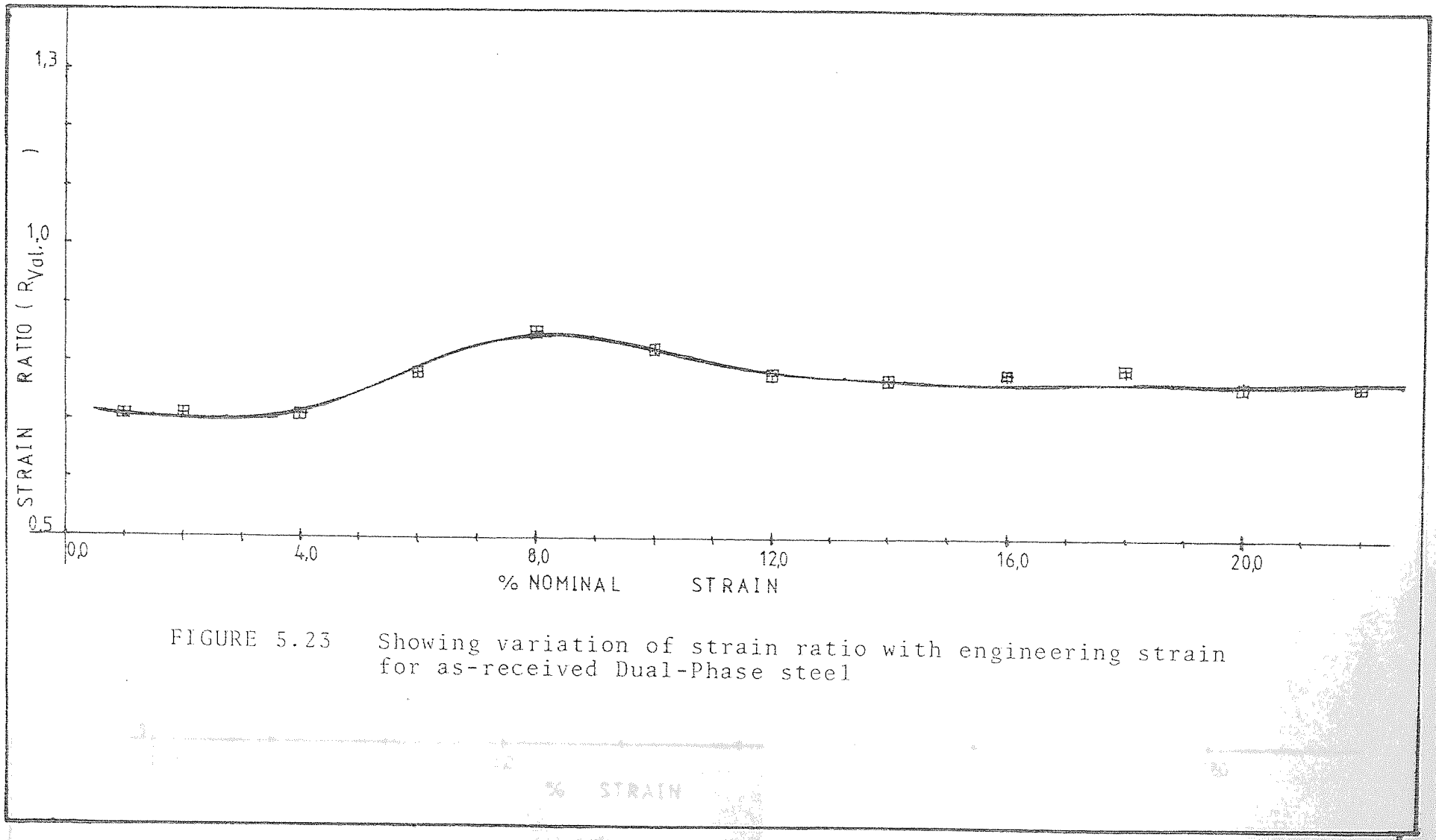

FIGURE 5.23 Showing variation of strain ratio with engineering strain for as-received Dual-Phase steel

FIGURE 5.24 Showing variation of strain rate sensitivity index (m) with % strain for as-received Dual-Phase steel

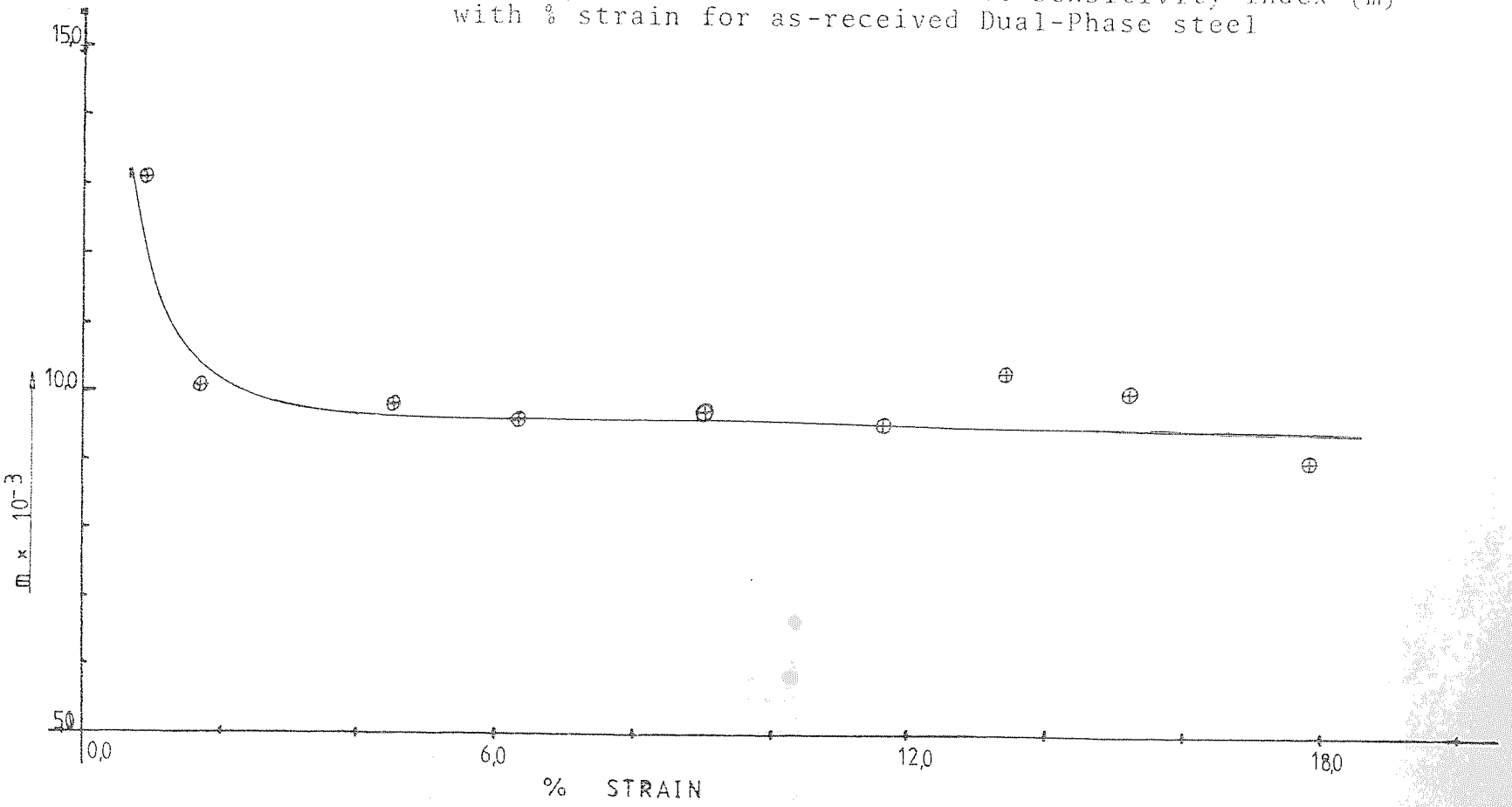

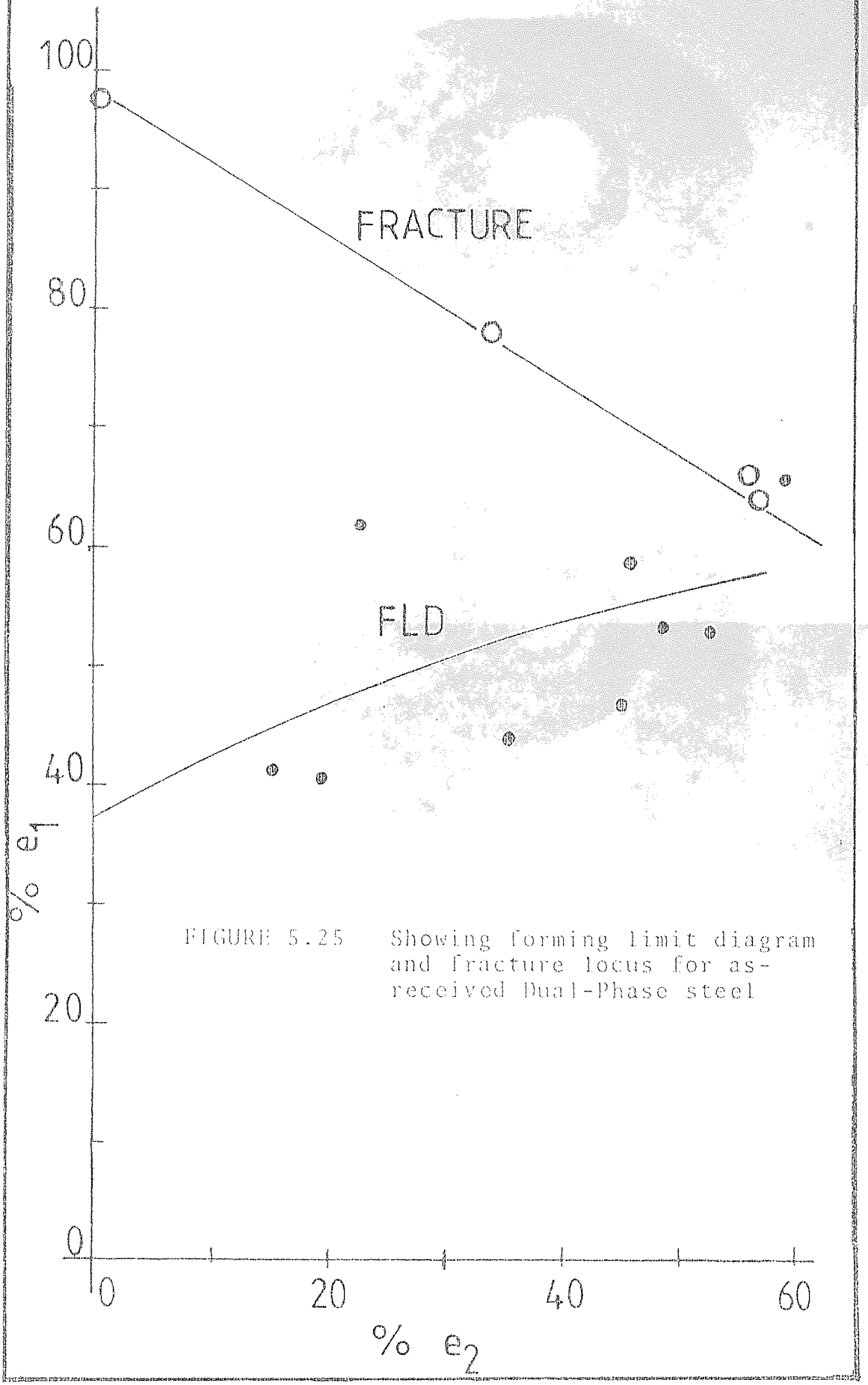

FIGURE 5.25 Showing forming limit diagram and fracture locus for as-received Dual-Phase steel

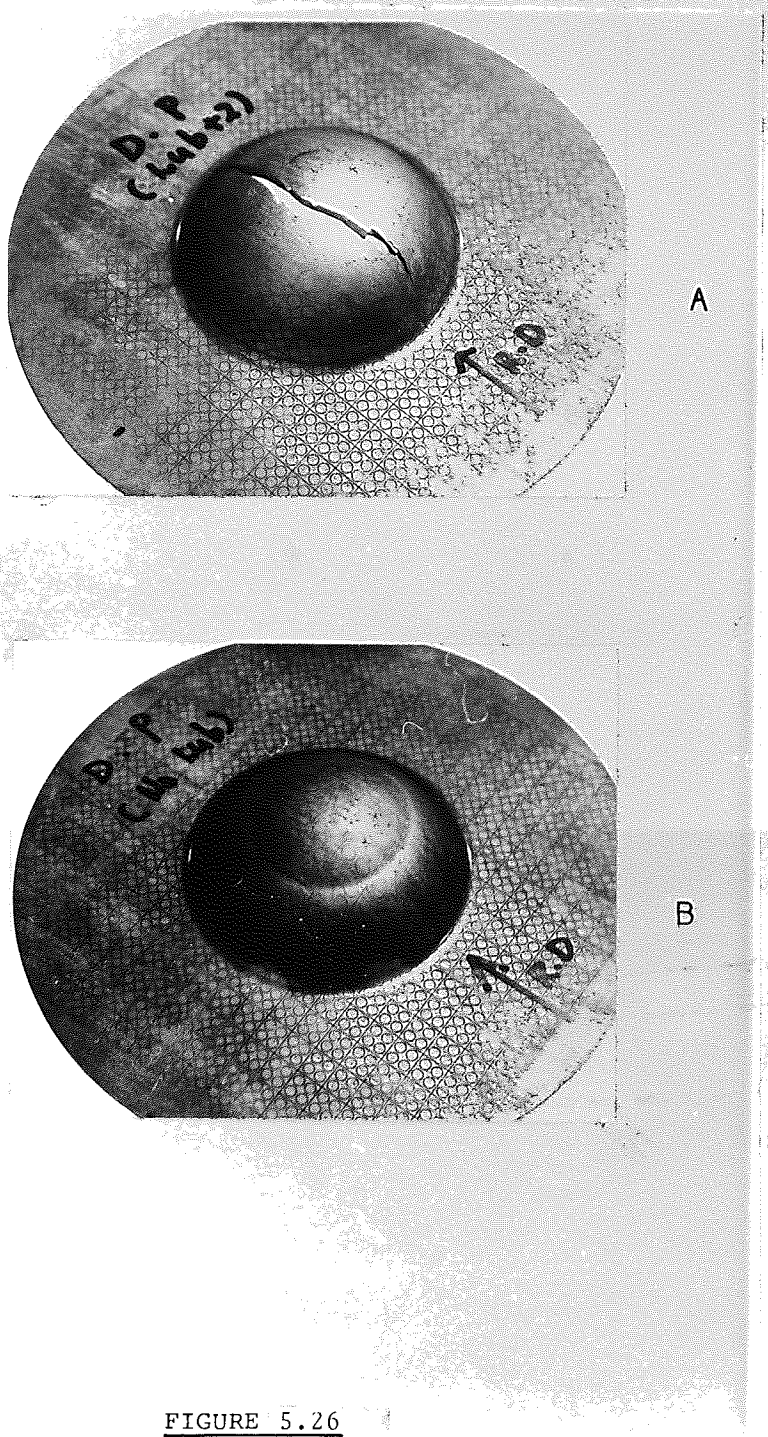

FIGURE 5.26

50mm punch stretch tests with and without lubrication

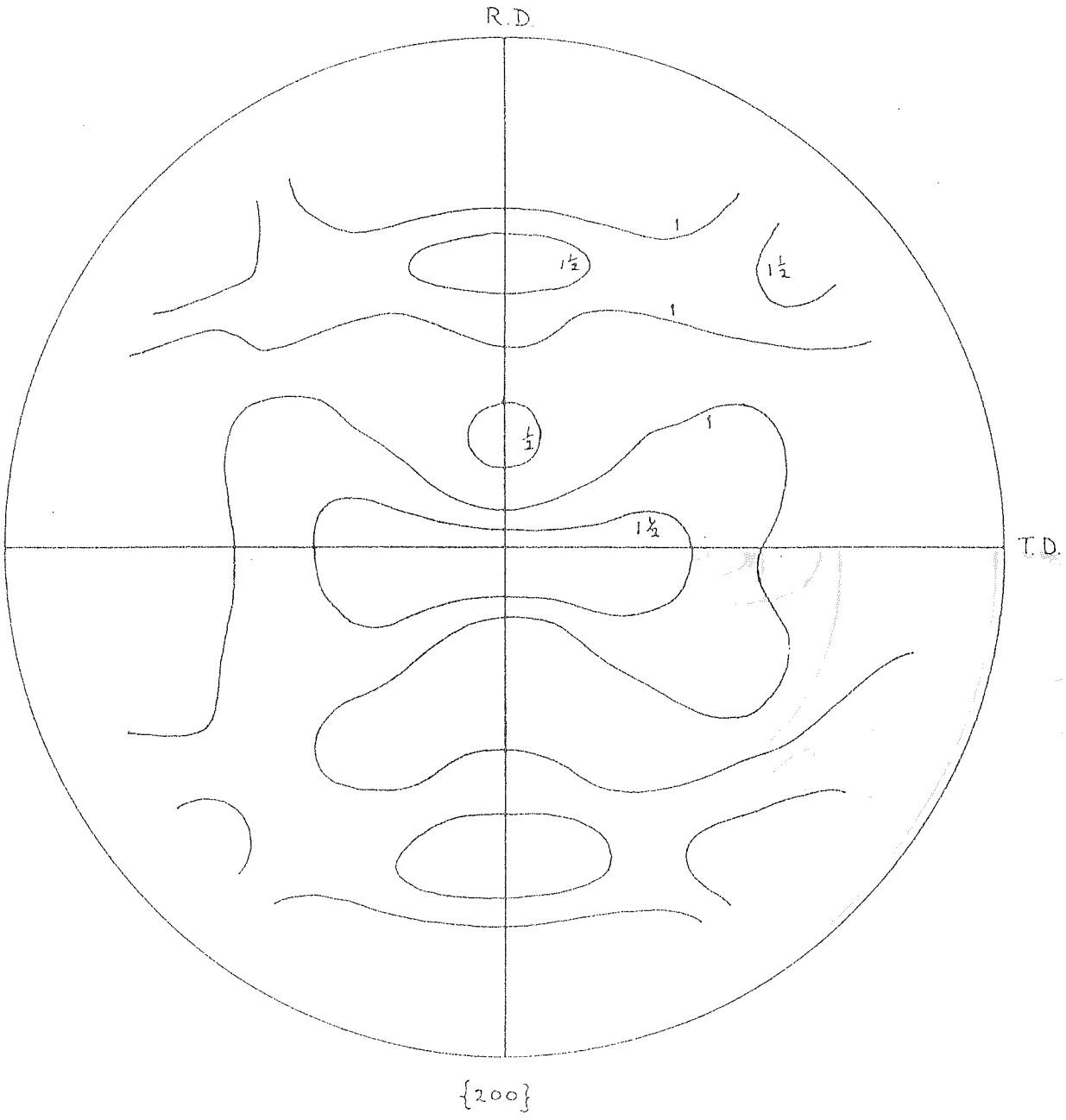

FIGURE 5.27 Showing the {200} pole figure

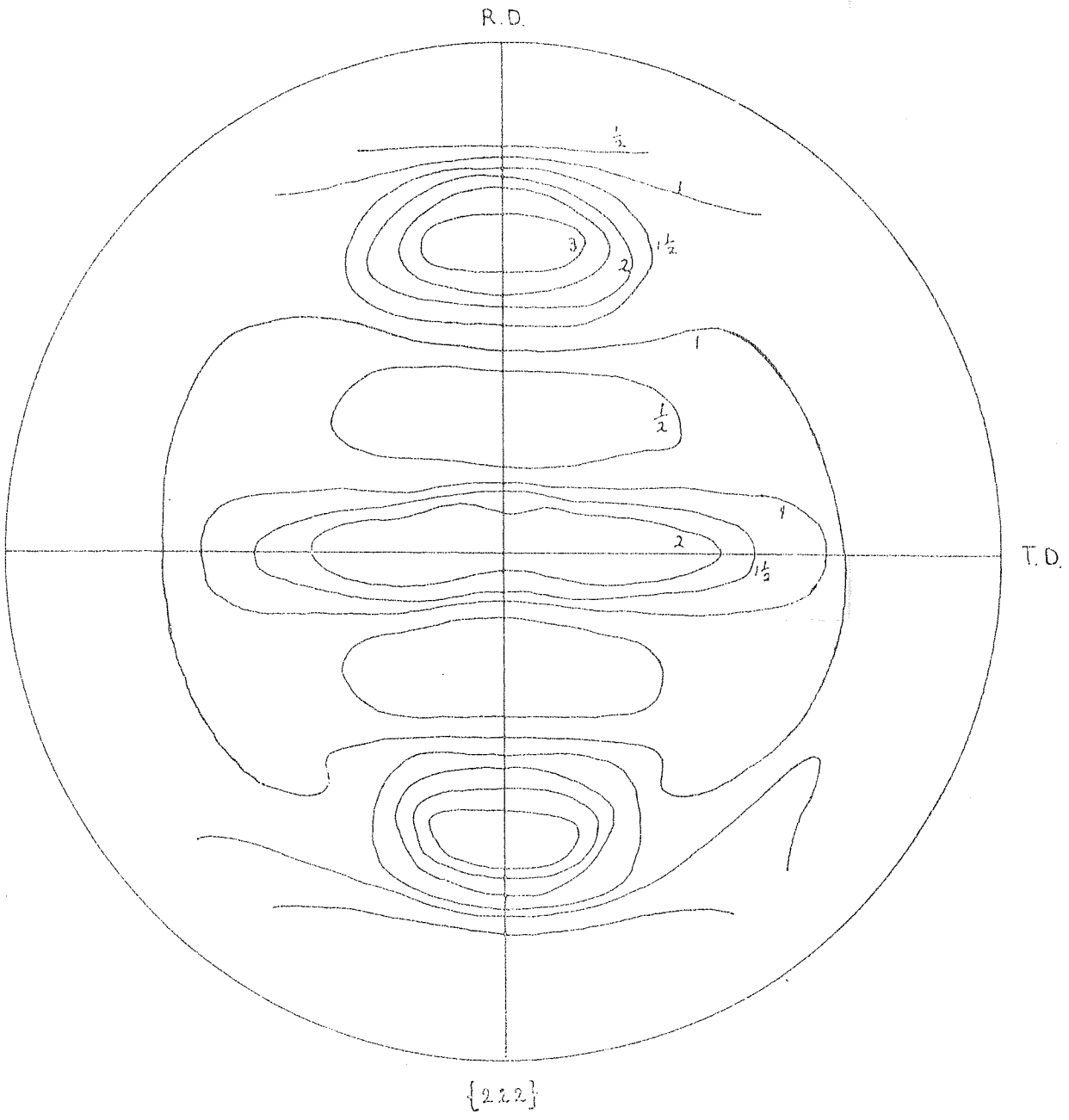

FIGURE 5.28 Showing the {222} pole figure

Table 5.2

Thickness mm	YS N/mm^2	TS N/mm^2	Total elongation %
0.93	324	631	24.7
0.97	292	603	24.8
1.95	307	650	30.0
1.98	287	638	32.0
2.90	323	612	36.0
2.93	389	631	31.0
2.95	267	634	32.0
2.97	341	645	27.0
3.30	339	622	31.0
3.32	398	636	33.6

Showing the thickness effect on tensile properties

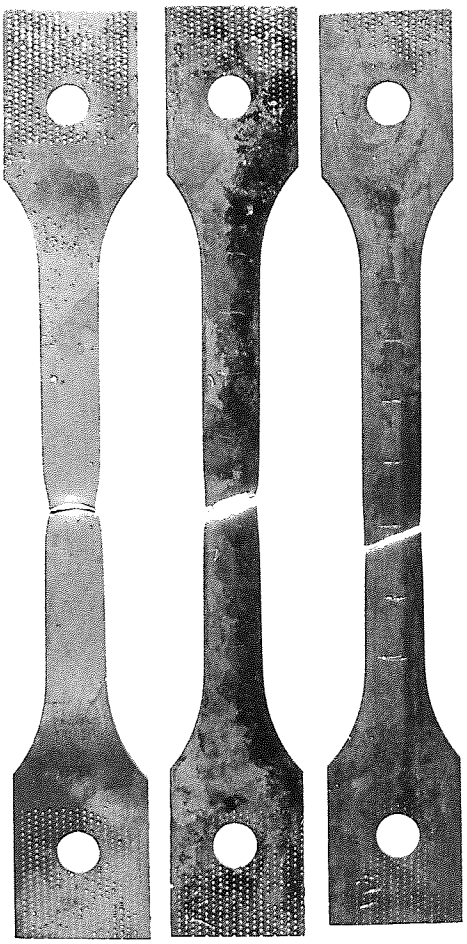

$t_A > t_B > t_C$

FIGURE 5.29

The variation of fracture appearance with thickness

FIGURE 5.30

FIGURE 5.30 Showing fracture surface

FIGURE 5.31 Showing longitudinal section to fracture surface. Voids are seen at particle/matrix interface.

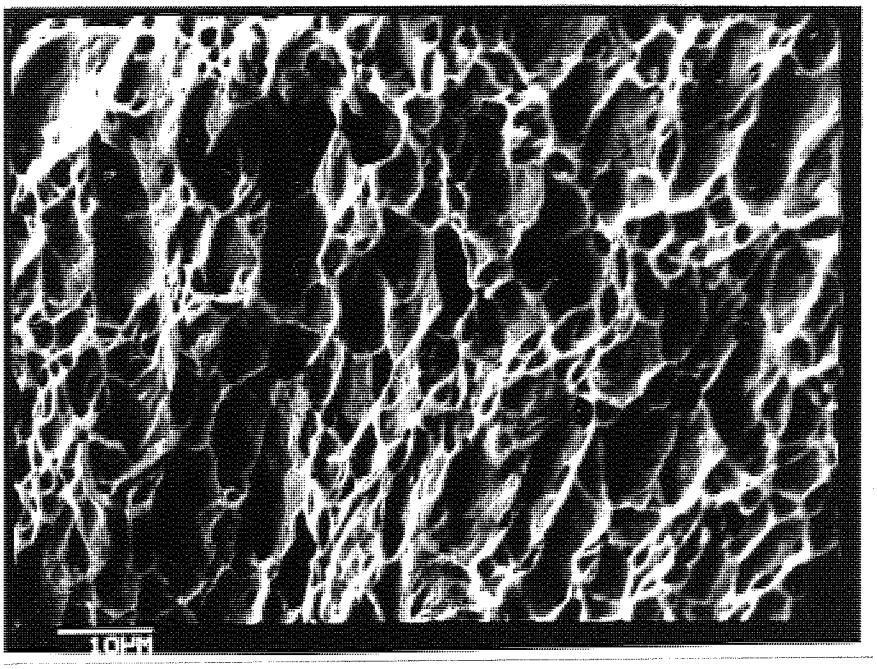

FIGURE 5.30 Typical Fracture Surface of as-received Dofasco steel

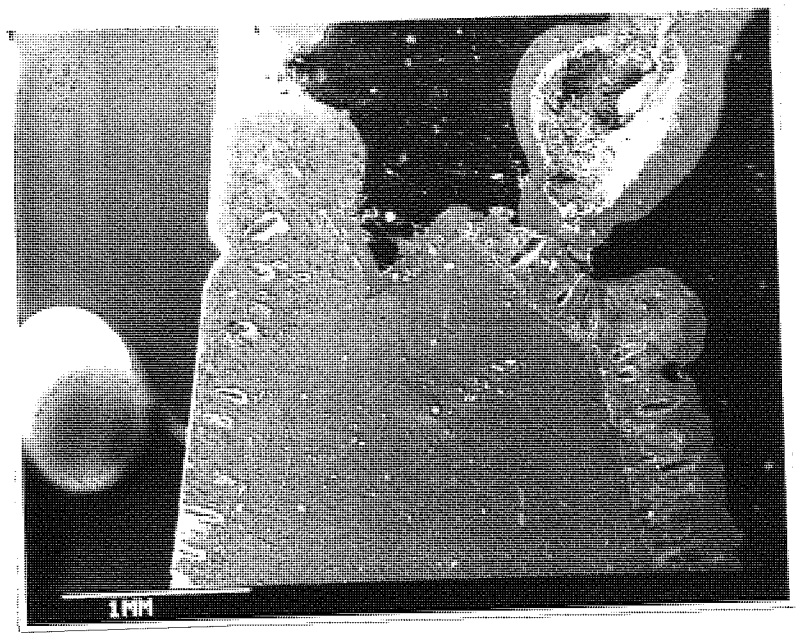

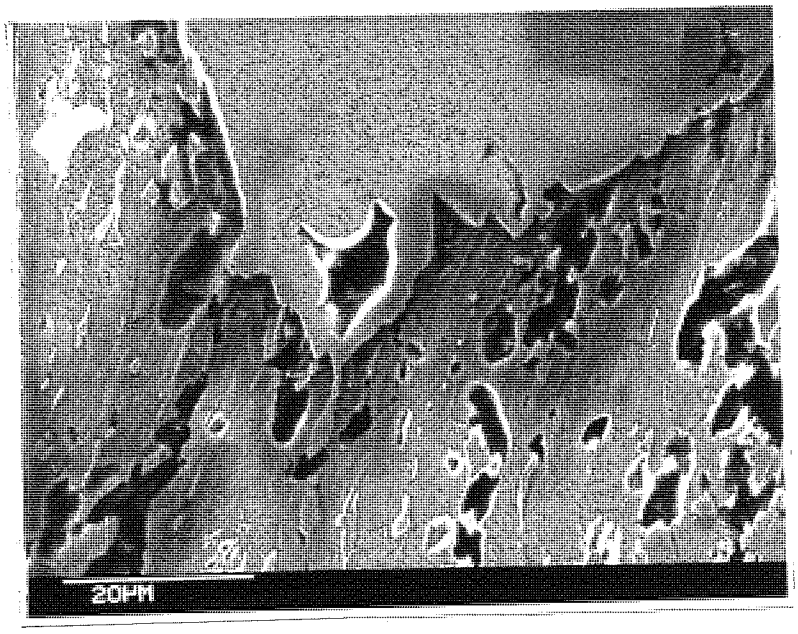

FIGURE 5.31a

FIGURE 5.31b

a. 1 mm from fracture surface
b. 2 mm from fracture surface
c. 3 mm from fracture surface

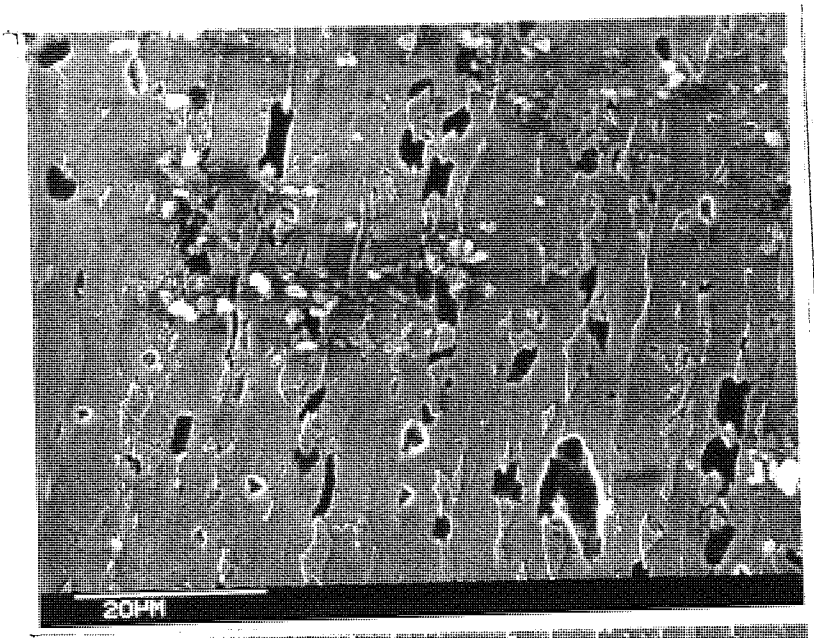

a.

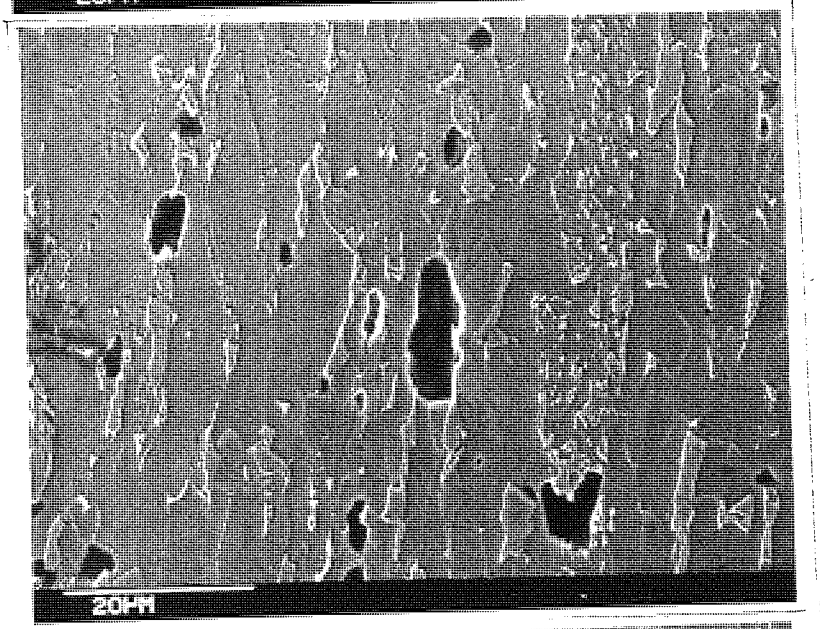

b.

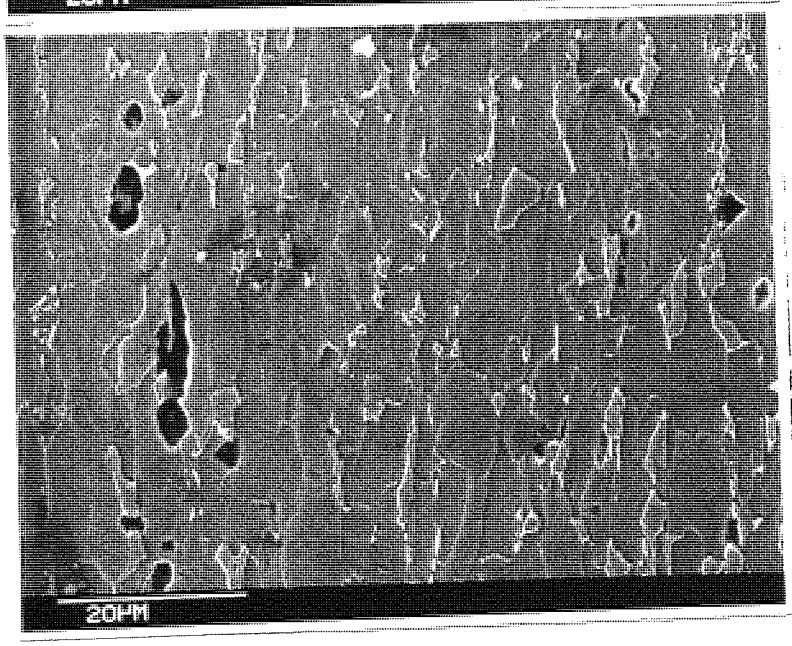

c.

FIGURE 5.31b

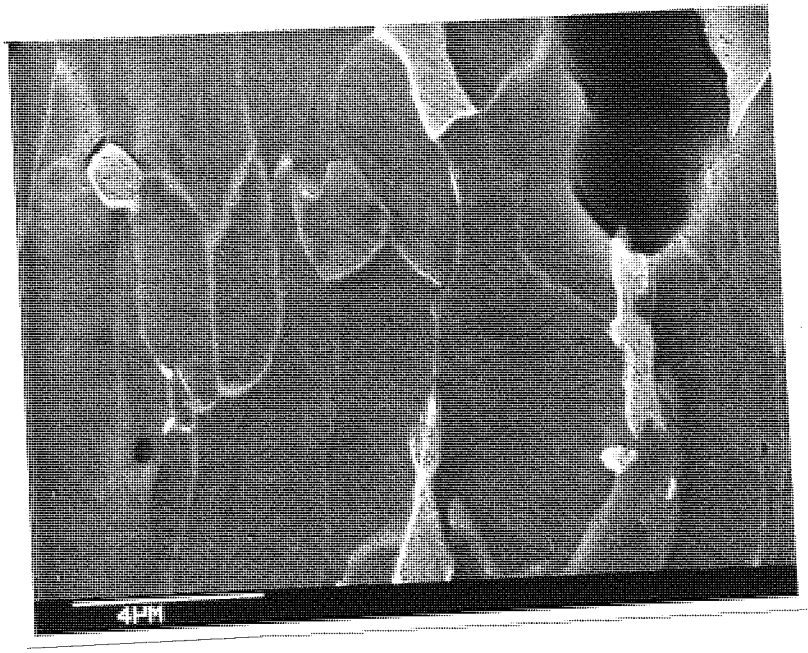

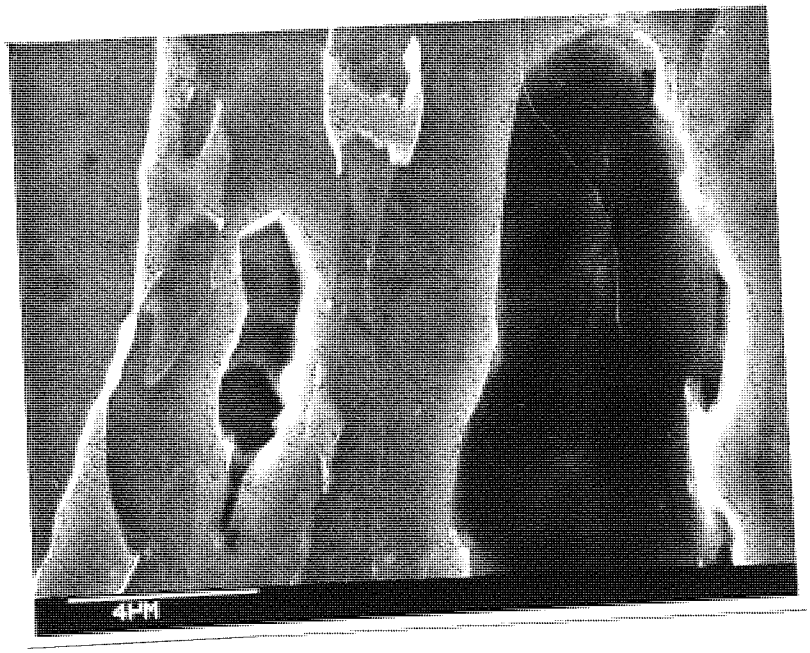

FIGURE 5.31c